Active noise control in the presence of uncertain and time-varying disturbances

Raúl Antonio Mélendez Márquez

Communauté UNIVERSITÉ Grenoble Alpes

THÈSE

Pour obtenir le grade de

DOCTEUR DE LA COMMUNAUTÉ UNIVERSITÉ GRENOBLE ALPES

Spécialité : **AUTOMATIQUE - PRODUCTIQUE**
Arrêté ministériel : 25 mai 2016

Presentée par

Raúl Antonio MELÉNDEZ MÁRQUEZ

Thèse dirigée par **Luc DUGARD**, **CNRS**, codirigée par **Ioan-Doré LANDAU**, **CNRS Emérite** et co-encadrée par **Tudor-Bogdan AIRIMIŢOAIE, Université de Bordeaux**

préparée au sein du **Laboratoire Grenoble Images Parole Signal Automatique**
dans **l'École Doctorale Electronique, Electrotechnique, Automatique, Traitement du Signal (EEATS)**

Active noise control in the presence of uncertain and time-varying disturbances

Thèse soutenue publiquement le **23 mai 2019,**
devant le jury composé de :

Monsieur Kouider Nacer M'SIRDI
Professeur, Aix-Marseille Université, Président
Monsieur Thomas HÉLIE
Directeur de Recherche CNRS, IRCAM Paris, Rapporteur
Monsieur Rogelio LOZANO-LEAL
Directeur de Recherche CNRS, UTC Compiègne, Rapporteur
Monsieur Luc DUGARD
Directeur de Recherche CNRS, CUGA Grenoble, Directeur de thèse
Monsieur Ioan-Doré LANDAU
Directeur de Recherche CNRS Emérite, CUGA Grenoble,
Co-directeur de thèse
Monsieur Tudor-Bogdan AIRIMIŢOAIE
Maître de Conférences, Université de Bordeaux, Examinateur

A mis padres y mi familia

TABLE OF CONTENTS

D . . . . Primary path model

G . . . . Secondary path model

M . . . . Reverse path model

N_s . . . . Number of samples in a test

$R(i)$ . . . . Autocorrelation

$R_n(i)$ . . . . Normalized Autocorrelation

S_{up} . . . . Input sensitivity function

S_{yp} . . . . Output sensitivity function

T_s . . . . Sampling time

W . . . . Image path model

f_s . . . . Sampling frequency

q^{-1} . . . . Delay operator for time domain

ANC . . . . Active Noise Control

ARMA . . . . Auto-Regressive Moving Average

ARMAX . . . . Auto-Regressive Moving Average with eXogenous input

AVC . . . . Active Vibration Control

BSF . . . . Band Stop Filter

FF . . . . Feedforward

FIR . . . . Finite Impulse Response

FuLMS . . . . Filtered-U Least Mean Squares

FuPLR . . . . Filtered-U Pseudo Linear Regression

FuSBA . . . . Filtered-U Stability Based Algorithm

FvLMS . . . . Filtered-V Least Mean Squares

FxLMS . . . . Filtered-X Least Mean Squares

HARF . . . . Hyperstable Adaptive Recursive Filter

IFAC . . . . International Federation of Automatic Control

IIR . . . . Infinite Impulse Response

IMP . . . . Internal Model Principle

IV . . . . Instrumental Variable

LMS . . . . Least Mean Squares

LS . . . . Least Squares

LTI . . . . Linear Time Invariant

MBD . . . . Model Based Design

MSE . . . . Mean Square Errors

NFuLMS . . . . Normalized Filtered-U Least Mean Squares

ODE . . . . Ordinary Differential Equation

OEEPM . . . . Output Error with Extended Prediction Model

PAA . . . . Parameter Adaptation Algorithm

PRBS . . . . Pseudo-Random Binary Sequence

PSD . . . . Power Spectral Density

RELS . . . . Extended Recursive Least Squares

RLMS . . . . Recursive Least Mean Squares

RLS . . . . Recursive Least Squares

SFuSBA . . . . Scalar Filtered-U Stability Based Algorithm

SHARF . . . . Simple Hyperstable Adaptive Recursive Filter

SPR . . . . Strictly Positive Real

TET . . . . Task Execution Time

YK . . . . Youla-Kučera

YK-FIR . . . . Finite Impulse Response Youla-Kučera

YK-IIR . . . . Infinite Impulse Response Youla-Kučera

International Journals with Peer Review

[J1] *Robust and Adaptive Feedback Noise Attenuation in Ducts*, Landau Ioan-Doré, Meléndez Raúl, Dugard Luc, Buche Gabriel, IEEE Transactions on Control Systems Technology, March 2019, 27 (2) 872-879, Institute of Electrical and Electronics Engineers. [Landau et al., 2019c]. DOI: 10.1109/TCST.2017.2779111

[J2] *Beyond the delay barrier in adaptive feedforward active noise attenuation*, Landau Ioan-Doré, Meléndez Raúl, Airimiţoaie Tudor-Bogdan, Dugard Luc, Journal of Sound and Vibration, Elsevier, 2019. ([Landau et al., 2019a]).

Internal Reports

[J3] *Algorithms for adaptive feedforward noise attenuation - A comparative experimental evaluation*, Tudor-Bogdan Airimiţoaie, Ioan-Doré Landau, Raúl Meléndez and Luc Dugard. [Airimiţoaie et al., 2018]

International Conferences with Peer Review

[C1] *Data driven design of tonal feedback cancellers*, Meléndez Raúl, Landau Ioan-Doré, Dugard Luc, Buche, Gabriel, 20th World Congress of the International Federation of Automatic Control, 9-14 July 2017, Toulouse, France. [Meléndez et al., 2017]. DOI: 10.1016/j.ifacol.2017.08.087

[C2] *Active Noise Control: Adaptive vs Robust Approach*, Landau Ioan-Doré, Meléndez Raúl, 25th Mediterranean Conference on Control and Automation, 3-6 July 2017, Valletta, Malta. [Landau and Meléndez, 2017]. DOI: 10.1109/MED.2017.7984216

[C3] *Why one should use Youla-Kučera parametrization in adaptive feedforward noise attenuation?*, Ioan-Doré Landau, Tudor-Bogdan Airimiţoaie, Raúl Meléndez and Luc Dugard, 58th IEEE Conference on Decision and Control, 11-13 December 2019, Nice, France. [Landau et al., 2019b]

National Presentations without proceedings

[C3] *Robust and adaptive approach for active noise control: Comparative study*, Meléndez Raúl, Dugard Luc, Landau Ioan-Doré, Airimiţoaie Tudor-Bogdan, Journées Automatique du GDR MACS 2016, Groupe de Recherche du CNRS en Modélisation, Analyse et Conduite des Systèmes dynamiques, 15-16 November 2016, Lille, France.

[C4] *Robust and Adaptive Approach for Feedback Active Noise Control: Comparative study*, Meléndez Raúl, 19th Journée des Doctorants EEATS 2017, Communauté Université Grenoble, June 2017, Grenoble, France.

[C5] *Robust and adaptive approach for active noise control: Comparative study*, Meléndez Raúl, Journée des Doctorants en Automatique 2017, Gipsa-Lab, November 2017, Grenoble France.

[C6] *Robust and Adaptive Active Noise Control*, Meléndez Raúl, Landau Ioan-Doré, Dugard Luc, Airimiţoaie Tudor-Bogdan, Journées Techniques de Contrôle en Vibrations, Acoustique et Musique 2017, Société Française d'Acoustique, 30 November - 1 December 2017, Grenoble, France.

[C7] *Evaluation Expérimentale des Techniques d'Atténuation Active de Bruit par Contre-réaction Adaptative*, Landau Ioan-Doré, Meléndez Raúl, Dugard Luc, 14ème Congrès Français d'Acoustique, Société Française d'Acoustique, 23-27 April 2018, Le Havre, France.

[C8] *Adaptive Active Noise Control: Principles and Applications of Anti-Noise*, Meléndez Raúl, Landau Ioan-Doré, Dugard Luc, Airimiţoaie Tudor-Bogdan, Journées Jeunes Chercheurs en vibration, Acoustique et Bruit, Société Française d'Acoustique, 15-16 November 2018, Le Mans, France.

RÉSUMÉ DÉTAILLÉ

Ce chapitre résume le contenu de cette thèse d'une manière brève avec des détails pertinents. Nous décrivons ici les problèmes liés à la commande active du bruit, ainsi que les différentes approches et propositions faites dans cette étude pour sa résolution. La première section décrit le banc d'essai utilisé pour effectuer les tests et les essais pertinents à ce travail. Ensuite, la méthodologie utilisée pour la modélisation du système requise dans le processus de conception des contrôleurs est décrite. Les sections suivantes décrivent les études proposées dans les configurations de feedback (rétroaction) et de feedforward (précompensation) pour le contrôle actif du bruit. Enfin, une dernière section présente les contributions et conclusions pertinentes de ce travail.

1.1 Introduction

1.1.1 Motivation

Sans entrer dans la théorie avancée ou approfondir les détails, les principes de base du contrôle actif du bruit (ANC) seront exposés et expliqués dans cette section. Quelques exemples de base seront donnés pour énoncer le problème de contrôle qui sera associé à notre recherche. Tout ceci est destiné à être présenté dans le contexte de notre travail.

Une des toutes premières mentions sur l'ANC a été faite par Henri Coandă dans les documents d'un brevet français en 1930 [Coanda, 1930]. Quelques années plus tard, Paul Lueg a fait quelque chose de similaire dans son travail et l'a mentionné dans un brevet [Lueg, 1934]. Quelque temps plus tard, le terme est apparu dans une publication de Harry F. Olson [Olson and May, 1953], cette fois dans un article de journal. En résumé, le problème à résoudre dans leur travail est celui de couper le son et de supprimer un bruit entrant d'une source donnée, en utilisant un

microphone pour les mesures, et l'ensemble formé d'un amplificateur et d'un haut-parleur pour agir comme un actionneur. On a constaté que dans ces conditions, si les systèmes proposés étaient capables de créer des ondes sonores avec des caractéristiques de fréquence similaires à celles du bruit, mais avec un décalage de phase de 180°, il était alors possible d'annuler les bruits dans la région d'action des ondes sonores produites par le haut-parleur. Par exemple, l'une des utilisations proposées de cette théorie est d'appliquer le système ANC près d'un opérateur de machines bruyantes et de moteurs d'avions pour réduire le bruit qu'ils produisent.

Dans ce domaine de recherche, trois approches différentes de contrôle actif du bruit sont considérées pour contrer le bruit, comme mentionné dans [Snyder, 2000] : celles avec un comportement passif, celles avec ce que nous pouvons appeler une action semi-active et enfin celles avec une action pleinement active. L'approche passive, qui est la plus courante, consiste principalement en l'utilisation de matériaux et de géométries aux caractéristiques spécifiques afin d'isoler et d'amortir les effets des bruits, lorsque aucun algorithme de contrôle n'est impliqué. Les avantages de cette technique sont la simplicité d'application dans les systèmes, avec une robustesse inhérente en termes de contrôle, et un excellent rapport coût-bénéfice dans la plupart des cas. Comme on pouvait s'y attendre, les inconvénients de l'utilisation d'une telle approche ont été constatés lors de l'atténuation des très basses fréquences. Cette approche se caractérise par un manque de flexibilité en termes de contrôle, ainsi que l'absence d'adaptation aux caractéristiques changeantes de l'environnement et une dépendance à la dynamique physique et naturelle du système. L'exemple le plus simple de l'insonorisation passive peut être vu dans l'isolation avec de la mousse haute densité utilisée dans les tuyaux et les murs des bâtiments. Le résonateur de Helmholtz, décrit dans [Olson and May, 1953, Fleming et al., 2007], est un exemple plus complexe, mais toujours un exemple de ce concept.

La seconde approche est dite semi-active, car elle ne nécessite pas d'énergie supplémentaire au système lui-même, mais elle utilise les informations acquises pour modifier les caractéristiques des actionneurs passifs. Cette conceptualisation requiert plus d'éléments impliqués dans son fonctionnement, comme un capteur ou un transducteur pour recueillir certaines informations données du système. Cela présente l'avantage d'être plus flexible aux changements de la dynamique du système, néanmoins la complexité de la mise en œuvre et les coûts augmentent considérablement. Suivant l'exemple de l'approche précédente, il existe des modèles de résonateurs de Helmholtz capables de modifier les dimensions de la chambre de résonance et donc de s'adapter entre une plage de fonctionnement déterminée à sa fréquence propre, comme le montrent [de Bedout et al., 1997] et [Matsuhisa et al., 1992].

Finalement, notre principal intérêt réside dans la troisième et dernière approche dans laquelle l'intégralité de ce travail est incluse, le contrôle actif. Cette implémentation présente une différence notable par rapport aux deux dernières options, car elle utilise des actionneurs qui constituent une source d'énergie supplémentaire et externe au système lui-même. Ceci permet de satisfaire différents objectifs. En ce qui concerne plus spécifiquement le contrôle actif du bruit

(ANC), le domaine fréquentiel d'intérêt couvre le spectre audible humain moyen des fréquences, approximativement entre 20 Hz et 20 000 Hz. Les approches passives, pour des raisons physiques, sont plus adaptées pour l'atténuation des hautes fréquences [Olson and May, 1953, Fuller and von Flotow, 1995, Elliott, 2001]. Ceci ouvre une fenêtre d'opportunités pour les ANC, d'agir dans le domaine des basses fréquences, où aucune autre approche ne peut fonctionner.

Parmi les nombreux exemples et utilisations de ces théories, l'un des exemples les plus courants dans les applications de la vie réelle est celui des écouteurs avec des capacités de réduction du bruit ambiant pour une meilleure qualité audio et expérience sonore. Pour ce faire, on mesure le bruit ambiant à l'aide d'un microphone intégré et on utilise cette information acquise par le biais d'un algorithme de commande et du haut-parleur interne comme actionneur. La Figure 1.1 détaille ce système. Dans le cas idéal, le signal ajouté doit être de même amplitude et avec un déphasage de 180° (négatif) afin d'annuler complètement le bruit gênant. Des présentations détaillées peuvent être trouvées dans les articles et documents de [Elliott and Nelson, 1993, Fuller and von Flotow, 1995, Guicking, 2007].
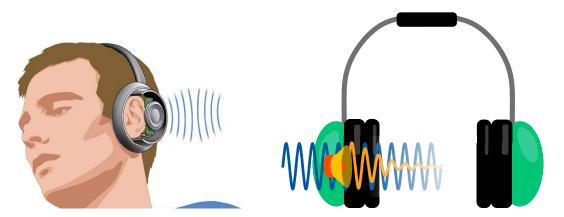
FIGURE 1.1. Atténuation externe du bruit dans les écouteurs grâce à un contrôle actif du bruit.

1.1.2 Description du Problème

La base de ce travail a d'abord été établie dans les études réalisées par Aurelian Constantinescu dans [Constantinescu, 2001], où le cas du contrôle actif des vibrations a été exposé. Par la suite, des travaux réalisés par Alma, Airimitoaie [Alma, 2011, Airimiţoaie, 2012] et plus récemment Castellanos [Silva, 2014] ont également été développés dans le domaine du contrôle des vibrations. Mais il existe des similitudes entre vibrations mécaniques et acoustiques, car ce sont deux phénomènes physiques qui peuvent être décrits par des ondes mécaniques, agissant simplement dans différents environnements. Chacun de ces travaux disposait de bancs d'essais adaptés à l'émulation de divers systèmes vibratoires mécaniques. Dans les conditions établies pour ces projets, des théories ont été élaborées et mises à l'essai sur les bancs d'essai.

Par exemple, il y a des études faites dans [Constantinescu and Landau, 2003] où un banc d'essai de système de suspension active est utilisé pour l'application des théories sur lesquelles cette thèse est basée. Dans [Alma et al., 2012] et [Landau et al., 2011a], nous pouvons trouver les applications de suivi de ces théories faites par Alma sur un autre banc de test. Une relation étroite entre les travaux décrits dans cette thèse est toujours présente parmi les études déjà réalisées, ainsi que les travaux en cours réalisés à ce stade par Airimiţoaie, vus dans [Airimiţoaie et al., 2011, Airimitoaie and Landau, 2016].

Il est remarquable de constater qu'il existe un vaste champ d'étude autour des AVC, et qu'il existe de nombreuses approches différentes ; néanmoins l'un des principaux objectifs de cette thèse est de garder trace de ces études spécifiques et de suivre le travail qui y est fait. Une fois les similitudes et les bases énoncées, l'objectif est alors de focaliser la somme des efforts réalisés dans le domaine ANC.

1.1.3 Configuration du système de contrôle

La Figure 1.2 représente un système de contrôle actif du bruit, ainsi qu'un contrôle actif des vibrations, qui envisage l'utilisation des compensateurs de feedback (rétroaction) et de feedforward (précompensation). Ce système peut être décrit comme un système à deux entrées, deux sorties. La première entrée correspond à la perturbation ou *Disturbance* $s(t)$, avec des caractéristiques inconnues et engendrée par une source non identifiée. La deuxième entrée peut être appelée *signal de commande* $u(t)$, soit la somme des signaux de commande de sortie individuels du régulateur feedback K, et du compensateur feedforward N, $u_{fb}(t)$ et $u_{ff}(t)$ respectivement. Les sorties de ce système seront celles obtenues à partir des mesures, puisque la première sortie correspond au *Bruit Résiduel* $y(t)$ du système, et la seconde sortie correspond à l'*Image de la Perturbation* $v(t)$. Dans notre cas, toutes les deux sont obtenues avec des microphones. Comme le montre la Figure 1.2, la voie qui transmet la perturbation $s(t)$ au bruit résiduel $y(t)$ est définie comme *voie primaire*. De la même façon, la *voie secondaire* est définie comme la voie qui transmet le signal de commande $u(t)$ au bruit résiduel $y(t)$. En tant que tel, le bruit résiduel est défini comme la somme de la sortie de la voie primaire, la perturbation $p(t)$, et de la sortie de la voie secondaire, désignée par $z(t)$.

Dans les systèmes de contrôle actif du bruit et de contrôle actif des vibrations, un effet secondaire appelé couplage positif interne est présent en raison du signal de contrôle $u(t)$. Le fait que les effets du signal de commande $u(t)$ sont distribués omnidirectionnellement à travers le système indique que cela aura également un effet sur les mesures $v(t)$, destinées à recueillir une information en corrélation avec la perturbation. Ce phénomène représente un couplage entre le signal de commande $u(t)$ et les mesures $v(t)$. Cette voie est appelée emphvoie inverse (reverse path), et ce couplage correspond à une retroaction positive interne. Il s'agit là d'un élément crucial dans le développement de la théorie de la commande par anticipation, car ses effets peuvent déstabiliser le système s'ils ne sont pas correctement pris en compte. Enfin, la voie entre la

perturbation $s(t)$ et les mesures à $v(t)$ est appelée la *voie image*. Ainsi, nous pouvons affirmer que les mesures $v(t)$ sont formées par la somme de la sortie de la voie inverse, définie comme $x(t)$ et de la sortie de la voie image, définie comme l'*image de la pertubation* $p_i(t)$.

Conformément à la terminologie de la théorie du contrôle, nous définirons la sortie $y(t)$ du système comme variable de performance, habituellement dénotée $e(t)$. Dans ce contexte, nous définissons notre objectif comme celui de minimiser le signal résultant $e(t)$ (au sens d'un certain critère), en compensant avec le signal de commande $u(t)$, calculé à partir des mesures $y(t)$ et $v(t)$.
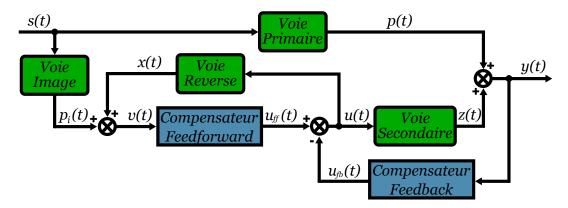
FIGURE 1.2. Représentation bloc-diagramme du problème de commande combiné de Feedback et Feedforward.

Les mesures du système peuvent être représentées sous forme vectorielle, telle que $Y(t) = [v(t), y(t)]^T$. De la même manière, en utilisant la notaion K pour le régulateur feedback et N pour le compensateur feedforward, nous pouvons les les représenter sous forme vectorielle telle que $\kappa = [N, -K]^T$. On peut donc définir le signal de commande comme suit :

$$(1.1) \qquad u(t) = u_{ff} - u_{fb} = N \cdot v(t) - K \cdot y(t) = \kappa^T \cdot Y(t).$$

Les notations utilisées pour les différentes parties du système sont : D correspond à la *voie primaire*, G est conçue comme la *voie secondaire*, W représente la *voie image* et M symbolise le *voie inverse*. Compte tenu de ces dénominations, nous pouvons redéfinir la figure 1.2, comme le montre la Figure 1.3.

1.2 Le Banc d'Essai

L'application des algorithmes et des théories développés dans le domaine du contrôle actif du bruit est une étape fondamentale, puisque les modèles sont basés sur des approximations de systèmes décrits par des équations au dérivées partielles et ont un comportement non linéaire. Cette condition inhérente crée un écart entre les résultats théoriques attendus et ceux que nous pouvons rencontrer dans des applications réelles. C'est pourquoi l'une des meilleures approches
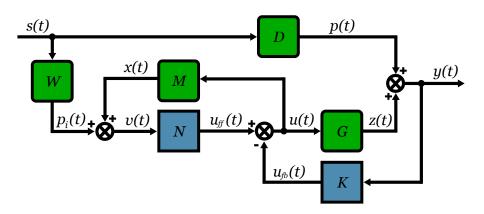
FIGURE 1.3. Schéma de diagramme de bloc du problème de commande combiné de feedback et de feedforward.

consiste à mettre à l'essai la théorie élaborée dans un environnement contrôlé, d'où la nécessité de concevoir un banc d'essai pour nos études.

Différentes approches existent lorsque l'on parle de systèmes et d'environnements de test pour le contrôle actif du bruit, comme dans [Venugopal and Bernstein, 2000, Cocchi et al., 2000, Hu and Lin, 2000, Bordeneuve-Guibé and Nistor, 2002], pour n'en citer que quelques-uns. Compte tenu de tout cela, il a été décidé d'adopter une approche légèrement différente de ce qui a été fait jusqu'à présent. Il a été choisi, comme conception générale, un environnement fermé avec un point initial fermé inhérent pour la source des perturbations agissant dans le système, et une limite ouverte à son extrémité.

Au départ, le système est conçu comme une section de conduit de distribution d'air idéalisé, comme ceux que l'on trouve dans les environnements industriels réels. Donnons, à titre d'exemple, une machinerie ou un équipement donné fonctionnant près d'une conduite de distribution d'air climatisé, qui est suffisamment près de la salle d'un bureau de l'installation pour être entendu. L'isolation passive qu'un mur et ses matériaux assurent est limitée, et les conduits fournissent un mode de transmission non isolé pour ces bruits. A titre d'exemple, nous pouvons voir le travail effectué par [Zeng and de Callafon, 2006].

Plusieurs configurations ont été utilisées au cours de cette thèse. À titre d'exemple, la première configuration est expliquée ici.

Les dimensions des composants et pièces utilisés dans cette première configuration se trouvent dans la Figure 1.4. Nous pouvons voir l'angle de 45° formé par le haut-parleur de contrôle, marqué (2) dans les Figures 3.3 et 1.6, et sa connexion au corps principal du banc de test. L'image de la Figure 1.5 montre le banc d'essai réel. Quatre éléments importants y sont représentés :

(1) *Haut-parleur de perturbation*, utilisé comme source artificielle de bruits. Peut reproduire une variété de perturbations avec des caractéristiques spécifiques. Utilisé pour alimenter le système avec des perturbations qui vont de simples signaux sinusoïdaux à des enregistrements audio dans des environnements réels.

(2) *Haut-parleur du contrôleur*, utilisé comme actionneur pour le signal de contrôle introduit dans le système par les algorithmes de commande. Il est connecté individuellement aux ordinateurs, ce qui signifie qu'il dispose de connecteurs et d'amplificateurs indépendants comme il le serait dans un système réel.

(3) *Microphone des bruits résiduels*, situé à l'extrémité ouverte du système et utilisé pour recueillir et enregistrer les données de mesure de la sortie du système. Les informations acquises par ce microphone sont mesurées en temps réel et utilisées dans des algorithmes feedback ou feedforward.

(4) *Microphone de l'image*, situé le plus près possible de la source de perturbation afin d'obtenir une première impression ou image de la perturbation avant qu'elle ne traverse le système. Ce second capteur ne peut être utilisé que pour les algorithmes avec une configuration en feedforward.
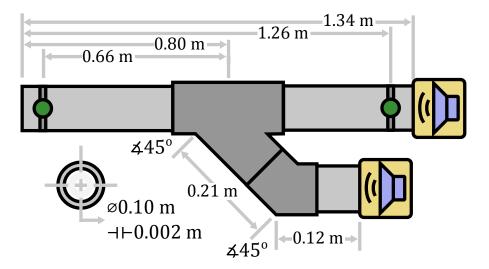
FIGURE 1.4. Première configuration du banc d'essai expérimental.

La Figure 1.6 présente les mêmes éléments dans une représentation plus schématique. Ici, nous pouvons voir inclus à la fois le PC de développement et le PC cible, utilisés pour développer les algorithmes et leur application directe sur le banc d'essai. Plus important encore, nous définissons pour la première fois la nomenclature utilisée tout au long de la thèse pour les différents signaux trouvés dans nos schémas. Tout d'abord nous avons $y(t)$ comme le *Bruit résiduel*, qui est acquis par des mesures du microphone du bruit résiduel et envoyé au PC cible. C'est le signal qu'un contrôleur testé vise à atténuer. Le deuxième en importance est $u(t)$, qui est le signal de contrôle. Il est calculé dans le PC cible et appliqué dans le système via un amplificateur de puissance connecté au haut-parleur du contrôleur. Indépendamment des différents algorithmes de calcul, un signal $s(t)$ est défini comme la *perturbation*. Il est appliqué
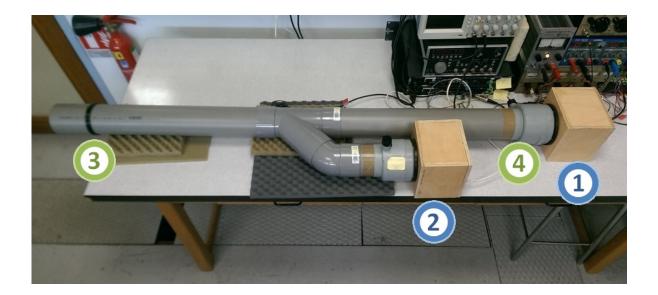
FIGURE 1.5. Photo de la première configuration du banc d'essai.

dans le système par l'intermédiaire d'un deuxième amplificateur indépendant connecté au haut-parleur de la perturbation. Finalement, $v(t)$ est *le signal image de la perturbation*, et n'est utilisé que pour les configurations de type feedforward.

En tant que partie fondamentale de notre approche, nous définissons maintenant les trajectoires internes ou chemins à l'intérieur du système. La voie située entre la source de perturbation située en *(1)* et le point où le bruit résiduel est mesuré, situé en *(3)*, est appelé *Voie Primaire*. Cette voie ainsi appelée est utile pour recréer la dynamique du système dans une simulation. Plus important est le chemin situé entre le haut-parleur du contrôleur en *(2)* et le point où le bruit résiduel est mesuré en *(3)*. Ce chemin qui s'appelle *Voie Secondaire* est crucial dans la conception des contrôleurs.

Puisque nous travaillons dans un environnement à temps discret, étant donné la fréquence de coupure du système, une fréquence d'échantillonnage $f_s = 2500\,\text{Hz}$ a été choisie. Nous pouvons maintenant décrire le système en nous basant sur un contrôleur feedback standard RST.

Dans ce cas, le système peut être décrit plus en détail par le diagramme donné dans la Figure 1.7, où nous avons le modèle des voies primaire et secondaire donné en temps discret tel que,

$$(1.2) \qquad G(q^{-1}) = \frac{q^{-d_G}B_G(q^{-1})}{A_G(q^{-1})}$$

définit la voie secondaire G avec un retard pur donné par d_G, et le contrôleur K est défini comme,

$$(1.3) \qquad K(q^{-1}) = \frac{R(q^{-1})}{S(q^{-1})}.$$
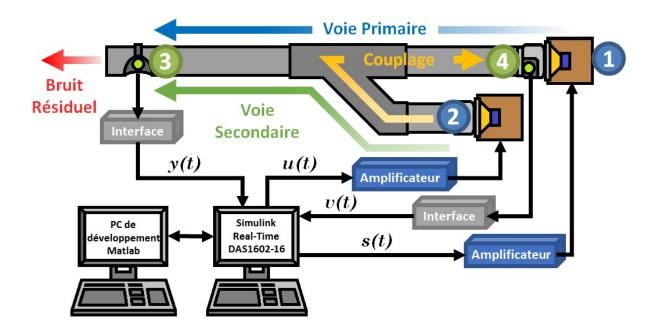
FIGURE 1.6. Schéma de la première configuration du banc d'essai.

Dans le cas des simulations, nous aurons aussi besoin d'avoir le modèle du chemin primaire, défini comme D de la même manière, de telle sorte que,

$$(1.4) \qquad D(q^{-1}) = \frac{q^{-d_D} B_D(q^{-1})}{A_D(q^{-1})}.$$

De cette manière, nous définissons le bruit résiduel comme suit

$$(1.5) \qquad y(t) = G(q^{-1}) \cdot u(t) + p(t),$$

et le signal de commande comme

$$(1.6) \qquad u(t) = -K(q^{-1}) \cdot y(t),$$

avec $p(t)$ comme les perturbations affectant le système (à ne pas confondre avec le signal de perturbation $s(t)$ envoyé par le PC cible).

1.3 Identification du Modèle

Étant donné que nous avons besoin de la connaissance de la voie secondaire à des fins de conception de contrôle, nous avons choisi une méthodologie d'identification de modèle à partir des données expérimentales. L'identification des systèmes est une approche expérimentale pour déterminer le modèle dynamique d'un système. Elle comprend quatre étapes :
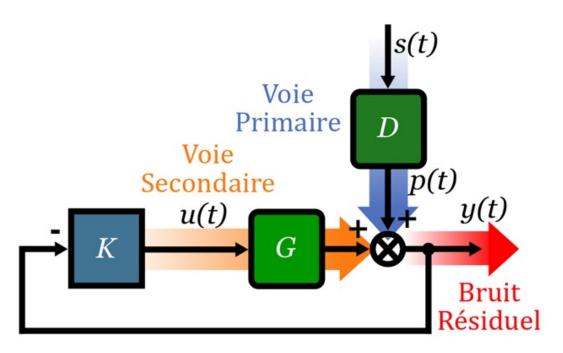
FIGURE 1.7. Schéma de commande Feedback.

1. Acquisition des données d'entrée-sortie dans le cadre d'un protocole expérimental et pré-traitement des données.

2. Estimation de la complexité de la structure du modèle.

3. Estimation des paramètres du modèle.

4. Validation du modèle identifié à la fois pour la complexité du modèle et pour les valeurs des paramètres.

Une opération d'identification complète doit comporter les quatre étapes indiquées ci-dessus. Le signal d'excitation d'entrée typique est une *Séquence binaire pseudo-aléatoire* PRBS, qui est un signal d'excitation persistant permettant une estimation unique des paramètres même pour les systèmes d'ordre supérieur. Le type de modèle à identifier est un modèle paramétrique à temps discret, qui permet de concevoir un algorithme de contrôle facilement implémentable sur un ordinateur. La validation du modèle est le dernier point clé. Il est important de souligner qu'il n'existe pas un seul algorithme qui puisse fournir un bon modèle dans tous les cas (c'est-à-dire qui passe les tests de validation du modèle). L'identification du système doit être considérée comme un processus itératif dont l'objectif est d'obtenir un modèle qui réussit l'essai de validation du modèle et qui peut ensuite être utilisé en toute sécurité pour la conception des contrôleurs. La procédure sera détaillée pour une identification de la voie secondaire de la première configuration du système G. La même méthodologie a également été utilisée pour l'identification de la voie inverse M (voie entre le signal de commande et la mesure de l'image de la perturbation), utilisée

dans l'approche feedforward. Par la suite, les voies primaire et d'image, D et W, ont également été identifiées de la même manière, bien qu'elles n'aient été utilisées que pour des simulations.

1.3.1 Acquisition des Données

Le système doit d'abord être excité avec un signal d'entrée riche en fréquences. Le protocole expérimental doit assurer une excitation persistante pour le nombre de paramètres à estimer. Il existe plusieurs méthodes pour y parvenir, néanmoins il a été montré dans [Ljung, 1999], que pour identifier $2n$ paramètres, le signal d'excitation doit contenir au moins $n+1$ sinusoïdes de fréquences distinctes. Pour aller au-delà de cette contrainte, lors des tests effectués à l'occasion de ce travail, la version en temps discret d'un signal de bruit blanc, appelé *Séquence Binaire Pseudo-Aléatoire*. (PRBS), a été utilisée car elle contient un grand nombre de sinusoïdes dont l'énergie est également répartie sur le domaine fréquentiel. De plus, l'amplitude du signal est constante, ce qui permet une sélection facile par rapport à la contrainte d'amplitude sur l'entrée de l'installation. Les séquences binaires pseudo-aléatoires sont des signaux d'impulsions rectangulaires modulées en largeur qui varient de façon aléatoire, mais qui ont une longueur finie et se répètent périodiquement à long terme, donc pseudo-aléatoires.

L'un des points-clés est la conception d'une PRBS afin de satisfaire un compromis entre la gamme de fréquences à couvrir, en particulier dans la région des basses fréquences, et la durée du test. Il faut appliquer au moins une séquence complète de PRBS, et ses caractéristiques, y compris sa durée, dépendront du nombre de cellules dans les registres utilisés pour sa génération. Les PRBS sont engendrées par des registres à décalage avec feedback. La longueur maximale d'une séquence est $L = 2^N - 1$, où N est le nombre de cellules du registre à décalage. Afin de couvrir tout le spectre de fréquence engendré par une PRBS particulière, la longueur d'un test doit être au moins égale à celle de la séquence.

L'amplitude de la PRBS doit aussi être prise en compte. Bien que la valeur choisie pour cette grandeur puisse être très faible, elle devrait entraîner des variations de sortie plus importantes que le niveau de bruit résiduel. Si le rapport signal/bruit est trop faible, la longueur d'essai doit être augmentée afin d'obtenir une estimation satisfaisante des paramètres. A noter que dans un grand nombre d'applications, l'augmentation significative du niveau de la PRBS peut être indésirable compte tenu du caractère non linéaire des systèmes à identifier, comme dans notre cas, car il s'agit d'identifier un modèle linéaire autour d'un point de fonctionnement.

1.3.2 Estimation de la Complexité

Il est extrêmement important de pouvoir estimer l'ordre du système à partir des données d'entrée/sortie, car il est difficile d'en obtenir une estimation fiable à partir du raisonnement physique. La sortie mesurée de l'installation est en général contaminée par le bruit. Ceci est dû soit à l'effet de perturbations aléatoires agissant en différents points de l'installation, soit à des bruits de mesure, soit à une (des) dynamique(s) du système non modélisée(s). Une façon

courante de décrire ce phénomène est de définir le système comme le *procédé + perturbations* $G + \eta$, donnant comme résultat $y(t) = G(q^{-1})u(t) + \eta(t)$. Si on ajoute ces perturbations aléatoires η, le système peut être représenté par une structure de type Auto-Regressive Moving Average with external input (ARMAX) [Landau et al., 2016, Landau and Zito, 2006].

La Figure 1.8 montre la configuration du processus ARMAX considérée pour l'identification de la voie secondaire, où $u(t)$ est le signal envoyé au haut-parleur du contrôleur, $y(t)$ est le bruit résiduel mesuré en sortie du système, $\delta(t)$ est une source inconnue de perturbations définissant η comme $\eta(t) = O(q^{-1})\delta(t)$.
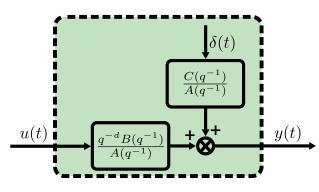
FIGURE 1.8. Diagramme de processus ARMAX.

On peut donc définir la sortie du système perturbé comme suit :

$$(1.7) \qquad y(t) = \frac{q^{-d}B(q^{-1})}{A(q^{-1})}u(t) + \frac{C(q^{-1})}{A(q^{-1})}\delta(t) = G(q^{-1})u(t) + O(q^{-1})\delta(t),$$

dans laquelle le premier terme $G(q^{-1})$ représente l'effet du contrôleur sur le système, et le second terme $O(q^{-1})$ concerne la somme des bruits de mesures.

Les polynômes $A(q^{-1})$ et $C(q^{-1})$ ont la forme

$$(1.8) \qquad A(q^{-1}) = 1 + \sum_{k=1}^{n_A} a_k q^{-k} = 1 + a_1 q^{-1} + a_2 q^{-2} + \cdots + a_{n_A} q^{-n_A},$$

et $B(q^{-1})$ est défini comme suit

$$(1.9) \qquad B(q^{-1}) = \sum_{k=1}^{n_B} b_k q^{-k} = b_1 q^{-1} + b_2 q^{-2} + \cdots + b_{n_B} q^{-n_B},$$

où n_B, n_A, n_C sont les ordres des polynômes A, B, C respectivement. La variable d correspond à un retard pur entrée-sortie dans le système. Ainsi, d, n_B, n_A, n_C sont les valeurs de commande à estimer dans cette étape du processus. Pour simplifier, nous assignons alors arbitrairement l'ordre de $C(q^{-1})$ comme $n_C = n_A$, et définissons l'ordre estimé du système global comme $\hat{n}$, avec $\hat{n} = \max(n_B + d, n_A)$.

1.3.3 Estimation des Paramètres

Les algorithmes utilisés pour l'estimation des paramètres dépendront des hypothèses faites sur les caractéristiques de bruit des mesures $\eta(t)$, qui doivent être confirmées par la validation du modèle. Il est important de souligner qu'il n'existe pas de structure unique qui puisse décrire toutes les situations rencontrées dans la pratique. De plus, il n'y a pas d'algorithmes d'estimation des paramètres utilisables avec toutes les structures *procédé + bruit* possibles menant toujours à des paramètres estimés non biaisés. C'est l'étape de validation qui permettra de décider quel algorithme, et implicitement quel modèle de bruit, doit être utilisé.

Parmi les différents modèles, il a été constaté que le modèle ARMAX donne la meilleure représentation dans ce cas, et entre les méthodes disponibles pour ce modèle, la méthode Output Error with Extended Prediction (OEEPM), appelée *XOLOE* dans certaines publications [Landau et al., 2016], donne les meilleurs résultats en matière de validation pour un modèle donné. Il s'avère que le OEEPM peut être interprété comme une variante des moindres carrés étendus (RELS) [Landau et al., 2016].

L'idée est d'identifier simultanément le modèle $G(q^{-1})$ du système et le modèle de bruit $O(q^{-1})$, afin d'obtenir un *erreur d'adaptation de prédiction* qui soit asymptotiquement un bruit blanc. En exprimant les polynômes en $B(q^{-1}) = q^{-1}B^*(q^{-1})$, le modèle générant les données peut être exprimé en:

$$(1.10) \quad \begin{aligned} y(t+1) &= -A^*(q^{-1})y(t) + B^*(q^{-1})u(t-d) + C^*(q^{-1})\delta(t) + \delta(t+1) \\ &= \theta^T \varphi_0(t) + \delta(t+1) \end{aligned}$$

avec

$$(1.11) \quad \theta^T = [a_1, a_2, \ldots, a_{n_A}, b_1, b_2, \ldots, b_{n_B}, c_1, c_2, \ldots, c_{n_C}],$$

$$(1.12) \quad \varphi_0^T(t) = [-y(t), \ldots, -y(t-n_A+1), u(t-d), \ldots, u(t-d-n_B+1), \delta(t), \ldots, \delta(t-n_C+1)].$$

Supposons que les paramètres sont connus et construisons un prédicteur qui donnera une erreur de prédiction blanche:

$$(1.13) \quad \hat{y}(t+1) = -A^*(q^{-1})y(t)y(t) + B^*(q^{-1})u(t-d) + C^*(q^{-1})\delta(t).$$

De plus, comme le montre [Landau and Zito, 2006], ce prédicteur minimise $E\left\{[y(t+1) - \hat{y}(t+1)]^2\right\}$, et ceci peut être manipulé pour implémenter un algorithme d'estimation (ou d'adaptation) de paramètre récursif (PAA) comme celui utilisé et décrit dans [Landau et al., 2016].

1.3.4 Validation du Modèle

Le protocole d'identification considéré OEEPM appartient à la classe des méthodes basées sur le blanchiment de l'erreur résiduelle, ce qui signifie que le prédicteur identifié ARMAX est optimal

si l'erreur résiduelle $\varepsilon(t) = y(t) - \hat{y}(t) = \delta(t)$ est un bruit blanc. Si l'erreur de prédiction résiduelle $\varepsilon(t)$ est une séquence de bruit blanc, en plus d'obtenir des estimations de paramètres non biaisées, cela signifie également que le modèle identifié donne la meilleure prédiction pour la sortie du système dans le sens où il minimise la variance de $\varepsilon(t)$. D'autre part, puisque l'erreur résiduelle est un bruit blanc, elle n'est corrélée à aucune autre variable, alors toutes les corrélations entre l'entrée et la sortie du système sont représentées par le modèle identifié et ce qui reste non modélisé ne dépend pas de l'entrée $u(t)$.

Avant de mettre en œuvre la méthode de validation, on suppose que I) la structure choisie est correcte et représentative de la réalité, II) une méthode appropriée d'estimation des paramètres pour la structure choisie a été utilisée, et III) les ordres polynomiaux n_A, n_B, n_C et le retard d ont été correctement choisis. Ensuite, l'erreur de prédiction $\varepsilon(t)$ tend asymptotiquement vers un bruit blanc, ce qui implique:

$$\lim_{t \to \infty} E\{\varepsilon(t) - \varepsilon(t-i)\} = 0; \qquad i = 1, 2, \ldots$$

Soit $\varepsilon(t)$ la séquence centrée des erreurs résiduelles de prédiction, ainsi nous avons:

$$(1.14) \qquad R(i) = \frac{1}{N_s} \sum_{t=1}^{N_s} \varepsilon(t) \varepsilon(t-i),$$

$$(1.15) \qquad R_n(i) = \frac{R(i)}{R(0)}, \qquad i = 0, 1, 2, \ldots, n_A, \ldots$$

avec $i_{\max} \geq n_A$, N_s nombre d'échantillons et $R(i)$, $R_n(i)$ les estimations d'autocorrélation et d'autocorrélation normalisée. Dans la situation théorique où l'erreur de prédiction résiduelle $\varepsilon(t)$ séquence est parfaitement blanche et le nombre d'échantillons N_s est grand ($N_s \to \infty$), alors $R_n(i) = 0$ pour tous les i. Cependant, dans la réalité, ce n'est jamais le cas et $R_n(i) \neq 0$ pour $i \geq 1$, puisque $\varepsilon(t)$ contient des erreurs structurelles résiduelles provenant de mauvais ordres polynomiaux, des effets non linéaires, des bruits non gaussiens, ou la valeur pour N_s est trop petite. Une validation pratique largement testée sur des critères d'application est définie par $|R_N(i)| \leq \frac{2.17}{\sqrt{N_s}}$, pour $i \geq 1$.

1.3.5 Modèles Identifiés

Des modèles ont été identifiés à partir d'expériences réalisées dans les différentes configurations du banc d'essai en appliquant la méthodologie d'identification des modèles décrite ci-dessus.

La figure 1.9 montre à titre d'exemple la caractéristique fréquentielle de la voie secondaire estimée pour la première configuration du banc d'essai.
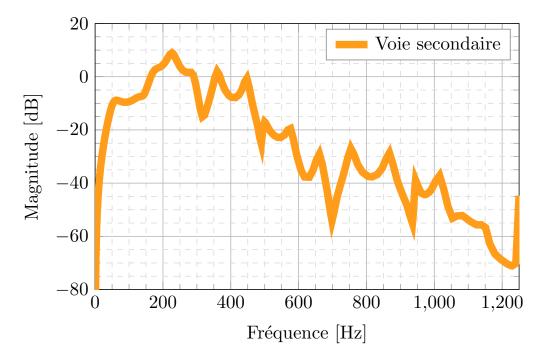
FIGURE 1.9. Caractéristique fréquentielle de la voie secondaire identifiée pour la première configuration du banc d'essai.

1.4 Configuration en Feedback

Le développement d'un contrôleur feedback (de rétroaction) adaptatif a été choisi pour le rejet des perturbations à bande étroite en commençant par un simple contrôleur fixe pour les perturbations tonales, puis en passant par un contrôleur fixe plus robuste en ce qui concerne les caractéristiques de la perturbation, pour finalement obtenir le contrôleur feedback adaptatif auto-réglable avec un paramétrage Youla-Kučera.

De la section précédente nous avons vu que le modèle à temps discret *linéaire et invariant dans le temps* (LTI) de la voie secondaire utilisée pour concevoir le contrôleur sera décrit comme:

$$(1.16) \qquad G(q^{-1}) = \frac{q^{-d_G} B_G(q^{-1})}{A_G(q^{-1})},$$

où les polynômes $A_G(q^{-1})$ et $B_G(q^{-1})$ sont définis comme:

$$(1.17) \qquad A_G(q^{-1}) = 1 + a_1 q^{-1} + \cdots + a_{n_{A_G}} q^{-n_{A_G}},$$

$$(1.18) \qquad B_G(q^{-1}) = b_1 q^{-1} + \cdots + b_{n_{B_G}} q^{-n_{B_G}},$$

avec d_G comme retard pur du système en nombre de périodes d'échantillonnage.

15

1.4.1 Contrôleurs linéaires

Nous avons aussi défini le contrôleur de feedback $K(q^{-1})$ comme $K(q^{-1}) = \frac{R_K(q^{-1})}{S_K(q^{-1})}$, de sorte que

$$(1.19) \qquad K(q^{-1}) = \frac{R_K}{S_K} = \frac{r_1 q^{-1} + \cdots + r_{n_{R_K}} q^{-n_{R_K}}}{1 + s_1 q^{-1} + \cdots + s_{n_{S_K}} q^{-n_{S_K}}}.$$
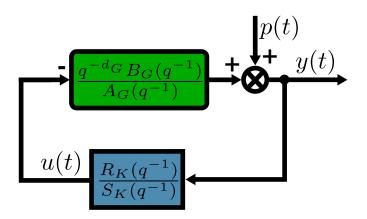
FIGURE 1.10. Schéma de régulation en Feedback.

La figure 1.4.1 montre le schéma de régulation en boucle fermée décrit par ces équations. La sortie du système $y(t)$ et l'entrée $u(t)$ sont décrites par $y(t) = G(q^{-1})u(t) + p(t)$ et $u(t) = -K(q^{-1})y(t)$, qui peuvent être écrites comme :

$$(1.20) \qquad y(t) = \frac{q^{-d_G} B_G(q^{-1})}{A_G(q^{-1})} u(t) + p(t),$$

$$(1.21) \qquad u(t) = -\frac{R_K(q^{-1})}{S_K(q^{-1})} y(t),$$

où $p(t)$ représente l'effet des perturbations sur la sortie mesurée. En développant ces équations, nous obtenons:

$$(1.22) \qquad y(t) = \frac{A_G S_K}{A_G S_K + q^{-d_G} B_G R_K} p(t) = \frac{A_G S_K}{P_{FB}} p(t),$$

avec $P_{FB}(q^{-1})$ comme *polynôme caractéristique* du système en feedback, qui spécifie les pôles en boucle fermée souhaités du système.

La fonction de transfert en boucle fermée entre la perturbation $p(t)$ et la sortie du système $y(t)$, est appelée *fonction de sensibilité de sortie* (S_{yp}) et est donnée par

$$(1.23) \qquad S_{yp} = \frac{y(t)}{p(t)} = \frac{A_G(q^{-1}) S_K(q^{-1})}{P_{FB}(q^{-1})}.$$

De la même manière, la fonction de transfert entre la perturbation $p(t)$ et l'entrée $u(t)$ du système est appelée *fonction de sensibilité d'entrée* (S_{up}) et est donnée par

$$(1.24) \qquad S_{up} = \frac{u(t)}{p(t)} = -\frac{A_G(q^{-1})R_K(q^{-1})}{P_{FB}(q^{-1})}.$$

Quelques contrôleurs linéaires fixes ont d'abord été conçus à l'aide de la technique de placement des pôles et de calibrage des fonctions de sensibilité. Premièrement, afin d'atténuer fortement les perturbations tonales, le principe du modèle interne (IMP) a été utilisé [Landau et al., 2016, Francis and Wonham, 1976]. En bref, le IMP indique que pour rejeter complètement une perturbation asymptotiquement (c'est-à-dire en état stationnaire), le contrôleur doit inclure le *modèle de la perturbation*.

Comme la fréquence des perturbations tonales peut varier ou n'est pas parfaitement connue dans un système ANC, un contrôleur robuste fixe a également été conçu pour prendre en compte les caractéristiques possibles de la perturbation. Pour réaliser cette fonction, des filtres à réjection de bande (band-stop filters) (BSF) ont été utilisés. La théorie de la conception des contrôleurs linéaires feedback est le sujet principal de l'annexe E [Meléndez et al., 2017].

1.4.2 Contrôleur adaptatif

L'approche adaptative utilise le paramétrage Youla-Kučera du contrôleur, combiné avec le principe du modèle interne. La référence de base pour cette approche utilisée dans le contrôle actif des vibrations est [Landau et al., 2016]. La théorie du contrôleur FIR adaptatif en feedback est le sujet principal de l'annexe A. [Landau et al., 2019c].

Pour adapter directement les paramètres du contrôleur, le paramétrage Youla-Kučera (YK) du contrôleur est utilisé. Dans ce contexte, on considère un filtre de réponse impulsionnelle finie (FIR) de la forme:

$$(1.25) \qquad Q(z^{-1}) = q_0 + q_1 z^{-1} + \cdots + q_{n_Q} z^{-n_Q},$$

à laquelle est associé le vecteur paramètres $\theta = [q_0 \ q_1 \ldots q_{n_Q}]^T$.

Sous le paramétrage Youla-Kučera, les polynômes équivalents $R_K(z^{-1})$ et $S_K(z^{-1})$ du contrôleur $K(q^{-1})$ prennent la forme:

$$(1.26) \qquad R_K(q^{-1}) = R_0 + A_G Q H_{S_0} H_{R_0}$$

$$(1.27) \qquad S_K(q^{-1}) = S_0 - q^{-d_G} B_G Q H_{S_0} H_{R_0},$$

où A_G, B_G et d_G correspondent au modèle identifié de la voie secondaire, $R_0(z^{-1})$, $S_0(z^{-1})$ sont les polynômes du contrôleur central, et H_{S_0}, H_{R_0} sont les éléments fixes du contrôleur. Il est remarquable de constater que sous le paramétrage YK utilisant une structure FIR pour le filtre $Q(z^{-1})$, les pôles en boucle fermée définis par le contrôleur central restent inchangés, de sorte

que:

$$
\begin{aligned}
P_{FB}(q^{-1}) &= A_G S_K + q^{-d_G} B_G R_K, \\
&= A_G[S_0 - q^{-d_G} B_G Q H_{S_0} H_{R_0}] + q^{-d_G} B_G[R_0 + A_G Q H_{S_0} H_{R_0}], \\
&= A_G S_0 + q^{-d_G} B_G R_0.
\end{aligned}
$$
(1.28)

L'objectif est d'estimer une valeur pour Q de sorte que $y(t)$ soit ramené à zéro.

Le schéma adaptatif est représenté dans la Figure 1.11, où PAA signifie *Algorithme d'adaptation paramétrique*.
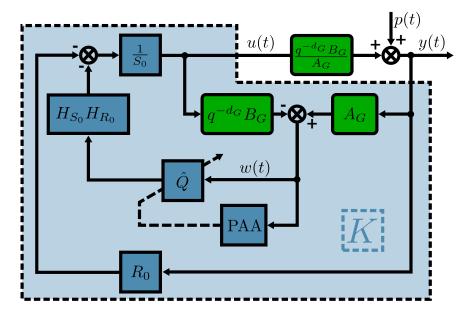
FIGURE 1.11. Schéma de paramétrage adaptatif Youla-Kučera.

L'observateur de la perturbation $w(t)$ est défini par

$$
w(t) = A_G(q^{-1})y(t) - q^{-d_G}B_G(q^{-1})u(t) = A_G(q^{-1})p(t).
$$
(1.29)

L'estimation du polynôme Q au temps t est donnée par:

$$
\hat{Q}(t, q^{-1}) = \hat{q}_0(t) + \hat{q}_1(t)q^{-1} + \cdots + \hat{q}_{n_Q}(t)q^{-n_Q},
$$
(1.30)

et est caractérisé par le vecteur de paramètres

$$
\hat{\theta}^T(t) = [\hat{q}_0(t)\ \hat{q}_1(t)\ldots\hat{q}_{n_Q}(t)].
$$
(1.31)

L'ordre n_Q du polynôme $\hat{Q}$ est lié à l'ordre du dénominateur du modèle de perturbation.

Ce type de configuration permet de développer un algorithme d'adaptation de la forme:

$$
\hat{\theta}(t+1) = \hat{\theta}(t) + F(t)\varphi(t)\varepsilon(t+1),
$$
(1.32)

où le vecteur $\varphi(t)$ est une fonction de l'observation $w(t)$ de la perturbation, de telle sorte que $\varphi(t) = f\{w(t), w(t-1), ...\}$, et

$$(1.33) \qquad \varepsilon(t+1) = \frac{\dfrac{S_0(q^{-1})}{P_{FB}(q^{-1})}w(t+1) - \hat{\theta}^T(t)\varphi(t)}{1 + \varphi^T(t)F(t)\varphi(t)},$$

et où la matrice de gain d'adaptation est définie comme:

$$(1.34) \qquad F(t+1) = \frac{1}{\lambda_1(t)}\left[F(t) - \frac{F(t)\varphi(t)\varphi^T(t)F(t)}{\dfrac{\lambda_1(t)}{\lambda_2(t)} + \varphi^T(t)F(t)\varphi(t)}\right],$$

avec $0 < \lambda_1(t) \le 1$, $0 \le \lambda_2(t) < 2$, $F(0) > 0$; où λ_1 et λ_2 permettent d'obtenir différents profils pour l'évolution du gain d'adaptation $F(t)$. Finalement, le contrôle à appliquer est donné par:

$$(1.35) \qquad u(t+1) = \frac{-1}{S_0}\left[R_0 y(t+1) + H_{R_0} H_{S_0} \hat{Q}(t+1)w(t+1)\right].$$

1.4.3 Résultats Expérimentaux

De nombreux essais expérimentaux ont été effectués pour prouver l'efficacité des controlleurs conçus pour le banc d'essai. L'un de ces essais a été appelé *essai d'interférence*. Il est divisé en trois parties principales. Le phénomène d'interférence apparait quand 2 perturbations sinusoïdales de fréquences très proches sont appliquées sur un système. Comme on peut le voir sur la Figure 1.12, la première partie correspond à un fonctionnement en boucle ouverte (perturbation dans le système sans atténuation du contrôleur); dans la seconde partie, la boucle est fermée et le contrôleur commence à atténuer le bruit, et la troisième partie montre le bruit résiduel après modification des caractéristiques fréquentielles des perturbations.

Il est clair que le niveau d'atténuation est proche d'un rejet complet de la perturbation, même dans le cas d'un éventuel changement des caractéristiques de la perturbation.

Un autre test a été désigné sous le nom de *changements en échelon des fréquences*, où la perturbation est définie par deux ondes sinusoïdales tonales dont les changements des caractéristiques fréquentielles sont décrits comme suit:

1. Référence pour le bruit ambiant, ni perturbations ni contrôle

2. Fréquences nominales, 170Hz + 285Hz

3. Perturbations -10Hz ,160Hz + 275Hz

4. Fréquences nominales, 170Hz + 285Hz

5. Perturbations +10Hz, 180Hz + 295Hz

6. Fréquences nominales, 170Hz + 285Hz

19
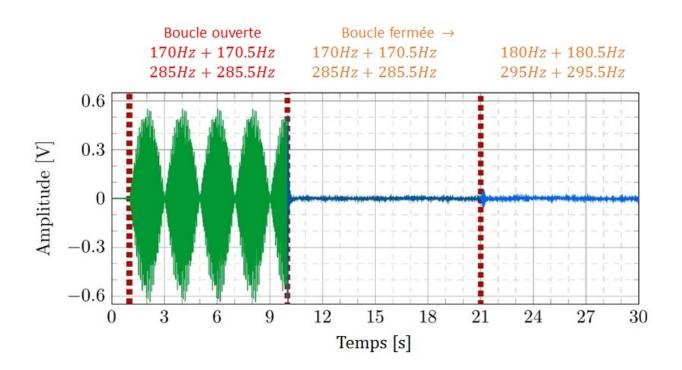
FIGURE 1.12. Atténuation des interférences acoustiques par un contrôleur adaptatif en feedback avec paramétrage YK.

La Figure 1.13 montre l'évolution dans le temps du bruit résiduel dans deux configurations. La première correspond au comportement du système en boucle ouverte (pas d'action du régulateur), tandis que la seconde affiche une excellente atténuation du bruit par le régulateur en boucle fermée, même en présence de changements brusques (échelons) dans les caractéristiques de la perturbation.

1.5   Configuration en Feedforward

La commande adaptative par feedforward pour la compensation des perturbations à large bande, est largement utilisée lorsqu'un signal corrélé avec la perturbation (image de la perturbation) est disponible [Kuo and Morgan, 1999, Elliott and Sutton, 1996, Elliott and Nelson, 1994]. Cependant, dans de nombreux systèmes, il existe un couplage physique positif entre le système de compensation à effet de feedforward et la mesure de l'image de la perturbation, ce qui entraîne souvent un état d'instabilité du système. En présence de ce couplage positif inhérent, le compensateur adaptatif de feedforward doit contrecarrer et minimiser les effets de la perturbation tout en assurant simultanément la stabilité de la boucle de couplage positive interne [Jacobson et al., 2001, Kuo and Morgan, 1996].

20
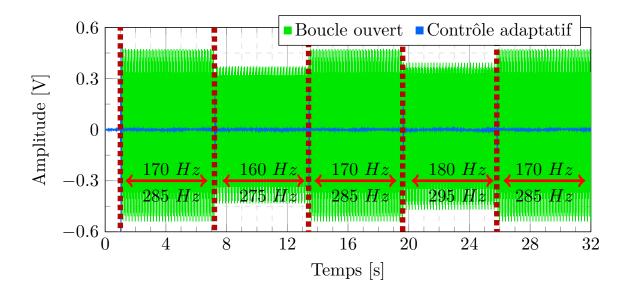
FIGURE 1.13. Changements en échelon des fréquences en utilisant le contrôleur adaptatif avec paramétrage YK.

1.5.1 Schéma de Commande Feedforward

En débutant par [Amara et al., 1999b] le contrôle adaptatif du bruit en feedback s'est révélé être une solution efficace pour atténuer les perturbations tonales simples ou multiples [Amara et al., 1999a], en profitant du modèle interne et du paramétrage Youla-Kučera du contrôleur du feedback [Landau et al., 2019c, Meléndez et al., 2017]. Néanmoins, l'utilisation efficace de cette approche dite de feedback pour l'atténuation du bruit à large bande est limitée par l'intégrale de Bode. Pour tenir compte des caractéristiques inconnues et variables des perturbations bande large, une approche adaptative est nécessaire. On peut donc dire que la compensation adaptative du bruit par feedforward est particulièrement dédiée à l'atténuation du bruit à large bande avec des caractéristiques inconnues et variables dans le temps.

Dans la Figure 1.14 on peut voir le diagramme général d'un schéma de commande en feedforward, où D représente la fonction de transfert de la voie primaire et G la voie secondaire de notre système. Dans cette configuration, le bloc N est utilisé pour le contrôleur feedforward. De plus, W caractérise la fonction de transfert entre le haut-parleur de la perturbation et le microphone de l'image, et la fonction de transfert M décrit le couplage feedback positif appelé *Voie Reverse*. En plus des signaux existants dans un diagramme feedback, nous trouvons les mesures $v(t)$ utilisées pour obtenir le signal corrélé avec l'image de la perturbation $i(t)$ qui est par nature biaisée par la boucle interne positive créée par le signal de contrôle.

Ce phénomène est désigné comme une *boucle de feedback interne positive* ; c'est un phénomène indésirable qui peut causer des instabilités dans ces systèmes et il doit être pris en compte lors de la conception du contrôleur. Le couplage de la sortie du compensateur de feedforward avec la
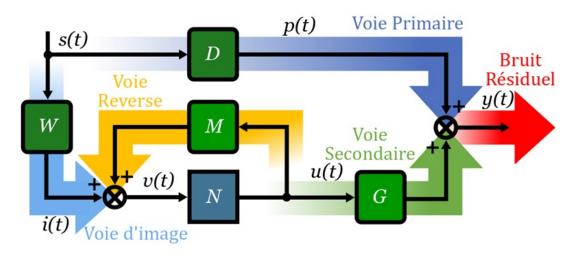
FIGURE 1.14. Schéma de commande Feedforward.

mesure $v(t)$ à travers est représenté par M.

Comme pour la voie secondaire, le couplage feedback positif est caractérisé par la fonction de transfert asymptotiquement stable:

$$(1.36) \qquad M(q^{-1}) = \frac{q^{-d_M} B_M(q^{-1})}{A_M(q^{-1})},$$

L'objectif est d'estimer et d'adapter les paramètres du compensateur feedforward en N, de sorte que le bruit résiduel mesuré soit minimisé au sens d'un certain critère. Le filtre feedforward optimal inconnu IIR est défini par:

$$(1.37) \qquad N(q^{-1}) = \frac{R_N(q^{-1})}{S_N(q^{-1})}.$$

1.5.2 Algorithmes Feedforward Adaptatifs

En accord avec la Figure 1.15, le compensateur estimé est indiqué par $\hat{N}(q^{-1})$. Il est défini comme $\hat{N}(t, q^{-1})$ lors de l'estimation (adaptation) de ses paramètres. Les compensateurs FIR sont obtenus en prenant $S_N = 1$.

L'entrée du compensateur de feedforward est notée $v(t)$, et elle correspond à la somme entre l'image perturbatrice en l'absence de compensation, et la sortie du chemin de feedback positif.

Comme nous l'avons vu précédemment, une formulation générale de l'algorithme d'adaptation des paramètres (PAA) peut être décrite par:
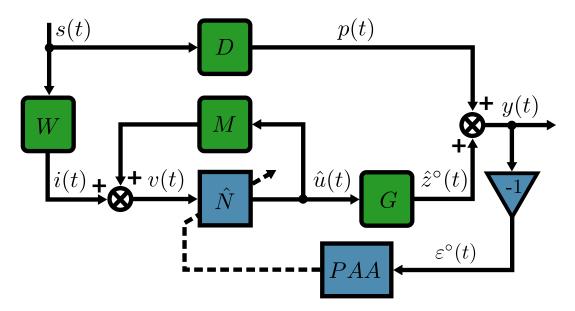
FIGURE 1.15. Schéma de commande Feedforward avec PAA.

$$\hat{\theta}(t+1) = \hat{\theta}(t) + F(t)\varphi(t)\varepsilon(t+1), \tag{1.38}$$

$$\varepsilon(t+1) = \frac{\varepsilon^\circ(t+1)}{1 + \varphi^T(t)F(t)\varphi(t)}, \tag{1.39}$$

$$F(t+1) = \frac{1}{\lambda_1(t)}\left[F(t) - \frac{F(t)\varphi(t)\varphi^T(t)F(t)}{\frac{\lambda_1(t)}{\lambda_2(t)} + \varphi^T(t)F(t)\varphi(t)}\right], \tag{1.40}$$

$$1 \geq \lambda_1(t) > 0, \quad 0 \leq \lambda_2(t) < 2, \quad F(0) > 0, \tag{1.41}$$

$$\varphi(t) = L\varphi_0(t) \tag{1.42}$$

où $\hat{\theta}(t)$ est un vecteur qui consiste en les paramètres estimés du contrôleur N au temps t, $\varphi(t)$ est un vecteur contenant les informations des mesures $v(t+1), v(t), \dots$ et $\hat{u}(t), \hat{u}(t), \hat{u}(t-1), \dots$ disponibles au temps t, L est un filtre défini par les paramètres système, et $\varepsilon^\circ(t)$ est l'erreur d'adaptation *a priori*.

En considérant la matrice de gain d'adaptation $F(t) = \gamma I$, où I est la matrice identité, on obtient un gain d'adaptation scalaire. De plus, le filtre L peut être défini de plusieurs façons. Il en résulte plusieurs configurations possibles pour le calcul du régulateur feedforward, qui ont été testées et comparées avec une approche couramment utilisée dans la littérature.

1.5.3 Paramétrage Youla-Kučera: Commande Feedforward

Afin d'isoler les problèmes liés à la stabilité de la boucle de feedback interne positif de l'objectif du contrôleur qui est la minimisation du bruit résiduel, un paramétrage Youla-Kučera (YK) a été utilisé. Au lieu d'un compensateur de feedforward standard IIR, une version similaire utilisant

un paramétrage Youla-Kučera du compensateur de feedforward adaptatif a été installée.

De cette façon, un contrôleur central assurera la stabilité de la boucle de feedback positif interne, tandis que ses performances sont améliorées en temps réel par l'adaptation directe des paramètres du filtre Youla-Kučera $Q(q^{-1})$. En prenant maintenant en compte un paramétrage YK, le schéma illustré à la Figure 1.16 présente le schéma fonctionnel du compensateur adaptatif avec un filtre Youla-Kučera $\hat{Q}(q^{-1})$ et un PAA. Les détails des algorithmes spécifiques peuvent être trouvés dans [Landau et al., 2013, Landau et al., 2012].
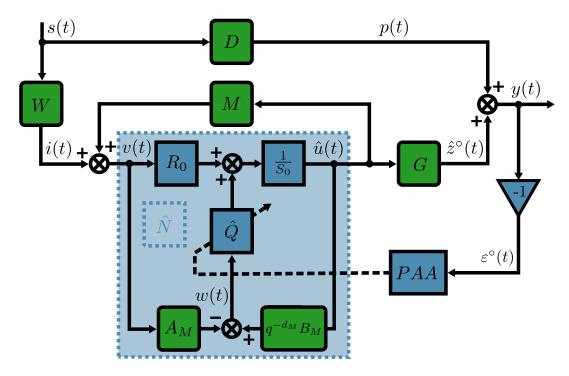
FIGURE 1.16. Schéma de commande Feedforward utilisant un paramétrage Youla-Kučera avec PAA.

En utilisant le paramétrage de Youla-Kučera, le compensateur IIR feedforward qui minimisera le bruit résiduel peut être appelé *Réponse Impulsionnelle Infinie Youla-Kučera* (YK-IIR), et il est décrit par:

$$(1.43) \qquad \hat{N}(q^{-1}) = \frac{R_N(q^{-1})}{S_N(q^{-1})} = \frac{R_0 A_Q - A_M B_Q}{S_0 A_Q - q^{-d_M} B_M B_Q},$$

où le filtre Youla-Kučera estimé $\hat{Q}(q^{-1})$ a une structure IIR, telle que

$$(1.44) \qquad \hat{Q}(q^{-1}) = \frac{\hat{B}_Q(q^{-1})}{\hat{A}_Q(q^{-1})} = \frac{\hat{b}_0^Q + \hat{b}_1^Q q^{-1} + \ldots + \hat{b}_{n_{B_Q}}^Q q^{-n_{B_Q}}}{1 + \hat{a}_1^Q q^{-1} + \ldots + \hat{a}_{n_{A_Q}}^Q q^{-n_{A_Q}}},$$

et ses paramètres sont donnés par:

$$(1.45) \qquad \hat{\theta}^T(t) = [\hat{b}_0^Q(t), \dots, \hat{b}_{n_{B_Q}}^Q(t), \hat{a}_1^Q(t), \dots, \hat{a}_{n_{A_Q}}^Q(t)].$$

Comme précédemment, l'algorithme d'adaptation des paramètres décrit dans Section 1.5.2 est à nouveau utilisé pour les compensateurs adaptatifs feedforward type Youla-Kučera, où il y a encore plusieurs choix pour le filtre L qui peuvent être considérés.

Il est également possible d'utiliser un gain d'adaptation scalaire. En prenant $A_Q(q^{-1}) = 1$, nous obtenons une configuration FIR Youla-Kučera (YK-FIR). Plusieurs options pour le filtre L et le gain d'adaptation sont possibles aussi dans la configuration YK-FIR.

1.5.4 Résultats Expérimentaux

Plusieurs séries de longs tests ont été effectuées pour comparer les différentes options proposées pour les algorithmes adaptatifs dans le cas de la compensation feedforward des bruits bande large. A titre d'exemple, la figure 1.17 montre l'évolution dans le temps du bruit résiduel mesuré pour un compensateur feedforward de type IIR. La première partie du test correspond à une opération en boucle ouverte sans compensateur. Ici, nous pouvons également voir l'évolution de l'atténuation globale dans le temps.
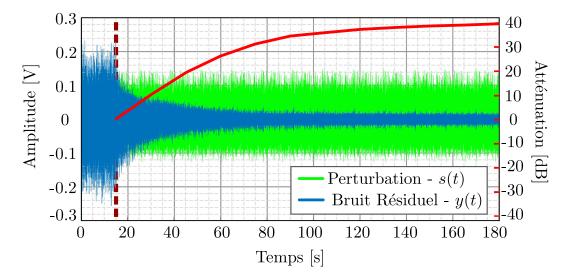
FIGURE 1.17. Performance du compensateur IIR. Le côté droit montre le niveau d'atténuation atteint à un moment donné.

En raison des caractéristiques plus complexes des perturbations, la vitesse de convergence est réduite par rapport à celle d'un régulateur en feedback, mais cela est tout à fait compréhensible et constitue un comportement attendu. Même en présence de bruits à large bande, le contrôleur feedforward atteint des niveaux élevés de rejet des perturbations.

INTRODUCTION

This introductory chapter describes the basic problems of adaptive Active Noise Control (ANC) and how this was related to the studies in Active Vibration control (AVC). This has motivated the research and gives an overview of the main results in the literature. To conclude, in the last two sections of this chapter, the original contributions of this work are summarized, and an outline of the dissertation is given.

2.1 Motivation

Without going into advanced theory or looking deeply into details, the basic principles of Active Noise Control (ANC) will be exposed and explained in this section. Some basic examples will be given to state the control problem which will be associated with our research. All this is intended to be presented as part of the context in our work.

One of the very first mentions about ANC was done by Henri Coandă in the documents of a French patent in 1930 [Coanda, 1930]. A couple of years later Paul Lueg did something similar in his work and mentioned it once again in [Lueg, 1934], yet another patent. Some time later the term appeared in a publication by Harry F. Olson [Olson and May, 1953], this time in a journal's article. In brief, the problem to solve in their work is that of mute and suppress an incoming noise of a given source, by using of a microphone for measurements, and the set of an amplifier and a loudspeaker to act as an actuator. It was found that under those given conditions, if the proposed systems were able to create sound waves with frequency characteristics similar to those of the noise, but with a shift in phase of 180°, then it was feasible to cancel noises in the action region of the sound waves produced by the loudspeaker. As an example, one of the proposed uses of this theory is to apply the ANC system near an operator of heavy machinery and airplanes engines to reduce the noise created by them.

In this field of research, three main different approaches of control methods are considered for counteracting the noise, as mentioned in [Snyder, 2000]: those with passive behavior, those with something we can call semi-active performance and finally those with a full active action. The passive approach, which is the most common one, since it consist mainly in the use of material and geometries with specific characteristics in order to isolate and damp the effects of noises, where no control algorithms are involved. The advantages of this technique is the simplicity of application into the systems, with an inherent robustness in terms of control, and a great cost-benefit ratio in most of the cases. As expected, the downside of using such an approach difficulties found when attenuating very low frequencies, its lack of flexibility in terms of control, as well as the absence of adaptation to the environment's changing characteristics and a dependency to the system's physical and natural dynamics. The most simple example of the passive noise control can be seen in the isolation with high density foam used in pipes and buildings walls. A more complex, but still an example of this concept is the Helmholtz resonator, which is described in [Olson and May, 1953, Fleming et al., 2007].

The second approach is denominated as semi-active, since it does not proportionate any additional energy to the system itself, but it uses information acquired from it to modify the passive actuators characteristics. This conceptualization requires more parts involved in its functioning, like a sensor or transducer to gather some given information from the system. This has the advantages of being more flexible to changes in the system's dynamics, nevertheless the implementation complexity and cost increase substantially. Following the previous approach example, there are designs of Helmholtz resonators with capacity to change the resonant chamber's dimensions and thus, to adapt between a determined range of operation its natural frequency, as shown by [de Bedout et al., 1997] and [Matsuhisa et al., 1992].

Finally our main interest resides in the third and last approach in which the integrity of this work is included, correspondingly called active control. This implementation has a distinguishable difference regarding the late two options, that refers to the fact that these actuators supply an additional and external source of energy to the system itself in the form of mechanical power, which targets its behavior to fulfill specific variable objectives. Speaking more specifically about Active Noise Control (ANC), the frequency domain of interest covers the average human audible spectrum of frequencies, roughly between 20 Hz and 20 000 Hz. Due to physical conditioning and inherent characteristics of passive approaches, their frequency range of operation is constrained to high frequencies, as stated in [Olson and May, 1953, Fuller and von Flotow, 1995, Elliott, 2001], where attenuations of 40 dB were achieved in frequencies above 500 Hz. This opens a window of opportunities for the ANC, to act at the low frequency domain, where no other approach can perform.

Amongst the many examples and uses of these theories, one of the most common examples found in real life applications is that of the headphones with environment noise reduction capabilities for a better audio quality and sound experience. This is done by measuring the

environmental noise with an embedded microphone and the use of this acquired information through control algorithm and the internal speaker as an actuator. Figure 2.1 details a reference to this system. In the ideal case, the added signal should be of equal magnitude and of 180° phase shift (negative) so as to completely cancel the disturbing noise. Further background analysis can be found in the articles and documents of [Elliott and Nelson, 1993, Fuller and von Flotow, 1995, Guicking, 2007].
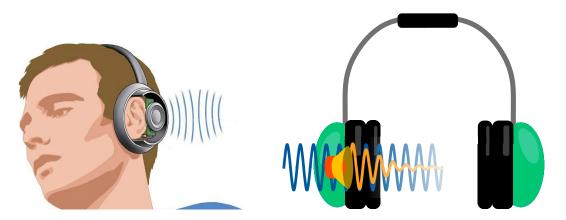
FIGURE 2.1. External noise attenuation in headphones by use of Active Noise Control.

2.2 Problem Description

This section describes some generalities of the Active Noise Control problems treated throughout this thesis. The main objective is to reduce the effects of a given perturbation in the system, corresponding in this case to the effects produced by acoustic noise, at the specified location of interest inside the system. A general overview and a description are given for the so called system, as well as the control approaches used which are given in the following subsections.

2.2.1 Active Vibration Control

The base of this work were settled first in the studies done by Aurelian Constantinescu in [Constantinescu, 2001], where the case of Active Vibration Control was exposed. Subsequently works done by Alma, Airimiţoaie [Alma, 2011, Airimiţoaie, 2012] and more recently Castellanos [Silva, 2014] were also developed in the field of vibration control, but there are similarities between mechanical vibrations and acoustics, since they are both physical phenomena that can be described by mechanical waves, just acting in different environments. Each of these works had at its disposal test benches fitted to emulate diverse mechanical vibrational systems. Under the conditions established for these projects, theories were developed and put to trial in the test benches.

An example, there are studies done in [Constantinescu and Landau, 2003] where an active suspension system test bench is used for the application of theories in which this thesis settle its basis. In [Alma et al., 2012] and [Landau et al., 2011a], we can find the follow up applications done by Alma of these theories on a different test bench. A close relationship between the work described in this thesis is still hold among the studies previously done, as well as the current works made at this point by Airimiţoaie, a seen in [Airimiţoaie et al., 2011, Airimitoaie and Landau, 2016].

It is remarkable to state that there exists a wide field of study around AVC, and there are many different approaches, nevertheless one of the main objectives of this thesis is to keep track of those specific studies and follow up the work done there. Once the similarities and bases are stated, the aim is then to focus the sum of efforts done in the ANC field.

2.2.2 Control System Configuration

Figure 2.2 represents an Active Noise Control system, as well as an Active Vibration Control, as we will see in the next subsection, which contemplates the use of both feedback and feedforward compensators. This system can be described as a two input, two output system. The first input corresponds to the perturbation or *Disturbance* $s(t)$, with unknown characteristics and generated by an as well unidentified source. The second input can be denominated as the *Control Signal* $u(t)$, being the sum of individual output control signals from the feedback regulator K, and the feedforward compensator N, $u_{fb}(t)$ and $u_{ff}(t)$ correspondingly. The outputs of this system will be those obtained from the measurements, as the first output corresponds to the system's *Residual Noise* $y(t)$, and the second output corresponds to the *Disturbance's Image* $v(t)$, in our case both gathered through microphones. As shown in Figure 2.2, the path that transmits the perturbation $s(t)$ to the residual noise $y(t)$ is defined as *Primary path*. Similarly, the *Secondary path* is defined as the path that transmits the control signal $u(t)$ to the residual noise $y(t)$. As such, the residual noise is defined as the sum of the primary path's output, the perturbation $p(t)$; and of the secondary path's output, denoted as $z(t)$.

Inherently in Active Noise Control and Active Vibration Control systems, a side effect called internal positive coupling is present due to the control signal $u(t)$. The fact that control signal $u(t)$ effects are omnidirectionally distributed through the system indicates that this will have an effect as well in the measurements $v(t)$, intended to gather an information correlated with the disturbance. This phenomenon represents a coupling between the control signal $u(t)$ and the measurements $v(t)$, where this path is defined as an internal positive feedback, or more commonly *Reverse path*. This is a crucial part in the development of feedforward control theory, since its effects can destabilize the system if not properly taken into account. Finally the path formed between the perturbation $s(t)$ and the measurements at $v(t)$ is described by the *Image path*. Thus, we can state that the measurements $v(t)$ are formed by the sum of the reverse path's output, defined as $x(t)$ and of the image path's output, defined as the *disturbance image* $p_i(t)$.

Accordingly with the control theory terminology, we will define the system's output $y(t)$ as the performance variable, usually denotated as $e(t)$. In this context we define our objective as that of minimizing the resulting signal $e(t)$, by compensating with the control signal $u(t)$, calculated by using the measurements $y(t)$ and $v(t)$.
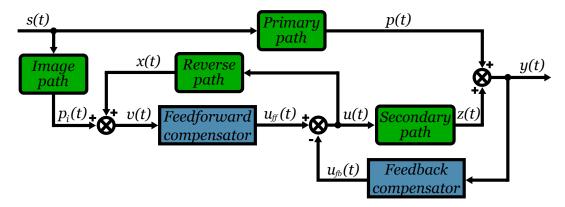
FIGURE 2.2. Block diagram representation of the combined feedback and feedforward control problem. In green we can identify the blocks corresponding to the system's plant, meanwhile in blue the corresponding *feedback K* and *feedforward N* compensators.

System's measurements can be displayed in a vectorial disposition, such that $Y(t) = [v(t), y(t)]^T$. In the same way using the previously stated definition of feedback regulator K, and feedforward compensator N, we can display them in a vectorial disposition such that $\kappa = [N, -K]^T$. Thus, we can define control signal as:

$$(2.1) \qquad u(t) = u_{ff} - u_{fb} = N \cdot v(t) - K \cdot y(t) = \kappa^T \cdot Y(t).$$

The feedforward controller denomination attributed to N is motivated by the fact that $v(t)$, also called *Correlated disturbance's image*, is measured upstream of the performance variable. This assumes also that it is physically possible to obtain such a measurement. The situations where this is not possible constitute feedback control problems, while the others are more generally addressed in the literature as hybrid control.

A standard feedback representation in the form of a 2 input - 2 output system can also be considered as shown in Figure 2.3. This representation is very well known in robust and optimal control, and similar representation can be found in [Tay et al., 1997, Zhou et al., 1996]. The equations associated with the feedback system representation are:

$$(2.2) \qquad Y(t) = \begin{bmatrix} y(t) \\ v(t) \end{bmatrix} = \begin{bmatrix} P_{11} & P_{12} \\ P_{21} & P_{22} \end{bmatrix} \begin{bmatrix} s(t) \\ u(t) \end{bmatrix} = \begin{bmatrix} D & G \\ W & M \end{bmatrix} \begin{bmatrix} s(t) \\ u(t) \end{bmatrix},$$

where the system, or *plant* parameters are defined, and D corresponds to the *Primary path*, G is designed as the *Secondary path*, W represents the *Image path* and M symbolizes the *Reverse*
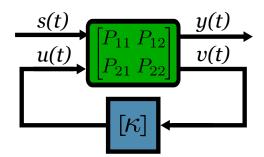
FIGURE 2.3. General representation of a 2 input - 2 output Active Noise Control / Active Vibration Control system.

path. Given these denominations, we can redefine the Figure 2.2, as displayed in the following Figure 2.4.
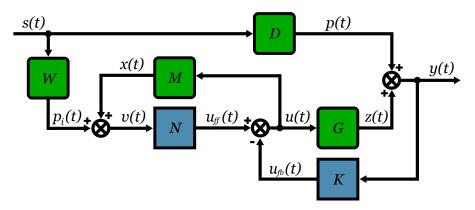
FIGURE 2.4. Block scheme of the combined feedback and feedforward control problem.

Equation (2.2), alongside with Equation (2.1), gives the overall representation of the ANC system and the corresponding control law. From here two specific cases for this problem will be addressed.

2.2.3 Feedback Control Problem

The feedback regulation is the first case. For this, it is common to provide a solution for reducing narrow band perturbation, talking about their frequency domain. In general, the disturbances will be supposed to represent vibrations coming from multiple narrow band disturbances sources. It should be observed that in this context there is no feedforward compensator and $N = 0$. As such, the previous general scheme can be reduced as in Figure 2.5.

Consequently we will have the residual noise measurement $y(t) = Y(t)$, and the control signal $u(t) = u_{fb}(t)$. For this configuration we will define the *performance variable* as the measured system's output, such that $e(t) = y(t)$. A schematic representation of this simplified situation is given in Figure 2.6.
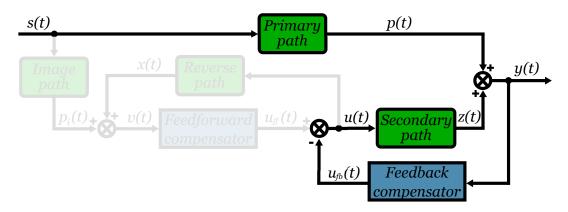
FIGURE 2.5. Reduced block diagram representation for a feedback control problem.
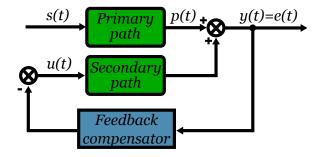
FIGURE 2.6. Feedback control problem scheme.

This came from the fact that there are situations where a second transducer to measure an image correlated with the disturbance cannot be used because the physical characteristics of the process prevent it, thus feedback control techniques have to be applied. The Bode integral limitations permit only narrow band disturbances to be reduced or rejected. Therefore, in this part of the dissertation, objectives will be those of developing techniques for the compensation of multiple stationary or variable sinusoidal disturbances.

2.2.4 Feedforward Control Problem

The feedforward noise compensation is the second case for this problem. A schematic representation of this situation is given in Figure 2.7. For this case, it can be observed that there is no feedback regulator, thus $K = 0$.

Therefore, in this situation we obtain $v(t) = Y(t)$ and $u(t) = u_{ff}(t)$. As mentioned earlier, it is supposed that a transducer can be used that provides a correlated image of the disturbance upstream of the performance variable $e(t) = y(t)$, therefore allowing a feedforward regulation approach to be implemented. Again a schematic representation of this simplified situation is given in Figure 2.8.

This method is used in practical situations where large or wide band perturbations need to be
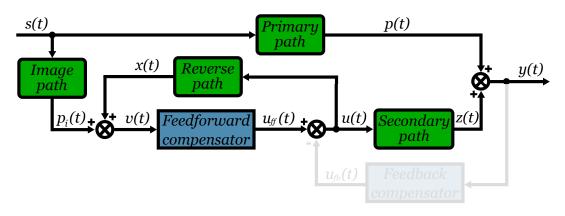
FIGURE 2.7. Reduced block diagram representation for a feedforward control problem.
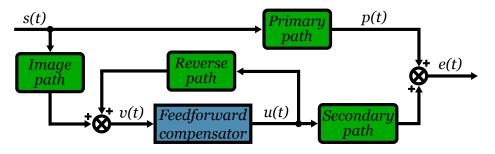
FIGURE 2.8. Feedforward control problem schema.

reduced. In these cases, a pure feedback approach would be hindered by the limitations imposed through the Bode integral [Hong and Bernstein, 1998] and only narrow band disturbances could be compensated (as it will be shown in the next section).

To deal with large band disturbances, the scheme in Figure 2.8 can be used. It can be immediately observed from this representation that the measured correlated image of the disturbance $v(t)$ will not only contain the significant information from the disturbance source but it will also be contaminated by the control signal transmitted through the positive coupling path, or *Reverse path*. The presence of this intrinsic positive feedback complicates the controller design because it can cause instability.

In many of the research studies that begun to propose solutions for this problem, the influence attributed to the positive feedback coupling was not taken into account [Widrow et al., 1975], because it was either considered that its influence could be compensated or that it was too weak to raise any problems. Several techniques have been reported in the literature for compensating the positive feedback coupling's effect, some being of mechanical nature and other being more related to the control algorithm. One example concerning the second technique, called feedback neutralization, has been described in [Kuo and Morgan, 1999, Nelson and Elliott, 1993] and relies on a very good estimation of the feedback path's model. However, it has been reported in [Nelson and Elliott, 1993, Mosquera et al., 1999] that if the estimation is not accurate, then the

possibility for instability still exists.

The algorithms presented in this dissertation are designed to provide good results in the presence of this feedback coupling path and therefore there is no need for positive feedback path cancellation. The use of adaptive control is motivated by the fact that in real applications, the disturbance's characteristics can vary in time or that the identified models might not be exact representations of the system's dynamics.

2.3 Literature Overview

It is important to note that the work done on this thesis is based on the studies previously conducted, in particular the research done on the thesis by Tudor-Bogdan Airimiţoaie [Airimiţoaie, 2012]. Here we can find references to the development of Active Noise Control throughout history, such as the description in [Miljković, 2016]. As described in 2.1, it is possible to differentiate three main control methods in noise control theory, as mentioned in [Snyder, 2000]. The first approach is referred to as *passive* in [Krysinski and Malburet, 2008], and new materials and configurations for the attenuation of unwanted sound waves are currently being researched and developed. An example is the so called *acoustic black hole* theory described in [Krylov, 2014], where basic physic concepts are applied into the surfaces to produce the passive dampening. A more recent concept is that of the *metamaterials* [Marchal, 2014], where the concept of internal structure and geometry of the materials are further manipulated to achieve the desired objective [Guo et al., 2018a, Guo et al., 2018b]. Regarding the semi-active approach, it is not part of the development of this thesis, and a definition and examples can be found in [Babaee et al., 2016] and [Hansen et al., 2007]. For the latter approach, a review of relevant contributions in the literature is made in this section, regarding noise control theories in feedback and feedforward configurations. A comparative study between these two approaches can be found in [Elliott and Sutton, 1996].

2.3.1 Feedback Rejection of Multiple Narrow Band Disturbances

In the field of applications it is not always possible to obtain the measurements necessary to perform a feedforward control, and in these cases the feedback approach is a relevant option. Given the characteristics and restrictions of this approach, especially the limitation of the Bode integral, it is established that feedback control will be used mainly for perturbations with narrow frequency bandwidths [Åström and Murray, 2008, Zhou et al., 1996]. In the case of this thesis, the study is carried out on multiple simultaneous sinusoidal tonal disturbances with time varying characteristics.

The basics of feedback control theory are described in [Landau et al., 2011b], where the difference between adaptive control and adaptive regulation is discussed. It is observed there that in classical *adaptive control* the objective is to track and attenuate a disturbance in the presence of unknown and time-varying plant model parameters. Thus, the focus of adaptive

control is put on the adaptation with respect to variations in the plant model's parameters, where the disturbance model is assumed to be known and invariant.

Adaptive regulation, on the other hand, can be described as an asymptotic attenuation of the effects caused by disturbances of unknown characteristics that may vary over time. It is also necessary to have a known model of the plant, and that it is possible to apply robust controls that can overcome small variations in the parameters that may happen. Given this approach, it is not necessary to make real-time estimations of the characteristics of the system model.

The studies conducted in this research are focused on the attenuation of disturbances with a known system model, therefore *adaptive regulation* is considered. In [Amara et al., 1999b, Amara et al., 1999a, Gouraud et al., 1997] is stated that it is possible to represent the perturbation in the system as filtered white noise or Dirac impulse. In order to represent the disturbance, these signals are filtered by a *disturbance's model*, and to counteract their effects one of the main proposals is the Internal Model Principle (IMP), described in [Valentinotti et al., 2003, Valentinotti, 2001, Hillerstrom and Sternby, 1994]. Using this method supposes that the disturbance's model is embedded into the controller, as done in [Tsypkin, 1997, Bengtsson, 1977, Francis and Wonham, 1976, Johnson, 1976]. In this way, its parameters must be continuously estimated, allowing the system to react to possible unexpected changes in the disturbance's characteristics. Although this entails indirect adaptive control, [Landau et al., 2005] that direct adaptation is possible if one uses the Youla-Kučera parametrization of all stable controllers.

A different approach is presented in [Marino and Tomei, 2007, Serrani, 2006, Ding, 2003, Marino et al., 2003], where an adaptive observer is part of the system. This approach is mainly focused on disturbances acting over the plant's input, and additional hypotheses should be taken into account before applying it to disturbances on the system's output, such as the plant having stable zeros, which is seldom the case for discrete time plant models. It is evident that although the Internal Model Principle is not explicitly considered in this approach, the use of the observer in the controller implies its use.

A direct approach that uses the concept of phase-locked loop is presented in [Bodson and Douglas, 1997] and experimental results are provided in [Bodson, 2005], where its use can be seen in the presence of sinusoidal disturbances with unknown characteristics. Using a single error signal a perturbation's frequency estimation is done alongside the disturbance cancellation. Here, an adequate plant's frequency response is required in the region which corresponds to our frequency range of interest.

More recently furthers applications have been developed using the same concept in different areas of interest, proving that the study of Active Noise Control for the narrow band disturbance rejection by means of a feedback configuration is still relevant. Industry has found a source of innovation for a growing market in environmental comfort as shown in [Carme et al., 2016], where the theory and experimental results on a test setup are displayed, and focused in the development of a specific product. Concerning also diverse problematic, [Sharma and Renu,

2016, Lu et al., 2014] have stated applications for these theories on medical related problematic.

2.3.2 Feedforward Control of Broad-band Noises

One of the main differences between the first studies carried out in adaptive Feedforward Active Noise Control and recent research is the fact of being aware of the existence of an internal feedback coupling, and taking into account its effects on the system. The majority of the work done in this field is based. Most of the work done in this area is based on the development of applications of the gradient search algorithm in the Least Mean Squares (LMS) theory, first introduced in introduced in [Widrow, 1971]. The main objective of the LMS method is to find the minimum point on the Mean Square Error (MSE) surface by updating the parameters of a Finite Impulse Response (FIR) filter in a direction which is an estimate of the steepest descent. For these purposes, this algorithm uses the current sample of the squared error.

An improvement to this method was presented by [Burges, 1981] and [Widrow et al., 1981] named Filtered-X Least Mean Squares (FxLMS), which uses a filtered version of the observations measured as correlated signal with the disturbance for the adaptation algorithm. Burges' research in adaptive sound controllers and Widrow's adaptive inverse control development, presented adaptation of a FIR filter, and a secondary path model that has a relevant role in the adaptation process. The observation vector had to be filtered through the secondary path's model in order to obtain good estimations. More important, both problems addressed by these authors presented schemes without feedback coupling.

Despite the stability and the convex performance surface of the FIR filters, it is possible to find situations when the use of Infinite Impulse Response (IIR) filters could be preferred. A good example appears when good performance is looked, since the FIR approach often has to use a large number of parameters because of their all zero form, while with a IIR filter, it is possible to obtain similar performances with a significantly reduced number of parameters. Feintuch proposed another method named Recursive Least Mean Squares (RLMS) in [Feintuch, 1976] to adapt IIR filters, which is a variant of the basic LMS filter adaptation to the IIR structure. This algorithm was later improved by using filtered observations in the same way as was done in FxLMS, providing the Filtered-U Least Mean Squares (FuLMS) algorithm. The FuLMS was first introduced in [Eriksson et al., 1987] for ANC and AVC applications, but no convergence and stability analysis were provided. As an application example of this algorithm, the reduction of noise inside jet aircraft, produced by the engines that are mounted directly on the fuselage is described in [Billoud, 2001]. In the neighborhood of LMS algorithms, normally it is used an approximate estimate of the steepest descent direction, obtained by taking the current sample's gradient of the squared error instead of taking that corresponding to the MSE gradient. An improvement can be obtained in the denominated Filtered-V Least Mean Squares (FvLMS) algorithm presented in [Crawford and Stewart, 1997], where the full-gradient is calculated. Nevertheless, considering a slow adaptation of the parameters, some approximations can been

done to reduce the algorithm's numerical complexity. A difficult problem for adaptive IIR filters in the context of ANC is their stability and convergence analysis. Compared to the output error algorithms, this is results rather complicated due to the secondary path and internal feedback coupling path. One way of analyzing the convergence, in a stochastic environment, is the ODE method of Ljung ([Ljung and Söderström, 1983], first presented in [Ljung, 1977a] and applied on the output error analysis estimation method of [Landau, 1976] in [Ljung, 1977b]). Using this, it was possible to analyze the FuLMS algorithm properties in [Fraanje et al., 1999, Wang and Ren, 2003]. Conditions are found so as to assure convergence with probability 1 in the case of positive feedback coupling but with some restricting conditions, two of them being that a vanishing adaptation gain has to be used and that the feedback path does not destabilize the system.

A different approach for the stability and convergence analysis of adaptive algorithms is the *hyperstability* theory. This was first proposed in the work of Vasile Mihai Popov presented in the original publications [Popov, 1960, Popov, 1966] and then translated in [Popov, 1963, Popov, 1973]. One of the most important repercussions of this theory is its use in the design of stable adaptive algorithms alongside positive dynamic systems. The initial framework for studying a given adaptive system using the hyperstability was established in [Landau and Silveira, 1979, Landau, 1979, Landau, 1980] and a complete theoretical analysis can be found in [Landau et al., 2011c]. Unlike the Lyapunov approach, which is limited by the difficulty in finding appropriate Lyapunov functions, a large family of adaptation laws leading to stable adaptive algorithms can be designed using the hyperstability theory.
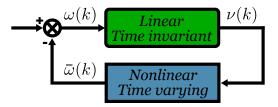
FIGURE 2.9. Standard representation of the analysis of adaptive systems using hyperstability theory.

The hyperstability mainly deals with the stability of systems class that can be represented as done by [Johnson, 1979] in the form given in Figure 2.9. On this configuration, it is supposed that the nonlinear and/or time-varying feedback block is such that it satisfies an input-output relation of the form

$$(2.3) \qquad \sum_{k=0}^{k_1} \bar{\omega}(k)\nu(k) \geq -\gamma^2, \text{ for all } k > 1$$

One of the early uses of hyperstability in the synthesis of adaptive algorithms was reported in [Treichler et al., 1978, Larimore et al., 1980]. The Simple Hyperstable Adaptive Recursive

Filter (SHARF) is convergent only for slow adaptation. The more complex Hyperstable Adaptive Recursive Filter (HARF) version has, instead, been proven convergent under less restrictive conditions [Johnson, 1979]. Both algorithms use filtering of the estimation error. A challenge encountered in these algorithms and which makes them difficult to use in ANC systems is the choice of a filter that assures the Strictly Positive Real (SPR) condition, especially due to the existence of the secondary and reverse paths. Furthermore, they are not presented in an ANC context, therefore the feedback coupling is not taken into account.

A filtered observations - filtered error variant of the HARF algorithm was presented in [Mosquera et al., 1999]. The convergence is then established, based on the previously developed theory. The implementation of this theory on an ANC system was experimented using feedback cancellation, but the results were not satisfactory. Similarly to the SHARF algorithms, in [Snyder, 1994] a method applicable in active control without positive feedback coupling is formulated. In contrast to the SHARF algorithms, filtering is done on the observation vector, whereas in the aforementioned algorithms it was done on the estimation error. A way of choosing the filtering is given. Yet another attempt to use the stability approach to design an adaptive algorithm for ANC was proposed in [Jacobson et al., 2001]. However, some assumptions made in the development of the theory restrict the application of this algorithm to specific cases and, as shown in [Landau et al., 2011a], the algorithm can even become unstable in a general ANC problem. More specifically, it was supposed that the secondary path is characterized by a SPR transfer function, which is seldom true. In addition to these directions of research, much work was done also on improving the numerical efficiency, especially in the case of RLS type algorithms and references belonging to these methods can be found in [Montazeri and Poshtan, 2010, Montazeri and Poshtan, 2011], but it has been limited to the case without positive feedback coupling. An equation error algorithm has been presented in [Sun and Chen, 2002]. The approach is globally convergent when the feedback coupling is not present and the measurement noise is zero. Where there is a presence of measurement noise, it is shown that the result is biased. Also when feedback exists, a local minimum is attained instead of a global one. In a way to overcome these problems, a Steiglitz-McBride type IIR algorithm has been published in [Sun and Meng, 2004]. Simulation results without feedback coupling are presented, yet another drawback of this algorithm appears where the stability is assumed before hand, when in practice, the poles of a IIR filter may move outside the unit circle and instability may then occur.

A different approach is considered in [Zeng and de Callafon, 2006], where a Model Based Design (MBD) controller obtained using the Youla-Kučera (YK) parametrization of all stabilizing controllers is implemented for a noise cancellation problem. The feedforward filter is first identified from open loop data and then an orthonormal basis function is designed, based on the method presented in [Heuberger et al., 1995]. A further difference with previously mentioned research results is that the parameters' adaptation is not done continuously but at certain intervals during which the system operates based on the last computed values. No stability analysis has been

performed in this case either.

To conclude on this review of the various methods developed in the field of ANC, it is necessary to mention also the H_∞ and H_2 MBD compensators. This approach has been considered in [Bai and H.H.Lin, 1997, Rotunno and de Callafon, 2003]. However, the resulting compensator does not have adaptation capabilities and its performance is not necessarily very good. Provided that the high dimension of the resulting compensator can be reduced, it just may constitute an initial value for the parameters of an adaptive or self-tuning feedforward compensator. In [Bai and H.H.Lin, 1997], it is shown experimentally that the results obtained with the H_∞ approach are better than those achieved using the FuLMS adaptation algorithm, for a disturbance with known spectral characteristics.

2.4 Contributions

The main objective of this work is the further development and comparison of diverse adaptive algorithms for acoustic noise attenuation in a determined system. These given algorithms have been used in previous projects for mechanical vibrations, and here they are extensively tested on a test bench designed specifically for this purpose. Having in mind the disturbances' characteristics, either a feedback control configuration for narrow band perturbations, or a feedforward control configuration for large band disturbances has been used.

In the initial Part I, aside of delivering an explanation of the test bench used for this work, the following contributions are presented:

- Development of methodology for systems' models identification based on measurements, applied on an acoustic environment,

- Study of geometry and physical disposition of elements and their effects on the active control and controllability over the resulting identified models.

As for the section corresponding to feedback in Part II, the contribution made can be summarized as:

- Development of methodology for feedback control to reject narrow band disturbances based on Band Stop Filters with adjustable frequency bandwidths and attenuations in order to shape the output sensitivity functions,

- Analysis and implementation of the Youla-Kučera parametrization on the control scheme of the feedback controller to improve the adaptation capabilities as well as the computation efficiency,

- Thorough comparison between different approaches and algorithms tested on the test bench designed for this purpose.

Finally in part III of this work, the feedforward approach is addressed, and the main contributions are:

- Analysis of different test bench configurations used and their effects on the control regarding the delay in the models.

- Development of generalized feedforward compensation adaptive algorithms that take into account the inherent existence of a positive feedback coupling in Active Noise Control systems,

- Application of Youla-Kučera parameterized adaptive feedforward filters, either in a FIR or IIR configuration,

- Exhaustive comparison between different algorithms and configurations, by analysis of experiments performed on the test bench,

- Comparison between both feedback and feedforward approaches made under similar conditions.

2.5 Dissertation Outline

After an explanation of the basis leading to this study in *Chapter 2*, we give a detailed description of the ANC test bench used for the trials done for this dissertation in *Chapter 3*. a comparison with more common approaches by other studies done in ANC is made. Geometries and dimensions are given for all the different configurations used throughout these studies, as well as the specification of the elements taking part in the test bench itself.

In the *Chapter 4*, the methodology utilized for the identification of all the linearized models, both for controller design and identifications, is described step by step. Later, similar models from different test bench configurations are discussed and compared.

In *Chapter 5* of this thesis, theory for attenuation of tonal or narrow band disturbances through a feedback control configuration is addressed. As a basis for comparison, non-adaptive controllers theory is developed and applied, focusing primordially in shaping the system's sensitivity functions. Then a more complex approach is taken into account when the Youla-Kučera (YK) parametrization is used for a self-tuning version of the previous controllers. Special care is taken for the computational stress due to complex calculations, and the optimization of the time required to perform them is done.

Finally, *Chapter 6* expose and studies the feedforward control theory for rejection of broad band disturbances, in the presence of an inherit internal coupling between the control signal and the measured disturbance's image present in ANC systems, that might induce a destabilization of the system itself. Common adaptive algorithms are tested and compared with the proposed Youla-Kučera parametrization.

Part I

Experimental Setup

PRACTICAL FIELD: TEST BENCH

pplication of algorithms and theories developed in the Active Noise Control domain
is a fundamental step, since the models are based on approximations of systems with
non-linear and dynamic behavior. This inherent condition creates a discrepancy between
the expected theoretical results and the ones we may encounter in real applications. Because
of that, one of the best approaches is to actually test the theory developed under a controlled
environment. From here the need to design a test bench for our studies.

In this chapter, first an explanation of the test bench used is given, comparing it with different
approaches. The physical disposition of key elements is explained and detailed, comparing to
other works and detailing the different test bench configurations used. Technical specifications
about the main components are given as well as detailed diagrams of configurations used.

3.1   From Theory to Reality: Test Bench Design

Different approaches exist when talking about test systems and environments for Active Noise
Control, as in [Venugopal and Bernstein, 2000, Cocchi et al., 2000, Hu and Lin, 2000, Bordeneuve-
Guibé and Nistor, 2002], just to mention a few. Taking all this into account, it was decided to take
a slight different approach to what has been done up until now. It was chosen, as general design,
an enclosed environment with an inherent closed initial point for the source of disturbances
acting in the system, and an open boundary at its end.

This was initially intended to act as a section of an idealized duct of air distribution, as the
ones we can find in real industrial environments. Let us give, as an example, a given machinery
or equipment working near one conduct of air conditioning distribution, which is close enough
to an office's room of the facility to be heard. The passive isolation that a wall and its materials

possess is limited, and the ducts provide a non usually isolated way of transmission for these noises. As an example we can see the work done by [Zeng and de Callafon, 2006].

A different application of the same idea is given in [Ben-Amara et al., 1999], where several controller adaptation algorithms are implemented in a test bench to solve the noise cancellation problem in a duct. In this work they address the fact that there are indeed differences between expected results and observed performances, that are attributed to the nonlinearities present in the test bench, and are not modeled in the design.

3.1.1 Control Actuator Placement

The main difference of the chosen configuration is seen at the control actuator positioning level. Amongst the most common configurations, we can find those in [Sharma and Renu, 2016, Zimmer et al., 2003, Carmona and Alvarado, 2000, Eriksson, 1991a], where there is a direct connection with the main section of the system in a complete perpendicular orientation, and taking into account the working fluid characteristics, allowing this actuator to be as close as possible to this main section.

Given the fact that a phenomenon of positive coupling is inherent to the system itself (as it will be explained in Section 6.3.1) and taken into account in some configurations for active control, such as measurement to decrease the effects of this, a new configuration was proposed. The basic scheme of the standard used setup in the field is displayed at Figure 3.1(a), where we can see a 90° connection, and the path that a reverse coupling would take. In order to decrease these undesirable but always present effects, a 45° connection, as in Figure 3.1(b), is implemented to create a smoother junction between the control signal heading to the flux of residual noise in the system, at the same time that makes a tougher path for the internal coupling.

More than one configuration were used during this thesis, due to some characteristics of the obtained models, and explained at section 6.1.

3.2 Test Bench Configurations

3.2.1 First Configuration

The first approach was taken just having in mind only the idea of decreasing the effects that an internal coupling presents. Dimensions of the components and parts used into this first configurations can be found in Figure 3.2. Here we can see the 45° angles formed by the control loudspeaker, marked as (2) in Figures 3.3 and 3.4, and its connection to the main body of the test bench.

The image in Figure 3.3 shows the real test bench in the facilities were it is used. Four important sections are depicted in it:
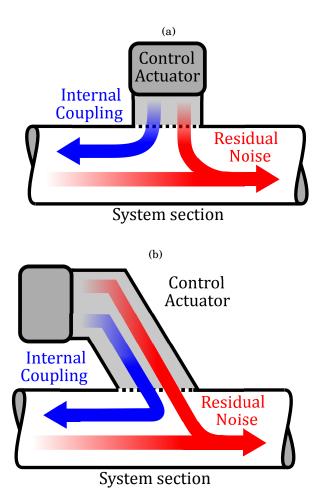
FIGURE 3.1. (a) Standard control actuator positioning. (b) Proposed control actuator positioning.

(1) *Disturbance's loudspeaker*, used as an artificial source of noises. Can reproduce variety of disturbances with specific characteristics. Used to feed the system with perturbations that go from simple sinusoidal signals, to audio recordings in real environments.

(2) *Controller's loudspeaker*, used as an actuator for the control signal fed into the system after calculations of the algorithms. It is individually connected to the computers, meaning that it has independent connectors and amplifier as it would be in a real system.

(3) *Residual noise's microphone*, located at the open end of the system and used to gather and record the measurements' data of the system exit. Information acquired by this microphone is measured in real time and used in algorithms with either a feedback or in feed-forward configuration.

(4) *Image's microphone*, a second sensor that may be used only for algorithms with a feed-forward configuration. It is located as close to the source of disturbance as possible in order to get a
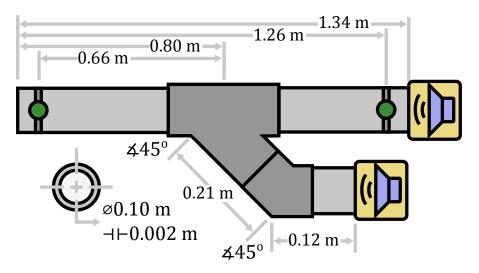
FIGURE 3.2. First experimental test bench configuration.

first impression or image of the disturbance before it crosses the system, thus called hereby image microphone.
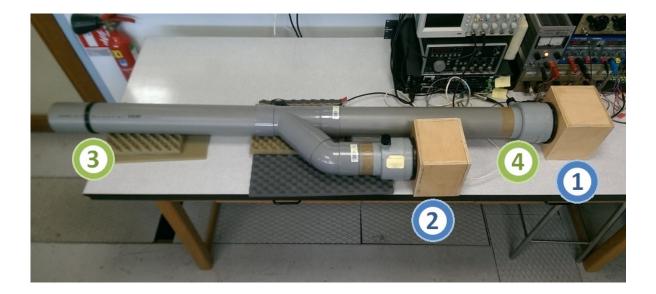
FIGURE 3.3. Photo of test bench's first configuration.

Figure 3.4 displays these same four remarks in a more schematic representation. Here we can see included both the development and target PC's, used to develop the algorithms and their direct application in the test bench. More important, we define for the first time the nomenclature used throughout the whole thesis for the different signals found in our schemes. First of all we have $y(t)$ as the *Residual Noise*, which is acquired by measurements of the residual noise's

microphone and sent to the target PC. This is the signal that a given controller being tested aims to attenuate. Second in importance is $u(t)$ as the *control signal*. It is calculated in the target PC and applied into the system through a power amplifier connected to the controller's loudspeaker. Independently to the different algorithms calculations, a signal $s(t)$ is defined as the *disturbance*. It is applied in the system through a second independent amplifier connected to the disturbance's loudspeaker. Lastly, $v(t)$ is the perturbation or *disturbance's image*, and is only used for the algorithms in a feed-forward configuration.

As a fundamental part of our approach, we define now the inner trajectories or paths inside the system. The path situated between the disturbance source located at *(1)*, and the point where residual noise is measured, located at *(3)* is named as *Primary Path*. This so called path is useful to recreate the system's dynamics in a simulation. More important is the path situated between the Controller's loudspeaker at *(2)* and the point where residual noise is measured in *(3)*. This is called *Secondary Path* and is crucial in the controllers' design, as it will be shown in the following sections.
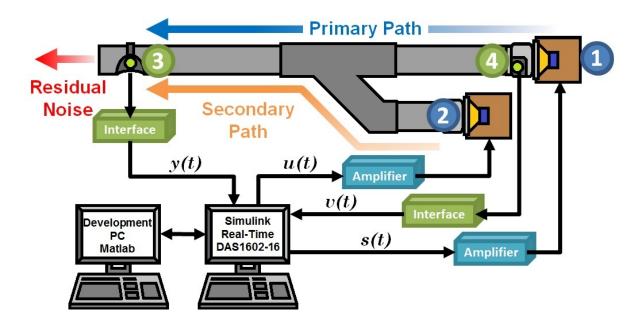
FIGURE 3.4. Schema of test bench's first configuration.

Since we are working in a discrete-time environment, given the cut-off frequency in the system a sampling frequency $f_s = 2500\,\text{Hz}$ was chosen. We may now describe the system based on a standard RST feedback controller as in figure 3.5, where $G = G(q^{-1})$ is the discrete time model of the plant, and where we will find that for our specific case, $r(t) = 0$.

Being that the case, the system can be further described by the diagram given in Figure 3.6,
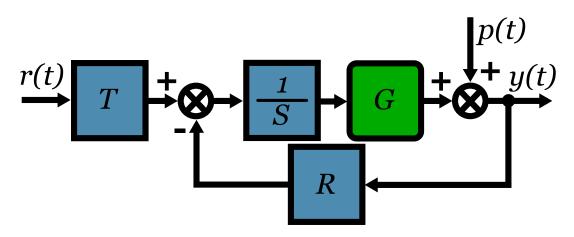
FIGURE 3.5. *RST* general controller scheme.

where we have the primary and secondary paths model given in discrete time such that,

$$(3.1) \qquad G(q^{-1}) = \frac{q^{-d_G} B_G(q^{-1})}{A_G(q^{-1})}$$

defines the secondary path G with a pure delay given by d_G, and the controller K is defined as,

$$(3.2) \qquad K(q^{-1}) = \frac{R(q^{-1})}{S(q^{-1})}.$$

For the case of simulations we will require to have the primary path's model as well, defined as D in the same way, such that,

$$(3.3) \qquad D(q^{-1}) = \frac{q^{-d_D} B_D(q^{-1})}{A_D(q^{-1})}.$$

In such manner, we define the residual noise as

$$(3.4) \qquad y(t) = G(q^{-1}) \cdot u(t) + p(t),$$

and the control signal as

$$(3.5) \qquad u(t) = -K(q^{-1}) \cdot y(t),$$

with $p(t)$ as the perturbations affecting the system (not to be confused with the disturbance signal $s(t)$ sent from the target PC). Further explanations will be given regarding the feed-forward configuration in the following sections (Chapter 6).

The resulting identified model for this first configuration's secondary path can be seen in Figure 3.7.
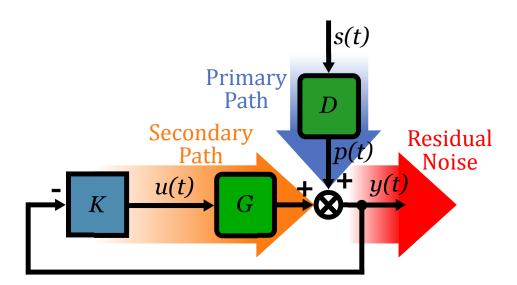
FIGURE 3.6. Feedback control scheme.
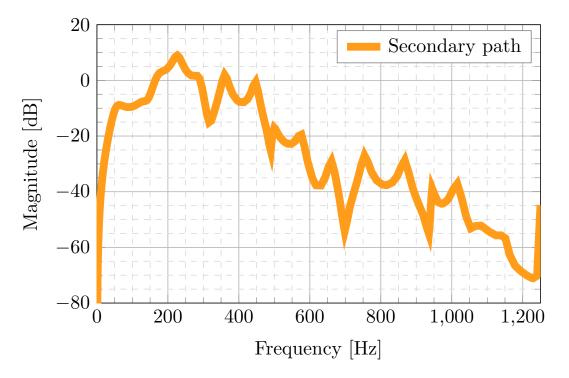
FIGURE 3.7. First test bench configuration's identified secondary path.

3.2.2 Second Configuration

For the second configuration used, as it can be seen in Figures 3.8 and 3.9, the geometry was changed to improve some characteristics of the secondary path, more specifically the controllability in some determined regions in the frequency domain, which is further explained in section

6.1.

In order to improve the secondary path's characteristics, it was found that since we use a loudspeaker as a disturbance's actuator, its diaphragm was acting as a passive damper [Baz, 2018, Krysinski and Malburet, 2008]. This introduced a series of setbacks that may not appear in a real system since disturbances are not configured to display passive dampening in real environment. This was related to a mechanic engineering term defined as *effective length* ([Stanfield and Skaves, 2012]). By shortening the disturbance's duct and changing the angles used as connection for the control loudspeaker, we were able to modify this length and thus, alter the undesired conditions present in the original design. However in this configuration the delay of the secondary path is larger than the delay of the primary path.
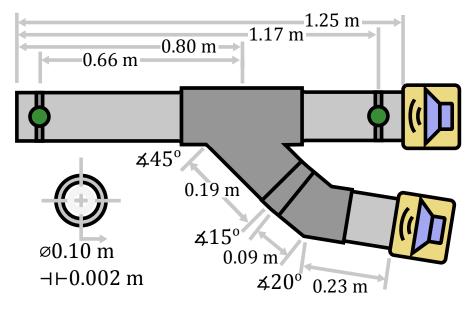
FIGURE 3.8. Second experimental test bench configuration.
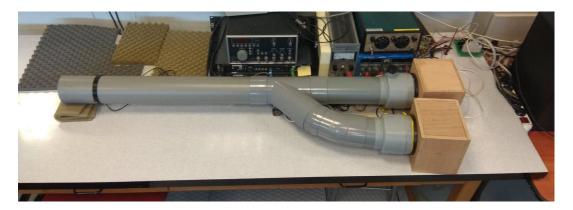
FIGURE 3.9. Photo of test bench's second configuration.

Results of the identified model for the second configuration's secondary path are displayed in

Figure 3.10.
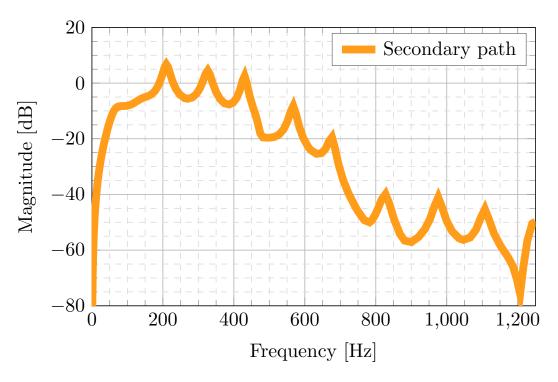
FIGURE 3.10. Second test bench configuration's identified secondary path.

3.2.3 Third Configuration

Finally a third and last configuration was implemented, where the test bench geometry was changed so that both feedback and feedforward approaches could be tested in similar conditions. The new geometrical dimensions are shown in Figure 3.11, and the actual test bench configuration can be seen in Figure 3.12.

Here, both previous test bench configurations advantages were considered. First, the unwanted zero in the secondary's path model was displaced to a mid-high frequency in order to allow the feedback controllers to operate in the desired frequency region of attenuation. Secondly, the difference between primary and secondary paths in terms of delay was taken into account to have favorable conditions for the feedforward controller.
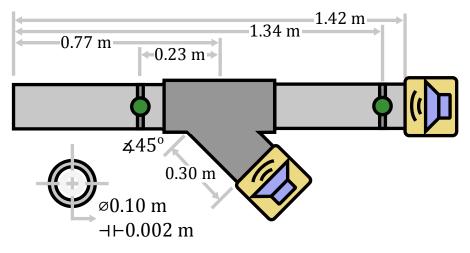
FIGURE 3.11. Third experimental test bench configuration.
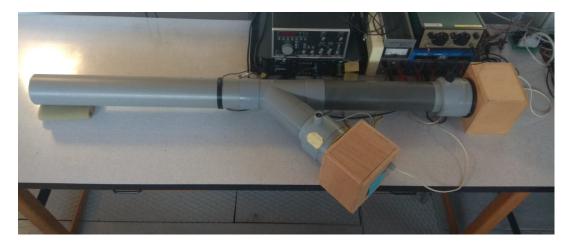
FIGURE 3.12. Photo of test bench's third configuration.

Further information regarding the differences between these configurations and the expla-

nation of their need are later done inChapter 6. Figure 3.13 shows the resulting identified path corresponding to this third configuration's secondary path is displayed. Figure 3.14 shows the comparison between all different configurations secondary path identified models and their differences in terms of frequency response.
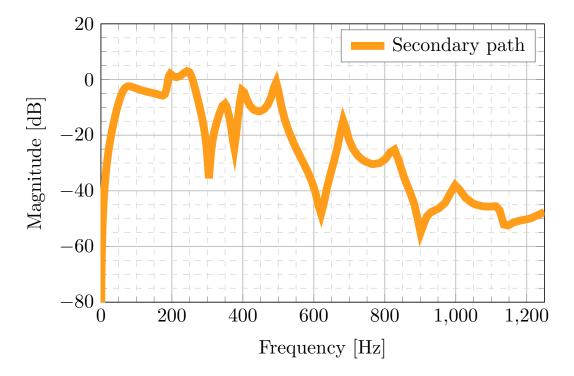
FIGURE 3.13. Third test bench configuration's identified secondary path.

3.3 Technical Specifications

Among the components used in the test bench we enlist here the most important ones. First of all, the pipes and connections are made of regular general purposes PVC non-scheduled, commonly used in low pressure sewer drain systems. All PVC parts have a nominal diameter of $0.10\,\mathrm{m}$.

The loudspeakers used are a couple of *Mark Audio Alpair 7 (Gen. 3) Extended Full-Range emitter, Gold color cone model*. In the attempt of creating an environment closer to reality, speakers were enclosed into anechoic chambers made out for reducing radiation noises done back the rear side of the speakers. They are made of half inch tick plywood, and filled with high density acoustic isolating foam. This custom made chambers have dimensions of $0.15\,\mathrm{m} \times 0.15\,\mathrm{m} \times 0.12\,\mathrm{m}$, with the configuration seen in Figure 3.15. Speakers are connected to two independent *Extron XPA 2004* power amplifiers, with a working range from $20\,\mathrm{Hz}$ to $20\,\mathrm{kHz}$ for frequency response. As for the microphones, a set of custom made *Hutchinson Paulstra* sensors are used for measurements.
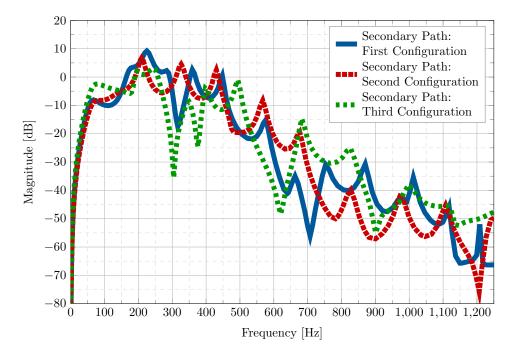
FIGURE 3.14. Secondary path models comparison. Frequency response of all test bench's configurations.
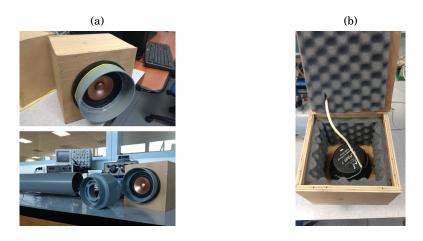
FIGURE 3.15. Anechoic boxes Set up.

3.4 Concluding Remarks

The physical description of elements conforming the test bench was given, as well as a brief explanation of the configuration and geometry used in its overall design, including the different configurations proposed. A basic introduction of the terms that will be used through this work is provided to start giving the basic notions and notations that will be recurring.

IDENTIFICATION OF MODELS

Design of noise controllers requires some knowledge of the system where it is intended to be applied. In this chapter, the methodology followed and the basic principles of dynamic systems identification are first introduced. The choice for this system's input signal used for identification and the influence of disturbances is later discussed, as well as the constrains imposed to high order models to agree with the parsimony principle, while keeping a good quality of the models. The whole model identification procedure is completely detailed for one of the models used in this project. Then the results obtained for the three configurations are displayed and compared before the concluding remarks.

4.1 Basis of Model Identification

Model identification from experimental data is a well established methodology as described in [Landau et al., 2016] and [Ljung, 1999]. Identification of systems is an experimental approach for determining a system's dynamic model. It includes four steps:

1. Input-output data acquisition under an experimental protocol and data pre-processing.

2. Estimation of the model's structure complexity.

3. Calculation of the model parameters.

4. Validation of the identified model for both complexity of the model and parameter's values.

A complete identification operation must comprise the four stages indicated above. The typical input excitation signal is a *Pseudo-Random Binary Sequence* PRBS, which is a persistent excitation signal allowing unique parameter estimation even for high order systems. The type

of model to be identified is a discrete-time parametric model, which allows to design a control algorithm straightforwardly implementable on a computer. Model validation is the final key point. It is important to emphasize that it does not exist one single algorithm that can provide a good model in all the cases (i.e. which passes the model validation tests). System identification should be viewed as an iterative process which has as objective to obtain a model which passes the model validation test and then can be used safely for control design. The procedure will be detailed for an identification of the system's first configuration secondary path G. The same methodology has been also used for the reverse path's M identification, used in the feedforward approach. Subsequently the primary and image paths, D and W correspondingly, were also identified in the same way, although they were used only for simulations.

4.2 Data Acquisition

For design and application reasons, since the objective was determined to reject tonal disturbances up to $400\,\mathrm{Hz}$, the sampling frequency was selected as $f_s = 2500\,\mathrm{Hz}$ (sampling time $T_s = 0.0004\,\mathrm{s}$) i.e. approximately 6 times the maximum frequency to attenuate, in accordance with recommendation given in [Landau et al., 2016]. The theoretical band pass of the system is $1975\,\mathrm{Hz}$, using formula given in [Zimmer et al., 2003].

4.2.1 Pseudo-Random Binary Sequence (PRBS)

In order to identify the corresponding models to each path, a methodology must be followed. First the system has to be excited with an input signal rich in frequencies. The experimental protocol should assure persistent excitation for the number of parameters to be estimated. There are several methods to achieve this, nevertheless it was shown in [Ljung, 1999], that for identifying $2n$ parameters, the excitation signal should contain at least $n + 1$ sines of distinct frequency. To go beyond this constraint, during this work's tests, the discrete-time version of a white noise signal, called *Pseudo-Random Binary Sequence* (PRBS), has been used; since it contains a large number of sines with energy equally distributed over the frequency domain. In addition, the signal's magnitude is constant, allowing an easy selection with respect to the magnitude constraint on the plant input. Pseudo-random binary sequences are signals of rectangular pulses modulated in width that vary randomly, but have a finite *sequence length* and repeat periodically in long term, thus Pseudo-Random.

One of the key points is the design of a PRBS in order to satisfy a compromise between the frequencies range to be covered, particularly those in the low frequencies region, and the test duration. One should apply at least on complete PRBS sequence, and its characteristics, including duration, will depend on the number of cells in the registers length used for its generation. The PRBS are generated by means of shift registers with feedback. The maximum length of a sequence is $L = 2^N - 1$, where N is the shift register's number of cells. In order to cover the entire

frequency spectrum generated by a particular PRBS, the length of a test must be at least equal to the sequence's length. In a large number of cases, the test duration L is chosen equal to the sequence's length.

The PRBS magnitude must also be considered. Although the value chosen for this magnitude may be very low, it should lead to output variations larger than the residual noise level. If the signal/noise ratio is too low, the test length must be augmented in order to obtain a satisfactory parameter estimation. Note that in a large number of applications, the significant increase in the PRBS level may be undesirable in view of the nonlinear character of the plants to be identified, as in our case, since we are concerned with the identification of a linear model around an operating point.

For identification in this work, the signal's characteristics used are: magnitude = 0.15 V, register length = 17, *sequence length* of $2^{17} - 1 = 131\,071$ samples, having a total duration of $L = 52.43$ s and guaranteeing a uniform power spectrum from about 50 Hz to 1250 Hz. This is beyond the system's band-pass estimated by using the non-parametric transfer function estimation technique in [Zimmer et al., 2003].

4.2.2 Data Preprocessing

Since we identify the secondary path, and since the relationship between the input/output signals $(u(t)/y(t))$, is that of a loudspeaker-microphone, the transfer functions will have a double differentiator behavior, since the input is determined by the speaker's coil position in [m], and the output is the acoustic pressure measured by the microphone's diaphragm in $[Pa] = [kg/(m\,s^2)]$. This is considered as the system's known part and so the objective is to identify the remaining unknown part only. To do this, the input sequence will be filtered by a discrete-time double differentiator

$$G_{dd}(q^{-1}) = (1 - q^{-1})^2 = 1 - 2q^{-1} + q^{-2}, \tag{4.1}$$

with q^{-1} as the delay operator for the time domain as in $q^{-n} y(t) = y(t-n)$, such that

$$u'(t) = G_{dd}(q^{-1}) \cdot u(t), \tag{4.2}$$

The double differentiator will be concatenated with the identified model of the unknown part in the final model. Finally the data acquired in $y(t)$ and the new defined $u'(t)$ are centered.

4.3 Order Estimation

It is extremely important being able to estimate the system's order from input/output data since it is hard from physical reasoning to get a reliable estimation of it. The plant measured output is in general contaminated by noise. This is due either to the effect of random disturbances acting at different points of the plant, to measurement noises, or unmodeled dynamics in the system's

plant. A common way of describe this phenomenon is define the system as the *plant + disturbance* $G + \eta$, thus giving as result $y(t) = G(q^{-1})u(t) + \eta(t)$. These random disturbances η are frequently modeled by ARMA models, thus the plant + disturbance process is given by an Auto-Regressive Moving Average with external input (ARMAX) model structure [Landau et al., 2016, Landau and Zito, 2006].

4.3.1 ARMAX Structure

Figure 4.1 shows the ARMAX process configuration taken for the secondary path's identification, where $u(t)$ is the signal sent to the controller's loudspeaker (as in 3.2), $y(t)$ is the system's output measured residual noise, $\delta(t)$ is an unknown source of disturbances defining η as $\eta(t) = O(q^{-1})\delta(t)$, and the discrete-time model of the disturbed secondary path is given by the linear transfer function $G^*(q^{-1})$ describing the system as $y(t) = G^*(q^{-1})u(t)$.
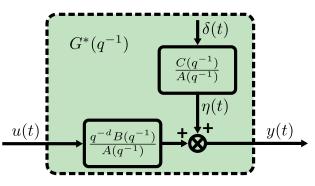
FIGURE 4.1. ARMAX process diagram.

Hence, we can define the disturbed plant's output as:

$$(4.3) \qquad y(t) = \frac{q^{-d}B(q^{-1})}{A(q^{-1})}u(t) + \frac{C(q^{-1})}{A(q^{-1})}\delta(t) = G(q^{-1})u(t) + O(q^{-1})\delta(t),$$

in which the first term $G(q^{-1})$ represents the controller effect or plant, and the second term $O(q^{-1})$ is attributed to the sum of measurements noise, random disturbances and unmodeled dynamics remaining out the effective model, since in practice we assume $\delta(t) = 0$, thus $G(q^{-1}) = G^*(q^{-1})$.

The polynomials $A(q^{-1})$ and $C(q^{-1})$ have the form

$$(4.4) \qquad A(q^{-1}) = 1 + \sum_{k=1}^{n_A} a_k q^{-k} = 1 + a_1 q^{-1} + a_2 q^{-2} + \cdots + a_{n_A} q^{-n_A},$$

and $B(q^{-1})$ is defined as

$$(4.5) \qquad B(q^{-1}) = \sum_{k=1}^{n_B} b_k q^{-k} = b_1 q^{-1} + b_2 q^{-2} + \cdots + b_{n_B} q^{-n_B},$$

where n_B, n_A, n_C are the polynomials orders respectively. The variable d corresponds to a pure input-output delay in the system. As such, d, n_B, n_A, n_C are the order values to estimate in this

step of the process. For simplicity, we then arbitrarily assign the order for $C(q^{-1})$ as $n_C = n_A$, and define the overall system's estimated order as $\hat{n}$, with $\hat{n} = \max(n_B + d, n_A)$.

4.3.2 Instrumental Variable

A simple way for identifying the polynomial orders and the quantity of pure delays is based on the least squares (LS) loss function. It is simple because it can be computed with only one pass through the data using an orthogonal transformation [Ljung, 1999, Söderström and Stoica, 1988, Söderström, 1977]. In general the LS method does not give a consistent estimate for orders when the second term $O(q^{-1})$ of Equation (4.3) models is colored noise. A solution in that case is to use the loss function of an ARMAX model, where $G(q^{-1})$ is also identified simultaneously.

However, the use of an ARMAX model is not appropriate when $O(q^{-1})$ is time-varying. Moreover, the identification of an ARMAX model is highly nonlinear, and the exact minimum of the loss function cannot be obtained. Finally, this approach has a high computational cost, because it requires many passes through the data, for identifying the model's parameters and computing the loss function of each model. Another approach, the rank test, has been proposed by [Guidorzi, 1981, Young et al., 1980, Wellstead, 1978] and others. The technique is based on testing the rank of some matrices, and often the problem is to define a criterion for deciding whether or not the considered matrix is of full rank [Söderström and Stoica, 1988]. Some solutions of the problem for a stationary noise case have been given by [Hall, 1991, Stoica, 1981], and others.

For explaining the rank test we, take as an example a simplified version of Equation (4.3), where the plant model is described by:

$$
\begin{aligned}
y(t) &= [-a_1 y(t-1) + b_1 u(t-1)] + [-a_2 y(t-2) + b_2 u(t-2)] + \cdots + [-a_{\hat{n}} y(t-\hat{n}) + b_{\hat{n}} u(t-\hat{n})], \\
&= -\left(\sum_{k=1}^{\hat{n}} a_k q^{-k}\right) y(t) + \left(\sum_{k=1}^{\hat{n}} b_k q^{-k}\right) u(t), \\
&= -A(q^{-1}) y(t) + B(q^{-1}) u(t),
\end{aligned}
\tag{4.6}
$$

with $A(q^{-1})$ and $B(q^{-1})$ of estimated order $\hat{n}$. From here we can define the data vectors acquired from the experiments system output $Y(t)$ and plant input $U(t)$ as

$$
Y^T(t) = [y(t), y(t-1), \ldots], \qquad U^T(t) = [u(t), u(t-1), \ldots],
\tag{4.7}
$$

and the parameters vector from the identified model as

$$
\theta^T = [a_1, a_2, \ldots, a_{\hat{n}}, b_1, b_2, \ldots, b_{\hat{n}}].
\tag{4.8}
$$

Afterwards we construct the $[2\hat{n}] \times [2\hat{n} + 1]$ matrix $[Y(t)|R(\hat{n})]$ as:

$$(4.9) \quad [Y(t)|R(\hat{n})] = \begin{bmatrix} y(t) & y(t-1) & u(t-1) & \dots & y(t-\hat{n}) & u(t-\hat{n}) \\ y(t-1) & y(t-2) & u(t-2) & \dots & y(t-\hat{n}-1) & u(t-\hat{n}-1) \\ \vdots & \vdots & \vdots & \ddots & \vdots & \vdots \\ y(t-2\hat{n}-1) & y(t-2\hat{n}) & u(t-2\hat{n}) & \dots & y(t-3\hat{n}-1) & u(t-3\hat{n}-1) \end{bmatrix},$$

with the square $[2\hat{n}] \times [2\hat{n}]$ matrix $R(\hat{n})$ defined by

$$(4.10) \qquad R(\hat{n}) = [Y(t-1), U(t-1), Y(t-2), U(t-2), \dots, Y(t-\hat{n}), U(t-\hat{n})].$$

From here we can say that, if the model order $\hat{n}$ given in Equation (4.6) is correct, the vector $Y(t)$ will be a linear combination of the columns in $R(\hat{n})$, since $Y(t) = R(\hat{n})\theta$ and the matrix will be rank deficient. If the real order of plant model is higher than $\hat{n}$, the matrix (4.9) will be full rank meaning that the estimated order $\hat{n}$ was too small.

Unfortunately, as a consequence of the disturbances that may appear, this procedure cannot directly be applied in practice. A more practical approach results from the observation that a rank test problem can be approached by looking for a $\hat{\theta}$ which minimizes the following criterion for an estimated value of the order $\hat{n}$. This is where the LS loss function intervenes [Söderström and Stoica, 1988], and we can define the criterion such that,

$$(4.11) \qquad V_{LS}(\hat{n}, N) = \min_{\hat{\theta}} \frac{1}{N} \left\| Y(t) - R(\hat{n})\hat{\theta} \right\|^2$$

where N is the number of samples acquired in the test for model identification.

Finally it has been shown that it is possible to replace the matrix $R(\hat{n})$, by a new reformulated *Instrumental Variable* (IV) auxiliary observation matrix $Z(\hat{n})$, as proposed in [Duong and Landau, 1996, Duong and Landau, 1994], whose elements are highly correlated with the uncontaminated variables, and therefore representative, but uncorrelated with the measurements noise and disturbances. Such an instrumental matrix $Z(\hat{n})$ can be obtained, by replacing in the matrix $R(\hat{n})$, the columns $Y(t-1), Y(t-2), \dots, Y(t-\hat{n})$ by a corresponding delayed version of $U(t-1)$ as in $Y(t) \rightarrow U(t-L)$, where $L \geq 2\hat{n}$ [Duong and Landau, 1996], such that

$$(4.12) \qquad Z(\hat{n}) = [U(t-1-L), U(t-1), U(t-L-2), U(t-2), \dots, U(t-\hat{n}-L), U(t-\hat{n})],$$

hence the criterion to minimize is defined as

$$(4.13) \qquad V_{IV}(\hat{n}, N) = \min_{\hat{\theta}} \frac{1}{N} \left\| Y(t) - Z(\hat{n})\hat{\theta} \right\|^2.$$

4.3.3 Penalization

One of the main objectives of the identification is to estimate lower order models, due to the parsimony principle, and therefore it is reasonable to add in the criterion a term which penalizes the model's complexity. Therefore, the penalized criterion for order estimation will take the form:

$$J_{IV}(\hat{n}, N) = V_{IV}(\hat{n}, N) + S(\hat{n}, N),$$ (4.14)

where the penalization term $S(\hat{n}, N)$ can take several forms. Results in this work were obtained by using the penalization term $S(\hat{n}, N) = 2\hat{n}\frac{\log N}{N}$, so Equation (4.14) is reformulated as

$$J_{IV}(\hat{n}, N) = V_{IV}(\hat{n}, N) + 2\hat{n}\frac{\log N}{N}.$$ (4.15)

Since we have a fixed amount of data and N is a constant, the value for this model order that the procedure is looking for can be described by

$$\hat{n} = \min_{\hat{n}} J_{IV}(\hat{n}).$$ (4.16)

A typical curve of the criterion $J_{IV}(\hat{n}, N)$ evolution as a function of $\hat{n}$ is shown in Figure 4.2.
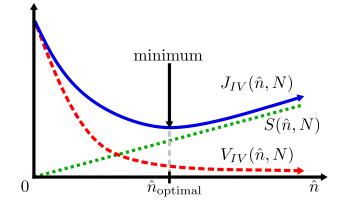
FIGURE 4.2. Evaluation of the penalized instrumental variable criterion for order estimation.

Once an estimated order $\hat{n}$ is selected, one can apply a similar procedure to individually estimate $\hat{n}_A$, $\hat{n} - \hat{d}$, $\hat{n}_B + \hat{d}$, from which $\hat{n}_A$, $\hat{n}_B$, $\hat{n}_C$ and $\hat{d}$ are obtained.

From Equation (4.1) we recall that a known part of the model is given by the second order polynomial $G_{dd}(q^{-1})$, hence the final value for the order of polynomial $B(q^{-1})$ will be expressed as $\hat{n}_{B'} + 2$. Examples of the results obtained for the real estimation of the example taken can be seen in Figure 4.3, where Figure 4.3(a) shows the results for $\hat{n}$, Figure 4.3(b) for $\hat{n}_{B'} + \hat{d}$, Figure 4.3(c) for $\hat{n}_A$, and Figure 4.3(d) for $\hat{n} - \hat{d}$. The order for polynomial $C(q^{-1})$ is taken as $\hat{n}_C = \hat{n}_A$.

As seen for the example in Figure 4.3(a), the minimum for criterion is very flat, which is understandable since we are trying to approximate an infinite-dimensional system. It is therefore necessary to explore the model's properties for $\hat{n}$ between 32 and beyond, in order to decide what order to take. Two additional criteria will be used to decide upon the best order estimation: I) comparison between the Power Spectral Densities (PSD) of the identified model's output and the output's real data, in order to see if the identified model captures all the vibration modes in the frequency range of operation, and II) comparison of the validation tests for the various models. This will be further explained in 4.5.
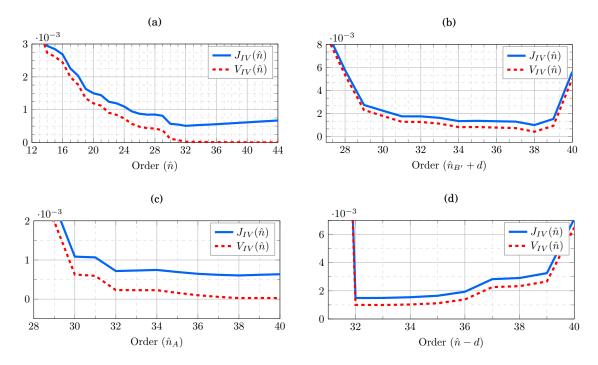
FIGURE 4.3. Order estimation using an Instrumental Variable and complexity penalty, with estimation for (a) $\hat{n}$, (b) $\hat{n}_{B'} + \hat{d}$, (c) $\hat{n}_A$, and (d) $\hat{n} - \hat{d}$.

The table 4.1 summarizes the estimated orders used for the secondary path model, along with the orders for all remaining system's paths models.

Path	n	n_A	n_B	d
Primary	38	34	27	9
Secondary	40	38	32	8
Reverse	37	33	30	7
Image	34	34	34	0

TABLE 4.1. First test bench configuration estimated orders used for the different system models.

A remark that can be done at this point is the fact that for the specific case of an ANC system,

the delays d can be sometimes calculated previously to the order estimation, since the sound speed and the relative distances between the signal source (a loudspeaker in this test bench), and the point of signal measurement, located at the microphone, can be determined.

4.4   Parameters Estimation

The algorithms used for parameter estimation will depend on the assumptions made on the measurements noise $\eta(t)$ characteristics, which have to be confirmed by the model validation (4.5). It is important to emphasize that no single *plant + noise* structure exists that can describe all the situations encountered in practice. Furthermore, there is no parameter estimation algorithms that may be used with all possible *plant + noise* structures such that the estimated parameters are always unbiased. It is the validation stage which will allow to decide what method, and implicitly what noise model, has to be used.

4.4.1   Identification Method: OEEPM

Among various models, it was found that ARMAX model gives the best representation in this case, and between the available methods for that model, Output Error with Extended Prediction method (OEEPM), called *XOLOE* in some literature [Landau et al., 2016], brought the best results in terms of validation for a given order model. It has been developed initially with the aim to remove the strictly positive real condition required by the output error algorithm. It turns out that the OEEPM can be interpreted as a variant of the Extended Least Squares (RELS) [Landau et al., 2016].

From Equation (4.3), we have:

$$(4.17) \qquad A(q^{-1})y(t) = q^{-d}B(q^{-1})u(t) + C(q^{-1})\delta(t).$$

The idea is to simultaneously identify the plant model $G(q^{-1})$ and the noise model $O(q^{-1})$, in order to obtain a *prediction adaptation error* which is asymptotically white. Expressing the polynomials as $B(q^{-1}) = q^{-1}B^*(q^{-1})$, the model generating data can be expressed as:

$$(4.18) \qquad \begin{aligned} y(t+1) &= -A^*(q^{-1})y(t) + B^*(q^{-1})u(t-d) + C^*(q^{-1})\delta(t) + \delta(t+1) \\ &= \theta^T \varphi_0(t) + \delta(t+1) \end{aligned}$$

with

$$(4.19) \qquad \theta^T = [a_1, a_2, \ldots, a_{n_A}, b_1, b_2, \ldots, b_{n_B}, c_1, c_2, \ldots, c_{n_C}],$$

$$(4.20) \qquad \varphi_0^T(t) = [-y(t), \ldots, -y(t-n_A+1), u(t-d), \ldots, u(t-d-n_B+1), \delta(t), \ldots, \delta(t-n_C+1)].$$

Assume that the parameters are known and construct a predictor that will give a white prediction error:

$$(4.21) \qquad \hat{y}(t+1) = -A^*(q^{-1})y(t) + B^*(q^{-1})u(t-d) + C^*(q^{-1})\delta(t).$$

Furthermore as shown in [Landau and Zito, 2006], this predictor will minimize $E\left\{[y(t+1)-\hat{y}(t+1)]^2\right\}$. The prediction error, in the case of known parameters, is given by:

$$(4.22) \qquad \varepsilon(t+1) = y(t+1) - \hat{y}(t+1) = \delta(t+1),$$

hence Equation (4.21) can be written as

$$(4.23) \qquad \hat{y}(t+1) = -A^*(q^{-1})y(t) + B^*(q^{-1})u(t-d) + C^*(q^{-1})\varepsilon(t),$$

and modifying Equation (4.18) with this new definition we get

$$(4.24) \qquad \varepsilon(t+1) = -C^*(q^{-1})[\varepsilon(t)-\delta(t)] + \delta(t+1),$$

thus $C^*(q^{-1})[\varepsilon(t)-\delta(t)] = 0$, and since $C(q^{-1})$ is an asymptotically stable polynomial, it results that $\varepsilon(t+1)$ will become white asymptotically.

In the adaptive version of this algorithm, the *a priori* adjustable predictor will take the form:

$$(4.25) \qquad \begin{aligned} \hat{y}^\circ(t+1) &= -\hat{A}^*(q^{-1},t)y(t) + \hat{B}^*(q^{-1},t)u(t-d) + \hat{C}^*(q^{-1},t)\delta(t) \\ &= -\hat{A}^*(q^{-1},t)\hat{y}(t) + \hat{B}^*(q^{-1},t)u(t-d) + \left\{\hat{C}^*(q^{-1},t)\delta(t) - \hat{A}^*(q^{-1},t)[y(t)-\hat{y}(t)]\right\}, \end{aligned}$$

that can be rewritten as

$$(4.26) \qquad \begin{aligned} \hat{y}^\circ(t+1) &= -\hat{A}^*(q^{-1},t)\hat{y}(t) + \hat{B}^*(q^{-1},t)u(t-d) + \hat{H}^*(q^{-1},t)\varepsilon(t) \\ &= \hat{\theta}^T(t)\varphi(t), \end{aligned}$$

with $\hat{H}^*(q^{-1},t) = \hat{C}^*(q^{-1},t) - \hat{A}^*(q^{-1},t) = \hat{h}_1(t) + q^{-1}\hat{h}_2(t) + \ldots$, with $\hat{h}_i(t) = \hat{c}_i(t) - \hat{a}_i(t)$ for $i = 1,2,\ldots,n_H$, where $n_H = \max(n_A, n_C)$; and also getting

$$(4.27) \qquad \hat{\theta}^T(t) = [\hat{a}_1, \hat{a}_2, \ldots, \hat{a}_{n_A}, \hat{b}_1, \hat{b}_2, \ldots, \hat{b}_{n_B}, \hat{h}_1, \hat{h}_2, \ldots, \hat{h}_{n_H}],$$

$$(4.28) \qquad \varphi^T(t) = [-\hat{y}(t), \ldots, -\hat{y}(t-n_A+1), u(t-d), \ldots, u(t-d-n_B+1), \varepsilon(t), \ldots, \varepsilon(t-n_H+1)].$$

Equation (4.26) corresponds to the adjustable predictor for the Output Error with Extended Prediction model (OEEPM). From here, the recursive parameter estimation (or adaptation) algorithm (PAA) used is described in [Landau et al., 2016], such that:

$$(4.29) \qquad \hat{\theta}(t+1) = \hat{\theta}(t) + F(t)\varphi(t)\varepsilon(t+1),$$

$$(4.30) \qquad F(t+1)^{-1} = \lambda_1(t)F(t)^{-1} + \lambda_2(t)\varphi(t)\varphi^T(t),$$

$$(4.31) \qquad \varepsilon(t+1) = \frac{\varepsilon^{\circ}(t+1)}{1 + \varphi^T(t)F(t)\varphi(t)},$$

with $0 < \lambda_1(t) \le 1$, $0 \le \lambda_2(t) \le 2$, $F(0) > 0$, $F^{-1}(t) > \alpha F^{-1}(0)$ for $\alpha > 0$.

4.5 Model Validation

The considered identification protocol OEEPM belongs to the class of methods based on the residual error's whitening, meaning that the identified ARMAX predictor is optimal if the residual error $\varepsilon(t)$ is a white noise. If the residual prediction error $\varepsilon(t)$ is a white noise sequence, in addition to obtaining unbiased parameter estimates, this also means that the identified model gives the best prediction for the plant output in the sense that it minimizes the variance of $\varepsilon(t)$. On the other hand, since the residual error is a white noise, it is not correlated with any other variable, then all correlations between the input and output of the plant are represented by the identified model and what remains unmodeled does not depend on the input $u(t)$.

Before implementing the validation method it is assumed that I) the *plant + noise* structure chosen is correct and representative of the reality, II) an appropriate parameter estimation method for the structure chosen has been used, and III) the polynomials orders n_A, n_B, n_C and delay d have been correctly chosen. Then the prediction error $\varepsilon(t)$ asymptotically tends toward a white noise, which implies:

$$\lim_{t \to \infty} E\{\varepsilon(t) - \varepsilon(t-i)\} = 0; \qquad i = 1, 2, \dots$$

4.5.1 Whitening Test

Let $\varepsilon(t)$ be the centered sequence of the residual prediction errors, so we have:

$$(4.32) \qquad R(i) = \frac{1}{N_s} \sum_{t=1}^{N_s} \varepsilon(t)\varepsilon(t-i),$$

$$(4.33) \qquad R_n(i) = \frac{R(i)}{R(0)}, \qquad i = 0, 1, 2, \dots, n_A, \dots$$

with $i_{\max} \ge n_A$, N_s number of samples and $R(i)$, $R_n(i)$ the autocorrelation and normalized autocorrelation estimations. In the theoretical situation where the residual prediction error $\varepsilon(t)$ sequence is perfectly white and the number of samples N_s is large ($N_s \to \infty$), then $R_n(i) = 0$ for all i. However, in real situations this is never the case and $R_n(i) \ne 0$ for $i \ge 1$, since $\varepsilon(t)$ contains

residual structural errors from wrong polynomial orders, nonlinear effects, non-Gaussian noises, or the value for N_s is too small.

A practical validation extensively tested on applications criterion is defined by:

$$(4.34) \qquad\qquad |R_N(i)| \le \frac{2.17}{\sqrt{N_s}}, \qquad i \ge 1.$$

This test has been defined taking into account the fact that for a white noise sequence $R_n(i) \ne 0$ has an asymptotically Gaussian (normal) distribution with zero mean and standard deviation $\sigma \frac{1}{\sqrt{N_s}}$. Equation (4.34) considers a confidence interval of 97% in the hypothesis test for Gaussian distribution (with a z-score $= 2.17$ we get $2.17\sigma = 97\%$).

If $R_n(i)$ obeys one-sided Gaussian distribution, there is only a probability of 1.5% that $|R_n(i)| > \frac{2.17}{\sqrt{N_s}}$. Therefore, if a computed value $R_n(i)$ falls outside the confidence interval range, the hypothesis stating that $\varepsilon(t)$ and $\varepsilon(t-i)$ are independent is not satisfied, and model should be rejected, since $\varepsilon(t)$ would not be a white noise sequence.

If several identified models have the same complexity, the model given by the methods that lead to the smallest $|R_n(i)|$ should be preferred. Also a "too good" validation criterion indicates that model simplifications may be possible.

Since for our example we estimate $n_A = n_C = 38$ from Table 4.1, we get that $i_{\max} = 38$. Results of the *Whitening Test* for the identified model example of the secondary path can be seen in Figure 4.4.
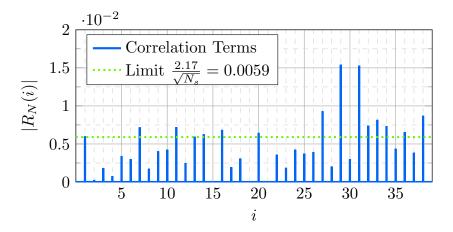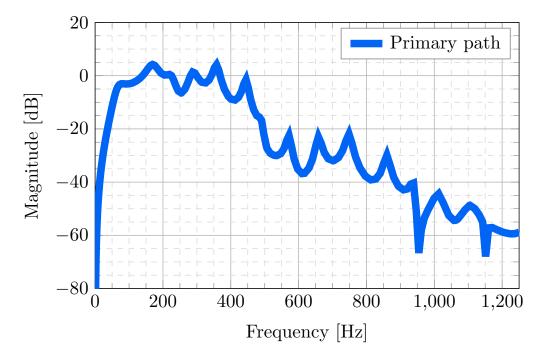
FIGURE 4.4. Whiteness test for identified secondary path.

It can be noticed that not all autocorrelations satisfy the criterion limit of $|R_n(i)| \le \frac{2.17}{\sqrt{N_s}}$, nevertheless among the several tests and approached realized for the models identifications, it was found that being close enough to this limit in the first autocorrelations, corresponding to the low frequencies in the identified model, gave good results.

4.6 Identified Models

Models identified from experiments done in the different configurations of the test bench by applying the model identification methodology are presented in this section. The primary and image paths are used only for simulations; they are presented only for the first test bench configuration.
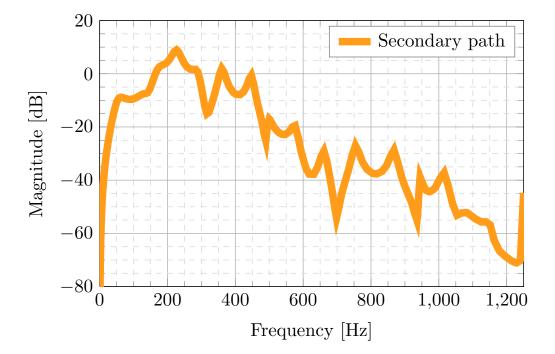
4.6.1 First Configuration Models

FIGURE 4.5. Identified primary path for first test bench configuration.

From Figure 4.5 we can see that the identified primary path of the first configuration has very low gain at frequencies over 500 Hz, meaning than disturbances above this frequency will be attenuated by the system itself and there is no use in apply a controller over those frequencies. Same phenomenon happens with frequencies under 50 Hz, where the effects of the double differentiator present on the model are evident.

In Figure 4.6 the most important point to highlight is the presence of a low damped zero around 315 Hz. This zero generates a region of low gain where the controller won't have attenuation capabilities and thus compensation at those given frequencies must be avoided.

FIGURE 4.6. Identified secondary path for first test bench configuration.
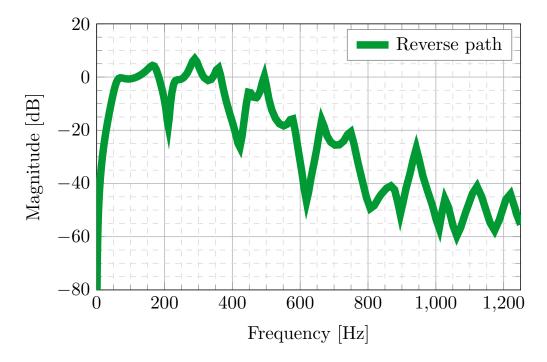
FIGURE 4.7. Identified reverse path for first test bench configuration.
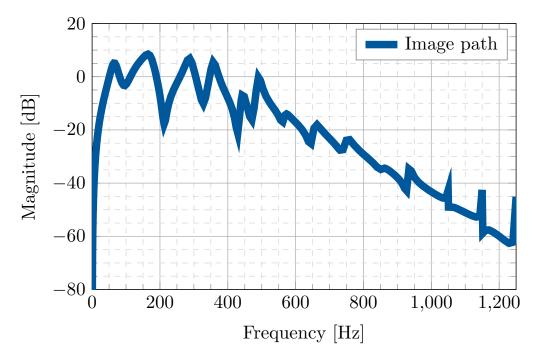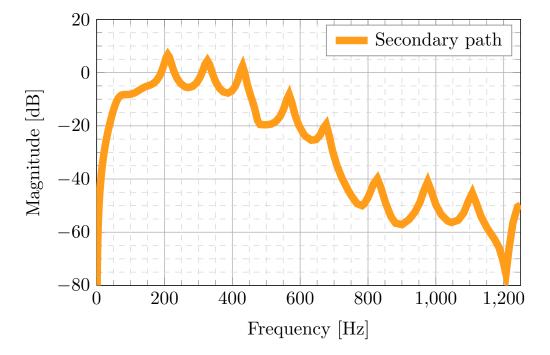
FIGURE 4.8. Identified image path for first test bench configuration.

Once the problem of this zero was pointed out, a solution was proposed and Figure 4.9 displays the secondary path of the second test bench configuration without low damped zeros in it, allowing us to have a larger attenuation region.

At last Figure 4.11 the third test bench configuration's secondary path, where the low damped zero is present again, but the gain at frequencies near 70 Hz is higher in comparison with those models of both previous configurations.

4.6.2 Second Configuration Models

FIGURE 4.9. Identified secondary path for second test bench configuration.
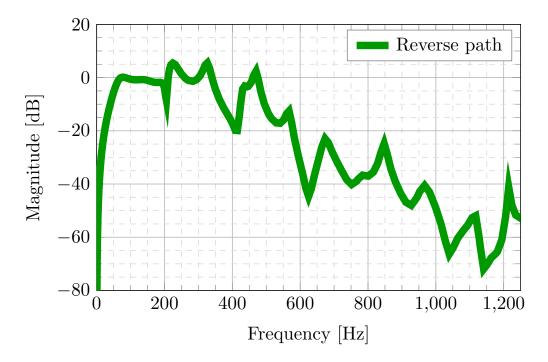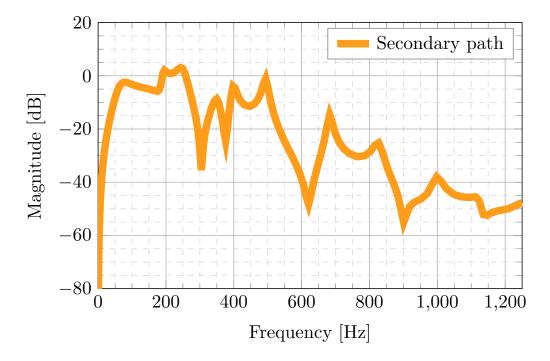
FIGURE 4.10. Identified reverse path for second test bench configuration.

4.6.3 Third Configuration Models

FIGURE 4.11. Identified secondary path for third test bench configuration.
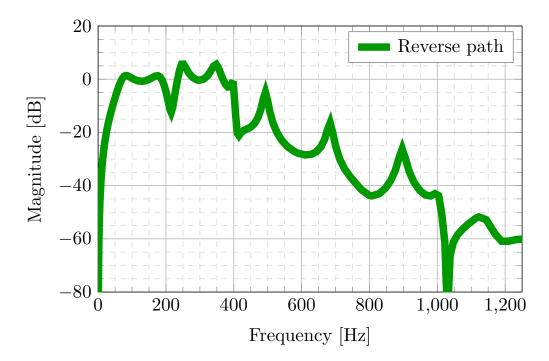
FIGURE 4.12. Identified reverse path for third test bench configuration.

4.7   Concluding Remarks

The basic elements for the identification of discrete-time models for dynamical systems have been laid down in this chapter. The following facts have to be emphasized:

1. System identification includes four basic steps:

   - input/output data acquisition under an experimental protocol,
   - estimation or selection of the model complexity,
   - estimation of the model parameters,
   - validation of the identified model (structure of the model and values of parameters);

   having in mind that this procedure has to be repeated (with appropriate changes at each step) if the model validation fails.

2. Recursive or off-line parameter estimation algorithms can be used for the identification of the plant model parameters.

3. The stochastic noises, which contaminate the measured output, may cause errors in the parameter estimates (bias). For a specific type of noise, appropriate recursive identification algorithms providing asymptotically unbiased estimates are available.

4. A unique *plant + noise* model structure that describes all the situations encountered in practice neither exists, nor is there a unique identification method providing satisfactory parameter estimates (unbiased estimations) in all situations.

5. Different test bench configurations have significant differences in terms of the models identified, more important in the secondary path, defining the controller capabilities.

Part II

Adaptive Feedback Disturbance Compensation

D evelopment of an adaptive feedback controller for narrow band disturbances is explained step by step in this chapter. Starting with a simple fixed controller for tonal disturbances, passing through a more robust fixed controller with respect to the disturbance's characteristics, and then finally get to the self tuning adaptive feedback controller in a Youla-Kučera parametrization.

First of all, the basic specifications are that the attenuation of two tonal disturbances located at 170 Hz and 285 Hz must be at least -40 dB, and the maximum amplification at any other frequencies be less than 7 dB. This choice is due to the fact that, as can be seen in Figure 4.5, the disturbance's frequency gains expected in the primary path have high gain at 170 Hz and 285 Hz. Nevertheless, as Figure 4.6 shows, the control signal's gains have a strong lost at 315 Hz that renders the zone as non controllable. Furthermore, in order to improve robustness, the input sensitivity function should be below -20 dB at frequencies over 600 Hz since they are beyond the system's band-pass.

5.1 Feedback Theory

For ease of notation, since in this chapter we make use exclusively of the secondary path models, in the this feedback context we will redefine $A(q^{-1}) = A_G(q^{-1})$, $B(q^{-1}) = B_G(q^{-1})$ and $d = d_G$. As stated in the previous Chapter 3 and Chapter 4, the *linear time invariant* (LTI) discrete-time model of the secondary path, or plant, used for controller design will be described as:

$$G(q^{-1}) = \frac{q^{-d}B(q^{-1})}{A(q^{-1})},$$

(5.1)

where the polynomials $A(q^{-1})$ and $B(q^{-1})$ are defined as:

(5.2)
$$A(q^{-1}) = 1 + a_1 q^{-1} + \cdots + a_{n_A} q^{-n_A},$$

(5.3)
$$B(q^{-1}) = b_1 q^{-1} + \cdots + b_{n_B} q^{-n_B},$$

with d as the plant pure time delay in number of sampling periods.

Also we defined the feedback controller $K(q^{-1})$ as $K(q^{-1}) = \frac{R_K(q^{-1})}{S_K(q^{-1})}$. Once again, since in this chapter we are working exclusively within the feedback context, we redefine our controller $R(q^{-1}) = R_K(q^{-1})$ and $S(q^{-1}) = S_K(q^{-1})$, such that

(5.4)
$$K(q^{-1}) = \frac{R}{S} = \frac{r_1 q^{-1} + \cdots + r_{n_R} q^{-n_R}}{1 + s_1 q^{-1} + \cdots + s_{n_S} q^{-n_S}}.$$
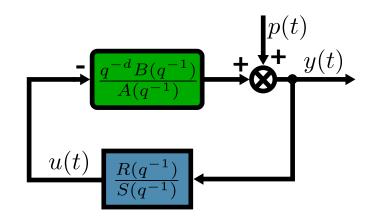
FIGURE 5.1. Feedback regulation scheme.

Figure 5.1 shows the closed loop feedback regulation scheme described by these equations, thus the plant's output $y(t)$ and the input $u(t)$ are described by $y(t) = G(q^{-1})u(t) + p(t)$ and $u(t) = -K(q^{-1})y(t)$, than may be written as:

(5.5)
$$y(t) = \frac{q^{-d}B(q^{-1})}{A(q^{-1})} u(t) + p(t),$$

(5.6)
$$u(t) = -\frac{R(q^{-1})}{S(q^{-1})} y(t),$$

where $p(t)$ represents the disturbances' effect on the measured output (Section 3.2). Developing these equations we obtain:

(5.7)
$$y(t) = \frac{AS}{AS + q^{-d}BR} p(t) = \frac{AS}{P} p(t),$$

with $P(q^{-1})$ as the system's *characteristic polynomial*, which specifies the desired closed loop poles of the system.

5.2 Linear Controller Design

As stated before, the performance specifications required for the controller are that the attenuation of two tonal disturbances located at $170\,\text{Hz}$ and $285\,\text{Hz}$ must be at least $-40\,\text{dB}$, meanwhile the maximum amplification at any other frequencies must be less than $7\,\text{dB}$. Furthermore, in order to improve robustness, the input sensitivity function should be below $-20\,\text{dB}$ at frequencies over $600\,\text{Hz}$. Moreover in a number of applications, the measured signal may contain specific frequencies which should not be attenuated by the regulator. In such cases the system should be in open-loop at these frequencies. Theory about feedback linear controller design was the main topic in the conference paper at Appendix E [Meléndez et al., 2017].

5.2.1 Sensitivity Function Shaping

In order to impose some specific constrains to the controller, we redefine $K(q^{-1})$ polynomials R and S as:

$$(5.8) \qquad R = H_R \cdot R' = H_R \cdot (r'_1 q^{-1} + \ldots + r'_{n_{R'}} q^{-n_{R'}}),$$

$$(5.9) \qquad S = H_S \cdot S' = H_S \cdot (1 + s'_1 q^{-1} + \ldots + s'_{n_{S'}} q^{-n_{S'}}),$$

where $H_S(q^{-1})$ and $H_R(q^{-1})$ represent prespecified fixed parts of the controller, used for example to incorporate the internal model of a disturbance, or to open the loop at some frequencies. Then $S'(q^{-1})$ and $R'(q^{-1})$ are solutions of the Bezout equation defined in Equation (5.7) as:

$$(5.10) \qquad P = P_D \cdot P_{\text{aux}} = (A \cdot H_S) \cdot S' + \left(q^{-d} B \cdot H_R \right) \cdot R',$$

where P_D represents the stable or dominant poles of the plant and P_{aux} are auxiliary poles. The dominant closed loop poles P_D have been chosen equal to those of the secondary path, thus P, P_D, P_{aux}, B, A, d, H_S, and H_R are given.

Equation (5.10) has unique solution for S' and R' of minimal degree for

$$(5.11) \qquad n_P = \deg\{P(q^{-1})\} \leq n_A + n_{H_S} + n_B + n_{H_R} + d - 1,$$

$$(5.12) \qquad n_{S'} = \deg\{S'(q^{-1})\} = n_B + n_{H_R} + d - 1,$$

$$(5.13) \qquad n_{R'} = \deg\{R'(q^{-1})\} = n_A + n_{H_S} - 1.$$

This means that, if not specified otherwise, the order n_P of polynomial $P(q^{-1})$ can be smaller in degree that the right side of the equation, and zeros will be added to pad $P(q^{-1})$ and match the right side. This zeros will be located at $0\,\text{Hz}$ and might cause undesirable conditions in the controller performance as it can be seen in Figure 5.3. Therefore, to overcome this problematic auxiliary real poles can be added, determined by the design requirements, without augmenting

the controller's order. These auxiliary poles are generally chosen as high-frequency real poles in the form:

$$(5.14) \qquad P_{\text{aux}}(q^{-1}) = (1 - p_i q^{-1})^{n_{P_{\text{aux}}}},$$

with $0.05 \leq p_i \leq 0.50$, and $n_{P_{\text{aux}}} \leq n_P - \hat{n}_P$, for $n_P = \max[\deg\{P(q^{-1})\}]$ and $n_{P_{\text{aux}}}$ calculated degree of $P(q^{-1})$. The introduction of auxiliary asymptotically stable real poles $P_{\text{aux}}(q^{-1})$ will cause in general a decrease of the modulus of the sensitivity function.

From Figure 5.1, the closed-loop transfer function between the disturbance $p(t)$ and the system's output $y(t)$, is denominated as *output sensitivity function* (S_{yp}) and is given by

$$(5.15) \qquad S_{yp} = \frac{y(t)}{p(t)} = \frac{A(q^{-1})S(q^{-1})}{P(q^{-1})}.$$

In the same way, the transfer function between the disturbance $p(t)$ and the plant's input $u(t)$ is named *input sensitivity function* (S_{up}) and is given by

$$(5.16) \qquad S_{up} = \frac{u(t)}{p(t)} = -\frac{A(q^{-1})R(q^{-1})}{P(q^{-1})}.$$

As previously stated, in a number of applications, the measured signal may contain specific frequencies which should not be attenuated by the regulator. In such cases the system should be in open-loop at these frequencies. Equation (5.16) can be further developed such that

$$(5.17) \qquad S_{up} = -\frac{A(q^{-1})H_R(q^{-1})R'(q^{-1})}{P(q^{-1})},$$

and therefore in order to make the input sensitivity function zero at a given frequency f, one should introduce a pair of undamped zeros in $H_R(q^{-1})$, i.e.

$$(5.18) \qquad H_R(q^{-1}) = 1 + \beta q^{-1} + q^{-2},$$

with

$$(5.19) \qquad \beta = -2\cos\left(2\pi \frac{f}{f_s}\right).$$

In many cases it is desired that the controller does not react to signals of frequencies close to $0.5 f_s$, corresponding to the Nyquist frequency, where the system's gain is in general very low. In such cases, we have $H_R(q^{-1}) = (1 + \beta q^{-1})^2$.

In active noise control systems, the secondary path gain at $0\,\text{Hz}$ is zero due to the double differentiator behaviour. It is therefore not reasonable to send a control signal at very low frequencies and the system should operate in open-loop at this frequency too. To achieve this, we get $H_R(q^{-1}) = (1 - \beta q^{-1})^2$.

5.2.2 Internal Model Principle

In order to strongly attenuate the two tonal disturbances the Internal Model Principle (IMP) has been used [Landau et al., 2016, Francis and Wonham, 1976]. In short, the IMP states that in order to completely reject a disturbance asymptotically (i.e., in steady state), the controller should include the *disturbance model*, so the designed of our RS controller requires a fixed part H_S to incorporate this disturbance's model. As described in Section 4.3.1, we suppose that $p(t)$ is a deterministic disturbance, so it can be modeled as a signal passing through a discrete filter and they can be modeled by:

$$(5.20) \qquad p(t) = \frac{C_p(q^{-1})}{A_p(q^{-1})}\delta(t),$$

with $\delta(t)$ as a Dirac impulse, and A_p, C_p co-prime polynomials. While in the case of stationary disturbances A_p has roots on the unit circle, in practice the contribution of C_p is weak asymptotically and negligible for steady state analysis in comparison with A_p. Hence, the disturbance's energy is essentially represented by A_p.

As such, from Equations (5.9) and (5.15) we have:

$$(5.21) \qquad y(t) = \frac{A(q^{-1})\left[S'(q^{-1})H_S(q^{-1})\right]}{P(q^{-1})} \cdot \frac{C_p(q^{-1})}{A_p(q^{-1})}\delta(t),$$

where $P(q^{-1})$ is an asymptotically stable polynomial that describes the system's closed loop poles, and where $y(t)$ will converge towards zero asymptotically if and only if the polynomial $S'(q^{-1})$ in the RS controller includes the disturbance's model as in $S'(q^{-1}) = A_p(q^{-1})$.

For the case of tonal disturbances, as stated in Equation 5.18, to make a sensitivity function zero qt q given frequency f it is needed to introduce a pair uf undamped zeros, for this case in H_S, as in

$$(5.22) \qquad H_S(q^{-1}) = 1 + \alpha q^{-1} + q^{-2},$$

again with

$$(5.23) \qquad \alpha = -2\cos\left(2\pi\frac{f}{f_s}\right).$$

Accordingly with the previously stipulated required specifications and constrains for the linear controller design at the beginning of this section, a fixed tonal disturbance compensator was designed using the tools hitherto described. By using the proper values in H_R, we can see in Figure 5.2 the effects of this fixed parts of the controller in its input sensitivity function S_{up}, where at 0 Hz and 1250 Hz we have no gain, and less that 20 dB are achieved after 600 Hz.
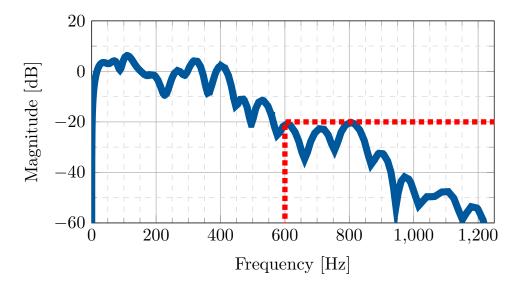
FIGURE 5.2. Input sensitivity function S_{up} of a fixed linear controller.

To display the effects and importance of each fixed component in the controller, Figure 5.3 shows the output sensitivity function S_{yp} evolution, when using just the IMP for defining filters H_S, then adding the corresponding values in H_R to modify S_{up}, and finally adding some auxiliary poles in $P_{\mathrm{aux}}(q^{-1})$ to fulfill the controller requirements.
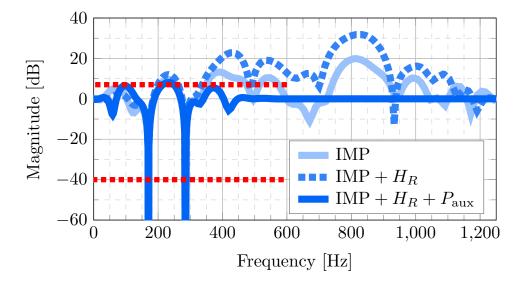
FIGURE 5.3. Evolution of the Output sensitivity function S_{yp} of a fixed linear controller.

5.3 Robust Controller Design

Since the tonal disturbances frequency may vary or is not perfectly known in an ANC system, a robust controller has to be designed to take into account the possible characteristics of the disturbance. Compensator is then designed to attenuate frequencies around $170\,\mathrm{Hz}$ and $285\,\mathrm{Hz}$, with a $\pm 5\,\mathrm{Hz}$ tolerance. Attenuation must be at least of $-18\,\mathrm{dB}$ in these regions and any undesired amplification should be less than $6\,\mathrm{dB}$. Also since the model's gain is low over $600\,\mathrm{Hz}$, and very low damped complex zeros are present in high frequencies, the input sensitivity function's magnitude should be below $-20\,\mathrm{dB}$ at frequencies over $600\,\mathrm{Hz}$, in order to improve robustness with respect to additive uncertainties and to avoid unnecessary control effort. Theory about feedback robust controller design was one of the main topics in the journal paper at Appendix A [Landau et al., 2019c].

5.3.1 Band Stop Filtering

Band Stop Filter (BSF) are used for shaping the output sensitivity function and the input sensitivity function in order to meet the design specifications. Without loss of generality for this explanation we make use of H_{S_i} but same would apply for H_{R_i}. We suppose now a simultaneous introduction of a fixed part H_{S_i}, and a pair of auxiliary poles P_{aux_i} in the form

$$(5.24) \qquad \frac{H_{S_i}}{P_{\mathrm{aux}_i}} = \frac{1 + \alpha_1 q^{-1} + \alpha_2 q^{-2}}{1 + \rho_1 q^{-1} + \rho_2 q^{-2}},$$

as result from the discretization of a continuous-time Band Stop Filter (BSF)

$$(5.25) \qquad F_{\mathrm{BSF}}(s) = \frac{s^2 + 2\zeta_{\mathrm{num}}\omega_0 s + \omega_0^2}{s^2 + 2\zeta_{\mathrm{den}}\omega_0 s + \omega_0^2},$$

using the bilinear transformation

$$(5.26) \qquad s = 2f_s \frac{1 - z^{-1}}{1 + z^{-1}},$$

with the complex variable z^{-1} used to characterize the system's behavior in the frequency domain. This bilinear transformation assures a better approximation of a continuous-time model by a discrete-time model in the frequency domain than the replacement of differentiation by a simple difference, as in $s = (1 - z^{-1})/f_s$.

These filters introduce a strong attenuation, or hole, at the normalized discretized frequency

$$(5.27) \qquad \omega_{\mathrm{BSF}} = 2\arctan\left(\frac{\omega_0}{2f_s}\right),$$

as a function of the ratio between $\zeta_{\text{num}}/\zeta_{\text{den}}$. The attenuation magnitude is described by

$$(5.28) \qquad\qquad M_{\text{BSF}} = 20 \log\left(\frac{\zeta_{\text{num}}}{\zeta_{\text{den}}}\right),$$

with $\zeta_{\text{num}} < \zeta_{\text{den}}$. In practice, the values used to define a BSF are the central normalized frequency f_{BSF}[Hz], the desired attenuation M_{BSF}[dB] at the given frequency, and the damping ζ_{den}, such that:

$$\omega_0 = 2f_s \tan(\pi f_{\text{BSF}}),$$
$$\zeta_{\text{num}} = 10^{\frac{M_{\text{BSF}}}{20}} \zeta_{\text{den}}.$$

The total set of BSF used with H_S for shaping of the output sensitivity functions can be obtained by the sum of 2nd order band-stop filters taking the form:

$$(5.29) \qquad\qquad \text{BSF}_{H_S} = \left.\frac{H_S(z^{-1})}{P_{\text{aux}}(z^{-1})}\right|_{\text{BSF}} = \prod_{i=1}^{n} \frac{H_{S_i}(z^{-1})}{P_{\text{aux}_i}(z^{-1})}.$$

Same characteristics are applied using H_R for shaping of the input sensitivity function in a similar way.

An example of the use if these filters can be seen at Figure 5.4(a), where the different usage of filters is displayed. If used alone, BSF create gains above the desired threshold, so auxiliary poles and fixed parts in H_R are added to correct and improve its performance. In Figure 5.4(b) we can clearly see the attenuation achieved at 170 Hz and 285 Hz, with similar control capabilities around those main frequencies, given them the desired ±5 Hz tolerance or *robustness*.

5.4 Adaptive FIR controller

The adaptive approach uses the Youla-Kučera parametrization of the controller combined with the Internal Model Principle. The basic reference for this approach used in active vibration control is [Landau et al., 2016]. A key aspect of this methodology is the use of aforementioned internal model principle (IMP), defined in Section 5.2.2. Feedback adaptive FIR controller theory was the main topics in the journal paper at Appendix A [Landau et al., 2019c].

5.4.1 Youla-Kučera Parametrization

To build a direct adaptive filter, the Youla-Kučera (YK) parametrization of the controller is used. In this context, one considers a finite impulse response (FIR) filter of the form:

$$(5.30) \qquad\qquad Q(z^{-1}) = q_0 + q_1 z^{-1} + \cdots + q_{n_Q} z^{-n_Q},$$
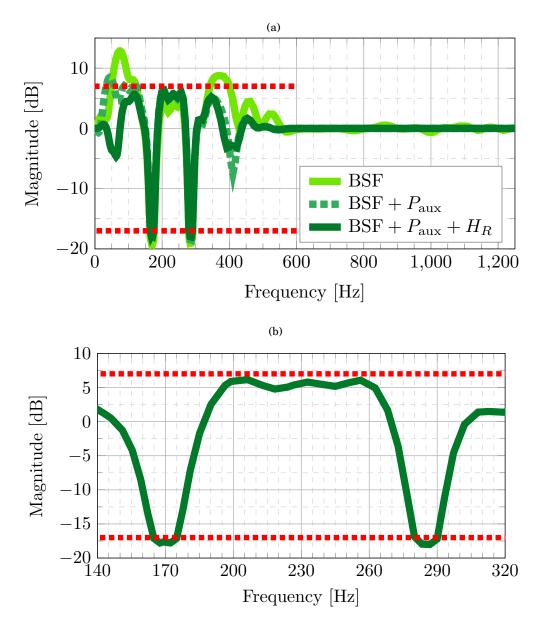
FIGURE 5.4. Output sensitivity function S_{yp}: a) Evolution of the fixed robust controller, and b) final controller zoomed region of interest.

to which is associated the parameters vector:

$$\theta = [q_0 \; q_1 \ldots q_{n_Q}]^T. \tag{5.31}$$

Under Youla-Kučera parametrization or *Q-parametrization*, the equivalent polynomials $R(z^{-1})$ and $S(z^{-1})$ of the controller $K(q^{-1})$ take the form:

$$(5.32) \qquad R(q^{-1}) = R_0 + AQH_{S_0}H_{R_0}$$

$$(5.33) \qquad S(q^{-1}) = S_0 - q^{-d}BQH_{S_0}H_{R_0},$$

with

$$(5.34) \qquad R_0(z^{-1}) = r_0^0 + r_1^0 z^{-1} + \ldots + r_{n_R}^0 z^{-n_{R_0}} = R_0' H_{R_0}$$

$$(5.35) \qquad S_0(z^{-1}) = 1 + s_1^0 z^{-1} + \ldots + s_{n_S}^0 z^{-n_{S_0}} = S_0' H_{S_0},$$

where A, B and d correspond to the identified model of the secondary path, $R_0(z^{-1})$, $S_0(z^{-1})$ are the central controller's polynomials, and H_{S_0}, H_{R_0} are the controller's fixed parts. It is remarkable to stand that under the YK parametrization using a FIR structure for the $Q(z^{-1})$ filter, the closed loop poles defined by the central controller remain unchanged, such that:

$$(5.36) \qquad \begin{aligned} P(q^{-1}) &= AS + q^{-d}BR, \\ &= A[S_0 - q^{-d}BQH_{S_0}H_{R_0}] + q^{-d}B[R_0 + AQH_{S_0}H_{R_0}], \\ &= AS_0 + q^{-d}BR_0. \end{aligned}$$

Using the output sensitivity function S_{yp}, the expression of system residual noise, or output can be written as:

$$(5.37) \qquad \begin{aligned} y(t) &= \frac{S_0 - q^{-d}BH_{S_0}H_{R_0}Q}{P}w(t) \\ &\frac{S_0}{P}w(t) - Q\frac{q^{-d}BH_{S_0}H_{R_0}}{P}w(t), \end{aligned}$$

with the disturbance's observer $w(t)$ defined by

$$(5.38) \qquad w(t) = A(q^{-1})y(t) - q^{-d}B(q^{-1})u(t) = A(q^{-1})p(t).$$

Hence, the objective is to estimate a value for Q such that $y(t)$ is driven to zero. Making the filter Q suitable of an adaptation will have as result the block diagram in Figure 5.5, with the *Parameters Adaptation Algorithm* PAA.

The polynomial Q estimation at time t is denoted:

$$(5.39) \qquad \hat{Q}(t, q^{-1}) = \hat{q}_0(t) + \hat{q}_1(t)q^{-1} + \cdots + \hat{q}_{n_Q}(t)q^{-n_Q},$$

and is characterized by the parameter vector

$$(5.40) \qquad \hat{\theta}^T(t) = [\hat{q}_0(t) \ \hat{q}_1(t) \ldots \hat{q}_{n_Q}(t)],$$
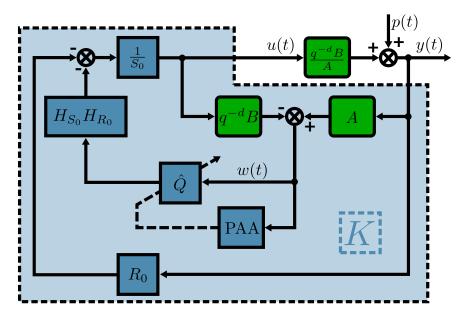
FIGURE 5.5. Adaptive Youla-Kučera parametrization scheme.

where the order n_Q of the polynomial $\hat{Q}$ is related to the disturbance's model denominator order n_{A_p}. As explained in Section 5.2.2 we suppose that $p(t)$ is a deterministic disturbance, like in Equation (5.20). As such we have $n_Q = n_{A_p} - 1$.

Since this is a regulation problem, $y(t)$ is expected to go towards zero and as such, it becomes an *a priori* adaptation error denoted $\varepsilon^0(t+1)$ for a given estimated polynomial $\hat{Q}(t, q^{-1})$, such that:

$$(5.41) \qquad \varepsilon^0(t+1) = \frac{S_0}{P} w(t+1) - \hat{Q}(t) \frac{q^{-d} B^* H_{S_0} H_{R_0}}{P} w(t),$$

with $B(q^{-1}) = q^{-1} B^*(q^{-1})$. In a similar way, one can define an *a posteriori* error as:

$$(5.42) \qquad \varepsilon(t+1) = \frac{S_0}{P} w(t+1) - \hat{Q}(t+1) \frac{q^{-d} B^* H_{S_0} H_{R_0}}{P} w(t),$$

which can be further expressed as

$$(5.43) \qquad \varepsilon(t+1) = [Q - \hat{Q}(t+1)] \frac{q^{-d} B^* H_{S_0} H_{R_0}}{P} w(t) + \eta(t+1)$$

where Q is the unknown optimal filter, and $\eta(t)$ tends asymptotically towards zero [Landau et al., 2011c].

Now, denoting filtered versions of the observer output $w(t)$ as:

(5.44)
$$w_1(t) = \frac{S_0(q^{-1})}{P(q^{-1})} w(t),$$

(5.45)
$$w_2(t) = \frac{q^{-d} B^* H_{R_0} H_{S_0}}{P} w(t),$$

and

(5.46)
$$\varphi^T(t) = [w_2(t) \, w_2(t-1) \ldots w_2(t - n_Q)],$$

Equation (5.43) can be rewritten as:

(5.47)
$$\varepsilon(t+1) = [\theta^T - \hat{\theta}^T(t+1)]\varphi(t) + \eta(t+1),$$

where η goes to zero. From here we can get:

(5.48)
$$\varepsilon(t+1) = w_1(t+1) - \hat{\theta}^T(t+1)\varphi(t),$$

(5.49)
$$\varepsilon^0(t+1) = w_1(t+1) - \hat{\theta}^T(t)\varphi(t).$$

This type of equation allows immediately to develop an adaptation algorithm, so the *Parameters Adaptation Algorithm* PAA is then defined by:

(5.50)
$$\hat{\theta}(t+1) = \hat{\theta}(t) + F(t)\varphi(t)\varepsilon(t+1),$$

with

(5.51)
$$\varepsilon(t+1) = \frac{\varepsilon^0(t+1)}{1 + \varphi^T(t)F(t)\varphi(t)},$$

(5.52)
$$\varepsilon^0(t+1) = w_1(t+1) - \hat{\theta}^T(t)\varphi(t),$$

and the Adaption Gain matrix defined as:

(5.53)
$$F(t+1) = \frac{1}{\lambda_1(t)}\left[F(t) - \frac{F(t)\varphi(t)\varphi^T(t)F(t)}{\frac{\lambda_1(t)}{\lambda_2(t)} + \varphi^T(t)F(t)\varphi(t)} \right]$$

with $0 < \lambda_1(t) \leq 1$, $0 \leq \lambda_2(t) < 2$, $F(0) > 0$; where λ_1 and λ_2 allow to obtain different profiles for the adaptation gain $F(t)$ evolution. Finally the control to be applied is given by:

(5.54)
$$u(t+1) = \frac{-1}{S_0}\left[R_0 y(t+1) + H_{R_0} H_{S_0}\hat{Q}(t+1)w(t+1) \right].$$

In adaptive regulation applications, one uses in general the *constant trace* profile, where $\lambda_1(t)$ and $\lambda_2(t)$ are automatically chosen at each step in order to ensure a constant trace value of the gain matrix $F(t)$, such that:

(5.55)
$$tr\{F(t+1)\} = tr\{F(t)\} = tr\{F(0)\} = nG_0$$

in which n is the number of parameters and G_0 is the initial adaptation gain. Hence, the diagonal matrix $F(0)$ has the form:

(5.56)
$$F(0) = \begin{bmatrix} G_0 & 0 & \dots & 0 \\ 0 & \ddots & \ddots & \vdots \\ \vdots & \ddots & \ddots & 0 \\ 0 & \dots & 0 & G_0 \end{bmatrix}$$

The values of $\lambda_1(t)$ and $\lambda_2(t)$ at each sampling instant are determined from the equation:

(5.57)
$$trF(t+1) = \frac{1}{\lambda_1(t)} tr\left[F(t) - \frac{F(t)\varphi(t)\varphi^T(t)F(t)}{\alpha(t) + \varphi^T(t)F(t)\varphi(t)}\right]$$

fixing the ratio $\alpha(t) = \lambda_1(t)/\lambda_2(t)$. This algorithm can be combined with the *decreasing adaptation gain* or with the *variable forgetting factor* profiles for initialization [Landau et al., 2016]. One switches to the *constant trace algorithm* when the adaptation gain's trace becomes equal or smaller than the assigned constant trace. Algorithms with constant scalar gain can be also implemented with $F(t) = F(0)$, but the results will be less good.

This scheme is implemented on top of the central controller R_0, S_0, which corresponds to the robust controller designed in Section 5.3 from which the BSF filters on S_{yp} have been removed, preserving however the characteristics of S_{up} in high frequencies over 600 Hz for robustness reasons.

5.4.2 U-D Parametrization

The calculation of parameters at each given sample can be highly demanding in terms of the task execution time (TET) of the operation. Additionally, the adaptation gain equation is sensitive to round-off errors. This problem is comprehensively discussed in [Landau et al., 2016, Bierman, 1977], where a U-D factorization has been developed to ensure the numerical robustness of the PAA. To this end, the adaptation gain matrix is rewritten as:

(5.58)
$$F(t) = U(t)\Delta(t)U^T(t),$$

where $U(t)$ is an upper triangular matrix with all diagonal elements equal to 1, and $\Delta(t)$ is a diagonal matrix. By reformulating $F(t)$ using this configuration allows the adaptation gain matrix to remain positive definite so that the rounding errors do not affect the solution significantly.

For a detailed explanation of its use, let

(5.59)
$$G(t) = \Delta(t)V(t),$$

(5.60)
$$V(t) = U(t)^T \varphi_f(t),$$

(5.61)
$$\beta(t) = 1 + V^T(t)G(t),$$

so we are able to define:

(5.62)
$$\Gamma(t) = \frac{U(t)G(t)}{\beta(t)} = \frac{F(t)\varphi_f(t)}{1 + \varphi_f^T(t)F(t)\varphi_f(t)}.$$

5.5 Comparative Results

Using the test bench described in Chapter 3 to apply the controllers designed in Sections 5.3 and 5.4 based on the model identified in Chapter 4, some real-time experiments were carried out in order to compare the different controllers performances.

To do so, we carried out a set of different tests allowing us explode the adaptive capabilities of the YK parametrization, but remaining in a fair ground for the fixed robust controller to enact.

5.5.1 Interference test

By interference, one refers to the physical effect occurring when two distinct waves with very close frequencies act together, creating periodic outbursts in the resulting wave magnitude. The interference test protocol is as follows:

- For 1 s, the system operates in open loop and without any disturbance in order to get a reference of the existing surrounding ambient noise.

- From 1 s to 10 s, the test bench works in open loop, in the presence of two pairs of sinusoidal noise disturbances located at 170 Hz and 170.5 Hz, and 285 Hz and 285.5 Hz respectively.

- At 10 s, the loop is closed and the controller begins to counteract the disturbance effect.

- The frequencies of the four signals are then increased at 21 s by 10 Hz. The corresponding new values are 180 Hz and 180.5 Hz for the first pair and 295 Hz and 295.5 Hz for the second pair, getting out of the attenuation regions of the robust controller.

Figure 5.6 shows the robust controller's performance for the interference experiment in a time domain, with delimited region for each of the four steps in the protocol. As long as the disturbance frequencies are in the region of designed operation, a residual noise's global attenuation of 39.86 dB is obtained (between 10 s and 21 s). After 21 s, since the disturbance's frequencies are
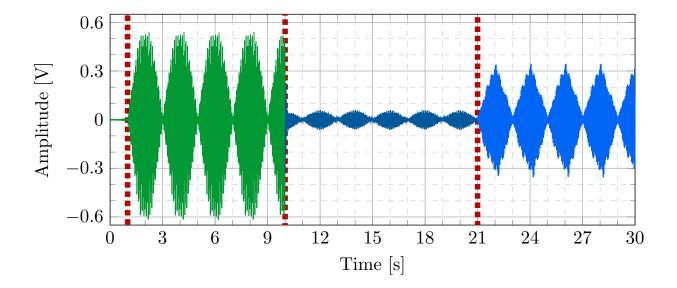
FIGURE 5.6. Acoustic interference attenuation using a robust controller.

outside the region of designed operation, the performance is unsatisfactory achieving a global attenuation of only 7.94 dB.

Figure 5.7 presents the results for a similar test using an adaptive controller. The number of adjustable parameters in the Q-filter is 4 ($n_Q = 3$) and an adaptation algorithm with *constant trace adaptation gain* is used, where the value for adaptation gain trace used was: $trF = 0.03 \cdot (n_Q + 1)$. It can be seen that after a negligible transient, a much better attenuation is obtained with respect to the robust controller between 10 s and 21 s. The global attenuation obtained is 70.56 dB. Excellent levels of attenuation are also obtained once the disturbances frequencies move away by 10 Hz, achieving a global attenuation of 67.65 dB, with a negligible adaptation transient. It is remarkable to state that the filter Q order is not directly related to the controller performance, and tests using $n_Q = 7$, or 8 adjustable parameter, did not improve the performance.

Figure 5.8 displays the evolution of each Q-parameter with respect to time. From 0 s to 10 s, all the parameters have values equal to zero since the controller is not working yet. Once the loop is closed, the Q-parameters take almost instantly stable mean values. At 21 s, the change in frequencies leads to a quick adaptation towards the new values.

5.5.2 Step changes test

In this experiment, step changes in the frequencies of a pair of tonal noise disturbances are considered, starting from their nominal values of 170 Hz and 285 Hz, with steps in the frequencies of ±10 Hz. The system is operated in open loop from 0 s to 1 s as reference for surrounding external noises. here, two simultaneous signals of constant frequency act as perturbations. After a given amount of time both frequencies are decreased or increased a determined value and remain

91
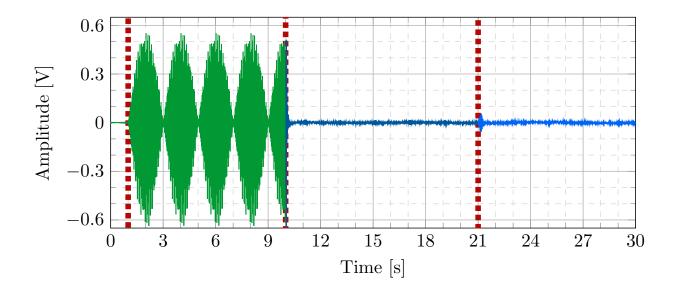
FIGURE 5.7. Acoustic interference attenuation using an adaptive controller with YK parametrization.
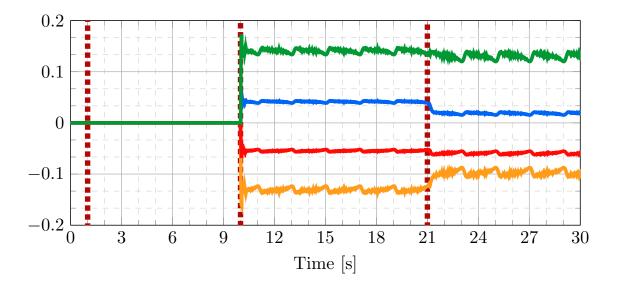
FIGURE 5.8. Parameters evolution for acoustic interference test using an adaptive controller with YK parametrization.

at those new constant frequencies for a period of time. At 1 s the system begin with both the controller and disturbances signals in closed loop with perturbations of 170 Hz and 285 Hz as nominal frequencies. After the next step, both signals are decreased −10 Hz. In the next span both perturbations go back to their nominal frequencies. At next step the signals have an increase of 10 Hz. Finally for the final period, disturbance's frequencies have once again the nominal

values. In order, the protocol for this test and corresponding step frequencies are:

- Reference for ambient noise, no disturbances nor control

- Nominal disturbances, $170\,\mathrm{Hz} + 285\,\mathrm{Hz}$

- $-10\,\mathrm{Hz}$ disturbances, $160\,\mathrm{Hz} + 275\,\mathrm{Hz}$

- Nominal disturbances, $170\,\mathrm{Hz} + 285\,\mathrm{Hz}$

- $+10\,\mathrm{Hz}$ disturbances, $180\,\mathrm{Hz} + 295\,\mathrm{Hz}$

- Nominal disturbances, $170\,\mathrm{Hz} + 285\,\mathrm{Hz}$

Figure 5.9 displays the robust controller performance. When the disturbances frequencies are inside the designed region of the controller, attenuation levels are satisfactory. However for $-10\,\mathrm{Hz}$ and $+10\,\mathrm{Hz}$ steps, since one operates outside the designed regions of attenuation, the performance is unsatisfactory.
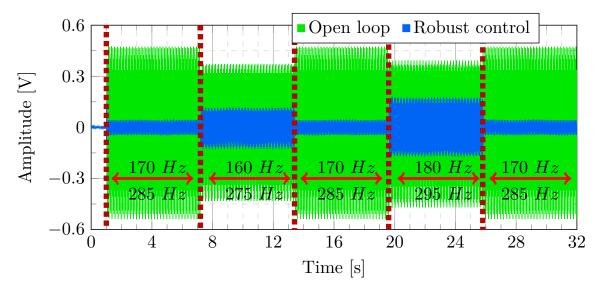
FIGURE 5.9. Step changes in frequencies using the robust controller. Residual noise: open loop vs closed loop.

The performance of the adaptive controller is illustrated in Fig. 5.10. The performance is almost the same for all frequencies values and the residual noise is close to the ambient noise. Adaptation transients are visible but very short. The same number of adjustable parameters and same adaptation gain as in the previous experiments have been used. Evolution of the Q-parameters is shown in Fig. 5.11.

Sinusoidal disturbances with continuously time- varying frequency
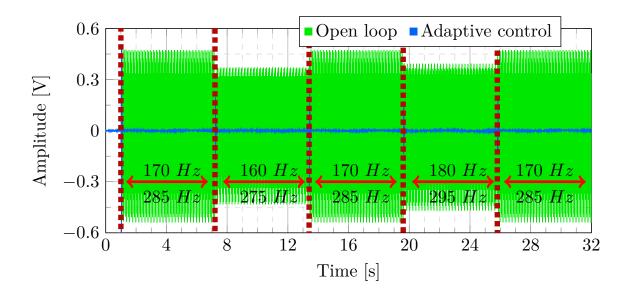
FIGURE 5.10. Step changes in frequencies using the adaptive controller with YK parametrization.
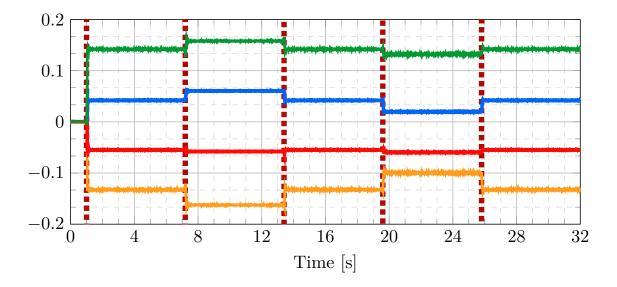
FIGURE 5.11. Parameters evolution for step changes in frequencies test using an adaptive controller with YK parametrization.

5.5.3 Continuously time-varying frequency test

In this experiment, a couple of tonal noise disturbances located at 160 Hz and 275 Hz are first applied to the system from 1 s to 6 s. Then, their frequencies linearly increase until they reach the values of 180 Hz and 295 Hz correspondingly at 27 s, after which their frequencies remain

constant until 32 s. A protocol for the test can be described as:

- Reference for ambient noise, no disturbances nor control until 1 s,

- Nominal disturbances $-10\,\mathrm{Hz}$, $160\,\mathrm{Hz} + 275\,\mathrm{Hz}$ from 1 s to 6 s,

- Linear increase in frequencies 6 s to 27 s

- Nominal disturbances $+10\,\mathrm{Hz}$, $180\,\mathrm{Hz} + 295\,\mathrm{Hz}$ from 27 s to 32 s.

Figure 5.12 displays a comparison between the system's residual noise when it is operated in open loop and in closed loop using the robust controller. As the frequencies move within the designed regions, a significant attenuation is obtained. However outside this zone, the performance is not satisfactory.
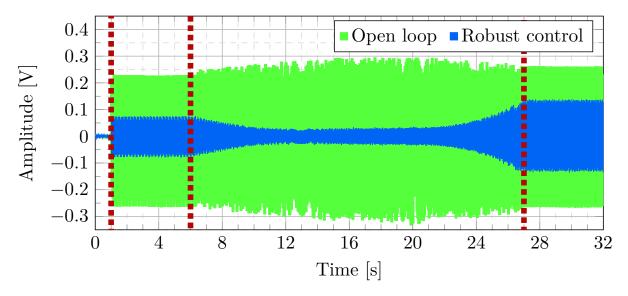
FIGURE 5.12. Residual noise in open loop vs closed loop using a robust controller under the effect of tonal disturbances with variable frequencies.

Correspondingly, Fig. 5.13 displays the residual noise in open loop operation and with the adaptive controller. Levels of attenuation achieved are globally much better.

The residual noise is comparable with the ambient noise measured between 0 s and 1 s. The Q-parameters evolution is shown in Fig. 5.14.

5.6 Concluding Remarks

This chapter has shown that if the frequencies variation regions of multiple tonal noise disturbances are known and limited, an efficient robust feedback controller can be designed. Adding an
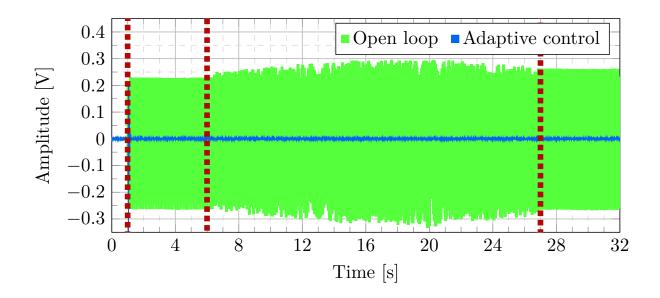
FIGURE 5.13. Residual noise in open loop vs closed loop using the adaptive controller with YK parametrization under the effect of tonal disturbances with variable frequencies.
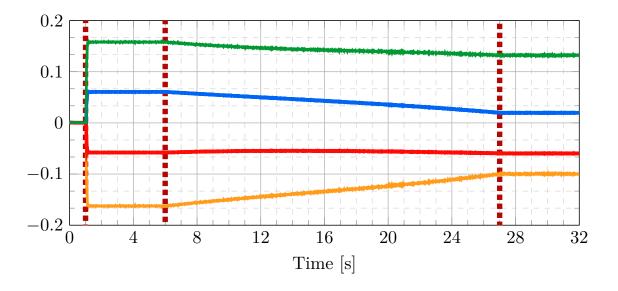
FIGURE 5.14. Parameters evolution for the tonal disturbances with variable frequencies test using an adaptive controller with YK parametrization.

adaptation feedback loop drastically enhances the performance of a robust controller in terms of achieved attenuation and expansion of the regions of attenuation in the frequency domain. It has been shown that techniques developed in the context of active vibration control [Landau et al., 2016] can be successfully used for robust and adaptive feedback attenuation of multiple narrow

band noise disturbances in ducts. The effective implementation of these techniques should take into account the identified model characteristics of the compensation path and design guidelines have been provided.

Part III

Adaptive Feedforward Disturbance Rejection

FEEDFORWARD CONFIGURATION

In the case of presence of broadband disturbances a Feedforward approach is proposed for the system. After undesirable conditions were found in the first test bench configuration, two more setups are proposed to enable a better performance of a control system working in a feedforward approach. Brief introduction about state of the art behind our denominated Feedforward approach is given, followed by a detailed explanation about its theory. These different approaches are described and then compared in a theoretical perspective. Using the same approaches, different parametrization of the controller is proposed using the denominated Youla-Kučera parametrization. The theory and use of Infinite Impulse Response compensators, as well as the simplified option using a Finite Impulse Response compensator are addressed. Finally a comparison of all the algorithms proposed is done in the test bench, and relevant results are discussed.

6.1   Test Bench Configurations

Active control is particularly dedicated to attenuate low frequency noise, and due to a undesired condition in the secondary path identified for the first test bench configuration, more specifically a zero located at 315 Hz, new configurations for the test bench had to be proposed in order to work under a feedforward configuration.

The effects of this undesired zero present in the secondary path model for the first test bench configuration are such that the controller won't have enough energy to perform any attenuation at that specific frequency and those around it. This effects are close to partially open the loop at those frequencies, leaving behind a region where the controller won't perform, thus being ineffective for a wide or broad brand attenuation attempt.

Nevertheless, this new second configuration brought a new problematic. Since the system to performs with a feedforward schema, according with the theory, pure delays in our identified

secondary path model should be less or equal than those delays found in the primary path; otherwise some conditions required for the proper application of theories won't be fulfilled.
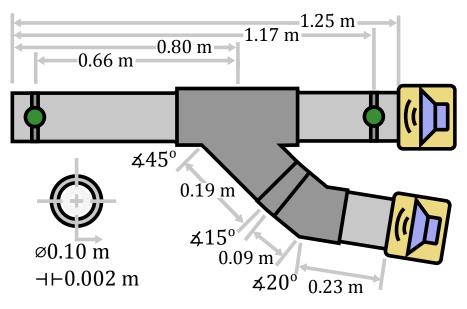
6.1.1   Second Test Bench Configuration

It was found that, since the test bench uses a loudspeaker as disturbance's actuator, its diaphragm acts as a passive damper [Baz, 2018, Krysinski and Malburet, 2008] for the control signal produced at the controller loudspeaker. In this disposition of the experimental setting, an unwanted reflection phenomenon is created, which lead to the presence of low damped complex zeros, where the position of these zeros in the frequency domain depends upon the geometry of the system. This was related to a mechanical engineering term defined as *effective length*, and a deeper explanation of the physics describing the phenomenon can be found in [Stanfield and Skaves, 2012]. This unwanted zeros introduced a series of inconvenient that may not appear in a real system, since disturbance sources are not configured to display passive dampening in a real environment.

As it can be seen in Figures 6.1 and 6.2, a second geometry was proposed for the test bench in order to modify the length between the control actuator and the passive damper located in the disturbance loudspeaker, named *second test bench configuration*. By shortening the duct connecting the disturbance's actuator with the rest of the system, and changing the angles used for connecting the control loudspeaker the rest of the system, we were able to modify this so called *effective length* and alter the undesired conditions present in our original design, thus displacing the position in the frequency domain of the zeros created by the unwanted passive damper.

An *effective length* between two points in a system includes the length of straight sections of duct, but it also contemplates the addition of equivalent lengths corresponding to all the fittings and couplings present to connect those straight sections, whose most of the time are longer than the real lengths due to the additional friction and changes of direction and pressure created in the flux of air. In this way, the dampening effect of the disturbance speaker's diaphragm, coupled with the control loudspeaker at that specific effective length gave as result the undesired zero in the identified secondary path for the first configuration.

Once again the process for identification of the different path's transfer functions was carried on and new identified models were estimated. Results and images of the frequency response of these paths can be found at 4.6.2. As a comparison between the first and second test bench configurations, Figure 6.1.1 displays secondary paths identified for each configuration. Here we can see the zero located at 315 Hz in the first configuration, and how this model differs from the second configuration model, where these low damped zeros are no longer present. This second configuration and its following identification of models brought as result a region in the frequency domain up to 450 Hz without interruptions due to zeros in the model of the secondary path, allowing us to have a control region roughly from 70 Hz to 450 Hz.

FIGURE 6.1. Second experimental test bench configuration.

FIGURE 6.2. Photo of test bench's second configuration.

Results of experiments performed on this second configuration of the test bench are not explicitly presented in this thesis, and can be found in Appendix C and Appendix D [Airimiţoaie et al., 2018, Landau et al., 2019a]. Even if the results and performance of the system were according to expectations, it was found that while this configuration managed to solve the problem of the zeros present due to unwanted dampening effects, it violates the conditions for *perfect matching* [Landau et al., 2016].
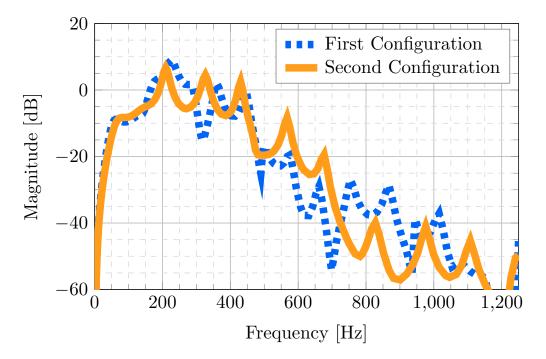
FIGURE 6.3. Identified secondary path for first and second test bench configurations.

6.1.2 Third Test Bench Configuration

To overcome the problematic regarding the model delay's orders and the fact that the perfect match conditions were not fulfilled, a third test bench configuration was proposed and presented as in 3.2.3. The new geometry of the system satisfy the perfect match conditions, but presents again a pair of low damped zeros located near 300 Hz, leaving a region for attenuation from 70 Hz to 270 Hz approximately.

Accordingly with the nomenclature previously stipulated in Figure 3.4, the updated schema for this third configuration can be seen in Figure 6.4. Here the residual noise's microphone located at (3) was displaced nearer the disturbance speaker (1). Similarly, sections of pipes connecting the main body with the control speaker at (2) were shortened and the angles connecting the sections were modified. The third and final configuration of the test bench can be seen in Figure 6.6, and its dimensions are described in Figure 6.5.

As a comparison between all the three different test bench configurations, Figure 6.7 shows the identified secondary paths for each of them, where we can a similar presence of a zero located around 300 Hz in the first and last configurations, nevertheless this last setup of the test bench allows us to have higher gain in frequencies between 50 Hz and 150 Hz.
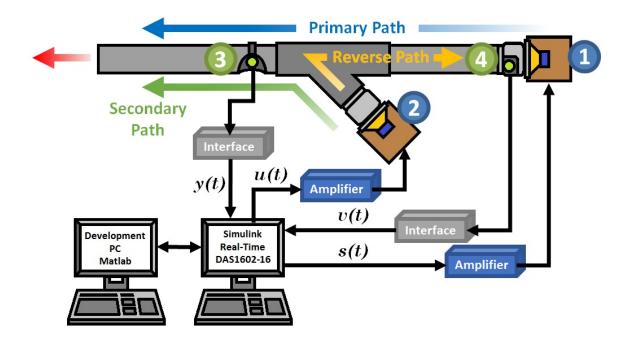
FIGURE 6.4. Schema of test bench's feedforward configuration.
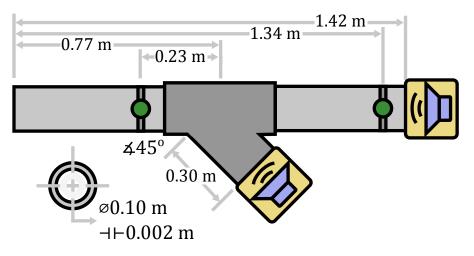
FIGURE 6.5. Third experimental test bench configuration.

6.2 Introduction to Adaptive Feedforward Noise Attenuation

Adaptive feedforward control for broadband disturbance compensation is widely used when a well correlated signal with the disturbance (image of the disturbance) is available [Kuo and Morgan, 1999, Elliott and Sutton, 1996, Elliott and Nelson, 1994]. However, in many systems there is a positive physical coupling between the feedforward compensation system and the disturbance's image measurement, which often leads to a condition of instability in the system.
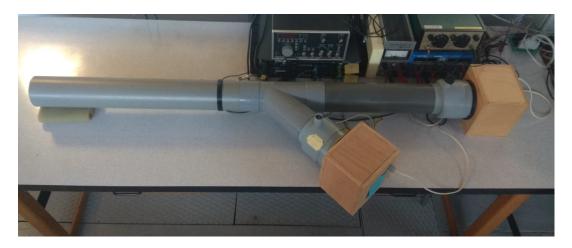
FIGURE 6.6. Photo of test bench's third configuration.
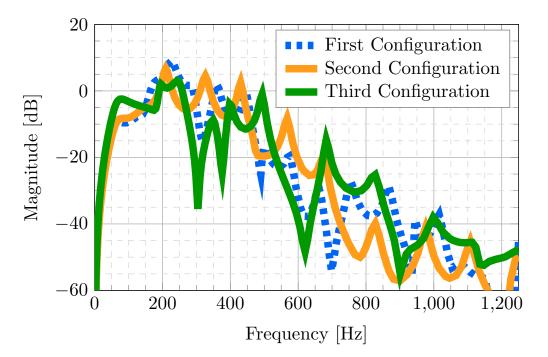
FIGURE 6.7. Identified secondary path for first, second and third test bench configurations.

About this inherent positive feedback, the adaptive feedforward compensator should counteract and minimize the disturbance effects while simultaneously assuring the stability related to the internal positive feedback loop [Jacobson et al., 2001, Kuo and Morgan, 1996].

Starting with [Amara et al., 1999b] adaptive feedback noise control emerged as an efficient solution for canceling single or multiple tonal disturbances [Amara et al., 1999a] taking advantage of the internal model principle and the Youla-Kučera parametrization of the feedback controller

[Landau et al., 2019c, Meléndez et al., 2017]. Nevertheless, the efficient use of this so called feedback approach for attenuation of broad-band noise is limited by the Bode integral. Giving the additional complexity that is inherent in the broadband disturbances, regarding unknown and variable characteristics, an adaptive approach is required. Therefore one can say that the adaptive feedforward noise compensation is particularly dedicated to the attenuation of broad-band noise with unknown and time varying characteristics in this cases.

A major component of an adaptive feedforward compensator is the PAA. In ANC field, the first algorithm used was the so called LMS [Widrow and Stearns, 1985] derived from a local minimization of a quadratic criterion in terms of the residual noise. Many contributions have been done on the properties analysis of this algorithm and the improvement of it. One of the ways for improving the adaptation is filtering of the regressor vector, giving as results the FuLMS [Eriksson, 1991b, Wang and Ren, 2003, Fraanje et al., 1999], which seems to be the most used algorithm in recent publications [Xie et al., 2016, Zhu et al., 2012].

For the analysis of these algorithms in the presence of an internal positive feedback an attempt is made in [Wang and Ren, 2003] where the asymptotic convergence in a stochastic environment of the so called *Filtered-U Least Mean Squares* (FuLMS) algorithm in this context is discussed. Further results on the same direction can be found in [Fraanje et al., 1999]. The authors use Ljung's ODE method [Ljung and Söderström, 1983] for the case of a scalar vanishing adaptation gain. Unfortunately, this is not enough because nothing is said about the system stability with respect to initial conditions and when a non vanishing adaptation gain is used in order to keep the controller capabilities of adaptation. The authors have assumed that the positive feedback does not destabilize the system which is not a realistic assumption.

A different approach emerged in the area of ANC, namely the adaptation algorithms design starting from a stability point of view and taking into account from the beginning an internal positive feedback. A first reference in ANC for a stability approach in the presence of an internal positive feedback is [Johnson, 1976]. Unfortunately, the results applicability is very limited since it is assumed that the secondary path has a simple positive gain, or it is characterized by a SPR transfer function, which is a unrealistic hypothesis. So then the study is based in the research done in AVC [Landau et al., 2011a], where it is provided a full synthesis procedure for asymptotically stable adaptation algorithms using IIR feedforward compensators in the presence of an internal feedback coupling. These algorithms can be used also in ANC as it will be shown throughout this work. It is interesting to note that most of the algorithms used for the adaptive feedforward compensation can be viewed as particular approximations of the algorithms derived from stability considerations.

6.3 Adaptive Feedforward Compensators Basic Theory

First, as it was done for the Feedback approach in Chapter 5, the primary path is characterized by the asymptotically stable transfer operator:

$$(6.1) \qquad D(q^{-1}) = \frac{q^{-d_D} B_D(q^{-1})}{A_D(q^{-1})},$$

where d_D corresponds to the pure delay in sample times for the primary path and

$$(6.2) \qquad B_D(q^{-1}) = b_1^D q^{-1} + \ldots + b_{n_{B_D}}^D q^{-n_{B_D}},$$

$$(6.3) \qquad A_D(q^{-1}) = 1 + a_1^D q^{-1} + \ldots + a_{n_{A_D}}^D q^{-n_{A_D}}.$$

In a similar way, the secondary path is characterized by the asymptotically stable transfer operator:

$$(6.4) \qquad G(q^{-1}) = \frac{q^{-d_G} B_G(q^{-1})}{A_G(q^{-1})},$$

where d_G corresponds to the pure delay in sample times for the secondary path and

$$(6.5) \qquad B_G(q^{-1}) = b_1^G q^{-1} + \ldots + b_{n_{B_G}}^G q^{-n_{B_G}} = q^{-1} B_G^*(q^{-1}),$$

$$(6.6) \qquad A_G(q^{-1}) = 1 + a_1^G q^{-1} + \ldots + a_{n_{A_G}}^G q^{-n_{A_G}}.$$

This can be represented in a feedforward diagram as in Figure 6.8,
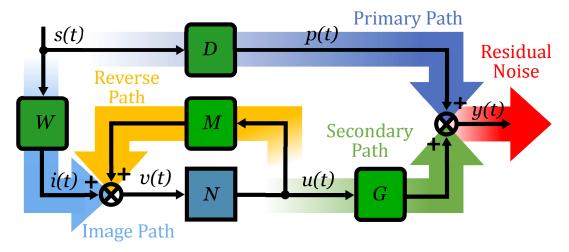
FIGURE 6.8. Feedforward control scheme.

where D represents the primary path transfer function and G denotes the secondary path of our system. In this configuration, the block N is used for the feedforward controller. Moreover, we found that W characterize the transfer function between the disturbance's speaker and the image's microphone, located in between (1) and (4) in Figure 6.4, and than the transfer function M describes the positive feedback coupling called reverse path.

In a similar fashion to a feedback configuration, $y(t)$ is the system's residual noise measured by the microphone located at (3) in Figure 6.4; $u(t)$ corresponds to the control signal sent to the controller speaker in (2), $s(t)$ is the disturbance signal sent to the disturbance's speaker in (1). Additionally to the signals seen in a feedback diagram, we find the measurements $v(t)$ used to get the signal correlated with the disturbance's image $i(t)$ which is inherently bias by the positive internal loop created by the control signal.

6.3.1 Feedforward Compensator Design

Since the measurements required for the feedforward configuration call for an image of the disturbance, it is acquired by the microphone located at (4) in Figure 6.4, nevertheless the control signal will also be captured by this measures as an indirect effect, and the resulting measurements are a sum of the the disturbance and the control signal. This phenomenon is denoted as a *positive internal feedback loop* and is an undesired condition than can cause instabilities in these systems and needs to be taken into account in the controller design stage. The feedforward compensator's output coupling with the measurement $v(t)$ through is denoted by M. As indicated in Figure 6.8, this coupling is a positive feedback.

Similarly to the primary and secondary paths, the positive feedback coupling is characterized by the asymptotically stable transfer operator:

$$(6.7) \qquad M(q^{-1}) = \frac{q^{-d_M} B_M(q^{-1})}{A_M(q^{-1})},$$

where d_M corresponds to the pure delay in sample times for the reverse path and,

$$(6.8) \qquad B_M(q^{-1}) = b_1^M q^{-1} + \ldots + b_{n_{B_M}}^M q^{-n_{B_M}} = q^{-1} B_M^*(q^{-1}),$$

$$(6.9) \qquad A_M(q^{-1}) = 1 + a_1^M q^{-1} + \ldots + a_{n_{A_M}}^M q^{-n_{A_M}}.$$

The objective is to estimate and adapt the feedforward compensator's parameters N, such that the measured residual noise be minimized in the sense of a certain criterion. The optimal unknown IIR feedforward filter is defined by:

$$(6.10) \qquad N(q^{-1}) = \frac{R(q^{-1})}{S(q^{-1})},$$

where the corresponding polynomials are defined as:

$$(6.11) \qquad R(q^{-1}) = r_0 + r_1 q^{-1} + \ldots + r_{n_R} q^{-n_R},$$

$$(6.12) \qquad S(q^{-1}) = 1 + s_1 q^{-1} + \ldots + s_{n_S} q^{-n_S} = 1 + q^{-1} S^*(q^{-1}).$$

Accordingly with Figure 6.9, the estimated compensator is denoted by $\hat{N}(q^{-1})$. It is defined as $\hat{N}(\hat{\theta}, q^{-1})$ when it is a linear filter with constant coefficients; and $\hat{N}(t, q^{-1})$ during estimation (adaptation) of its parameters. FIR compensators are obtained by taking $S = 1$ (i.e. $s_i = 0$, $\forall i = 1 : n_S$).
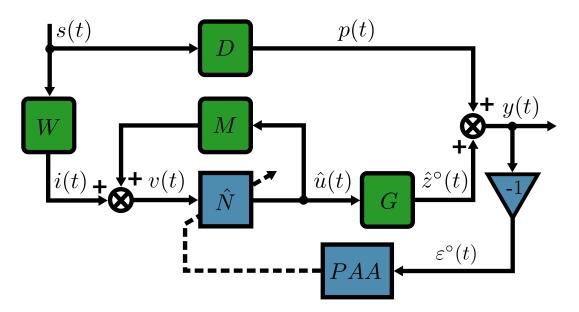
FIGURE 6.9. Feedforward control scheme with PAA.

The feedforward compensator's input is denoted by $v(t)$, and it corresponds to a sum between the disturbance image in the absence of compensation, and of the positive feedback path's output. When there is no compensation, meaning to operate in a open-loop configuration, we have $v(t) = i(t)$.

We now remember that in adaptive control and estimation theory, a predicted output at a given time t can be computed either on basis of the current parameter estimations, named *a posteriori*; or on the basis of previous parameter estimations, denominated *a priori*. The *a posteriori* output of the feedforward compensator, which is the control signal applied to the secondary path, is denoted by $\hat{u}(t+1) = \hat{u}(t+1|\hat{\theta}(t+1))$. The input-output relationship for the estimated feedforward compensator is given by an equation of the *a priori* output, such that:

$$\hat{u}^{\circ}(t+1) = \hat{u}(t+1|\hat{\theta}(t)) = \hat{R}(t, q^{-1})v(t+1) - \hat{S}^{*}(t, q^{-1})\hat{u}(t)$$

(6.13)
$$= \hat{\theta}^{T}(t)\varphi_0(t) = \left[\hat{\theta}_R^{T}(t), \hat{\theta}_S^{T}(t)\right]\begin{bmatrix}\varphi_v(t)\\\varphi_{\hat{u}}(t)\end{bmatrix},$$

where the controller's estimated parameters vector $\hat{\theta}(t)$ and $\varphi_0(t)$ are defined as

(6.14)
$$\hat{\theta}^{T}(t) = [\hat{r}_1(t), \ldots, \hat{r}_{n_R}(t), \hat{s}_0(t), \ldots, \hat{s}_{n_S}(t)] = [\hat{\theta}_R^{T}(t), \hat{\theta}_S^{T}(t)],$$

(6.15)
$$\varphi_0^{T}(t) = [v(t+1), \ldots, v(t-n_R+1), -\hat{u}(t), \ldots, -\hat{u}(t-n_S+1)]$$
$$= [\varphi_v^{T}(t+1), \varphi_{\hat{u}}^{T}(t)],$$

and $\hat{u}(t), \hat{u}(t-1), \ldots$ are the *a posteriori* outputs of the feedforward compensator generated by

(6.16)
$$\hat{u}(t) = \hat{u}(t|\hat{\theta}(t)) = \hat{\theta}^{T}(t)\varphi_0(t-1),$$

and where $v(t+1)$, $v(t)$, ... are the measurements provided by the microphone located at (4) in Figure 6.4, since $v(t+1)$ is available before adaptation of parameters starts at time $t+1$.

The *a priori* output of the secondary path will be denoted $\hat{z}°(t+1)$:

$$(6.17) \qquad \hat{z}°(t+1) = \hat{z}(t+1|\hat{\theta}(t)) = \frac{q^{-d_G}B_G^*(q^{-1})}{A_G(q^{-1})}\hat{u}(t),$$

meanwhile the *a posteriori* unmeasurable value of the secondary path's output is denoted by:

$$(6.18) \qquad \hat{z}(t+1) = \hat{z}(t+1|\hat{\theta}(t+1)) = \frac{q^{-d_G}B_G(q^{-1})}{A_G(q^{-1})}\hat{u}(t+1) = G(q^{-1})\hat{u}(t).$$

The measured primary signal, also called reference, satisfies the equation:

$$(6.19) \qquad v(t+1) = \frac{q^{-d_M}B_M^*(q^{-1})}{A_M(q^{-1})}\hat{u}(t) + i(t+1),$$

while the residual error measured at (3) in 6.4, is described by the equation:

$$(6.20) \qquad y(t+1) = p(t+1) + \hat{z}°(t+1),$$

so the *a priori* adaptation error can be defined as

$$(6.21) \qquad \varepsilon°(t+1) = -y(t+1) = -p(t+1) - \hat{z}°(t+1).$$

Finally, the calculated *a posteriori* adaptation error, in this case similar to the residual error, will be given by:

$$(6.22) \qquad \varepsilon(t+1) = \varepsilon(t+1|\hat{\theta}(t+1)) = -p(t+1) - \hat{z}(t+1).$$

The development of a PAA for estimating in real-time the parameter's vector $\hat{\theta}$ assumes that:

- A *perfect matching condition* can be satisfied and there exist a set of values θ for the feedforward filter $N(q^{-1})$, such that:

$$(6.23) \qquad \frac{N(q^{-1})W(q^{-1})}{1 - N(q^{-1})M(q^{-1})}G(q^{-1}) = -D(q^{-1})$$

- The characteristic polynomial $P_{\text{int}}(q^{-1})$ of the internal feedback loop,

$$(6.24) \qquad P_{\text{int}}(q^{-1}) = A_M(q^{-1})S(q^{-1}) - q^{-d_M}B_M(q^{-1})R(q^{-1}),$$

is a Hurwitz polynomial.

Now we can state that the parameter adaptation algorithm's (PAA) objective will be then to allow the compensator $\hat{N}(q^{-1},\hat{\theta}(t))$ to approach the optimal compensator $N(q^{-1})$, at least in the frequency range of interest but assuring the asymptotic stability of the internal loop.

From the user point of view and taking into account the type of adaptive compensation system's operation, one has to consider two approaches for the adaptive schemes:

- *Adaptive* operation. The adaptation is performed continuously with a non-vanishing adaptation gain and the feedforward compensator is updated at each sampling.

- *Self-tuning* operation. The adaptation procedure starts either on demand or when the performance is unsatisfactory. A vanishing adaptation gain is used.

In this chapter, only the adaptive operation will be considered in the experimental evaluation

6.3.2 Parameter Adaptation Algorithm

As seen in Chapter 5, a general formulation for the parameter adaptation algorithm (PAA) can be described by:

$$\hat{\theta}(t+1) = \hat{\theta}(t) + F(t)\varphi(t)\varepsilon(t+1), \tag{6.25}$$

$$\varepsilon(t+1) = \frac{\varepsilon^{\circ}(t+1)}{1 + \varphi^T(t)F(t)\varphi(t)}, \tag{6.26}$$

$$F(t+1) = \frac{1}{\lambda_1(t)}\left[F(t) - \frac{F(t)\varphi(t)\varphi^T(t)F(t)}{\frac{\lambda_1(t)}{\lambda_2(t)} + \varphi^T(t)F(t)\varphi(t)}\right], \tag{6.27}$$

$$1 \geq \lambda_1(t) > 0, \quad 0 \leq \lambda_2(t) < 2, \quad F(0) > 0, \tag{6.28}$$

$$\varphi(t) = L\varphi_0(t) \tag{6.29}$$

where L is a filter defined by the system parameters, and $\lambda_1(t)$ and $\lambda_2(t)$ allow to obtain various profiles for the adaptation gain matrix $F(t)$. Four cases are of interest:

- *Constant trace* profile. $\lambda_1(t)$ and $\lambda_2(t)$ are adjusted continuously to maintain constant the trace of the adaptation gain matrix. This allows to move in the optimal direction but maintaining the adaptation capabilities. Nevertheless, for accelerating the adaptation transient it may be useful to use a larger adaptation gain transiently.

- *Decreasing adaptation gain*. With $\lambda_1 = 1$ and $\lambda_2 = 1$, a self-tuning regime is defined. Can also be used for initialization of the constant trace profile.

- *Variable forgetting factor*. This option can be also used for initialization of the constant trace algorithm. The difference is that in this option $\lambda_1(0) < 1$ but it will tend asymptotically to 1. This allows to get transiently a higher adaptation gain than the one used in the constant trace algorithm.

- *Constant scalar adaptation gain*. This is obtained by taking $F(t) = \gamma I$ where I is the identity matrix, and γ is a chosen constant value. This approach gives a scalar adaptation gain.

As stated before, in order to initialize the algorithms, it is often the combined use of *decreasing gain* with the *constant trace*, allowing the adaptation process to have a larger gain at beginning. Once the adaptation gain matrix's trace tr$[F(t)]$ reaches the specific constant trace's value desired,

λ_1 and λ_2 switches to a constant trace profile. Same can be said about an initialization using a *variable forgetting factor* instead of decreasing adaptation gain.

As previously, the adaptation gain matrix evolution is given by defined in Equation (6.27). For the *decreasing gain* profile one chooses $\lambda_1(t) = \lambda_1 = 1$ and $\lambda_2(t) = \lambda_2 = 1$; meanwhile for the *variable forgetting factor* profile we define $\lambda_2(t) = \lambda_2 = 1$, $\lambda_1(t) = \lambda_0\lambda_1(t-1) + 1 - \lambda_0$ and $0 < \lambda_0 < 1$, with typical values being $\lambda_1(0) = 0.95$ to 0.99, and $\lambda_0 = 0.95$ to 0.99. The difference with respect to the *decreasing gain* profile is that the maximum value for adaptation gain occurs not at instant $t = 0$, but after a certain horizon related to the particular values of $\lambda_1(0)$, λ_0 and the number of parameters to adapt.

Finally, in order to maintain a *constant the trace* profile, the values of $\lambda_1(t)$ and $\lambda_2(t)$ of the adaptation gain matrix $F(t)$ are determined from the equation:

$$(6.30) \qquad \operatorname{tr}[F(t+1)] = \frac{1}{\lambda_1(t)}\operatorname{tr}\left[F(t) - \frac{F(t)\varphi(t)\varphi^T(t)F(t)}{\alpha + \varphi^T(t)F(t)\varphi(t)}\right]$$

fixing the ratio $\alpha = \lambda_1(t)/\lambda_2(t)$.

Moreover, by taking $F(t) = \gamma I$, where I is the identity matrix, one gets a scalar adaptation gain as in Table 6.1 and 6.2. The equation (6.25) for updating the parameter vector then becomes:

$$(6.31) \qquad \hat{\theta}(t+1) = \hat{\theta}(t) + \gamma\varphi(t)\frac{\varepsilon^\circ(t+1)}{1 + \gamma\varphi^T(t)\varphi(t)}.$$

When using a scalar adaptation gain, it can be seen that for very small values of γ one can approximate the above equation by

$$(6.32) \qquad \hat{\theta}(t+1) = \hat{\theta}(t) + \gamma\varphi(t)\varepsilon^\circ(t+1),$$

which is close to the adaptation algorithm used in FuLMS, who uses $\varphi(t-1)\varepsilon^\circ(t)$ instead of $\varphi(t)\varepsilon^\circ(t+1)$, since the adaptation gain is small and the residual error would vary slowly otherwise.

In this experimentation setup, the updating of matrix $F(t)$ is again done using the $U-D$ factorization for reasons of numerical robustness. The details of this algorithm are given in Section 5.4.2. At this point the adaptation gain matrix $F(t)$ is rewritten as:

$$(6.33) \qquad F(t) = U(t)\Delta(t)U^T(t),$$

where $U(t)$ is an upper triangular matrix with all diagonal elements equal to 1, and $\Delta(t)$ is a diagonal matrix. This allows $F(t)$ to remain positive definite so that the rounding errors do not affect the solution significantly. An interesting option, taking into account the $U-D$ factorization, is to apply the desired profile on $\operatorname{tr}[\Delta(t)]$ instead of $\operatorname{tr}[F(t)]$ for simplification of calculations and ease of computation time consumption, while the PAA objectives remains unchanged.

6.4 Feedforward Adaptive Algorithms Comparison

Table 6.1 and Table 6.2 summarize the most important algorithms used with an IIR configuration of the feedforward compensator. In every case it is possible to perform with a FIR controller by

using a fixed value for $S = 1$. These tables give a brief comparison between different approaches exposed throughout this Chapter. The proposed approach with an adaptation based on a matrix gain $F(t)$, as well as its simplified counterpart who uses a scalar gain $\gamma(t)$ in a similar fashion, are compared with a more common approach FuLMS, than can be described as an even more simplified scalar version of the previous two methodologies.

Table 6.1 starts showing the differences between them, by exposing the diverse ways of computing and estimate the controller's parameters vector $\hat{\theta}(t+1)$ at the future instant in $t+1$ while using just past information from instants t and $t-1$. The complexity inherent to the matrix structure is clear when comparing its adaptation gains calculation with those of a scalar approach. Even though the vector $\varphi_0(t)$ definition remains unchanged, Table 6.2 shows a difference for computing the vector $\varphi(t)$ for each case. Derived from stability considerations, using a matrix gain $F(t)$ gives as result the adaptation algorithms *Filtered-U Pseudo Linear Regression* (FuPLR) and *Filtered-U Stability Based Algorithm* (FuSBA). In a similar way and also derived from stability considerations, the adaptation algorithms using scalar gain *Normalized Filtered-U Least Mean Squares* (NFuLMS) and *Scalar Filtered-U Stability Based Algorithm* (SFuSBA). Lastly we can find FuLMS approach, an algorithm that has been extensively used and is still common to be found [Xie et al., 2016, Zhu et al., 2012].

A comparison that summarize the stability conditions in a deterministic context os also shown, being a global asymptotic stability condition for any initial conditions on the IIR compensator's parameters, or a local asymptotic stability condition. A key element for assuring the stability of the various algorithms is the filter L, as in Table 6.2. The definition of this filter helps to satisfy the *strictly positive real* (SPR) condition for asymptotic stability and parameter convergence.

	$\hat{\theta}(t+1)$	Adaptation Gain
Matrix Approach	$\hat{\theta}(t) + F(t)\varphi(t)\dfrac{\varepsilon^\circ(t+1)}{1+\varphi^T(t)F(t)\varphi(t)}$	$F(t+1)^{-1} = \lambda_1(t)F(t) + \lambda_2(t)\varphi(t)\varphi^T(t)$ $0 \le \lambda_1(t) < 1,\ 0 \le \lambda_2(t) < 2,\ F(0) > 0$
Scalar Approach	$\hat{\theta}(t) + \gamma(t)\varphi(t)\dfrac{\varepsilon^\circ(t+1)}{1+\gamma\varphi^T(t)\varphi(t)}$	$\gamma(t) > 0$
FuLMS	$\hat{\theta}(t) + \gamma(t)\varphi(t-1)\varepsilon^\circ(t)$	$\gamma(t) > 0$

TABLE 6.1. Comparison of algorithms for direct adaptive feedforward compensation in an ANC system with acoustic coupling (1).

6.4.1 Adaptation Algorithm Stability: The Filter L

In order to clarify the importance of filtering the observation vector though the filter L, it is important to note that the residual error equation can be expressed as [Landau et al., 2011a]:

$$(6.34) \qquad \varepsilon(t+1) = H(q^{-1})[\theta - \hat{\theta}(t+1)]^T \varphi(t),$$

	$\varphi_0^T(t)$	$\varphi(t) = L\varphi_0(t)$	Stability Condition
Matrix Approach	$[v(t+1),\ldots,v(t-n_R+1),$ $-\hat{u}(t),\ldots,-\hat{u}(t-n_S+1)]$	FuPLR: $L = G$ FuSBA: $L = \dfrac{A_M}{\hat{P}}G,$ $\hat{P} = A_M\hat{S} - q^{-d_M}B_M\hat{R}$	$\dfrac{A_MG}{PL} - \dfrac{\lambda}{2} = \text{SPR}$ $\lambda = \max[\lambda_2(t)]$
Scalar Approach	$[v(t+1),\ldots,v(t-n_R+1),$ $-\hat{u}(t),\ldots,-\hat{u}(t-n_S+1)]$	NFuLMS: $L = G$ SFuSBA: $L = \dfrac{A_M}{\hat{P}}G,$ $\hat{P} = A_M\hat{S} - q^{-d_M}B_M\hat{R}$	$\dfrac{A_MG}{PL} = \text{SPR}$
FuLMS	$[v(t),\ldots,v+1(t-n_R+1),$ $-\hat{u}(t),\ldots,-\hat{u}(t-n_S+1)]$	FuLMS: $L = G$	$A_M = 1$, unknown stability condition

TABLE 6.2. Comparison of algorithms for direct adaptive feedforward compensation in an ANC system with acoustic coupling (2).

where function $H(q^{-1})$ is defines as

$$(6.35) \qquad H(q^{-1}) = \frac{A_M(q^{-1})G(q^{-1})}{P(q^{-1})L(q^{-1})}$$

and as stated before, the filtered vector $\varphi(t)$ is defined by

$$(6.36) \qquad \varphi(t) = L\varphi_0(t).$$

From these equations, one can understand that there is a phase difference between the residual error $\varepsilon(t+1)$ and $\varphi(t)$, and that $\varphi(t)\varepsilon(t+1)$ is an approximation of the gradient vector's inverse. Therefore, for convergence purposes, the angle created between the directions of adaptation, and that of the true gradient's inverse, which is not computable, should be less than 90°, fact that is effectively assured by the SPR condition on $H(q^{-1})$. For time-varying adaptation gains, the condition is sharper, where

$$(6.37) \qquad H'(q^{-1}) = H(q^{-1}) - \frac{\lambda_2}{2}, \quad \max_t[\lambda_2(t)] \le \lambda_2 < 2$$

is required to be SPR.

Several choices for the filter L are considered, each one leading to a different algorithm. In the specific case where one uses a matrix adaptation gain $F(t)$ is done, we can describe the following algorithms:

FuPLR: $L = \hat{G}$

FuSBA: $L = \frac{A_M}{\hat{P}}G$ with $\hat{P} = A_M\hat{S} - q^{d_M}B_M\hat{R}$

The algorithm FuPLR, assuming that the SPR condition given in Table 6.2 is satisfied, assures a global stability of the algorithm for any initial given conditions. This condition can be relaxed for low adaptation gain provided that in the average, a SPR condition is true but the performance will be impacted, as described in the works of [Landau et al., 2011a, Anderson et al., 1986]. In order to improve the performance, it is needed to use the FuSBA algorithm, which tries to make the $H(q^{-1})$ transfer function close to 1. This will depend on how good the estimation in real-time of $\hat{P}$ is. This can be achieved once an acceptable estimation of the parameters in $\hat{N}$ is available. Therefore in order to use this approach, an initialization with the FuPLR algorithm should be done. Is important to remember that in terms of stability, the FuSBA algorithm's condition is a local result. Strictly speaking, it is valid only in the

neighborhood of the equilibrium point. This algorithm assumes also that FuPLR despite that the SPR is not satisfied, which means that ans SPR condition is satisfied in the average. Note that in order to consider averaging arguments the adaptation gains should be enough small. It also assumes that the estimated $\hat{P}$ is asymptotically stable, which implies that requires an inclusion of a stability test on $\hat{P}$.

For the scalar adaptation gain one has the same choices for the filter L and the corresponding algorithms issued from stability consideration have th same considerations as for the matrix adaptation gain, as given in Table 6.2. These algorithms are described as:

NFuLMS: $L = G$

SFuSBA: $L = \frac{A_M}{\hat{P}} G$ with $\hat{P} = A_M \hat{S} - q^{d_M} B_M \hat{R}$

Where, in a similar way that the matrix approach, the SFuSBA should be initialized using the NFuLMS.

The procedure followed at each sampling time for implementing the adaptive feedforward compensation, in a given sample at time $t+1$, can be describes ass:

1. Get the measured image of the disturbance $v(t+1)$, and the measured residual error $y(t+1)$. Then compute $\varepsilon^{\circ}(t+1) = -y(t+1)$.

2. Update the values in $\varphi_0(t)$ with the new acquired measure $v(t+1)$, and $\hat{u}(t)$ from the previous sampling period.

3. Using filter L, calculate $\varphi(t)$ as $\varphi(t) = L\varphi_0(t)$

4. Estimate the parameter vector $\hat{\theta}(t+1)$ using the corresponding PAA defined at Table 6.1, in accordance with the chosen approach.

5. Calculate the adaptation gain for the current sample, also in accordance with the chosen approach, as described in Table 6.1.

6. Using Equation (6.16), compute and apply the control $\hat{u}(t+1)$.

6.5 Youla-Kučera Parametrized Adaptive Feedforward Controller

In order to isolate the issues related with the positive internal feedback loop stability, from the controller's objective which is the residual noise's minimization, and as previously done for the feedback control approach in Section 5.4.1, a Youla-Kučera (YK) parametrization was used. Instead of a standard IIR feedforward compensator, a similar version using a Youla-Kučera parametrization of the adaptive feedforward compensator was settled.

In such way, a central controller will assure the internal positive feedback loop stability, while its performance are enhanced in real-time by the direct parameters adaptation of the Youla-Kučera $Q(q^{-1})$ filter. In an extended format of the diagram presented in Figure 6.9, and now taking into account a YK parametrization, the scheme shown in Figure 6.10 presents the block diagram of the adaptive feedforward compensator with a Youla-Kučera estimated $\hat{Q}(q^{-1})$ filter and a PAA. Details of the specific algorithms can be found in [Landau et al., 2013, Landau et al., 2012].
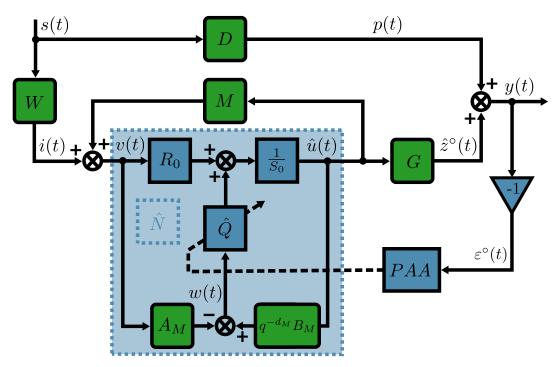
FIGURE 6.10. Feedforward control scheme using a Youla-Kučera parametrization with PAA.

6.5.1   Infinite Impulse Response Youla-Kučera Controller

Using the Youla-Kučera parametrization, the optimal IIR feedforward compensator which will minimize the residual noise can be denominated as *Infinite Impulse Response Youla-Kučera* (YK-IIR) filter, and it is described by:

$$(6.38) \qquad N(q^{-1}) = \frac{R(q^{-1})}{S(q^{-1})} = \frac{R_0 A_Q - A_M B_Q}{S_0 A_Q - q^{-d_M} B_M B_Q},$$

where the optimal Youla-Kučera filter $Q(q^{-1})$ has an IIR structure

$$(6.39) \qquad Q(q^{-1}) = \frac{B_Q(q^{-1})}{A_Q(q^{-1})} = \frac{b_0^Q + b_1^Q q^{-1} + \ldots + b_{n_{B_Q}}^Q q^{-n_{B_Q}}}{1 + a_1^Q q^{-1} + \ldots + a_{n_{A_Q}}^Q q^{-n_{A_Q}}},$$

with $R_0(q^{-1})$, $S_0(q^{-1}) = 1 + q^{-1} S_0^*(q^{-1})$ as the central controller's polynomials meant to work as a stabilizing filter, and $A_M(q^{-1})$, $q^{-d_M} B_M(q^{-1})$ are given in (6.7). As such, the estimated YK-IIR filter can be expressed as:

$$(6.40) \qquad \hat{Q}(q^{-1}) = \frac{\hat{B}_Q(q^{-1})}{\hat{A}_Q(q^{-1})} = \frac{\hat{b}_0^Q + \hat{b}_1^Q q^{-1} + \ldots + \hat{b}_{n_{B_Q}}^Q q^{-n_{B_Q}}}{1 + \hat{a}_1^Q q^{-1} + \ldots + \hat{a}_{n_{A_Q}}^Q q^{-n_{A_Q}}},$$

and its parameters are given by:

$$(6.41) \qquad \hat{\theta}^T(t) = [\hat{b}_0^Q(t), \ldots, \hat{b}_{n_{B_Q}}^Q(t), \hat{a}_1^Q(t), \ldots, \hat{a}_{n_{A_Q}}^Q(t)] = [\hat{\theta}_{B_Q}^T(t), \hat{\theta}_{A_Q}^T(t)].$$

In a similar way as it was done in Section 6.3.1, the *a priori* output of the estimated feedforward compensator using a YK parametrization for the case of time-varying parameter estimates is given by:

$$(6.42) \qquad \begin{aligned} \hat{u}^\circ(t+1) = \hat{u}(t+1|\hat{\theta}(t)) &= -\hat{S}^*(t,q^{-1})\hat{u}(t) + \hat{R}(t,q^{-1})v(t+1), \\ &= -S_0^* \hat{u}(t) + R_0 v(t+1) - \hat{A}_Q^*(t,q^{-1})\psi(t) + \hat{B}_Q(t,q^{-1})w(t+1), \end{aligned}$$

and

$$(6.43) \qquad \hat{u}(t+1) = -S_0^* \hat{u}(t) + R_0 v(t+1) - \hat{A}_Q^*(t+1,q^{-1})\psi(t) + \hat{B}_Q(t+1,q^{-1})w(t+1),$$

where we define $\psi(t)$ as filter $Q(q^{-1})$ output, such that $\psi(t) = S_0 \hat{u}(t) - R_0 v(t)$, and the resulting signal $w(t) = q^{-d_M} B_M \hat{u}(t) - A_M v(t)$ used as input for the filter $Q(q^{-1})$.

Then, the *perfect matching condition* for the YK-IIR parametrized feedforward filter becomes

$$(6.44) \qquad \frac{A_M(R_0 A_Q - A_M B_Q)}{A_Q(S_0 A_M - q^{-d_M} B_M R_0)} G = -D.$$

Neglecting the time-varying operators property of non-commutativity, the residual noise equation of is then given by:

$$(6.45) \qquad \varepsilon(t+1|\hat\theta) = \frac{A_M(q^{-1})G(q^{-1})}{A_Q(q^{-1})P_0(q^{-1})L(q^{-1})}[\theta - \hat\theta]^T \varphi(t),$$

with

$$(6.46) \qquad P_0 = A_M S_0 - q^{-d_M} B_M R_0,$$

and $\varphi(t) = L(q^{-1})\varphi_0(t)$. We then redefine $\varphi_0(t)$ as:

$$(6.47) \qquad \begin{aligned} \varphi_0^T(t) &= [w(t+1), w(t), \ldots, w(t-n_{B_Q}+1), \psi(t), \psi(t-1), \ldots, \psi(t-n_{A_Q})], \\ &= [\varphi_w^T(t+1), \varphi_\psi^T(t)]. \end{aligned}$$

The parameter adaption algorithm described in Section 6.3.2 is again used for the Youla-Kučera feedforward compensators, and in the same way, there are several choices for the filter L that can be considered, leading to different algorithms:

YK FuPLR: $\quad L = G,$

YK FuSBA: $\quad L = \frac{A_M}{\hat P} G \qquad$ with $\qquad \hat P = \hat A_Q(A_M S_0 - q^{-d_M} B_M R_0) = \hat A_Q P_0,$

where $\hat A_Q$ is an estimation of the denominator for an ideal YK-IIR filter computed on the basis of available parameters estimations of the filter $\hat Q$. In order to implement the YK-IIR - FuSBA algorithm, it is necessary to make an initialization over a certain horizon for obtaining an estimation of $\hat A_Q$. This can be done by running the YK-IIR - FuPLR for a certain time to get an estimate of $\hat A_Q$.

6.5.2 Finite Impulse Response Youla-Kučera Controller

For the case where a FIR Youla-Kučera (YK-FIR) configuration is desired, filters are obtained by taking $A_Q(q^{-1}) = 1$.

The parameters vector of the optimal YK-FIR filter assuring perfect matching will be denoted by:

$$(6.48) \qquad \theta^T(t) = [b_0^Q(t), \ldots b_{n_{B_Q}(t)}^Q] = \theta_{B_Q}^T(t),$$

The vector of parameters for the estimated $\hat Q$ filter is described by:

$$(6.49) \qquad \hat Q(q^{-1}) = \frac{\hat B_Q(q^{-1})}{1} = \hat b_0^Q + \hat b_1^Q q^{-1} + \ldots + \hat b_{n_{B_Q}}^Q q^{-n_{B_Q}},$$

so the estimation vector $\hat\theta^T$ is denoted by

$$(6.50) \qquad \hat\theta^T(t) = [\hat b_0^Q(t), \ldots, \hat b_{n_{B_Q}}^Q(t)] = \hat\theta_{B_Q}^T(t).$$

The major difference between the YK-IIR configuration and that proposed as YK-FIR, is reflected in the residual noise evolution's equation, described by::

$$(6.51) \qquad \varepsilon(t+1|\hat{\theta}) = \frac{A_M(q^{-1})G(q^{-1})}{P_0(q^{-1})L(q^{-1})}[\theta - \hat{\theta}]^T \varphi(t),$$

with $\varphi(t) = L\varphi_0(t)$, and

$$(6.52) \qquad \varphi_0(t) = [w(t+1), \dots w(t - n_{B_Q} + 1)].$$

In Equation (6.51), the current poles of the internal closed loop, which will depend on the time-varying parameters of $A_Q(q^{-1})$, are now fixed and defined by the central controller.

The objective will be then to select a filter, such that the transfer function

$$(6.53) \qquad H = \frac{A_M(q^{-1})G(q^{-1})}{P_0(q^{-1})L(q^{-1})}$$

is SPR when we use a constant adaptation gain, or the transfer function

$$(6.54) \qquad H'(q^{-1}) = H(q^{-1}) - \frac{\lambda_2}{2}, \quad \max_t[\lambda_2(t)] \le \lambda_2 < 2$$

is SPR for time-varying adaptation gains.

Like for the IIR type compensators, condition in Equation (6.53) can be interpreted as that of the gradient's angle approximation implemented in the algorithm, and the non-computable true gradient is less than 90° in all the directions [Landau et al., 2011c].

Several choices for the filter L will be considered, leading to different algorithms, as seen in see Tables 6.3 and 6.4:

YK FuPLR: $\quad L = \hat{G}$,

YK FuSBA: $\quad L = \frac{A_M}{P_0}G \qquad$ with $\qquad \hat{P}_0 = A_M S_0 - q^{-d_M}B_M R_0$.

The major difference with respect to the IIR compensators is that the FuSBA algorithm assures in this case global stability and can be implemented from the start, since our polynomial P is known from the beginning and remains unchanged during adaptation process. This is a significant advantage.

As previously done in Section 6.4, Tables 6.3 and 6.4 give the adaptation gain's details used in the various cases proposed. Also as it was done before, the following procedure is applied at each sampling time for implementing the adaptive feedforward compensation using a Youla-Kučera structure. At a given time $t+1$, we have:

1. Get the measured image of the disturbance $v(t+1)$, and the measured residual error $y(t+1)$. Then compute $\varepsilon°(t+1) = -y(t+1)$.

2. Update the values in $\varphi_0(t)$ with the new acquired measure $v(t+1)$, and $\hat{u}(t)$ from the previous sampling period.

3. Using filter L, calculate $\varphi(t)$ as $\varphi(t) = L\varphi_0(t)$

4. Estimate the parameter vector $\hat{\theta}(t+1)$ using the corresponding PAA defined at Table 6.3, in accordance with the chosen approach.

5. Calculate the adaptation gain for the current sample, also in accordance with the chosen approach, as described in Table 6.3.

6. Using Equation (6.43), compute and apply the control $\hat{u}(t+1)$.

	$\hat{\theta}(t+1)$	Adaptation Gain
Matrix YK-IIR	$\hat{\theta}(t) + F(t)\varphi(t)\dfrac{\varepsilon^\circ(t+1)}{1+\varphi^T(t)F(t)\varphi(t)}$	$F(t+1)^{-1} = \lambda_1(t)F(t) + \lambda_2(t)\varphi(t)\varphi^T(t)$
Matrix YK-FIR		$0 \le \lambda_1(t) < 1,\ 0 \le \lambda_2(t) < 2,\ F(0) > 0$
Scalar YK-IIR	$\hat{\theta}(t) + \gamma(t)\varphi(t)\dfrac{\varepsilon^\circ(t+1)}{1+\gamma\varphi^T(t)\varphi(t)}$	$\gamma(t) > 0$
Scalar YK-FIR		

TABLE 6.3. Comparison of algorithms for direct adaptive feedforward compensation in an ANC system with acoustic coupling, using a YK parametrization (1).

Two major observations when using the Youla-Kučera parametrization can be made at this point:

- If a FIR Q filter is used, the internal closed loop poles will be defined by the central controller R_0, S_0 and they will remain unchanged independently of the Q filter parameters values. The stability condition for the FuSBA algorithm is global.

- If an IIR Q filter is used, the internal closed loop poles will be defined by the central controller, but additional poles corresponding to the denominator A_Q from Q filter will be added. The stability condition for the FuSBA algorithm is local and an initialization with the FuPLR algorithm is necessary.

When using an YK-FIR structure, $\hat{A}_Q \equiv 1$, so implementation of a FuSBA-YK-FIR algorithm is much simpler since $\hat{P} = \hat{P}_0$ is constant and known once the central controller is designed.

As for the direct feedforward algorithms described in Section 6.4, scalar adaptation gains can also be used. The same choices for the filter L apply and the corresponding algorithms issued from stability consideration are NFuLMS and SFuSBA, as seen in Tables 6.3 and 6.4.

	$\varphi_0^T(t)$	$\varphi(t) = L\varphi_0(t)$	Stability Condition
Matrix YK-IIR	$[w(t),\dots,w(t-n_{B_Q}+1),$ $\psi(t+1),\dots,\psi(t-n_{A_Q})]$ $w(t) = q^{-d_M}B_M\hat{u}(t) - A_M v(t)$ $\psi(t) = S_0\hat{u}(t) - R_0 v(t)$	FuPLR: $L = G$ FuSBA: $L = \dfrac{A_M}{\hat{P}}G,$ $\hat{P} = A_Q(A_M S_0 - q^{-d_M}B_M R_0)$	$\dfrac{A_M G}{PL} - \dfrac{\lambda}{2} = \text{SPR}$
Matrix YK-FIR	$[w(t),\dots,w(t-n_{B_Q}+1)]$ $w(t) = q^{-d_M}B_M\hat{u}(t) - A_M v(t)$	FuPLR: $L = G$ FuSBA: $L = \dfrac{A_M}{\hat{P}}G,$ $\hat{P} = A_M S_0 - q^{-d_M}B_M R_0$	$\lambda = \max[\lambda_2(t)]$
Scalar YK-IIR	$[w(t),\dots,w(t-n_{B_Q}+1),$ $\psi(t+1),\dots,\psi(t-n_{A_Q})]$ $w(t) = q^{-d_M}B_M\hat{u}(t) - A_M v(t)$ $\psi(t) = S_0\hat{u}(t) - R_0 v(t)$	NFuLMS: $L = G$ SFuSBA: $L = \dfrac{A_M}{\hat{P}}G,$ $\hat{P} = A_Q(A_M S_0 - q^{-d_M}B_M R_0)$	$\dfrac{A_M G}{PL} = \text{SPR}$
Scalar YK-FIR	$[w(t),\dots,w(t-n_{B_Q}+1)]$ $w(t) = q^{-d_M}B_M\hat{u}(t) - A_M v(t)$	NFuLMS: $L = G$ SFuSBA: $L = \dfrac{A_M}{\hat{P}}G,$ $\hat{P} = A_M S_0 - q^{-d_M}B_M R_0$	

TABLE 6.4. Comparison of algorithms for direct adaptive feedforward compensation in an ANC system with acoustic coupling, using a YK parametrization (2).

6.6 Test Bench Experimental Results

For the realization of experiments, experimental test were carried in the second and third test bench configurations. Those obtained with the second configuration are presented in [Landau et al., 2019a], found in Appendix D. As previously stated in Section 6.1, the third configuration of the test bench was chosen as the best option to satisfy the proposed requirements. As it can be seen in Figures 6.11 and 6.7, the frequency region of the third test bench configuration's identified secondary path has enough gain to perform roughly starting from 70 Hz to 270 Hz. It is not recommended to enforce a controller's performance beyond this point, since the existence of a zero located at 300 Hz is quite clear and would let the control in a operation close to an open loop behavior around those frequencies. So the following experiments will have as objective to test the performance of diverse algorithms and approaches attempting the attenuation of disturbances located between 70 Hz and 270 Hz.

A discretized version of a Gaussian white noise, in this case a PRBS, is filtered by a band-pass filter, with band frequencies of 70 Hz to 270 Hz an used as disturbance signal. A first approach for
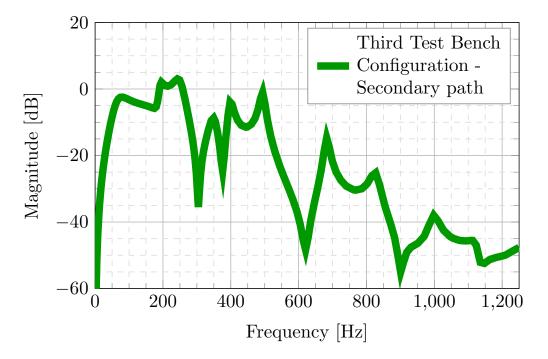
FIGURE 6.11. Identified secondary path for the third test bench configuration.

these tests includes the use a single disturbance that remains unchanged throughout the whole experiment, with a range of 70 Hz to 270 Hz. A regular test horizon of 180 s has been chosen as a compromise between the time required to achieve many of the experiments, and the convergence horizon. Longer tests have been carried on with a length of 600 s as horizon, showing the expected improvement in performance.

After the disturbance characteristics and experiment length have been decided, we proceed then to determine the optimal order for the controller adaptive filters, in this case $N(q^{-1})$ for the standard FF approach, and $Q(q^{-1})$ for the YK parametrization. Here it is taken into account the parsimony concept stating that a simpler controller should be chosen over a more complex in the case that improvements in performance are not enough in relation to the additional computational time required at each step inherent to a more complex controller, and may be an implicit over-parametrization of the compensator.

Once we have decided the adaptive filter's order, we test an compare the results given by different *Parameter Adaptation Algorithms* (PAA). This include the test of approaches whom use a scalar gain, and since it is intended to have a fair comparison between all the proposed algorithms in this chapter, a profile of *Constant Trace* has been chosen for the algorithms using a matrix gain. This is also done in this way since the controllers are intended to represent the application in a real environment, where the constant trace profile is used for letting the controller remain with adaptive capabilities in the case of changes in the disturbances characteristics.

At last, a small comparison of the selected choices using different initial conditions is done.

Since all experiments are carried using a constant trace profile, the value for this trace is increased gradually to look at the changes in performance, and eventually find a threshold for the value that the system working under such conditions can handle.

6.6.1 Standard Feedforward Adaptive Results

As stated before, the first step is to select a proper order for the controller filter, and Table 6.5 shows the results obtained after a series of experiments different orders for the $N(q^{-1})$ filter, either in a IIR or FIR configuration. Results show that for a 180 s horizon in the experiments, IIR controllers have an average better performance in comparison with the FIR counterpart. Speaking now exclusively about the results gathered from IIR filters, is evident that the best response came from the order 30 15/15 filter. In this particular case there seems to be a local maximum for the parameter's order, since a larger filter, 20/20 has a lost in performance and the attenuation achieved is smaller that the lesser order controller.

Filter Type	Filter Order [Num/Den]	Attenuation [dB]	Test Duration
IIR	10/10	23.4	
	15/15	26.7	
	20/20	25.6	
FIR	20/0	18.4	180 s
	30/0	21.0	
	40/0	21.0	
	50/0	20.8	

TABLE 6.5. *Standard controller* order comparison for tests with 180 s horizon and a 70 Hz to 270 Hz disturbance. This comparison was done using standard FuSBA algorithm and a profile of *constant trace* with a value of 0.002 per parameter.

Table 6.6 shows results from similar versions of the previous tests, where different order for the $N(q^{-1})$ filter were reviewed, but this time a 600 s horizon was chosen. This longer version of the tests allowed to see the improvement in performance of controllers. Once again we found that the results of IIR filter with order 30 and values of 15/15 is amongst the best performances, alongside with the IIR filter of order 40 and values of 20/20. Increasing the complexity by 10 just gives a 5% improvement in the performance, thus not giving enough arguments to change the previous selection and keeping a complexity of 30 for the IIR filter, and values of 15/15 for its numerator and denominator.

Table 6.7 show the results of test with similar experimental conditions, but using different PAA. An horizon of 180 s was again used as test length, and a signal with frequencies between 70 Hz and 270 Hzis used as disturbance. Results for FuSBA are still showing good levels of

Filter Type	Filter Order [*Num/Den*]	Attenuation [dB]	Test Duration
IIR	10/10	unstable	
	15/15	39.5	
	20/20	41.5	600 s
FIR	30/0	32.4	
	40/0	32.2	

TABLE 6.6. *Standard controller* order comparison for tests with 600 s horizon and a 70 Hz to 270 Hz disturbance. This comparison was done using standard FuSBA algorithm and a profile of *constant trace* with a value of 0.002 per parameter.

attenuation, nevertheless experiment with its scalar counterpart, SFuSBA, displayed a even better performance.

Adaptation Algorithm	Attenuation [dB]	Filter [Num/Den]	Test Duration
FuPLR	23.7		
FuSBA	26.7		
NFuLMS	26.3	IIR [15/15]	180 s
SFuSBA	28.5		
FuLMS	24.7		

TABLE 6.7. *Standard controller* adaptation algorithms comparison for tests with 180 s horizon and a 70 Hz to 270 Hz disturbance. This comparison was done using a *constant trace* with a value of 0.002 per parameter ($\mathrm{tr}[F(t)] = \mathrm{tr}[F] = 0.002(n_R + n_S)$) for the matrix gain, and 0.002 per parameter ($\gamma = 0.002(n_R + n_S)$) for the scalar gain approach.

As previously done, Table 6.8 presents longer duration experiments, with a length of 600 s as horizon. Here is evident that for a longer duration, controller with a FuSBA approach has outperform SFuSBA, and will be chosen as the best choice.

Since one of the most common algorithms used now a days is FuLMS, Table 6.9 shows a comparison of results between performance of tests done with FuLMS, and the choice we made of algorithm FuSBA. Since different approaches for the PAA have diverse limitations, we push to their limits the performance of both algorithms by modifying the initial conditions of the PAA. In order to have a fair comparison, one again the matrix approach was done using a constant trace profile to have a similar base for comparison with the scalar case, as well as conditions of operation closer to a real environment. The selected value for a constant trace $\mathrm{tr}[F(t)] = \mathrm{tr}[F]$ in the FuSBA experiments was chosen as $\mathrm{tr}[F] = \mathrm{tr}[F]_{pp}(n_R + n_S)$, where n_R and n_S are the corresponding numerator and denominator orders of filter $N(q^{-1})$, [15/15] accordingly with our experimental results; and $\mathrm{tr}[F]_{pp}$ is the desired value for the constant trace per parameter. In

Adaptation Algorithm	Attenuation [dB]	Filter [Num/Den]	Test Duration
FuPLR	35.5		
FuSBA	39.5		
NFuLMS	35.1	IIR [15/15]	600 s
SFuSBA	36.8		
FuLMS	34.6		

TABLE 6.8. *Standard controller* adaptation algorithms comparison for tests with 600 s horizon and a 70 Hz to 270 Hz disturbance. This comparison was done using a *constant trace* with a value of 0.002 per parameter ($\mathrm{tr}[F(t)] = \mathrm{tr}[F] = 0.002(n_R + n_S)$) for the matrix gain, and 0.002 per parameter ($\gamma = 0.002(n_R + n_S)$) for the scalar gain approach.

the case of experiments using a scalar FuLMS PAA, several values for γ were considered as $\gamma = \gamma_{pp}(n_R + n_S)$, where γ_{pp} is the desired value for the gain per parameter.

Adaptation Algorithm	Initial Condition (per parameter)		Attenuation [dB]	Filter [Num/Den]	Test Duration
FuSBA	$\mathrm{tr}[F]_{pp} =$	0.002	26.7		
		0.005	36.2		
		0.010	39.6		
		0.020	unstable	IIR [15/15]	180 s
FuLMS	$\gamma_{pp} =$	0.002	24.7		
		0.008	34.2		
		0.020	37.8		
		0.040	unstable		

TABLE 6.9. *Standard controller* initial condition comparison for tests with 180 s horizon and a 70 Hz to 270 Hz disturbance. This comparison was done using different *constant trace* values $\mathrm{tr}[F]_{pp}$ ($\mathrm{tr}[F(t)] = \mathrm{tr}[F] = \mathrm{tr}[F]_{pp}(n_R + n_S)$) for the matrix gain, and different values for γ ($\gamma = \gamma_{pp}(n_R + n_S)$) for the scalar gain approach.

In Table 6.9 we can see that even though augmenting the initial values for the gain has a clear improvement in the performance and attenuation achieved, the PAA have limitations and there are thresholds for them in terms of capabilities that must not be surpassed. Finally we can see that FuSBA algorithm has a better performance than the FuLMS scalar approach, even if we have different initial conditions for each one of them.

Figures 6.12 to 6.15 show results from the highlighted experiment in Table 6.9. First at Figure 6.12 we have a comparison between the signal sent as disturbance to the system, denominated $s(t)$, and the measurements gathered as residual noise in $y(t)$. In this experiment, first 15 s displays the system behavior in open loop, meaning that there is no compensation. Starting from

15 s is clear that the controller had a positive effect counteracting the disturbance. Right axis displays the attenuation's value achieved at any given point with respect to the open loop section, as

(6.55)
$$\text{Attenuation}(t)[dB] = 20\log_{10}\left(\frac{\|y_{\text{OL}}\|_2^2}{\|y_{\text{CL}}(t)\|_2^2}\right),$$

where y_{OL} corresponds to the measures of residual noise while the system is in open loop such that $y_{OL} = [y(15\,\text{s}),\ldots,y(0\,\text{s})]$, and y_{CL} corresponds to the measures of residual noise while the system is already being compensated by the controller, meaning that is performing in a closed loop, and $y_{CL}(t) = [y(t),\ldots,y(t-15\,\text{s})]$. Even thou the experimental horizon is just 180 s, the attenuation achieved is already 39.6 dB at that time, seemingly reaching a steady state.
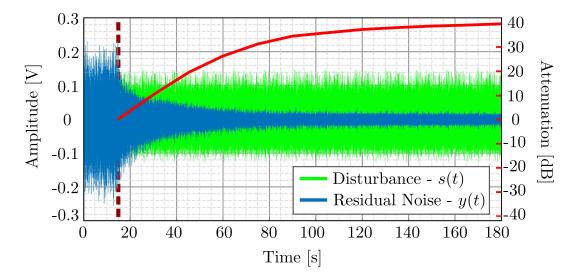
FIGURE 6.12. Performance of IIR compensator of order [15/15] with FuSBA PAA and *constant trace* profile ($\text{tr}[F]_{pp} = 0.010$). Right side shows the level of attenuation achieved at a given point in time, with 39.6 dB achieved at 180 s. Compensation starts at 15 s.

Figure 6.13 show results in the frequency domain of this experiment. Here we can see compared the *power spectral densities* (PSD) of y_{OL} for the *Open loop*, and $y_{CL}(180\,\text{s})$ for the *Closed loop*. As expected from the open loop section where only the disturbance is present in the measurements, its PSD show a clear high gain in the region corresponding to 70 Hz - 270 Hz. On the other hand we have the closed loop PSD taken at $t = 180\,\text{s}$, where is evident the compensation achieved at those given frequencies. As we remember from Figure 6.11, there are region with very low gain in the secondary path and this becomes observable at the gain peak created around 325 Hz, where the controller is trying to perform and creating a perturbation with similar levels to those of the attenuated disturbances.

Parameters adaptation evolution through time is displayed in Figure 6.14, where all the 30 estimated parameters from the filter $N(q^{-1}) = \frac{R}{S}$ of order [15/15] are displayed. Here it can be
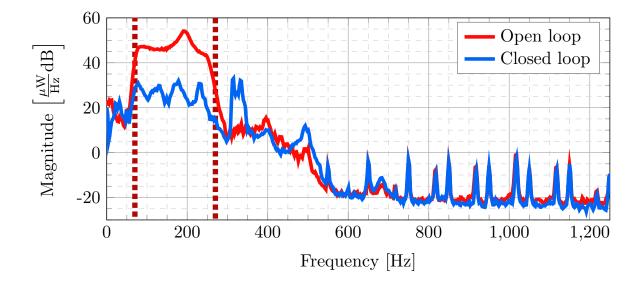
FIGURE 6.13. Comparison between measured noise's PSD of a disturbance with frequencies between 70 Hz and 270 Hz without compensation (Open loop), and measured residual noise of the system at 180 s, using a standard FuSBA PAA with a constant trace profile and $\text{tr}[F]_{pp} = 0.010$ (Closed loop).

seen that many of the parameters values have reached a steady state and converged to a constant value.

FIGURE 6.14. Filter $N(q^{-1}) = \frac{R}{S}$ parameters evolution for a [15/15] standard IIR filter using FuSBA PAA with a constant trace profile. Compensation starts at 15 s.

Finally Figure 6.15 show the values of adaptation gain matrix trace $\text{tr}[F(t)]$, where a constant

value of 0.3 is reached immediately after compensations starts.

FIGURE 6.15. Evolution of adaptation matrix F's trace for a *constant trace* profile of a FuSBA PAA. A value of $\text{tr}[F]_{pp} = 0.010$ was chosen, so $\text{tr}[F(t)] = \text{tr}[F] = 0.3$

6.6.2 Youla-Kučera Feedforward Adaptive Results

In a similar fashion than the procedures for standard feedforward compensation, the first step is to select a proper order for the controller filter, and identical experimental conditions were used, with a 70 Hz to 270 Hz disturbance applied in the third test bench configuration. Table 6.10 shows the results obtained after a series of experiments different orders for the $Q(q^{-1})$ filter, either in a IIR or FIR configuration with 180 s horizon. Even if experimental results for YK-FIR are stable for small order of the $Q(q^{-1})$ filter, corresponding orders in a YK-IIR configuration display better performance in terms of attenuation levels reached in an overall perspective. Between the use of filters 30/30 and 40/40 there is a 3 dB improvement, but an increment of 20 additional parameters, which increments considerably the computational process time, thus 30/30 filter is chosen.

Filter Type	Filter Order [Num/Den]	Attenuation [dB]	Test Duration
YK-IIR	20/20	unstable	
	25/25	29.0	
	30/30	30.2	
	40/40	33.2	
YK-FIR	20/0	17.2	
	30/0	20.9	180 s
	40/0	22.7	
	50/0	25.7	
	60/0	27.0	
	80/0	28.9	
	100/0	31.2	

TABLE 6.10. *YK controller* orders comparison for test with 180 s horizon and a 70 Hz to 270 Hz disturbance. This comparison was done using YK FuSBA algorithm and a profile of *constant trace* with a value of 0.02 per parameter in the IIR case, and 0.5 for FIR case.

As done for the standard approach Table 6.11 shows the experimental results of test with the chosen order 30/30 YK-IIR FuSBA, but an extended horizon of 600 s, as well as its counterpart 60/0 YK-FIR for comparison. The differences here are even higher, since even both tests shows an improved attenuation level reached, YK-FIR has a 1.3 dB increase from its shorter test, while YK-IIR has a 5.5 dB improvement. This shows once again that for the YK approach, an IIR filter is the best choice for this configuration.

Table 6.12 show the results of test with similar experimental conditions with an 180 s horizon and a signal with frequencies between 70 Hz and 270 Hz used as disturbance; but again using different PAA for comparison proposes. Results were just a $L = G$ filtering is used show similar and unacceptable levels of attenuation, conditioning the system to use the more complex filtering of

Filter Type	Filter Order [Num/Den]	Attenuation [dB]	Test Duration
YK-IIR	30/30	35.7	600 s
YK-FIR	60/0	28.3	

TABLE 6.11. *YK controller* order comparison for tests with 600 s horizon and a 70 Hz to 270 Hz disturbance. This comparison was done using YK FuSBA algorithm and a profile of *constant trace* with a value of 0.02 per parameter in the IIR case, and 0.5 for FIR case.

FuSBA and SFuSBA. As in the standard case, FuSBA was the final choice due to its performance was the one with best levels of attenuation.

Adaptation Algorithm	Attenuation [dB]	Filter [Num/Den]	Test Duration
FuPLR	6.1		
FuSBA	30.2	YK-IIR [30/30]	180 s
NFuLMS	6.1		
SFuSBA	27.5		

TABLE 6.12. *YK controller* adaptation algorithms comparison for tests with 180 s horizon and a 70 Hz to 270 Hz disturbance. This comparison was done using a *constant trace* with a value of 0.02 per parameter ($\mathrm{tr}[F(t)] = \mathrm{tr}[F] = 0.02(n_R + n_S)$) for the matrix gain, and 0.02 per parameter ($\gamma = 0.02(n_R + n_S)$) for the scalar gain approach.

Finally experimental results were gathered for tests with a 30/30 YK-IIR filter and a FuSBAPAA with constant trace profile. The value used to define the trace calculation was augmented gradually and the results are displayed in Table 6.13.

Filter Order [Num/Den]	Initial Condition (per parameter)	Attenuation [dB]	PAA	Test Duration
[30/30]	$\mathrm{tr}[F]_{pp} =$	0.02 → 30.2	FuSBA	180 s
		0.05 → 34.4		
		0.10 → 35.6		
		0.12 → unstable		

TABLE 6.13. *YK controller* initial condition comparison for tests with 180 s horizon and a 70 Hz to 270 Hz disturbance. This comparison was done using different *constant trace* values $\mathrm{tr}[F]_{pp}$ ($\mathrm{tr}[F(t)] = \mathrm{tr}[F] = \mathrm{tr}[F]_{pp}(n_R + n_S)$) for the matrix gain, and different values for γ ($\gamma = \gamma_{pp}(n_R + n_S)$) for the scalar gain approach.

Figures 6.16 to 6.15 show results from the highlighted experiment in Table 6.13. Once again Figure 6.16 shows a comparison between the signal sent as disturbance to the system $s(t)$, and

the measurements gathered as residual noise in $y(t)$. First 15 s represent the system behavior in open loop. From 15 s the controller positive effects counteracting the disturbance are evident. In this case the experimental horizon is just 180 s, and the attenuation achieved is 35.6 dB at that time, but without reaching a steady state.
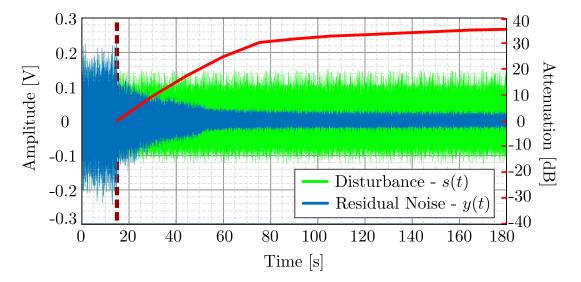
FIGURE 6.16. Performance of YK-IIR compensator order 30/30 with FuSBA PAA and *constant trace* profile ($\text{tr}[F]_{pp} = 0.10$). Right side shows the level of attenuation achieved at a given point in time, with 35.6 dB achieved at 180 s. Compensation starts at 15 s.

Figure 6.17 show results in the frequency domain of this experiment. Comparison between the *power spectral densities* (PSD) of y_{OL} for the *Open loop*, and $y_{CL}(180\text{s})$ for the *Closed loop* is done here. The open loop section show a clear high gain in the region corresponding to 70 Hz - 270 Hz accordingly with the disturbance frequencies. On the other hand we have the closed loop PSD taken at $t = 180\text{s}$, where the compensation achieved at those given frequencies is shown. An improvement regarding the standard approach is the fact that there are no more high-gain peaks outside the attenuation region, with an almost negligible undesired gain in very low frequencies.

Parameters adaptation evolution through time is displayed in Figure 6.18, where all the 60 estimated parameters from the filter $Q(q^{-1}) = \frac{Q_B}{Q_A}$ of order [30/30] are displayed. Here it can be seen that many of the parameters values have yet to reach a steady state and have not completely converged to a constant value.

Finally Figure 6.19 show the values of adaptation gain matrix trace $\text{tr}[F(t)]$, where a constant value of 6.0 is reached immediately after compensations starts.
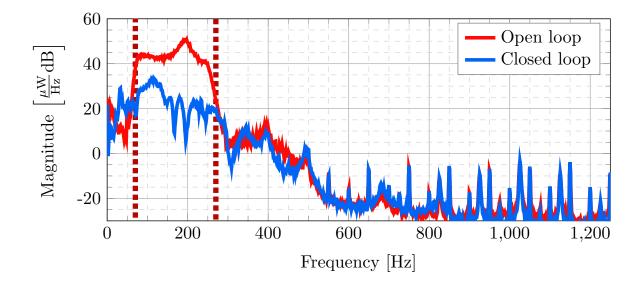
FIGURE 6.17. Comparison between measured noise's PSD of a disturbance with frequencies between 70 Hz and 270 Hz without compensation (Open loop), and measured residual noise of the system at 180 s, using a YK FuSBA PAA with a constant trace profile and $\text{tr}[F]_{pp} = 0.10$ (Closed loop).
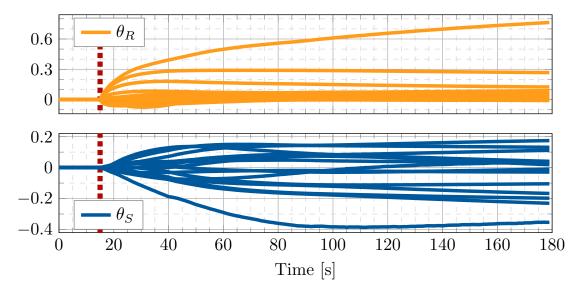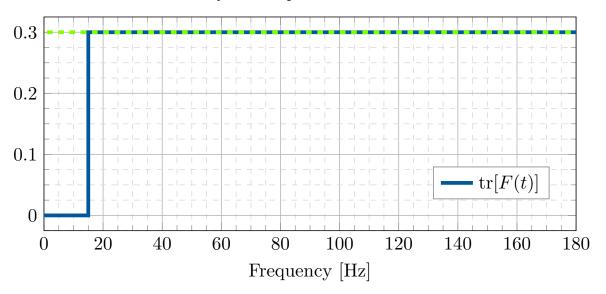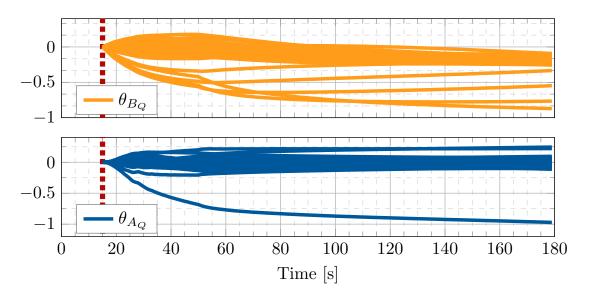

FIGURE 6.18. Filter $Q(q^{-1}) = \frac{B_Q}{A_Q}$ parameters evolution for a [30/30] YK-IIR filter using FuSBA PAA with a constant trace profile. Compensation starts at 15 s.
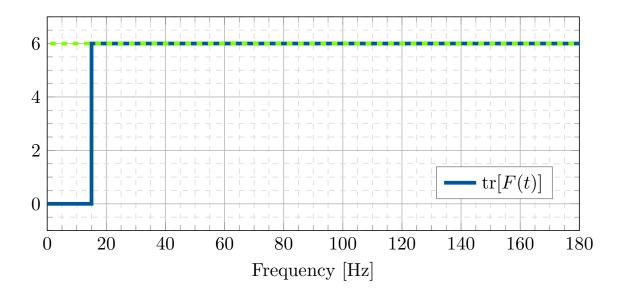
FIGURE 6.19. Evolution of adaptation matrix F's trace for a *constant trace* profile of a YK FuSBA PAA. A value of $\text{tr}[F]_{pp} = 0.10$ was chosen, so $\text{tr}[F(t)] = \text{tr}[F] = 6.0$

6.7 Concluding Remarks

New configurations of the test bench were presented, where diverse physical phenoms affecting controller's performance were described. Basis and theory about the Feedforward approach were given and related to the previous explained Feedback theory. Similar Parameter Adaptation Algorithms were presented as it was done for in previous Chapters, but this time focused in a Feedforward approach. The Youla-Kučera parametrization was again applied to improve some characteristics in the control system. A full methodology for comparison between all different variants in the configuration of controllers was established and tested in the test bench for examination of real experimental results.

No definitive conclusion can be done about the general case of Active Noise Control, nevertheless results presented give an idea of the differences that diverse approaches and their variants can bring. It is not yet possible to assure that the standard approach is better just because it excels in attenuation levels regarding a YK parametrized system, if for example we found that this last has a neater performance in terms of frequencies attenuated and lack of gain outside the desired regions of performance, as well as a better ratio of computation time per parameter.

CONCLUSIONS AND PERSPECTIVES

7.1 Concluding Remarks

The main concern of this thesis was the control of active noise systems. Depending on the disturbance's characteristics, either feedback or feedforward control methods are proposed. Both operation approaches rely on accurate models of the system. Physical modeling can provide qualitative results but fails to yield models that are usable in control design, since their high order of complexity and the fact that they are not always an available solution rend them not suitable for this scenario. Thus data based modeling was emphasized for acquiring such required dynamic model identification. The main point in the methodology defined for identification based on data, is to find a simplified approximate discrete transfer function of an infinite order dynamic model of system's secondary path, located between the compensator's actuator and the residual noise measurement point, used in both control design and active compensation. Additional transfer functions have been identified as well, including a reverse path model of the inherent internal coupling present while implementing feedforward compensation, located between the control actuator and the source of the disturbance's image required for this approach.

Part I

The procedure was investigated in detail starting with transfer the functions' orders estimation and continuing with parameters estimation and model's validation, as well as related topics developed in Chapter 4. This settled the basis for the first section in the paper published in IEEE Transactions on Control Systems Technology, found in Appendix A [Landau et al., 2019c]. Methodology for identification of models was also one of the main topics approached during the 20th IFAC World Congress Toulouse 2017, with the presentation of Appendix E [Meléndez et al.,

2017]. Shorter introductions to the topic are given in the following publications since it continued to be a relevant point throughout subsequent theories and their applications.

To develop the theory of both identification and control design, as well as obtaining data from experimental results, a relevant reconfigurable test-bench was designed and built. The geometry and dimensions of such an experimental setup are indeed subject to redesign and changes in order to explore different configurations, allowing to get various identified models which, at the same time, permit us to have slightly distinct control capabilities. The active control uses a loudspeaker as an actuator, so the main objective was to minimize the residual noise at the considered point of measurement. A detailed explanation is given in Chapter 3, where specifications of the test bench were given, alongside the relevant differences between all the different geometrical configurations of the test bench and their corresponding identified models. The first configuration was used in the first part of the thesis, and was described in [Meléndez et al., 2017, Landau and Meléndez, 2017, Landau et al., 2019c]. The second configuration was the main topic developed in the internal report [Landau et al., 2019a], while the third configuration was used in the studies done in [Landau et al., 2019b, Airimiţoaie et al., 2018].

Part II

The feedback control approach was addressed in Chapter 5 for the case where the frequency characteristics of the disturbances are either tonal or narrow-band time-varying. First, in order to be able to compare the proposed adaptive noise control approach with simpler controllers, the theory for a linear fixed controller design based on the identified models was presented, by introducing and developing the concept of Internal Model Principle, later used as a base for an adaptive controller in a more complex approach. A robust canceler was then proposed and developed as a better variant of the linear controller, while keeping the non adaptability characteristics. The concept of Band-Stop Filters was introduced to reduce the so called water-bed effects, settling a base for the sensitivity function shaping theory also applied in the adaptive control approach. A direct adaptive control algorithm was then proposed, still based on the use of the internal model principle, but with a extended theory meant to be combined with the Youla-Kučera parametrization of the controller. The estimated model's quality for control design was illustrated by the experimental performance of the controllers implemented on the test bench in diverse tests setup conditions.

The most relevant results are on one hand those obtained in the case of multiple narrow band disturbances located in distinct frequency regions which vary through time, and on the other hand, those obtained in the case of frequency interference, occurring in the presence of disturbances with very close frequencies creating a dynamic and non stationary perturbation. Results gathered from these experiments were presented in the IEEE Transactions on Control Systems Technology, Appendix A [Landau et al., 2019c], and the 20th IFAC World Congress held on Toulouse in 2017, Appendix E [Meléndez et al., 2017]. Results achieved with the test

bench were satisfactory, and a seemingly total attenuation was reached in many of the cases for the experimental conditions of the tests, proving the efficiency of the developed feedback theory applied to disturbances with either tonal or narrow-band time-varying characteristics.

Part III

Concerning the attenuation of broadband disturbances, a feedforward scheme was studied. This approach requires a perturbation's image, thus a signal highly correlated with the disturbance needs to be obtained from the system. Given the flexible characteristics of the test bench, a second sensor was added to perform this task, such that an additional measurement was available to be integrated into the active noise control system. As explained in Chapter 6, this configuration generates an internal positive acoustical feedback in the system between the compensation actuator and the reference measurements source, which is a cause of instabilities in several cases of compensators. Adaptive algorithms for feedforward active compensation have been developed from a stability point of view. Nevertheless, in order to separate the problem of stabilizing the internal positive feedback loop from the minimization of the residual noise, the Youla-Kučera parametrization of the feedforward compensator had been proposed as a second available optional approach; hence algorithms have been developed from a stability point of view for both standard and YK parametrized configurations.

Experimental tests with for a feedforward system were done in the test bench and results were obtained and studied. Since the different configurations proposed for the test bench have diverse advantages and disadvantages, the feedforward experiments were designed accordingly for each of the configurations as well. The second proposed test bench configuration is extensively detailed and acts as the main topic in [Landau et al., 2019a] found at Appendix D, where the system performs under undesirable conditions related to the minimal difference required between the pure delays in the primary and secondary paths. Even though this topic was addressed and extensive studies were done, this is not presented in this thesis since research about the phenomenon and theories backing up the results are still under development and research, as can be seen in [Landau et al., 2019b], found at Appendix B

The third test bench configuration was used for the experiments shown in Chapter 6, and in [Airimiţoaie et al., 2018], see Appendix C. In [Landau et al., 2019b], a brief comparison between second and third test bench configurations was made. It was proved that if taken into account, the stability issues inherent to the feedforward approach can be properly managed while keeping a good performance in terms of attenuation, even in the presence of broadband noises. Since the frequency characteristics of the disturbances present a wide spectrum and portray a time-variant dynamic, it is very hard to achieve a full attenuation of them; nevertheless very good and interesting results were achieved using the proposed approaches.

7.2   Future Work

Thorough the length of this thesis, feedback and feedforward algorithms have been addressed individually, and the disturbances each methodology attempts to attenuate are as well individual for each approach, using a feedback configuration for narrow band perturbations and a feedforward for broadband disturbances. Nevertheless, the simultaneous study of them is still a promising field of research, that can be a followup of the work already done in this project.

First of all, a comparison under identical disturbances conditions can be done from the point of view where both approaches, feedback and feedforward, are tested under perturbations with similar frequency characteristics. The use of a feedback approach is preferred in some cases, since it requires one measurement less and does not present as many instabilities issues as its feedforward counterpart, however it use is limited to narrow band disturbances. This threshold can be further tested to find an equilibrium point where more complex perturbation can still be approached with a simpler feedback control, before appealing to a more complex feedforward system. In the same way, the broadband control of the feedforward approaches can be expanded to the narrow disturbances in some extent, enlarging the control capabilities of a system already implementing this kind methodology.

This studies can lead as well to a simultaneous combined *Feedback + Feedforward* control scheme, where the stability issues will be an important part of the system and will play a fundamental role in the design of the controllers. Whit this new combined approach, the disturbances could be as well of combined characteristics, enlarging even further the control capabilities already achieved by the individual components of the scheme. Theory enclosing the use of both approaches simultaneously from a stability point of view can be developed with basis in the individual theories of its components. Here could be more important the need of algorithms and calculus simplification, since both control systems performing at the same time may increase significantly the computation time required at each sample.

Part IV

Appendices

Robust and Adaptive Feedback Noise Attenuation in Ducts

Robust and Adaptive Feedback Noise Attenuation in Ducts

Ioan Doré Landau [ID], Raúl Meléndez, Luc Dugard, and Gabriel Buche

Abstract— In this brief, the attenuation of sound propagation in an air-handling duct using robust and adaptive feedback active noise control (ANC) strategies is investigated. The case of multiple narrow-band disturbances located in distinct frequency regions and the interference occurring in the presence of disturbances with very close frequencies are considered. The active control uses a loudspeaker as a compensatory system. The objective is to minimize the residual noise at the end of the duct segment considered. The system does not use any additional sensors for receiving real-time information upon the disturbances. This brief illustrates the application of the techniques for active vibration control presented by Landau *et al.* to this problem. A hierarchical feedback control approach will be used. At the first level, a robust linear controller will be designed taking advantage of the knowledge of the domains of variation of the frequencies of the noise disturbances. To further improve the performance, a direct adaptive control algorithm will be added. Its design is based on the use of the internal model principle combined with the Youla–Kučera parameterization of the controller. Guidelines for the design of the baseline (central) controller are provided. Both robust and adaptive controls require the knowledge of the discrete-time model of the compensation path, which is obtained by identification from experimental data. Experimental results on a relevant duct ANC test bench will illustrate the performance of the proposed methodology.

Index Terms— Active noise control (ANC), adaptive control, internal model principle (IMP), robust control, system identification, Youla–Kučera (YK) parameterization.

I. INTRODUCTION

IN MOST cases, feed-forward noise compensation is currently used for active noise control (ANC) when a disturbance's image is available (a correlated measurement with the disturbance) [2]–[5]. However, these solutions, inspired by Widrow's technique for adaptive noise cancellation [6], ignore the possibilities offered by feedback control systems and have a number of disadvantages: 1) they require the use of an additional transducer; 2) difficult choice for its location; and 3) in most cases, presence of a "positive" coupling between the compensatory system and the disturbance image's measurement, which can cause instabilities [5]. To achieve the

attenuation of the disturbance without measuring it, a feedback solution can be considered. This is particularly suitable for attenuating multiple time-varying narrow-band noise.

Residual noise can be described as the result of acoustic waves that pass through the system, and the noise canceller's objective is to minimize it. In many cases, these waves can be characterized in the frequency domain either as tonal disturbances or as narrow-band disturbances, both with unknown and time-varying frequencies. The common framework is the assumption that a narrow-band disturbance is the result of a white noise or a Dirac impulse passed through the "disturbance's model." More specifically, in discrete time, the model for a single narrow-band or tonal disturbance is a notch filter with poles on the unit circle and zeros inside the unit circle (for details see [1]). In the context of this brief, robustness should be understood as performance robustness with respect to the variations of the characteristics of the disturbance noise. This will be achieved by using either a linear robust controller or an adaptive controller.

In managing the noise attenuation by feedback, the shape of the modulus of the *output sensitivity function* (the transfer function between the disturbance and the residual noise) is fundamental both from performance and robustness considerations. The output sensitivity function should be appropriately shaped in order to avoid unwanted amplifications in the neighborhood of the frequencies of the disturbances which will be attenuated.

The problem of robust feedback noise attenuation in ducts by shaping the output sensitivity function has been addressed in [7]. This paper [8] considers the use of H_∞ combined with LMI for a robust control design of noise attenuation in ducts. This paper [9] considers an H_∞ approach to noise attenuation in headphones. If the frequency of the tonal or narrow-band disturbance is known, the "internal model principle" (IMP) can be used to achieve a very strong attenuation. However, since the frequencies of these noise disturbances vary, an adaptive approach has to be considered. The combination of the IMP with the Youla–Kučera (YK) parameterization has allowed the development of a direct adaptive regulation scheme for active vibration control [1] and this approach will be used in this brief for active noise attenuation in ducts. This approach is different from the approaches considered in [10]–[12], which ignore IMP and YK parameterization and require adaptation of a very large number of parameters. One should mention the pioneering work of [13] in using IMP and YK parameterization. However, this paper uses different adaptation algorithms and a different design for the central controller and goes beyond the case of a single tonal disturbance.

Several problems have been considered in the field of ANC. In this paper, one considers multiple unknown and

time-varying tonal disturbances located within two distinct relatively small frequency ranges. To be specific, two cases will be considered: 1) the case of two time-varying tonal disturbances located in two distinct frequency regions and 2) the case of four simultaneous tonal disturbances, two located in one limited frequency range and the other two in another frequency range. In this context, a very important problem is to be able to counteract the very low frequency oscillations (interference), which are generated when the two frequencies are very close. Since these disturbances are located within two relatively small frequency ranges, it is possible to consider a robust linear control design. The first case, in the context of ANC in ducts, was considered in [7] and the shaping of the output sensitivity function was achieved using the convex optimization procedure introduced in [14]. It will be shown in this brief that an elementary procedure for shaping appropriately the modulus of the sensitivity functions can be implemented by using stopband filters as shaping tools (see [1] for details).

To further improve the performance, an algorithm for direct adaptive rejection of the disturbances will be added [1]. This algorithm uses the IMP and the YK parameterization of the controller. The design of the central controller associated with the YK parameterization should consider the presence of low damped complex zeros in the plant model.

The real-time performance of the noise cancellers depends upon the quality of the secondary path dynamic model used for designing the feedback control law. Despite long years of effort [15], [16], physical modeling is not relevant for obtaining good models for control design. What is needed in practice is a finite-dimension discrete-time model, which reproduces the system's dynamical behavior. Once such a model is available, one can use digital control design techniques readily implementable on a real-time computer. These models can be obtained directly from data using system identification techniques [1], [7], [17].

This brief is organized as follows. Section II describes the experimental setup. Section III presents briefly the equations describing the system model and the controller. Section IV summarizes the identification procedure and provides the model of the secondary path used in the controller design. Section V gives the specifications and the design of the robust controller. Section VI provides the algorithm used for adaptive disturbance rejection using the internal model principle. Section VII presents the experimental results obtained. Conclusions are given in Section VIII.

II. EXPERIMENTAL SETUP

The view of the test bench used for experiments is shown in Fig. 1 and its detailed scheme is given in Fig. 2.

The speaker used as the source of disturbances is labeled as 1, the control speaker is 2, and finally, at the pipe's open end, the microphone that measures the system's output (residual noise) is denoted as 3. The transfer function between the disturbance's speaker and the microphone (1→3) is denominated *Primary Path*, while the transfer function between the control speaker and the microphone (2→3) is denominated *Secondary Path*. Both speakers are connected to an xPC Target
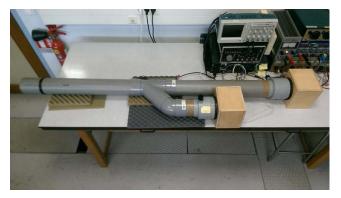
Fig. 1. Duct ANC test bench (photograph).
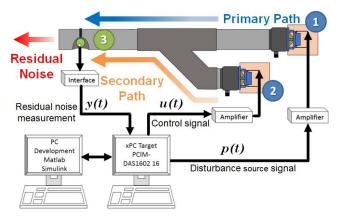
Fig. 2. Duct ANC test bench diagram.

computer with Simulink Real Time environment. $y(t)$ is the system's output (residual noise measurement), $u(t)$ is the control signal, and $p(t)$ is the disturbance. Both primary and secondary paths have a double differentiator behavior, since as input we have the voice coil displacement, and as output the air acoustic pressure. A second computer is used for development, design, and operation with MATLAB.

III. SYSTEM DESCRIPTION

The linear time invariant discrete-time model of the secondary path, or plant, used for the controller design is

$$G(z^{-1}) = \frac{z^{-d}B(z^{-1})}{A(z^{-1})} = \frac{z^{-d}B'(z^{-1})D_F(z^{-1})}{A(z^{-1})} \quad (1)$$

where $D_F(z^{-1}) = (1 - z^{-1})^2$ is a double differentiator filter and

$$A(z^{-1}) = 1 + a_1 z^{-1} + \cdots + a_{n_A} z^{-n_A} \quad (2)$$

$$B'(z^{-1}) = b_1 z^{-1} + \cdots + b_{n_{B'}} z^{-n_{B'}} \quad (3)$$

with d as the plant pure time delay in a number of sampling periods.[1] The system's order (without the double differentiator) is

$$n = \max(n_A, n_{B'} + d). \quad (4)$$

---

[1]The complex variable z^{-1} is used to characterize the system's behavior in the frequency domain and the delay operator q^{-1} for the time-domain analysis.
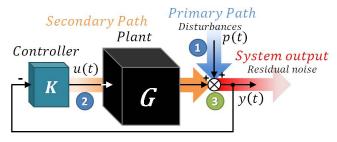
Fig. 3.   Feedback regulation scheme.

Fig. 3 shows the closed-loop feedback regulation scheme, where the controller K is described by

$$K(z^{-1}) = \frac{R}{S} = \frac{r_0 + r_1 z^{-1} + \cdots + r_{n_R} z^{-n_R}}{1 + s_1 z^{-1} + \cdots + s_{n_S} z^{-n_S}}. \qquad (5)$$

The plant's output $y(t)$ and the input $u(t)$ may be written as (see Fig. 3)

$$y(t) = \frac{q^{-d} B(q^{-1})}{A(q^{-1})} \cdot u(t) + p(t) \qquad (6)$$

$$S(q^{-1}) \cdot u(t) = -R(q^{-1}) \cdot y(t). \qquad (7)$$

In (6), $p(t)$ is the disturbances' effect on the measured output[2] and $R(z^{-1})$ and $S(z^{-1})$ are the polynomials in z^{-1} having the following expressions:

$$R = H_R \cdot R' = H_R \cdot (r_0' + r_1' z^{-1} + \ldots + r_{n_{R'}}' z^{-n_{R'}}) \qquad (8)$$

$$S = H_S \cdot S' = H_S \cdot (1 + s_1' z^{-1} + \ldots + s_{n_{S'}}' z^{-n_{S'}}) \qquad (9)$$

where $H_S(z^{-1})$ and $H_R(z^{-1})$ represent prespecified parts of the controller (used, for example, to incorporate the internal model of a disturbance, or to open the loop at some frequencies) and $S'(z^{-1})$ and $R'(z^{-1})$ are, in the present context, the solutions of the Bezout equation

$$P = (A \cdot H_S) \cdot S' + (z^{-d} B \cdot H_R) \cdot R'. \qquad (10)$$

In (10), $P(z^{-1})$ represents the characteristic polynomial, which specifies the desired closed-loop poles of the system.

The transfer functions between the disturbance $p(t)$ and the system's output $y(t)$ and the control input $u(t)$, denoted, respectively, *output sensitivity* and *input sensitivity* functions, are given by

$$S_{yp}(z^{-1}) = \frac{A(z^{-1}) S(z^{-1})}{P(z^{-1})} \qquad (11)$$

and

$$S_{up}(z^{-1}) = -\frac{A(z^{-1}) R(z^{-1})}{P(z^{-1})}. \qquad (12)$$

IV. SYSTEM IDENTIFICATION

The design of the ANC requires the knowledge of the dynamic model of the compensator system (the secondary path). This model will be obtained by system identification from experimental data [1], [17].

For design and application reasons (the objective is to reject tonal disturbances up to 400 Hz), the sampling frequency was

---

[2]The disturbance passes through the *primary path*, and $p(t)$ is its output.

selected as $f_s = 2500$ Hz ($T_s = 0.0004$ s), i.e., approximately six times the maximum frequency to attenuate, in accordance with the recommendation given in [1].

The characteristics of the pseudorandom binary sequences used as excitation signal are: magnitude = 0.15 V, register length = 17, frequency divider of 1, and sequence length: $2^{17} - 1 = 131,071$ samples, guaranteeing a uniform power spectrum from about 70 to 1250 Hz. Since the transfer functions have a double differentiator behavior (input: speaker's coil position and output: acoustic pressure), this is considered as a system's known part and the objective is to identify the unknown part only. To do this, the input sequence is filtered by a double discrete-time differentiator $D_F = (1 - q^{-1})^2$, such that $u'(t) = D_F \cdot u(t)$. The double differentiator will be concatenated with the identified model of the unknown part in the final models.

The next step in the identification procedure is the estimation of the order n of the model from the experimental data. The method of [1] and [18] has been used. Once an estimated order $\hat{n}$ is selected, one can apply a similar procedure to estimate $\hat{n}_A$, $\hat{n} - \hat{d}$, and $\hat{n}_{B'} + \hat{d}$, from which $\hat{n}_A$, $\hat{n}_{B'}$, and $\hat{d}$ are obtained. The estimated order $\hat{n}$ is selected as the value which minimizes a certain criterion. The value of $\hat{n} = 36$ has been obtained, but since the minimum was relatively flat, nearby values have also been considered. The final selection has been done by checking what order allows: 1) to capture all the oscillatory modes in the model and 2) to lead to the best statistical validation once the parameters are identified.

Comparative parameter estimation considering various plant and noise models and estimation algorithms led to the conclusion that an ARMAX model representation is the most appropriate for this system, and the best results in terms of statistical validation (whiteness test on the residual error) have been obtained using the output error with extended prediction model (OEEPM) (see [1] for the detail of the methodology). Therefore, the OEEPM model $n_A = 38, n_B' = 30$, and $d = 8$ ($n = 38$) has been chosen. It has 18 oscillatory modes with damping comprised between 0.0097 and 0.3129. It has also 13 pairs of stable and unstable oscillatory zeros with damping comprised between -0.0159 and 0.5438. The very low damped complex zeros and the unstable zeros are located in the frequency domain over 500 Hz. The presence of these low damped zeros makes the control system's design difficult. Fig. 4 gives the frequency characteristics of the identified complete models for the primary and secondary paths.[3]

V. ROBUST CONTROL DESIGN

A. Control Specifications

The controller is designed to attenuate frequencies around 170 and 285 Hz, with a ±5 Hz tolerance. Attenuation must be at least of -18 dB in these regions and any undesired amplification should be less than 6 dB. In addition, since the gain of the model is low over 600 Hz, and very low damped complex zeros are present in high frequencies, the magnitude of the input sensitivity function should be below -20 dB

---

[3]Primary path model has been identified using the same procedure. This model is used for simulations only.

Fig. 4. Frequency characteristics of the identified primary and secondary paths' models.

Fig. 5. Robust controller design—output sensitivity function evolution.

Fig. 6. Robust controller's output sensitivity function evolution—zoomed-in view.
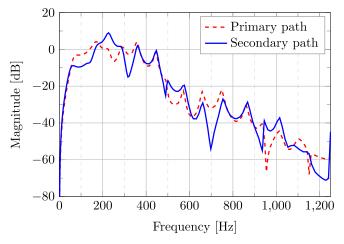
at frequencies over 600 Hz (in order to improve robustness with respect to additive uncertainties and to avoid unnecessary control effort).

In addition, the controller's gain should be zero at 0 Hz since the plant does not have gain at zero frequency, and the controller's gain should be zero also at the Nyquist frequency $(0.5 \, f_s)$, for robustness reasons (the unstable zeros are close to $0.5 \, f_S$). These control specifications will be achieved through the sensitivity functions' shaping.

B. Design Procedure

To achieve the constraints at 0 Hz and at $0.5 f_s$, a fixed part $(H_R)^4$ is introduced in the controller

$$H_R(q^{-1}) = (1 - q^{-1})(1 + q^{-1}) = 1 - q^{-2}. \qquad (13)$$

The use of auxiliary poles is done such that the characteristic polynomial takes the form

$$P(z^{-1}) = P_D(z^{-1}) \cdot P_F(z^{-1}) \qquad (14)$$

where P_D contains the dominant poles corresponding to the poles of the identified dynamic model and P_F includes the auxiliary poles determined by the design requirements.

It is shown in [1] that a very accurate shaping of the output or the input sensitivity functions can be obtained by the use of the second-order band-stop filters (BSFs) of the form: $[H_{S_i}(z^{-1})/P_{FS_i}(z^{-1})]$ and, respectively $[H_{R_i}(z^{-1})/P_{FR_i}(z^{-1})]$. Depending on whether the filter is designed for shaping the output or the input sensitivity function, the numerator of the filter is included in the fixed part of the controller denominator H_{S_0} or numerator H_{R_0}, respectively. The filter denominator is always included in the closed-loop characteristic polynomial. As such, the filter denominator influences the design of the controller indirectly in the computation of S' and R' as solutions of the Bezout equation (10).

The steps for the linear controller's design are as follows.

---

[4] H_{R_i}, H_{S_i}, P_{FR_i}, and P_{FS_i} will denote any given controller's fixed part.
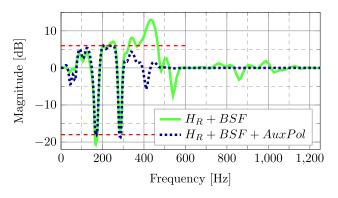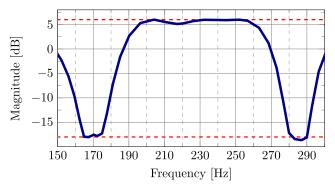
1) Include all (stable) secondary path poles in the closed-loop characteristic polynomial.
2) Open the loop at 0 and 1250 Hz by setting the fixed part of the controller numerator as in (13).
3) Nine BSFs on S_{yp} have been used around each of the frequencies, where attenuation is desired in order to assure the desired attenuation within ± 5 Hz.
4) Eight BSFs have been used on S_{up} to reduce its magnitude above 600 Hz.
5) To improve robustness, 17 auxiliary real poles located at 0.17 have been added to the characteristic polynomial.

Fig. 5 shows the characteristics of the output sensitivity function. The effect of auxiliary poles is illustrated. A zoom of the final characteristics is shown in Fig. 6.[5]

VI. ADAPTIVE CONTROL DESIGN

The adaptive approach uses the YK parameterization of the controller combined with the IMP. The basic reference for this approach used in active vibration control is [1].

A key aspect of this methodology is the use of the IMP. It is supposed that $p(t)$ is a deterministic disturbance given by

$$p(t) = \frac{N_p(q^{-1})}{D_p(q^{-1})} \cdot \delta(t) \qquad (15)$$

where $\delta(t)$ is a Dirac impulse and N_p and D_p are the coprime polynomials of degrees n_{N_p} and n_{D_p}, respectively. In the case

---

[5] The models and the robust controller can be downloaded from: http://www.gipsa-lab.fr/raul.melendez/.

of stationary narrow-band disturbances, the roots of $D_p(z^{-1})$ are on the unit circle.

A. Internal Model Principle [19]

The effect of the disturbance (15) upon the output

$$y(t) = \frac{A(q^{-1})S(q^{-1})}{P(q^{-1})} \cdot \frac{N_p(q^{-1})}{D_p(q^{-1})} \cdot \delta(t) \qquad (16)$$

where $D_p(z^{-1})$ is a polynomial with roots on the unit circle and $P(z^{-1})$ is an asymptotically stable polynomial, converges asymptotically toward zero if and only if the polynomial $S(z^{-1})$ in the RS controller has the form [based on (9)]

$$S(z^{-1}) = D_p(z^{-1})H_{S_0}(z^{-1})S'(z^{-1}). \qquad (17)$$

Thus, the prespecified part of $S(z^{-1})$ should be chosen as $H_S(z^{-1}) = D_p(z^{-1})H_{S_0}(z^{-1})$ and the controller is computed solving

$$P = AD_pH_{S_0}S' + z^{-d}BH_{R_0}R' \qquad (18)$$

where P, D_p, A, B, H_{R_0}, H_{S_0}, and d are given.[6]

To build a direct adaptive controller, the YK parameterization of the controller is used. In the context of this brief, one considers a finite impulse response (FIR) filter of the form

$$Q(z^{-1}) = q_0 + q_1 z^{-1} + \cdots + q_{n_Q}z^{-n_Q} \qquad (19)$$

to which is associated the vector of parameters

$$\theta = [q_0 \; q_1 \ldots q_{n_Q}]^T. \qquad (20)$$

Under YK parameterization or Q-parameterization, the equivalent polynomials $R(z^{-1})$ and $S(z^{-1})$ of the controller $K(q^{-1})$ take the form of

$$R(q^{-1}) = R_0 + A \cdot Q \cdot H_{S_0} \cdot H_{R_0} \qquad (21)$$

$$S(q^{-1}) = S_0 - q^{-d}B \cdot Q \cdot H_{S_0} \cdot H_{R_0} \qquad (22)$$

with

$$R_0(z^{-1}) = r_0^0 + r_1^0 z^{-1} + \ldots + r_{n_R}^0 z^{-n_R} = R_0' \cdot H_{R_0} \qquad (23)$$

$$S_0(z^{-1}) = 1 + s_1^0 z^{-1} + \ldots + s_{n_S}^0 z^{-n_S} = S_0' \cdot H_{S_0} \qquad (24)$$

where A, B, and d correspond to the identified model of the secondary path, $R_0(z^{-1})$ and $S_0(z^{-1})$ are the central controller's polynomials, and H_{S_0} and H_{R_0} are the controller's fixed parts.[7]

Using the output sensitivity function, the expression of the output can be written as

$$y(t) = \frac{S_0}{P} \cdot w(t) - Q \cdot \frac{q^{-d}BH_{S_0}H_{R_0}}{P} \cdot w(t) \qquad (25)$$

with

$$w(t) = A \cdot y(t) - q^{-d}B \cdot u(t) = A \cdot p(t) \qquad (26)$$

as a disturbance's observer. The objective is to find a value of Q such that $y(t)$ is driven to zero.

A block diagram of the adaptive scheme is given in Fig. 7.

[6]Of course, it is assumed that D_p and B do not have common factors.

[7]Under YK parameterization using an FIR structure for the Q filter, the closed-loop poles defined by the central controller remain unchanged.
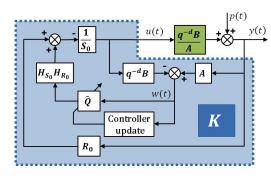
Fig. 7. Adaptive YK parameterization scheme.

The estimation of the polynomial Q at time t is denoted as

$$\hat{Q}(t, q^{-1}) = \hat{q}_0(t) + \hat{q}_1(t)q^{-1} + \cdots + \hat{q}_{n_Q}(t)q^{-n_Q} \quad (27)$$

and is characterized by the parameter vector [8]

$$\hat{\theta}^T(t) = [\hat{q}_0(t) \; \hat{q}_1(t) \ldots \hat{q}_{n_Q}(t)]. \qquad (28)$$

Since this is a regulation problem, $y(t)$ is expected to go toward zero and as such, it is an *a priori* adaptation error denoted $\varepsilon^0(t+1)$ for a given estimated polynomial $\hat{Q}(t, q^{-1})$

$$\varepsilon^0(t+1) = \frac{S_0}{P} \cdot w(t+1) - \hat{Q}(t)\frac{q^{-d}B^*H_{S_0}H_{R_0}}{P} \cdot w(t) \qquad (29)$$

with $B(q^{-1}) = q^{-1} \cdot B^*(q^{-1})$. In a similar way, one can define an *a posteriori* error as

$$\varepsilon(t+1) = \frac{S_0}{P} \cdot w(t+1) - \hat{Q}(t+1)\frac{q^{-d}B^*H_{S_0}H_{R_0}}{P} \cdot w(t) \qquad (30)$$

which can be further expressed as

$$\varepsilon(t+1) = [Q - \hat{Q}(t+1)] \cdot \frac{q^{-d}B^*H_{S_0}H_{R_0}}{P} \cdot w(t) + \eta(t+1) \qquad (31)$$

where Q is the unknown optimal filter, and $\eta(t)$ tends asymptotically toward zero (see [20] for details).

Denoting filtered versions of the observer output $w(t)$ as

$$w_1(t) = \frac{S_0(q^{-1})}{P(q^{-1})} \cdot w(t) \qquad (32)$$

$$w_2(t) = \frac{q^{-d}B^*H_{R_0}H_{S_0}}{P} \cdot w(t) \qquad (33)$$

and

$$\varphi^T(t) = [w_2(t) \; w_2(t-1) \ldots w_2(t-n_Q)] \qquad (34)$$

Equation (31) can be rewritten as

$$\varepsilon(t+1) = [\theta^T - \hat{\theta}^T(t+1)] \cdot \varphi(t) + \eta(t+1) \qquad (35)$$

[8]The order of the polynomial $\hat{Q}$ is related to the order of the denominator of the model of the disturbance n_{D_p} as $n_{\hat{Q}} = n_{D_p} - 1$.

where η goes to zero. This type of equation allows immediately to develop an adaptation algorithm [20]

$$\hat{\theta}(t+1) = \hat{\theta}(t) + F(t)\varphi(t)\varepsilon(t+1) \tag{36}$$

$$\varepsilon(t+1) = \frac{\varepsilon^0(t+1)}{1 + \varphi^T(t)F(t)\varphi(t)} \tag{37}$$

$$\varepsilon^0(t+1) = w_1(t+1) - \hat{\theta}^T(t)\varphi(t) \tag{38}$$

$$F(t+1) = \frac{1}{\lambda_1(t)}\left[F(t) - \frac{F(t)\varphi(t)\varphi^T(t)F(t)}{\frac{\lambda_1(t)}{\lambda_2(t)} + \varphi^T(t)F(t)\varphi(t)}\right] \tag{39}$$

$$0 < \lambda_1(t) \le 1; \quad 0 \le \lambda_2(t) < 2; \quad F(0) > 0 \tag{40}$$

where λ_1 and λ_2 allow to obtain different profiles for the evolution of the adaptation gain $F(t)$. Finally, the control to be applied is given by

$$S_0 \cdot u(t+1) = -R_0 \cdot y(t+1) - H_{R_0}H_{S_0}\hat{Q}(t+1) \cdot w(t+1). \tag{41}$$

For the stability analysis of this algorithm, see [20].

In adaptive regulation applications, one uses in general the *constant trace algorithm*. In this case, $\lambda_1(t)$ and $\lambda_2(t)$ are automatically chosen at each step in order to ensure a constant trace of the gain matrix (constant sum of the diagonal terms)

$$\text{tr}F(t+1) = \text{tr}F(t) = \text{tr}F(0) = \text{nGI} \tag{42}$$

in which n is the number of parameters and GI is to be suppressed the initial adaptation gain. The matrix $F(0)$ has the form

$$F(0) = \begin{bmatrix} GI & & 0 \\ & \ddots & \\ 0 & & GI \end{bmatrix}. \tag{43}$$

The values of $\lambda_1(t)$ and $\lambda_2(t)$ at each sampling instant are determined from the equation

$$\text{tr}F(t+1) = \frac{1}{\lambda_1(t)}\text{tr}\left[F(t) - \frac{F(t)\phi(t)\phi^T(t)F(t)}{\alpha(t) + \phi^T(t)F(t)\phi(t)}\right] \tag{44}$$

fixing the ratio $\alpha(t) = \lambda_1(t)/\lambda_2(t)$. This algorithm can be combined with the *decreasing adaptation gain* algorithm or with the *variable forgetting factor* algorithm for initialization [1]. One switches to the *constant trace algorithm* when the trace of the adaptation gain becomes equal or smaller than the assigned constant trace. Algorithms with constant scalar gain can also be implemented [$F(t) = F(0)$], but the results will be inferior.

This scheme is implemented on top of the central controller, which corresponds to the robust controller designed in Section V from which the BSF filters on S_{yp} have been removed (preserving, however, the characteristics of S_{up} in high frequencies over 600 Hz for robustness reasons).

VII. EXPERIMENTAL RESULTS

The robust controller and the adaptive controller have been tested on the experimental setup described in Section II under several protocols.
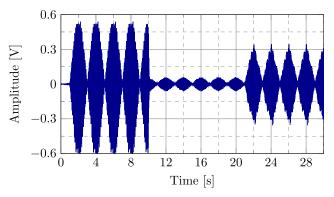
Fig. 8. Acoustic interference attenuation using a robust controller. Noise frequencies: 170 + 170.5 Hz and 285 + 285.5 Hz then 180 + 180.5 Hz and 295 + 295.5 Hz. Loop closed at 10 s.
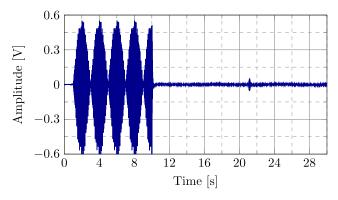
Fig. 9. Acoustic interference attenuation using an adaptive controller. Noise frequencies: 170+170.5 Hz and 285+285.5 Hz then 180+180.5 Hz and 295+295.5 Hz. Loop closed at 10 s.

A. Interference Test

The protocol is as follows. For 1 s, the system operates in open loop and without any disturbance in order to get a reference for the ambient noise. From 1 to 10 s, the test bench works in open loop, in the presence of two pairs of sinusoidal noise disturbances located at 170 and 170.5 and 285 and 285.5 Hz, respectively. At 10 s, the loop is closed and the controller begins to counteract the disturbance effect. The frequencies of the four signals are then increased at 21 s by 10 Hz. The corresponding new values are 180 and 180.5 Hz for the first pair and 295 and 295.5 Hz for the second pair (leaving the attenuation regions of the robust controller).

Fig. 8 shows the robust controller's performance for the interference experiment. As long as the disturbance frequencies are in the region of designed operation, a global attenuation of 39.86 dB is obtained (between 10 and 21 s). After 21 s, since the frequencies of the disturbances are outside the region of designed operation, the performance is unsatisfactory achieving a global attenuation of only 7.94 dB.[9] Fig. 9 presents the results for a similar test using the adaptive controller. The number of adjustable parameters in the Q filter is 4 ($n_Q = 3$) and an adaptation algorithm with *constant trace adaptation gain* is used. The trace of the adaptation gain used was: $trF = 0.03 \cdot (n_Q + 1)$. It can be seen that after a negligible transient, a much better attenuation is obtained

[9]Audio files available at http://www.gipsa-lab.fr/raul.melendez/.
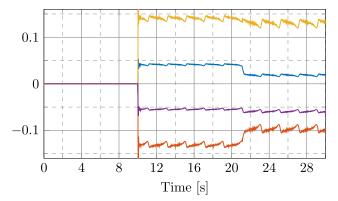
Fig. 10. Parameters evolution for acoustic interference test using an adaptive controller.
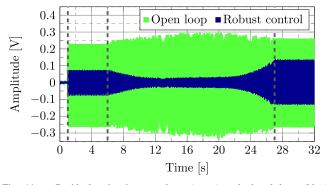
Fig. 11. Residual noise in open loop (green) and closed loop (blue) using a robust controller under the effect of tonal disturbances with variable frequencies.

Fig. 12. Residual noise in open loop (green) and closed loop (blue) using an adaptive controller under the effect of tonal disturbances with variable frequencies.

Fig. 13. Evolution of the controller parameters under the effect of tonal disturbances with variable frequency

Fig. 14. Step changes in frequencies using the robust controller. Residual noise in open loop (green) and in closed loop (blue).

with respect to the robust controller between 10 and 21 s. The global attenuation obtained is 70.56 dB. Excellent levels of attenuation are also obtained once the disturbances frequencies move away by 10 Hz (global attenuation 67.65 dB), with a negligible adaptation transient.[10]

Fig. 10 shows the evolution of each Q-parameter with respect to time. From 0 to 10 s, all the parameters have values equal to zero, since the controller is not working yet. Once the loop is closed, the Q-parameters take almost instantly stable mean values. At 21 s, the change in frequencies leads to a quick adaptation toward the new values.

B. Sinusoidal Disturbances With Continuously Time-Varying Frequency

In this experiment, two tonal noise disturbances located at 160 and 275 Hz are first applied to the system from 1 to 6 s. Then, their frequencies linearly increase until they reach the values of 180 and 295 Hz correspondingly at 27 s, after which their frequencies remain constant.

Fig. 11 shows a comparison between the system's residual noise when it is operated in open loop and in closed loop using the robust controller. As the frequencies move within the designed attenuation regions, a significant attenuation is obtained. However, outside this zone, the performance is not satisfactory. Correspondingly, Fig. 12 shows the residual noise in open-loop operation and with the adaptive controller. The

---

[10]Using $n_Q = 7$ (eight adjustable parameters) does not improve the performance.

---
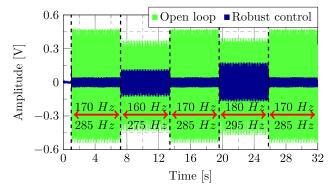
levels of attenuation achieved are globally much better. The residual noise is comparable with the ambient noise measured between 0 s and 1 s. The evolution of the parameters is shown in Fig. 13.

C. Step Changes in Frequencies

In this experiment, step changes in the frequencies of a pair of tonal noise disturbances are considered, starting from their nominal values of 170 and 285 Hz. The steps are of ± 10 Hz and applied every 6.2 s. The system is operated in open loop from 0 to 1 s. Fig. 14 shows the robust controller performance. When the disturbances' frequencies are inside the attenuation region of the controller, the attenuation is satisfactory. However, for -10 Hz and $+10$ Hz steps, since one operates outside the designed regions of attenuation,
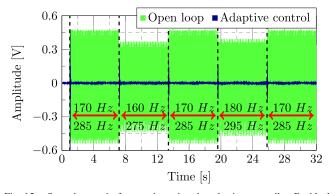
Fig. 15. Step changes in frequencies using the adaptive controller. Residual noise in open loop (green) and in closed loop (blue).
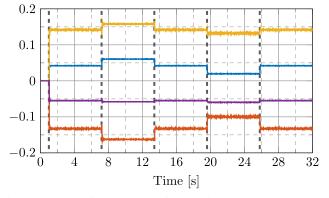
Fig. 16. Evolution of the parameters of the adaptive controller in the presence of step changes in disturbances frequencies.

the performance is unsatisfactory. The performance of the adaptive controller is shown in Fig. 15. The performance is almost the same for all frequencies values and the residual noise is close to the ambient noise. The adaptation transients are visible but very short. The same number of adjustable parameters and the same adaptation gain as in the previous experiments have been used. The evolution of the Q-parameters is shown in Fig. 16.

VIII. Conclusion

This brief has shown that techniques developed in the context of active vibration control [1] can be successfully used for robust and adaptive feedback attenuation of multiple narrowband noise disturbances in ducts. The effective implementation of these techniques should consider the characteristics of the identified model of the compensation path, and design guidelines have been provided.

References

[1] I. D. Landau, T.-B. Airimitoaie, A. Castellanos-Silva, and A. Constantinescu, *Adaptive and Robust Active Vibration Control*. London, U.K.: Springer, 2016.

[2] S. Elliott and P. Nelson, "Active noise control," *Noise/News Int.*, vol. 2, no. 2, pp. 75–98, Jun. 1994. [Online]. Available: http://www.ingentaconnect.com/content/ince/nni/1994/00000002/00000002;jsessionid=1phrui4jwquft.x-ic-live-02

[3] S. J. Elliott and T. J. Sutton, "Performance of feedforward and feedback systems for active control," *IEEE Trans. Speech Audio Process.*, vol. 4, no. 3, pp. 214–223, May 1996.

[4] S. M. Kuo and D. R. Morgan, "Active noise control: A tutorial review," *Proc. IEEE*, vol. 87, no. 6, pp. 943–973, Jun. 1999.

[5] J. Zeng and R. de Callafon, "Recursive filter estimation for feedforward noise cancellation with acoustic coupling," *J. Sound Vibrat.*, vol. 291, nos. 3–5, pp. 1061–1079, 2006.

[6] B. Widrow and S. D. Stearns, *Adaptive Signal Processing*. Englewood Cliffs, NJ, USA: Prentice-Hall, 1985.

[7] J. C. Carmona and V. M. Alvarado, "Active noise control of a duct using robust control theory," *IEEE Trans. Control Syst. Technol.*, vol. 8, no. 6, pp. 930–938, Nov. 2000.

[8] S. Tansel, A. S. Yucelen, and F. Pourboghrat, "Active noise control in a duct using output feedback robust control techniques," in *Proc. Amer. Control Conf.*, 2010, pp. 3506–3511.

[9] S. Liebich, C. Anemüller, P. Vary, P. Jax, D. Rüschen, and S. Leonhardt, "Active noise cancellation in headphones by digital robust feedback control," in *Proc. 24th Eur. Signal Process. Conf. (EUSIPCO)*, 2016, pp. 1843–1847.

[10] J. Shaw, "Adaptive control for sound and vibration attenuation: A comparative study," *J. Sound Vibrat.*, vol. 235, no. 4, pp. 671–684, 2000.

[11] H. S. Sane, R. Venugopal, and D. S. Bernstein, "Disturbance rejection using self-tuning ARMARKOV adaptive control with simultaneous identification," *IEEE Trans. Control Syst. Technol.*, vol. 9, no. 1, pp. 101–106, Jan. 2001.

[12] S. Manikandan, "Literature survey of active noise control systems," vol. 17, 2006. [Online]. Available: https://www.semanticscholar.org/paper/Literature-Survey-of-Active-Noise-Control-Systems-Manikandan/f0660fb6cc537824ac2830ff8c391925974bf649

[13] F. Ben Amara, P. T. Kabamba, and A. G. Ulsoy, "Adaptive sinusoidal disturbance rejection in linear discrete-time systems—Part II: Experiments," *J. Dyn. Syst. Meas. Control*, vol. 121, no. 4, pp. 655–659, 1999.

[14] J. Langer and I. D. Landau, "Combined pole placement/sensitivity function shaping method using convex optimization criteria," *Automatica*, vol. 35, no. 6, pp. 1111–1120, 1999.

[15] P. A. Nelson and S. J. Elliott, *Active Control of Sound*. San Diego, CA, USA: Academic, 1993.

[16] B. J. Zimmer and S. P. Lipshitz, "An improved acoustic model for active noise control in a duct," *J. Dyn. Syst., Meas., Control*, vol. 125, pp. 382–395, Sep. 2003.

[17] L. Ljung, *System Identification—Theory for the User*, 2nd ed. Englewood Cliffs, NJ, USA: Prentice-Hall, 1999.

[18] H. N. Duong and I. D. Landau, "An IV based criterion for model order selection," *Automatica*, vol. 32, no. 6, pp. 909–914, 1996.

[19] B. A. Francis and W. M. Wonham, "The internal model principle of control theory," *Automatica*, vol. 12, no. 5, pp. 457–465, Sep. 1976.

[20] I. D. Landau, R. Lozano, M. M'Saad, and A. Karimi, *Adaptive Control Algorithms, Analysis and Applications*, 2nd ed. London, U.K.: Springer, 2011.

Beyond the delay barrier in adaptive feedforward active noise attenuation

Beyond the delay barrier in adaptive feedforward active noise control using Youla–Kučera parametrization

Ioan Doré Landau[a], Raul Melendez[a], Tudor-Bogdan Airimitoaie[b], Luc Dugard[a]

[a]*Univ. Grenoble Alpes, CNRS, Grenoble INP, GIPSA-lab, 38000 Grenoble, France*[1]
[b]*Univ. Bordeaux, Bordeaux INP, CNRS, IMS, UMR 5218, 33405 Talence, France*

Abstract

Adaptive feedforward broad-band noise compensation is currently used when a correlated measurement with the disturbance (an image of the disturbance) is available. Most of the active feedforward noise control systems feature an internal "positive" acoustical feedback between the compensation system and the reference source (a correlated measurement with the disturbance) that has to be taken into account. Adaptive algorithms for active feedforward noise attenuation have been implemented such that the propagation delay between the compensatory actuator and the measurement of the residual noise (the secondary path) be much smaller than the propagation delay between the reference source (image of the incoming noise) and the measurement of the residual noise (the primary path). Nevertheless, there are potential fields of applications in which the propagation delay of the secondary path may be larger than the one of the primary path. The present paper explores the behaviour of the available adaptive feedforward compensation algorithms in this new context. The algorithms have been tested experimentally on a relevant test bench. All the algorithms except the Youla–Kučera finite impulse response (YKFIR) adaptive compensator and the standard FIR adaptive compensator using a stability based filtered adaptation (FUSBA) lead to an unstable behavior. In terms of performance the YKFIR provides the best performance.

Keywords: active noise control, adaptive feedforward compensation, Youla–Kučera parametrization, positive feedback coupling

1. Introduction

Adaptive feedforward broad-band noise compensation is currently used when a correlated measurement with the disturbance (an image of the disturbance) is available. Most of the active feedforward noise control systems feature an internal "positive" acoustic feedback between the compensation system and the reference source (a correlated measurement with the disturbance) that has to be taken into account.

Figure 1 gives the basic block diagram of the adaptive feedforward compensation in the presence of the internal positive coupling between the output of the compensator and the measurement of the image of the incoming noise. The incoming noise propagates through the so called *primary*

---

[1]Corresponding author: Ioan Doré Landau (ioan-dore.landau@gipsa-lab.grenoble-inp.fr)
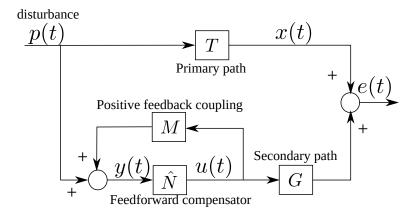
Figure 1: Adaptive active noise feedforward compensation.

path and its effect is compensated through a secondary noise source (*secondary path*) driven by a feedforward compensator. The input to the feedforward compensator is the sum of the image of the incoming noise and of the internal acoustic positive feedback. Since this feedback is positive, it raises of course stability problems. Stability analysis of the adaptive feedforward compensation schemes became an important issue [1–3]. The stability analysis make the assumption that there exists a compensator N such that the internal positive loop (formed by M and N in feedback) is stable and such that the perfect matching of the primary path is achieved.[2]

One of the important aspects in active noise feedforward control is the transportation delay related to the sound propagation speed [4]. Most of the implementations of the adaptive feedforward compensation systems are close to a collocation of the residual noise measurement and of the secondary source used for compensation (see for example [5],[6]). More generally speaking, the length between these two objects is much smaller than the length of the primary path (between the reference microphone and the residual noise microphone). See for example [7]. A ratio of 3 to 6 seems to be the case in a number of applications (particularly true in the active noise compensation in ducts).

Nevertheless, there are potential applications fields where the length of the secondary path may be longer than the length of the primary path.[3] In this case the delay associated with the dynamics of the secondary path will be larger than the delay associated with the primary path.

When the delay characterizing the dynamic model of the secondary path is larger than the delay of the primary path, even in the absence of the internal positive feedback, it just simply does not exist a stable compensator assuring the "perfect matching".[4] One needs algorithms which will minimize the residual noise and which will assure the stability of the scheme (and of course the stability of the internal loop). The present paper does not propose new algorithms but tries to

---

[2]This hypothesis of perfect matching of the primary path can be relaxed under certain conditions taking into account that the perfect matching should be achieved in practice in a limited frequency band (see [2]).

[3]This can occur when there are thermal constraints for the positioning of the secondary source.

[4]In the case of the internal feedback the effective compensator is the feedback connection of the compensator N and of the reverse path M.

evaluate in this context the available algorithms for adaptive feedforward compensation using a relevant experimental test-bench.

As it will be shown in this paper, only the adaptive Youla–Kučera (YK) parametrized compensator using a Finite Impulse Response (FIR) filter [3] and the Filtered u stability based algortithm (FUSBA) associated to a standard FIR compensator [2, 8] assure a stable operation of the system. All the other algorithms tested do not assure a stable operation. In terms of performance it is the Youla–Kučera FIR adaptive feedforward compensator which has provided the best performance. The reason for the good behavior of the Youla–Kučera parametrized FIR (YKFIR) algorithm is that from the beginning the internal loop will be stable (by the appropriate design of the central compensator) independently of the values of the parameters of the YKFIR filter which will be adapted in order to minimize the residual noise. The standard FUSBA FIR adaptive compensator provides less good performance and does not offer the possibility to assign the poles of the internal closed-loop which unfortunately go extremely close to the unit circle. This raises questions about its robustness.

All the algorithms have been tested in real-time on a relevant test bench and in simulation using the identified models of the test bench. The performance of the Youla–Kučera FIR algorithm will be thoroughly investigated.

The paper is organized as follows: In Section 2, the experimental setup will be described. In Section 3, the basic equations describing the system will be presented in order to make understandable the various algorithms which will be reviewed in Sections 4 and 5. Section 6 will show simulation results. The experimental results obtained on the test bench are summarized in Section 7. Conclusions are given in Section 8. Appendix A provides an analysis of the possible stable/unstable equilibrium points for the various schemes. Appendix B provides simulation results for a simplified YKFIR adaptive feedforward compensator.

2. Experimental Setup

The view of the test bench used for experiments is shown in Fig. 2 and in more detail in Fig. 3. The actual dimensions of the test bench are given in Fig. 4.

The speaker used as the source of disturbances is labelled as 1, while the control speaker is marked as 2. At pipe's open end, the microphone that measures the system's output (residual noise $e(t)$) is denoted as 3. Inside the pipe, close to the source of disturbances, we can find the second microphone, labelled as 4, for measuring the perturbation's image, denoted as $y(t)$. Additionally, we denote $u(t)$ the control signal and $s(t)$ the disturbance. The transfer function between the disturbance's speaker and the microphone (1→3) is called *Global Primary Path*, while the transfer function between the control speaker and the microphone (2→3) is denoted *Secondary Path*. The transfer function between microphones (4→3) is called *Primary Path*. The internal coupling found between (2→4) is denoted *Reverse Path*. These marked paths have a double differentiator behaviour, since as input we have the voice coil displacement and as output the air acoustic pressure.

Both speakers are connected to a xPC Target computer with Simulink Real-time® environment through a pair of high definition power amplifiers and a data acquisition board. A second computer is used for development, design and operation with Matlab®. The sampling frequency
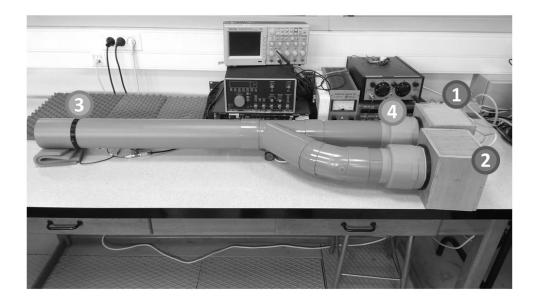
Figure 2: Duct active noise control test bench (Photo).
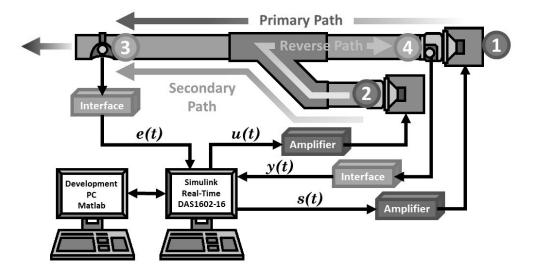
Figure 3: Duct active noise control test bench diagram.
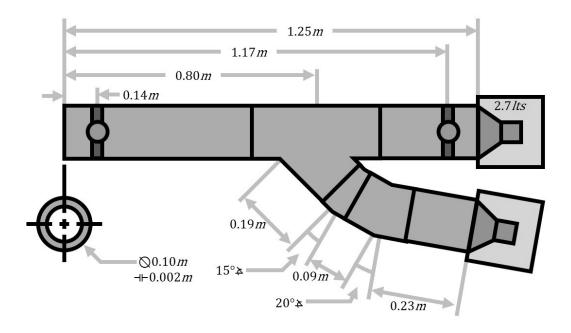
Figure 4: Duct active noise control test bench dimensions.

has been chosen in accordance with the recommendations given in [8]. Taking into account that disturbances up to 400 Hz need to be attenuated, a sampling frequency $f_s = 2500$ Hz has been chosen ($T_s = 0.0004$ sec), i.e., approximately six times the maximum frequency to attenuate.

In this configuration, speakers are isolated inside wood boxes filled with special foam in order to create anechoic chambers and reduce the radiation noise produced. These boxes have dimensions $0.15\,\mathrm{m} \times 0.15\,\mathrm{m} \times 0.12\,\mathrm{m}$, giving a chamber volume of $2.7\,\mathrm{L}$.

3. System Description

The primary (T), secondary (G), and reverse (positive coupling) (M) paths are characterized by the asymptotically stable transfer operators:

$$X(q^{-1}) = q^{-d_x} \frac{B_X(q^{-1})}{A_X(q^{-1})} = q^{-d_x} \frac{b_1^X q^{-1} + \ldots + b_{n_{B_X}}^X q^{-n_{B_X}}}{1 + a_1^X q^{-1} + \ldots + a_{n_{A_X}}^X q^{-n_{A_X}}}, \tag{1}$$

with $B_X = q^{-1} B_X^*$ for any $X \in \{G, M, T\}$. $\hat{G} = q^{-d_G} \frac{\hat{B}_G}{a_G}$, $\hat{M} = q^{-d_M} \frac{\hat{B}_M}{a_M}$, and $\hat{T} = q^{-d_T} \frac{\hat{B}_T}{a_T}$ denote the identified (estimated) models of G, M, and T. The system's order is defined by (the indexes G, M, and T have been omitted):

$$n = max(n_A, n_B + d). \tag{2}$$

The models of the systems have been identified experimentally using the identification procedure described in [9].
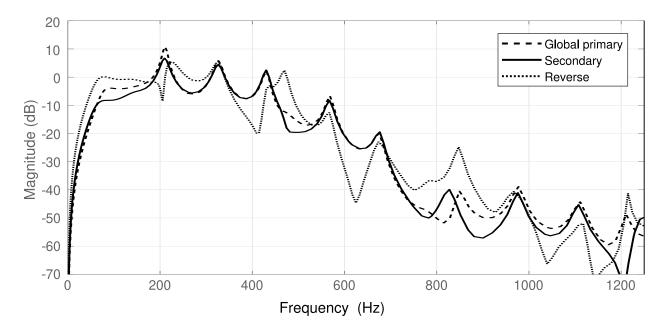
Figure 5: Frequency characteristics of the Primary, Secondary and Reverse paths identified models.

The frequency characteristics[5] of the identified models for the primary[6], secondary and reverse paths are shown in Fig. 5. These characteristics present multiple resonances (low damped complex poles) and anti-resonances (low damped complex zeros).

One can see that the secondary path has sufficient gain between 150 to 425 Hz, which means that disturbances can be efficiently attenuated in this zone. It is also clear that the reverse path has a significant gain on a large frequency range so its effect can not be neglected.

The orders and the pure delays of the various identified models are given in Table 1. One observes that the secondary path transfer operator has a pure delay of 9 sampling periods and the primary path has a pure delay of 8 sampling periods (coherent values with the length of the two paths - see Fig. 4).

Model	n_B	n_A	d
Primary	20	27	8
Secondary	20	27	9
Reverse	33	33	4

Table 1: Orders of the identified system paths.

---

[5]It expresses the gain of the system in the frequency domain. The gain is a non-dimensional quantity.

[6]The primary path model has been exclusively used for simulation purposes only.

4. Adaptive Infinite/Finite Impulse Response (IIR/FIR) feedforward compensators for Active Noise Control (ANC)

The corresponding block diagrams in open-loop operation and with the compensator system are shown in Fig. 6. The signal $p(t)$ is the image of the disturbance measured when the compensator system is not used (open-loop). The signal $\hat{y}(t)$ denotes the effective output provided by the measurement device when the compensator system is active and which will serve as input to the adaptive feedforward compensator $\hat{N}$. The output of this filter, denoted by $\hat{u}(t)$, is applied to the actuator through an amplifier. The transfer function G (the secondary path) characterizes the dynamics from the output of the filter $\hat{N}$ to the residual noise measurement (amplifier + actuator + dynamics of the acoustic system). The unmeasurable value of the output of the primary path (when the compensation is active) is denoted $x(t)$.
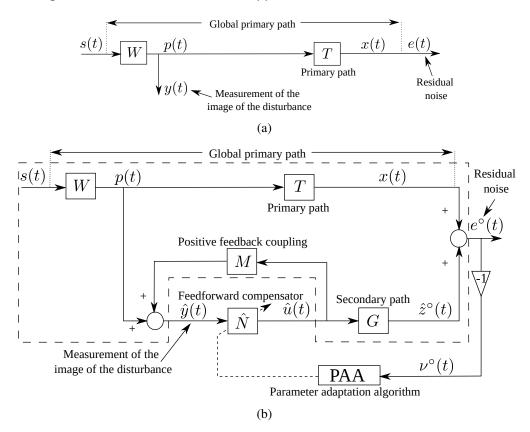
Figure 6: Feedforward active noise control (ANC): in open-loop (a) and with adaptive feedforward compensator (b).

The coupling between the output of the feedforward compensator and the measurement $\hat{y}(t)$ through the compensator actuator is denoted by M. As indicated in Fig. 6, this coupling is a "positive" feedback. The positive feedback may destabilize the system.[7] The system is no longer a pure feedforward compensator.

---

[7]Different solutions for reducing the effect of this internal positive feedback are reviewed in [10, 11].

The objective is to adapt the parameters of the feedforward compensator $N(q^{-1})$ such that the measured residual noise be minimized in the sense of a certain criterion while assuring the stability of the internal positive feedback loop. The optimal IIR feedforward filter (unknown) is defined by:

$$N(q^{-1}) = \frac{R(q^{-1})}{S(q^{-1})}, \tag{3}$$

where

$$R(q^{-1}) = r_0 + r_1 q^{-1} + \ldots + r_{n_R} q^{-n_R}, \tag{4}$$

$$S(q^{-1}) = 1 + s_1 q^{-1} + \ldots + s_{n_S} q^{-n_S} = 1 + q^{-1} S^*(q^{-1}). \tag{5}$$

The estimated compensator is denoted by $\hat{N}(q^{-1})$ or $\hat{N}(\hat{\mathbf{w}}, q^{-1})$ when it is a linear filter with constant coefficients or $\hat{N}(t, q^{-1})$ during estimation (adaptation) of its parameters. The optimal FIR compensator structure is obtained by taking $S = 1$ (i.e. $s_i = 0$, $\forall i = 1 : n_S$).

The input of the feedforward compensator is denoted by $\hat{y}(t)$ and it corresponds to the sum between the disturbance image in the absence of compensation and of the output of the positive feedback path. In the absence of the compensation loop (open-loop operation): $\hat{y}(t) = p(t)$. The *a posteriori*[8] output of the feedforward compensator (which is the control signal applied to the secondary path) is denoted by $\hat{u}(t+1) = \hat{u}(t+1|\hat{\mathbf{w}}(t+1))$. The input-output relationship for the estimated feedforward compensator is given by the equation of the *a posteriori* output:

$$\hat{u}(t+1) = \hat{u}(t+1|\hat{\mathbf{w}}(t+1)) = -\hat{S}^*(t+1, q^{-1})\hat{u}(t) + \hat{R}(t+1, q^{-1})\hat{y}(t+1)$$

$$= \hat{\mathbf{w}}^T(t+1)\mathbf{u}(t) = \left[\hat{\mathbf{w}}_S^T(t), \hat{\mathbf{w}}_R^T(t)\right] \begin{bmatrix} \mathbf{u}_{\hat{u}}(t) \\ \mathbf{u}_{\hat{y}}(t) \end{bmatrix}, \tag{6}$$

where $\hat{\mathbf{w}}$ is the estimated parameter vector and $\mathbf{u}$ is the measurement vector. Their expressions are given below:

$$\hat{\mathbf{w}}^T(t) = [\hat{s}_1(t), \ldots \hat{s}_{n_S}(t), \hat{r}_0(t), \ldots \hat{r}_{n_R}(t)] = [\hat{\mathbf{w}}_S^T(t), \hat{\mathbf{w}}_R^T(t)], \tag{7}$$

$$\mathbf{u}^T(t) = [-\hat{u}(t), -\hat{u}(t-n_S+1), \hat{y}(t+1), \ldots \hat{y}(t-n_R+1)] = [\mathbf{u}_{\hat{u}}^T(t), \mathbf{u}_{\hat{y}}^T(t)], \tag{8}$$

and $\hat{u}(t), \hat{u}(t-1), \ldots$ are the *a posteriori* outputs of the feedforward compensator generated by

$$\hat{u}(t) = \hat{u}(t|\hat{\mathbf{w}}(t)) = \hat{\mathbf{w}}^T(t)\mathbf{u}(t-1), \tag{9}$$

while $\hat{y}(t+1), \hat{y}(t), \ldots$ are the measurements provided by the primary transducer.[9]

The measured residual error satisfies the following equation:

$$e^\circ(t+1) = x(t+1) + \hat{z}^\circ(t+1). \tag{10}$$

---

[8] In adaptive control and estimation the predicted output at t can be computed either on the basis of the previous parameter estimates (*a priori*) or on the basis of the current parameter estimates (*a posteriori*).

[9] $\hat{y}(t+1)$ is available before adaptation of parameters starts at $t+1$.

The *a priori* adaptation error is defined as

$$v°(t+1) = -e°(t+1) = -x(t+1) - \hat{z}°(t+1). \tag{11}$$

The development or analysis of the PAA for estimating in real-time the parameter vector $\hat{\mathbf{w}}$ assumes that

- (Perfect matching condition) There exists a value of the feedforward filter parameters such that[10]

$$\frac{N}{(1-NM)}G = -T \tag{12}$$

- and the characteristic polynomial of the "internal" feedback loop:

$$P(z^{-1}) = A_M(z^{-1})S(z^{-1}) - B_M(z^{-1})R(z^{-1}) \tag{13}$$

is a Hurwitz polynomial.

So the objective of the adaptation algorithm will be to allow the compensator $\hat{N}$ to approach the optimal value at least in the frequency range of interest.

Nevertheless, in the context of the present paper these hypothesis are violated. What it is expected is that the minimization of the residual error in a frequency band will lead to a stable internal loop.

The various FIR/IIR adaptive compensation algorithm which have been tested are summarized in Table 2. All the algorithms can be characterized by the use of a particular form of the parameter adaptation algorithm (PAA) which will be presented next and of a specific "regressor vector" (observation vector) generated through the filtering of available measurements.

4.1. Parameter Adaptation Algorithm (PAA)

Based on stability considerations, a general form for the PAAs has been proposed in [12] which can be expressed using the formalism of [13] as:

$$\mathbf{r}(t) = \mathbf{u}_f(t) = L(q^{-1})\mathbf{u}(t) \tag{14}$$

$$\mathbf{k}(t) = \frac{\mathbf{F}(t)\mathbf{r}(t)}{1 + \mathbf{r}^T(t)\mathbf{F}(t)\mathbf{r}(t)} \tag{15}$$

$$\hat{\mathbf{w}}(t+1) = \hat{\mathbf{w}}(t) + \mathbf{k}(t)v°(t+1) \tag{16}$$

$$v(t+1) = \frac{v°(t+1)}{1 + \mathbf{r}^T(t)\mathbf{F}(t)\mathbf{r}(t)} \tag{17}$$

$$\mathbf{F}(t+1) = \frac{1}{\lambda_1(t)}\left[\mathbf{F}(t) - \frac{\mathbf{F}(t)\mathbf{r}(t)\mathbf{r}^T(t)\mathbf{F}(t)}{\frac{\lambda_1(t)}{\lambda_2(t)} + \mathbf{r}^T(t)\mathbf{F}(t)\mathbf{r}(t)}\right] \tag{18}$$

$$1 \geq \lambda_1(t) > 0 \quad ; \quad 0 \leq \lambda_2(t) < 2 \quad ; \quad F(0) > 0 \tag{19}$$

$\lambda_1(t)$ and $\lambda_2(t)$ allow to obtain various profiles for the adaptation gain matrix $\mathbf{F}(t)$. Four cases are of interest:

---

[10]The parenthesis (q^{-1}) or (z^{-1}) will be omitted in some of the following equations to make them more compact.

- Constant trace algorithm. $\lambda_1(t)$ and $\lambda_2(t)$ are adjusted continuously to maintain constant the trace of the adaptation gain matrix. This allows to move in the optimal direction of the least squares while maintaining the adaptation capabilities. Nevertheless, for accelerating the adaptation transient it may be useful to use a larger adaptation gain transiently.

- Decreasing adaptation gain ($\lambda_1 = 1$, $\lambda_2 = 1$). This is used in self-tuning regime and for initialization of the constant trace algorithm with a higher gain as well as for self-tuning operation (convergence towards a fixed feedforward compensator).

- Variable forgetting factor. This option can be also used for initialization of the constant trace algorithm. The difference is that in this option $\lambda_1(0) < 1$ but it will tend asymptotically to 1. This allows to get transiently a higher adaptation gain than the one used in the constant trace algorithm [12].

- Constant scalar adaptation gain. This is obtained by taking $\mathbf{F}(t) = \gamma\mathbf{I}$, where $\mathbf{I}$ is the identity matrix. One gets a scalar adaptation gain. In this case $\mathbf{k(t)}$ is given by:

$$\mathbf{k}(t) = \frac{\gamma\mathbf{r}(t)}{1 + \gamma\mathbf{r}(t)^T\mathbf{r}(t)} \tag{20}$$

In order to maintain constant the trace of the adaptation gain matrix the values of $\lambda_1(t)$ and $\lambda_2(t)$ are determined from the equation:

$$tr\left(\mathbf{F}(t+1)\right) = \frac{1}{\lambda_1(t)}tr\left(\mathbf{F}(t) - \frac{\mathbf{F}(t)\mathbf{r}(t)\mathbf{r}^T(t)\mathbf{F}(t)}{\alpha(t) + \mathbf{r}^T(t)\mathbf{F}(t)\mathbf{r}(t)}\right) \tag{21}$$

fixing the ratio $\alpha(t) = \lambda_1(t)/\lambda_2(t)$.

The updating of matrix $\mathbf{F}(t)$ is done using the U-D factorization for numerical robustness reason. The details of this algorithm can be found in [8, 12].[11]

When using a scalar adaptation gain, one can see that for very small values of γ one can approximate Eq. (20) by $\mathbf{k}(t) = \gamma\mathbf{r}(t)$ and therefore Eq. (16) by

$$\hat{\mathbf{w}}(t+1) = \hat{\mathbf{w}}(t) + \gamma\mathbf{r}(t)\nu^\circ(t+1), \tag{22}$$

which corresponds almost to the adaptation algorithm used in Filtered u least mean square (FULMS) for IIR compensators [14] and to the filtered x least mean squares (FXLMS) for FIR compensators[15] algorithms except that since the adaptation gain is small and the residual error will vary slowly the quantity $\mathbf{r}(t)\nu^\circ(t+1)$ is replaced by $\mathbf{r}(t-1)\nu^\circ(t)$.

In Table 2, column 1 gives the adaptation algorithms using a matrix adaptation gain derived from stability considerations: Filtered u pseudo linear regression (FUPLR) and Filtered u stability based (FUSBA). Column 2 gives the adaptation algorithms using scalar adaptation gain also derived from stability considerations: normalized filtered u least mean squares (NFULMS) and

---

[11]Routines for the implementation of the algorithm can be downloaded from `http://www.gipsa-lab.grenoble-inp.fr/~ioandore.landau/adaptivecontrol/`

	Paper (Matrix gain)	Paper (Scalar gain)	FULMS (FXLMS) (Scalar gain)
$\hat{\mathbf{w}}(t+1) =$	$\hat{\mathbf{w}}(t) + \frac{F(t)\mathbf{r}(t)}{1+\mathbf{r}^T(t)F(t)\mathbf{r}(t)}v^\circ(t+1)$	$\hat{\mathbf{w}}(t) + \frac{\gamma(t)\mathbf{r}(t)}{1+\gamma(t)\mathbf{r}^T(t)\mathbf{r}(t)}v^\circ(t+1)$	$\hat{\mathbf{w}}(t) + \gamma(t)\mathbf{r}(t-1)v^\circ(t)$
Adapt. gain	$F(t+1)^{-1} = \lambda_1(t)F(t) + $ $+\lambda_2(t)\mathbf{r}(t)\mathbf{r}^T(t)$ $0 \le \lambda_1(t) < 1, 0 \le \lambda_2(t) < 2$ $F(0) > 0$	$\gamma(t) > 0$	$\gamma(t) > 0$
Adaptive	Decr. gain and const. trace	$\gamma(t) = \gamma = const$	$\gamma(t) = \gamma = const$
Self tuning	$\lambda_2 = const.$ $\lim_{t\to\infty} \lambda_1(t) = 1$	$\sum_{t=1}^{\infty} \gamma(t) = \infty, \quad \lim_{t\to\infty}\gamma(t) = 0$	$\sum_{t=1}^{\infty} \gamma(t) = \infty, \quad \lim_{t\to\infty}\gamma(t) = 0$
$\mathbf{u}^T(t) =$	$[-\hat{y}(t),\dots,\hat{u}(t+1),\dots]$	$[-\hat{y}(t),\dots,\hat{u}(t+1),\dots]$	$[-\hat{y}(t),\dots,\hat{u}(t+1),\dots]$
$\mathbf{r}(t) =$	$L\mathbf{u}(t)$ FUPLR: $L = \hat{G}$ FUSBA: $L = \frac{a_M}{\hat{P}}\hat{G}$ $\hat{P} = a_M\hat{S} - \hat{B}_M\hat{R}$	$L\mathbf{u}(t)$ NFULMS: $L = \hat{G}$ SFUSBA: $L = \frac{a_M}{\hat{P}}\hat{G}$ $\hat{P} = a_M\hat{S} - \hat{B}_M\hat{R}$	$L\mathbf{u}(t)$ $L = \hat{G}$
$M = \frac{B_M}{A_M}$	$B_M = b_{1_M}z^{-1} + b_{2_M}z^{-2} + \dots$		
	$A_M = 1 + a_{1_M}z^{-1} + a_{2_M}z^{-2} + \dots$		$A_M = 1$
Stability condition	$\frac{A_M G}{PL} - \frac{\lambda}{2} = SPR$ $\lambda = \max \lambda_2(t)$	$\frac{A_M G}{PL} = SPR$	Unknown

Table 2: Algorithms for IIR (FIR) adaptive feedforward compensation in active noise control (ANC) with acoustic coupling.

scalrar filtered u stability based (SFUSBA). Column 3 gives the now classical FULMS algorithm which uses a scalar adaptation gain (and which corresponds to the FXLMS algorithm when using an FIR compensator). The connections with the NFULMS have been enhanced above. An important observation is that the compensator can be implemented as a FIR or an IIR filter.

The last row of Table 2 summarizes the stability conditions in a deterministic context (asymptotic stability condition for any initial condition on the parameters of the IIR/FIR compensator assuming that a perfect matching solution exist). Despite the fact that the basic hypotheses for stability analysis are violated, it was observed that these "strictly positive real" (SPR) conditions play a fundamental role even in the present context. The reason is that these SPR conditions can be interpreted as approximation conditions with respect to the true gradient [16], namely the approximated gradient used should be within an angle of $\pm 90^\circ$ with respect to the true gradient.

A key role in the various adaptation algorithms is played by the filter L, that helps to satisfy the "strictly positive real condition".

The following procedure is used at each sampling time for implementing the adaptive feedforward compensation:

1. Get the measured image of the disturbance $\hat{y}(t+1)$, the measured residual error $e^\circ(t+1)$, and compute $v^\circ(t+1) = -e^\circ(t+1)$.

11

2. Compute $\mathbf{u}(t)$ and $\mathbf{r}(t)$ using Eqs (8) and (14).
3. Estimate the parameter vector $\hat{\mathbf{w}}(t+1)$ using the PAA given in Eqs (14)-(16).
4. Compute and apply the control $\hat{u}(t+1)$ given in Eq. (6).

5. Youla–Kučera Parametrized Adaptive Feedforward Compensators

The rationale behind the use of the Youla–Kučera parametrized feedforward compensator is to separate the problem of the stabilization of the positive internal loop from the problem of the minimization of the residual noise [5]. In order to achieve this, instead of a standard FIR or IIR feedforward compensator, one can use an Youla–Kučera parametrization of the adaptive feedforward compensator. The central compensator will assure the stability of the internal positive feedback loop and its performance are enhanced in real-time by the direct adaptation of the parameters of the Youla–Kučera Q filter.
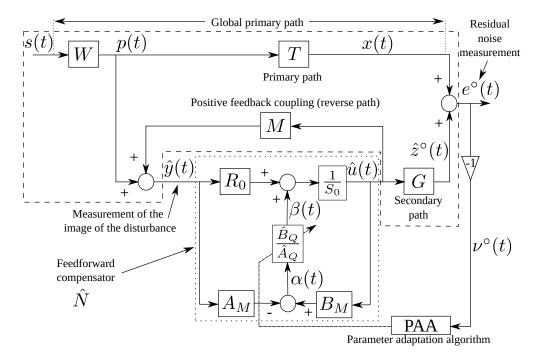
Figure 7: Adaptive feedforward disturbance compensation using Youla–Kučera parametrization.

A block diagram of such an adaptive feedforward compensator is shown in Fig. 7. FIR and IIR Q filters can be used. Details of the specific algorithms can be found in [3, 16]. The transfer operators of the various paths of the ANC system have been given in Section 3.

The optimal Youla–Kučera IIR (YKIIR) feedforward compensator which will minimize the residual noise can be written, using this parametrization, as:

$$N(q^{-1}) = \frac{R(q^{-1})}{S(q^{-1})} = \frac{A_Q(q^{-1})R_0(q^{-1}) - B_Q(q^{-1})A_M(q^{-1})}{A_Q(q^{-1})S_0(q^{-1}) - B_Q(q^{-1})B_M(q^{-1})} \tag{23}$$

where the optimal Youla–Kučera filter $Q(q^{-1})$ can have an IIR or a FIR structure:

$$Q(q^{-1}) = \frac{B_Q(q^{-1})}{A_Q(q^{-1})} = \frac{b_0^Q + b_1^Q q^{-1} + \ldots + b_{n_{B_Q}}^Q q^{-n_{B_Q}}}{1 + a_1^Q q^{-1} + \ldots + a_{n_{A_Q}}^Q q^{-n_{A_Q}}} \tag{24}$$

$R_0(q^{-1})$, $S_0(q^{-1}) = 1 + q^{-1}S_0^*(q^{-1})$ are the polynomials of the central (stabilizing) filter and $A_M(q^{-1})$, $B_M(q^{-1})$ are given in Eq. (1). The FIR Q filter corresponds to $A_Q = 1$, i.e. $a_i^Q = 0$ for $i = 1$ to n_{A_Q}.

An equivalent representation for the YK feedforward compensator is shown in Figure 8. This equivalent representation allows to enhance the fact that for the particular case $R_0 = 0$ the YK feedforward compensator contains implicitly a "neutralization filter" in order to compensate the internal positive feedback present in the system.
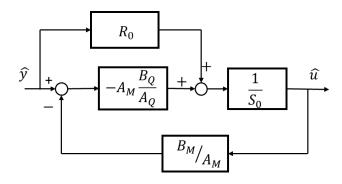
Figure 8: Equivalent representation of the Youla Kučera compensator.

Details on YK algorithms for adaptive feedforward compensation can be found in [2],[16]. Table 3 summarizes the YK type adaptation algorithms used in the various cases as well as the structure of the filters introduced for stability reasons. We will focus next on the YKFIR algorithm which is the algorithm assuring a stable operation in the context of a delay of the secondary path larger than the delay of the primary path.

5.1. Youla–Kučera Finite Impulse Response (YKFIR) Filter

Let's begin by considering Youla–Kučera FIR filters, for which $A_Q(q^{-1}) = 1$. The estimated YKFIR filter is denoted by $\hat{Q}(q^{-1})$ or $\hat{Q}(\hat{\mathbf{w}}, q^{-1})$ when it is a linear filter with constant coefficients or $\hat{Q}(t, q^{-1})$ during estimation (adaptation). The vector of parameters for the estimated $\hat{Q}$ filter

$$\hat{Q}(q^{-1}) = \frac{\hat{B}_Q(q^{-1})}{1} = \hat{b}_0^Q + \hat{b}_1^Q q^{-1} + \ldots + \hat{b}_{n_{B_Q}}^Q q^{-n_{B_Q}} \tag{25}$$

is denoted by

$$\hat{\mathbf{w}}^T = [\hat{b}_0^Q, \ldots, \hat{b}_{n_{B_Q}}^Q] = \hat{\mathbf{w}}_{B_Q}^T. \tag{26}$$

The PAAs have been developed from a stability point of view assuming that:

13

- (Perfect matching condition) There exists a value of the Q filter parameters such that

$$\frac{G \cdot A_M (R_0 - A_M B_Q)}{A_M S_0 - B_M R_0} = -D \qquad (27)$$

- There exists a central feedforward compensator N_0 (R_0, S_0) which stabilizes the internal positive feedback loop formed by N_0 and M and the characteristic polynomial of the closed-loop

$$P_0(z^{-1}) = A_M(z^{-1})S_0(z^{-1}) - B_M(z^{-1})R_0(z^{-1}) \qquad (28)$$

is a Hurwitz polynomial[12].

What it is important to underline, is that in the context of this paper while the first hypothesis is violated, the second is definitely true since the central controller is designed such that the poles of the internal closed loop be asymptotically stable (These poles remain constant independently of the values of the parameters of the FIR Q filter[13]). This is a fundamental difference with respect to the case of using a standard FIR adaptive compensator (see Section 4).

The control signal for the YKFIR is expressed as:

$$\hat{u}(t+1) = \hat{u}(t+1|\hat{\mathbf{w}}(t+1)) = -S_0^*(q^{-1})\hat{u}(t) + R_0(q^{-1})\hat{y}(t+1) + \hat{\mathbf{w}}^T(t+1)\mathbf{u}(t) \qquad (29)$$

where $\hat{\mathbf{w}}(t)$ and $\mathbf{u}(t)$ are given in Table 3. The PAAs are exactly of the same structure as those given in Eqs (14)-(18). All the considerations regarding the type of adaptation gain and its profile remain valid. In order to satisfy the positive real condition for stability, the introduction of the filter L on the measured quantities is important.

Several choices for the filter L will be considered, leading to different algorithms (see Table 3):

FUPLR and NFULMS: $\quad L = \hat{G}$

FUSBA and SFUSBA: $\quad L = \frac{A_M}{\hat{P}_0}\hat{G} \qquad$ with $\qquad \hat{P}_0 = \hat{A}_M S_0 - \hat{B}_M R_0$

The major difference with respect to the standard IIR or FIR compensators as well as with respect to YKIIR compensators is that the FUSBA algorithm can be implemented from the beginning since the polynomial $\hat{P}_0$ is known and remains unchanged during the adaptation process (for YKIIR the filter to be used will depend on currently estimated parameters). This is a significant advantage and this is the key point for assuring a stable operation when the delay of the secondary path is larger than the delay of the primary path.

---

[12]For $R_0 = 0$ and $S_0 = 1$ one has $P_0 = A_M$

[13]Connecting in positive feedback the YK compensator given in Eq. (23) for $A_Q = 1$ with the reverse path $M = \frac{B_M}{A_M}$, it can be verified by simple calculations that the closed loop poles of the internal loop are given by Eq. (28) independently of the values of the Q filter.

	YKIIR	YKFIR	YKIIR	YKFIR
	Matrix adaptation gain		Scalar adaptation gain	
$\hat{\mathbf{w}}(t+1) =$	$\hat{\mathbf{w}}(t) + \frac{F(t)\mathbf{r}(t)}{1+\mathbf{r}^T(t)F(t)\mathbf{r}(t)}v^\circ(t+1)$		$\hat{\mathbf{w}}(t) + \frac{\gamma(t)\mathbf{r}(t)}{1+\gamma(t)\mathbf{r}^T(t)\mathbf{r}(t)}v^\circ(t+1)$	
Adapt. gain	$F(t+1)^{-1} = \lambda_1(t)F(t) + \lambda_2(t)\mathbf{r}(t)\mathbf{r}^T(t)$ $0 \le \lambda_1(t) < 1,\ 0 \le \lambda_2(t) < 2,\ F(0) > 0$		$\gamma(t) > 0$	
Adaptive	Decr. gain and const. trace		$\gamma(t) = \gamma = const$	
Self tuning	$\lambda_2 = const.,\quad \lim\limits_{t\to\infty}\lambda_1(t) = 1$		$\sum\limits_{t=1}^{\infty}\gamma(t) = \infty,\quad \lim\limits_{t\to\infty}\gamma(t) = 0$	
$\hat{\mathbf{w}}(t) =$	$[\hat{b}_0^Q,\dots,a_1^Q,\dots]$	$[\hat{b}_0^Q,\dots]$	$[\hat{b}_0^Q,\dots,a_1^Q,\dots]$	$[\hat{b}_0^Q,\dots]$
$\mathbf{u}^T(t) =$	$[\alpha(t+1),\dots,\beta(t),\dots]$ $\alpha(t) = B_M\hat{u}(t) - A_M\hat{y}(t)$ $\beta(t) = S_0\hat{u}(t) - R_0\hat{y}(t)$	$[\alpha(t+1),\dots]$ $\alpha(t) = B_M\hat{u}(t)$ $-A_M\hat{y}(t)$	$[\alpha(t+1),\dots,\beta(t),\dots]$ $\alpha(t) = B_M\hat{u}(t) - A_M\hat{y}(t)$ $\beta(t) = S_0\hat{u}(t) - R_0\hat{y}(t)$	$[\alpha(t+1),\dots]$ $\alpha(t) = B_M\hat{u}(t)$ $-A_M\hat{y}(t)$
$\hat{P} =$	$A_Q(A_MS_0 - \hat{B}_MR_0)$	$A_MS_0 - \hat{B}_MR_0$	$A_Q(A_MS_0 - \hat{B}_MR_0)$	$A_MS_0 - \hat{B}_MR_0$
$P =$	$A_Q(A_MS_0 - B_MR_0)$	$A_MS_0 - B_MR_0$	$A_Q(A_MS_0 - B_MR_0)$	$A_MS_0 - B_MR_0$
$\mathbf{r}(t) =$	$\mathbf{L}u(t)$ FUPLR: $L = \hat{G}$ FUSBA: $L = \frac{a_M}{\hat{P}}\hat{G}$		$\mathbf{L}u(t)$ NFULMS: $L = \hat{G}$ SFUSBA: $L = \frac{a_M}{\hat{P}}\hat{G}$	
Stability condition	$\frac{A_MG}{PL} - \frac{\lambda}{2} = SPR\quad (\lambda = \max\lambda_2(t))$		$\frac{A_MG}{PL} = SPR$	

Table 3: Algorithms for Youla–Kučera parametrized adaptive feedforward compensation in ANC with acoustic coupling.

5.2. Design of the Central Controller

The main objective of the central controller $N_0(q^{-1}) = \frac{R_0(q^{-1})}{S_0(q^{-1})}$ is to guarantee the stability of the internal positive feedback loop. This can be achieved by using a pole placement design technique (see also [8, Chapter 7]) taking into account that the feedback is positive. All stable poles of the reverse path can be assigned as poles of the closed loop. In order to obtain a small attenuation of the high amplitude picks, one can modify the damping of the poles at the frequencies of those picks. Additional stable poles can be assigned and some fixed part can be added in order to reach some specifications (opening of the loop at 0 Hz and at $0.5f_S$, reducing the maximum of the disturbance–residual noise sensitivity function, etc.). A very interesting particular case which drastically simplify the implementation is to choose the desired poles of the internal closed loop as $P_0 = A_M$. This can be achieved by taking $S_0 = 1$ ($S_0^* = 0$) and $R_0 = 0$. Not only the central controller is drastically simplified but the FUPLR and FUSBA algorithms become identical and therefore the filter L is simpler (simulation results for this algorithm are presented in Appendix B.

5.3. Youla–Kučera Parametrization—Some Remarks

Two major observations when using the Youla–Kučera parametrization have to be made:

15

- If an FIR Q filter is used, the poles of the internal closed loop will be defined by the central compensator R_0, S_0 and they will remain unchanged independently of the values of the parameters of the Q filter.

- If an IIR Q filter is used, the poles of the internal closed loop will be defined by the central controller but additional poles corresponding to the denominator of the estimated Q filter will be added. When the delay of the secondary path is larger than the delay of the primary path, it was observed that the denominator of the estimated Q filter becomes unstable. The use of lattice form algorithms [17], [18] may be an issue in order to force the denominator of the IIR Q filter to remain stable.

As for the standard IIR (FIR) feedforward adaptive compensators described in Section 4, scalar adaptation gains can also be used. The implementation procedure is similar to that for the FIR compensators except that $\hat{\mathbf{w}}(t)$ and $\mathbf{r}(t)$ are given in Table 3 and the control $u(t+1)$ is given in Eq. (29).

6. Simulation Results

The objective of this section is to assess comparatively the performance of the various adaptive feedforward compensation schemes for attenuating broad-band noise disturbances with unknown and time-varying characteristics. All the algorithms mentioned in Tables 3 and 4 have been tested, but only the FIR FUSBA and the YKFIR algorithms have assured a stable operation of the test bench and of the simulations. Decreasing of the adaption gain only pushes forward in time the instability phenomenon. As a consequence only the FIR FUSBA and the YKFIR FUSBA will be further evaluated in terms of performance.

6.1. Number of Adjustable Parameters

The performance of the various compensators will depend on the number of parameters. For a selected PAA various complexities of the feedforward compensator have been tested. A compromise between performance/complexity has to be considered and this value is used for further investigation.

6.2. Type of Parameter Adaptation Algorithms

For a given complexity of the feedforward compensator (60 parameters) the performance obtained with various PAAs have been evaluated. The attenuation is measured on a sample of 3s as the ratio between the variance of the residual noise in the absence of the compensator and the variance of the residual noise in the presence of the compensator. The obtained result is then transformed into decibels.

6.3. Description of Simulations and Results

In this section, simulation results for the Youla-Kučera FIR and the standard FIR feedforward compensators are presented. The disturbance signal used in these simulations is a pseudo random binary sequence (PRBS) generated by a register with $N = 15$ cells passed through a band-pass filter with cut-off frequencies at 150 Hz and 350 Hz. To make these simulation closer to the

Filter type	No. params. [num/den]	Attenuation (dB)
YKFIR	20/0	13.28
YKFIR	30/0	14.55
YKFIR	40/0	19.25
YKFIR	50/0	19.53
YKFIR	60/0	21.02
YKFIR	70/0	21.82
YKFIR	80/0	22.01

Table 4: Influence of the number of parameters on the performance of the YKFIR adaptive compensator (150-350 Hz broad-band disturbance, decreasing gain, 180 sec, simulation).

experimental case, we have introduced small changes in the poles and zeros of the reverse and secondary path models used for the simulation of the system by making these closer to the unit circle (as such there will be a difference between the values of the identified model parameters used in the filters and the values of the parameters used in the simulator).

Filter type	No. params. [num/den]	Adaptation algorithm	Att. (dB)
YKFIR	60/0	NFULMS (scalar gain)	unstable
YKFIR	60/0	FUPLR (matrix gain)	unstable
YKFIR	60/0	SFUSBA (scalar gain)	15.23
YKFIR	60/0	FUSBA (matrix gain)	21.02

Table 5: Influence of the adaptation algorithm on the performance of YKFIR adaptive compensators (150-350 Hz broad-band disturbance, decreasing gain, 180 sec, simulation).

Table 4 summarizes the obtained attenuation results for the YKFIR adaptive filter for various filter orders and the FUSBA adaptation algorithm with decreasing gain. The initial gain is chosen to be of 0.1 per parameter, which implies an initial trace of the adaptation matrix of 0.1 times the number of adapted parameters. The simulation is done over a time duration of 180 sec, where the control algorithm is activated after 15 sec. From these results, it seems that the 60/0 filter order is a good compromise in terms of attenuation vs. complexity. For the reamining simulation results, the 60/0 order filter is used.

Table 5 shows a comparison of various adaptation algorithms for the 60/0 YKFIR feedforward filter. For the scalar gain adaptation, an initial gain of 0.02 is used. Decreasing gain adaptation is obtained by dividing the initial gain by $(1 + \frac{t}{10})$, where the variable t represents the time in seconds since the beginning of the adaptation. The instability of the FUPLR and NFULMS alorithms is the consequence of the violation of the SPR condition over a large frequency range.

For the standard FIR adaptive algorithm, Table 6 shows the influence of the number of parameters on the obtained attenuation. These simulations results have been obtained by closing the loop first at 15 sec using the FUPLR algorithm and then switching to the FUSBA algorithm at 50 sec. The total simulation duration is of 180 sec. The decreasing gain algorithm is used to adapt the

Filter type	No. params. [num/den]	Attenuation (dB)
FIR	20/0	6.66
FIR	30/0	7.67
FIR	40/0	8.16
FIR	50/0	8.33
FIR	60/0	8.37
FIR	70/0	8.43
FIR	80/0	8.51

Table 6: Influence of the number of parameters on the performance of the FIR adaptive compensator (150-350 Hz broad-band disturbance, decreasing gain, 180 sec, simulation).

parameters with an initial gain of 0.01 per parameter. As for the YKFIR adaptive compensator, the disturbance's spectrum is between 150 and 350 Hz. An adaptive FIR compensator with 60 parameters has been considered for further evaluation.
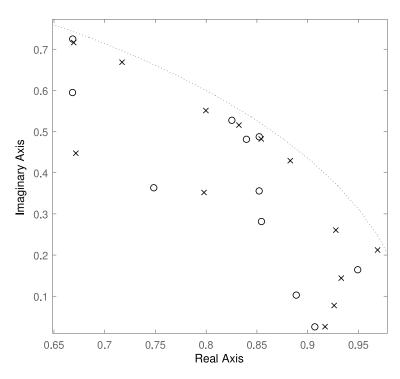
Figure 9: Zoom for the comparison of the positive feedback loop poles when using YKFIR (○) and FIR (×) adaptive compensators (simulation).

Figure 9 can be used to compare the poles of the internal positive feedback loop when using the adaptive YKFIR and the adaptive FIR compensators (it is a zoom of the poles map showing the 1/4 of the map). For the standard FIR there is a pair of poles in low frequencies which are very close to the unit circle.

18

7. Experimental Results

The objective of this section is to compare experimentally on the test bench described in Section 2 the algorithms that showed stable results in simulation.

7.1. Protocols used for performance evaluation

In defining the experimental protocols, a number of performance indicators have to be taken into account: definition of the testing signals, number of parameters to be adapted, type of PAA used, duration of the experiment.

7.2. Testing Signals

The following type of disturbances have been considered

- broad-band noise with a flat DSP between 150 to 200 Hz, 225 to 275 Hz, 300 to 350 Hz,150 to 250 Hz, 250 to 350 Hz, 150 to 350 Hz and 150 to 350 Hz.

- PRBS noise with a flat DSP from 80 to 1250 Hz

- step change from a broad-band disturbance 150 -250 Hz to a broad-band disturbance 250 -350 Hz

A test horizon of 180 s has been chosen as a compromise between the time required to achieve many of the experiments and the convergence horizon. Few tests have been carried on a larger horizon showing the expected improvement in performance.

An important issue is the adaptation capabilities in the presence of step changes in the disturbance characteristics. The step changes occur at 180 sec.

7.3. Experimental Results for Adaptive Youla-Kučera FIR Feedforward Compensators

Filter type	No. params. [num/den]	Attenuation (dB)
YKFIR	40/0	19.79
YKFIR	60/0	20.58
YKFIR	80/0	20.66

Table 7: Influence of the number of parameters on the performance of the YKFIR (150-350 Hz broad-band disturbance, 180 s experimental).

Table 7 gives results obtained with YKFIR FUSBA for various complexities of the Q FIR filter on a 180 s experiment using a broad-band disturbance 150-350 Hz and a decreasing matrix adaptation gain. The Q FIR filter with 60 parameters has been selected for further investigation. Table 8 gives the performance of the 60 parameters YKFIR for various PAAs and a duration of 180 s for the experiment. It can be seen that the FUSBA (matrix adaptation gain) and the SFUSBA (scalar adaptation gain) algorithms give the best results[14].

---

[14]The lower perfance of the FUPLR and NFULMS algorithms can be explained by the fact that the strictly positive real condition is violated over a significant frequency range.

Filter type	No. params. [num/den]	Adaptation algorithm	Att. (dB)
YKFIR	60/0	NFULMS (scalar gain)	5.57
YKFIR	60/0	FUPLR (matrix gain)	5.65
YKFIR	60/0	SFUSBA (scalar gain)	19.90
YKFIR	60/0	FUSBA (matrix gain)	20.94

Table 8: Influence of the adaptation algorithm on the performance of YKFIR adaptive compensators, 180 sec, experimental.

Figure 10 gives the time-domain performance of the YKFIR configuration with 60 parameters using the FUSBA algorithm. A constant trace adaptation gain has been used with a trace of $trace = 60 \times 0.002$. The system operates in open loop for 15 s. The attenuation is evaluated every 15 secs on a horizon of 15s. One can say that the system almost reaches final attenuation after 700 s. Table 9 gives information about the transient behaviour. One can see that after 180 s almost 90% of the final performance is achieved.

Filter type	No. params. [num/den]	Duration	Attenuation (dB)
YKFIR	60/0	180s	20.58
YKFIR	60/0	800s	22.76

Table 9: Influence of the experiment's length on the performance (150-350 Hz broad-band disturbance).
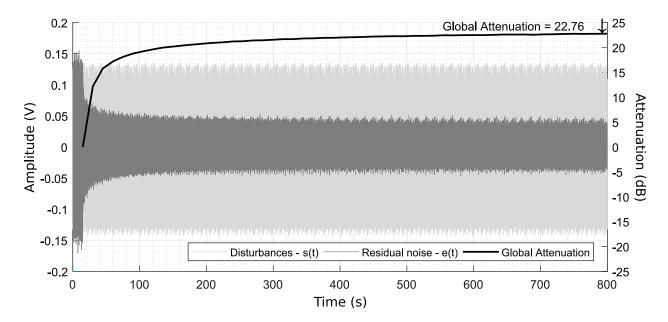
Figure 10: Performance of YKFIR adaptive compensator with 60 parameters (experimental).

20

Filter type	No. params. [num/den]	Bandwidth	Disturbance	Att. (dB)
YKFIR	60/0	50Hz	150Hz-200Hz	32.33
YKFIR	60/0	50Hz	225Hz-275Hz	33.19
YKFIR	60/0	50Hz	300Hz-350Hz	29.30
YKFIR	60/0	100Hz	150Hz-250Hz	31.68
YKFIR	60/0	100Hz	250Hz-350Hz	23.94
YKFIR	60/0	200Hz	150Hz-350Hz	20.57
YKFIR	60/0	1250Hz	PRBS	5.20

Table 10: Influence of the disturbance characteristics on the performance of the YKFIR adaptive compensator (experimental).

Table 10 gives the performance of the YKFIR for various types of broad-band disturbances. The duration of the experiment is of 180 sec. As expected, the attenuation depends on the bandwidth of the disturbance.

Figure 11 shows the evolution of the output of the system using YKFIR adaptive feedforward compensator with constant trace adaptation gain for a change in the characteristics of the disturbance at t=180 sec. The first disturbance is a broad band disturbance located between 150 and 250 Hz, while the second one is a broad band disturbance located between 250-350 Hz (the system operates in open-loop for the first 15 sec).

7.4. Experimental Results for FUSBA FIR adaptive compensators

Filter type	No. params.	Attenuation (dB)
FIR	20/0	9.20
FIR	30/0	9.95
FIR	40/0	9.98
FIR	50/0	10.04
FIR	60/0	10.35
FIR	80/0	10.07

Table 11: Influence of the number of parameters on the performance of standard FIR compensator (150-350 Hz broad-band disturbance, 180sec experiment).

Table 11 gives results obtained with a standard FIR FUSBA compensator for various complexities of the FIR filter on a 180 sec experiment using a broad-band disturbance 150-350 Hz. The FIR filter with 60 parameters has been selected for further investigation.

Nevertheless, the difference observed on this shorter horizon does not allow to conclude clearly for the compromise performance/complexity.

Figure 12 illustrates the performance of the FUSBA FIR using a constant trace adaptation gain over a horizon of 800 sec (60 parameters). One can see that the steady-state operation has not yet been obtained.
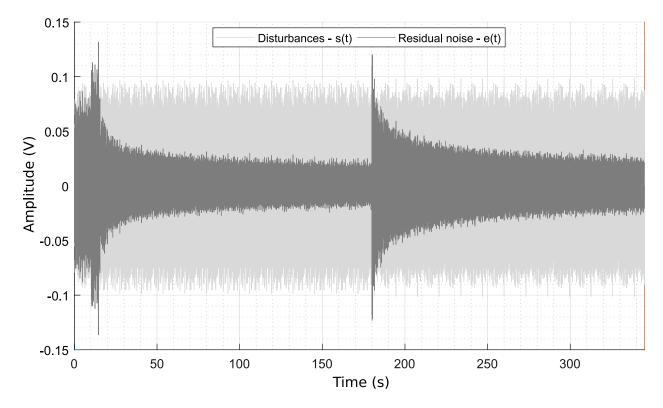
Figure 11: Transient performance of YKFIR adaptive compensator (experimental). 0 to 180s: broad-band disturbance 150-250 Hz; 180 to 345 s: broad-band disturbance 250-350 Hz; open loop operation: 0 to 15 sec.

Figure 13 shows comparatively the PSD in open-loop and under the effect of the FUSBA FIR compensator and of the FUSBA YKFIR compensator (each with 60 parameters, and the same constant trace adaptation gain with $trace = 60 \times 0.002$). Experiment duration: 800 sec. It can be seen on this figure that the performance of the FUSBA YKFIR is better than the performance of the FUSBA FIR compensator for the same complexity and the same adaptation gain. When using FUSBA FIR scheme, the PSD of the residual noise shows the presence of two very significant peaks (around 50 Hz and 450 Hz) correspondng to very low damped poles of the internal closed loop. This questions the robustness of the scheme (instability risk).

8. Conclusions

Based on the experimental and simulation results presented, it can be concluded that the YK-FIR adaptive compensator provides a stable operation and good performance of the adaptive feed-forward active noise compensation system when the delay of the compensator path is larger than the delay of the primary path (between the reference source and the residual noise measurement). Its performance is much better than the one of a standard FIR adaptive compensator using the FUSBA algorithm. In addition there are doubts upon the robustness of the FIR adaptive feed-forward compensator. The main explanations for this good behaviour for the YKFIR adaptive compensator using a FUSBA algorithm are that the internal positive closed-loop will remain sta-

22
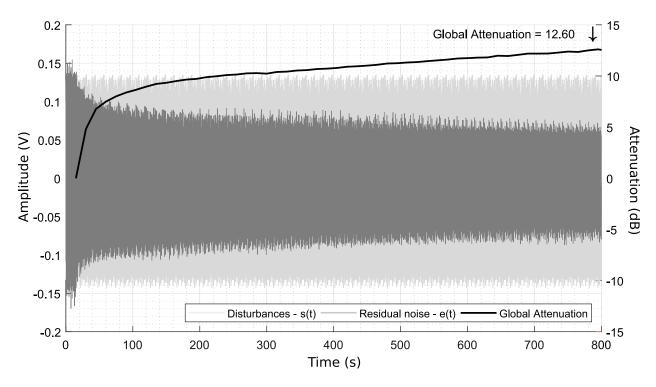
Figure 12: Performance of FUSBA FIR adaptive compensator (60 parameters, experimental).

ble independently of the values of the adaptive parameters and that the filter to be used for the implementation of the parameter adaptation algorithm is fixed and provides a better approximation of the gradient than the other filtering options used in the various algorithms. Unfortunately, the FULMS and FXLMS algorithms as well as the standard IIR compensators using FUPLR or NFULMS algorithms do not work properly in this configuration (instability). While the YKIIR configuration considered is also unstable, the use of a lattice type algorithms may lead to a stable implementation and this is a subject of further investigation.

Appendix A. Stability/Instability Issues. A Qualitative Analysis

The objective of this appendix is to show that certain adaptive feedforward configurations, in the presence of delay of the secondary path larger than the one of the primary path, present instability risks. One considers the following example:

Primary path:[15] $T = \frac{B_T}{A_T} = \frac{q^{-2}}{1}$.

Reverse path: $M = \frac{B_M}{A_M} = \frac{q^{-1}}{1}$.

Secondary path: $G = \frac{B_G}{A_G} = \frac{q^{-2}(1+a_{1_G}q^{-1})}{1}$.

The secondary path is characterized by a pure delay of 2 sampling periods and a fractional delay defined by the term $(1+a_{1_G}q^{-1})$ (with a d.c. gain $(1+a_{1_G})$). For $a_{1_G} > 1$, the fractional

---

[15]In some examples, in order to simplify the analysis, we will consider $T = \alpha q^{-2}$.
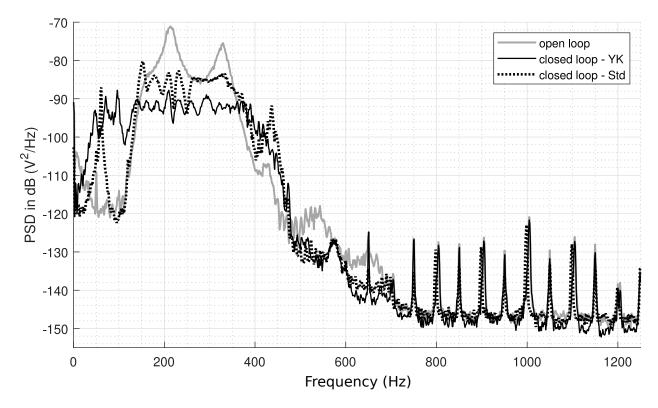
Figure 13: Power spectral density for FUSBA FIR and FUSBA YKFIR (60 parameters, experimental).

delay is larger than $0.5T_s$ and the associated zero is unstable (outside the unit circle) [19]. As such, the delay of the secondary path is larger than the delay of the primary path. We will analyse the system for various configurations of the adaptive feedforward compensator.

When "perfect matching" is achieved, we implicitly assume "persistance of excitation", i.e. residual error equal zero implies that parameters converge towards the values assuring perfect matching.

Appendix A.1. IIR adaptive compensator

The IIR adaptive compensator considered has the following structure

$$\hat{N} = \frac{\hat{r}_0}{1 + \hat{s}_1 q^{-1}} \tag{A.1}$$

(the time argument has been omitted). The effective compensator constituted by $\hat{N}$ in positive feedback with M will be characterized by the transfer operator:

$$\hat{N}_{CL} = \frac{\hat{r}_0}{1 + (\hat{s}_1 - \hat{r}_0)q^{-1}}. \tag{A.2}$$

The stability of the internal loop requires that the $|\hat{s}_1 - \hat{r}_0| < 1$. The possibility that this value becomes > 1 asymptotically should be avoided.

24

The compensation path (concatenation of the effective compensator and the secondary path) denoted by C is characterized by the transfer operator:

$$C = \frac{\hat{r}_0 q^{-2}(1 + a_{1_G} q^{-1})}{1 + (\hat{s}_1 - \hat{r}_0) q^{-1}}. \tag{A.3}$$

For perfect matching, one should have

$$\frac{\hat{r}_0 q^{-2}(1 + a_{1_G} q^{-1})}{1 + (\hat{s}_1 - \hat{r}_0) q^{-1}} = -q^{-2}. \tag{A.4}$$

Clearly this can be achieved for $\hat{r}_0 = -1$; $\hat{s}_1 - \hat{r}_0 = a_{1_G}$ and the adaptation mechanism will drive the adjustable parameters towards these values. Therefore for $a_{1_G} > 1$, the internal loop will be unstable.

Appendix A.2. FIR adaptive compensator

The adaptive compensator in this case will have the structure

$$\hat{N} = \frac{\hat{r}_0}{1} \tag{A.5}$$

The effective compensator will be characterized by

$$\hat{N}_{CL} = \frac{\hat{r}_0}{1 - \hat{r}_0 q^{-1}}. \tag{A.6}$$

The compensation path will be characterized by

$$C = \frac{\hat{r}_0 q^{-2}(1 + a_{1_G} q^{-1})}{1 - \hat{r}_0 q^{-1}}. \tag{A.7}$$

For perfect matching one should have (in this case $T = a_{1_G} q^{-2}$)

$$\frac{\hat{r}_0 q^{-2}(1 + a_{1_G} q^{-1})}{1 - \hat{r}_0 q^{-1}} = -a_{1_G} q^{-2}. \tag{A.8}$$

Clearly the equilibrium point will be $-\hat{r}_0 = a_{1_G}$ and the system can become unstable for $a_{1_G} > 1$ (fractional delay larger than $0.5 T_s$).

Appendix A.3. YKIIR adaptive compensator

The adaptive compensator has a Youla-Kučera structure with

$$\hat{Q} = \frac{\hat{b}_0^Q}{1 + \hat{a}_1^Q q^{-1}} \tag{A.9}$$

25

The central controller is characterized by $R_0 = r_0$ and $S_0 = 1$ ($|r_0| < 1$). The compensator will be given by

$$\hat{N} = \frac{(1 + \hat{a}_1^Q q^{-1}) r_0 - \hat{b}_0^Q}{(1 + \hat{a}_1^Q q^{-1}) - \hat{b}_0^Q q^{-1}} \tag{A.10}$$

The effective compensator will be characterized by

$$\hat{N}_{CL} = \frac{(1 + \hat{a}_1^Q q^{-1}) r_0 - \hat{b}_0^Q}{(1 + \hat{a}_1^Q q^{-1})(1 - r_0 q^{-1})}. \tag{A.11}$$

The compensation path will be characterized by

$$C = \frac{\left[(1 + \hat{a}_1^Q q^{-1}) r_0 - \hat{b}_0^Q \right] q^{-2} (1 + a_{1_G} q^{-1})}{(1 + \hat{a}_1^Q q^{-1})(1 - r_0 q^{-1})} \tag{A.12}$$

For perfect matching one should have

$$\frac{\left[(1 + \hat{a}_1^Q q^{-1}) r_0 - \hat{b}_0^Q \right] q^{-2} (1 + a_{1_G} q^{-1})}{(1 + \hat{a}_1^Q q^{-1})(1 - r_0 q^{-1})} = -a_{1_G} q^{-2} \tag{A.13}$$

It can be verified that $\hat{a}_1^Q = a_{1_G}$ and $r_0 - \hat{b}_0^Q = -a_{1_G}$ assure the perfect matching and this equilibrium point corresponds to an internal loop which will be unstable for $a_{1_G} > 1$.

Appendix A.4. YKFIR adaptive compensator

In this case

$$\hat{Q} = \frac{\hat{b}_0^Q}{1}; \qquad R_0 = r_0, \; S_0 = 1 \quad (|r_0| < 1). \tag{A.14}$$

The YKFIR feedforward compensator will be characterized by

$$\hat{N} = \frac{r_0 - \hat{b}_0^Q}{1 - \hat{b}_0^Q q^{-1}} \tag{A.15}$$

The effective feedforward compensator will be characterized by

$$\hat{N}_{CL} = \frac{r_0 - \hat{b}_0^Q}{1 - r_0 q^{-1}}. \tag{A.16}$$

Therefore, the internal closed-loop can not become unstable since the closed loop pole is fixed and depends only upon r_0. This pole is asymptotically stable since $|r_0| < 1$. The transfer operator of the compensation path is characterized by

$$C = \frac{\left(r_0 - \hat{b}_0^Q \right) q^{-2} (1 + a_{1_G} q^{-1})}{1 - r_0 q^{-1}} \tag{A.17}$$

26

and the perfect matching condition becomes

$$\frac{\left(r_0 - \hat{b}_0^Q\right) q^{-2}(1 + a_{1_G}q^{-1})}{1 - r_0 q^{-1}} = -q^{-2} \tag{A.18}$$

Clearly the "perfect matching" condition can not be achieved for $a_{1_G} > 1$. The error will be characterized by

$$\varepsilon(t) = q^{-2} \left(1 + \frac{\left(r_0 - \hat{b}_0^Q\right)(1 + a_{1_G}q^{-1})}{1 - r_0 q^{-1}}\right) p(t) \tag{A.19}$$

The adaptation will try to minimize the error, but the internal loop will remain stable for all possible values of $\hat{b}_0^Q$. Augmenting the order of $\hat{B}_Q$ will allow to further reduce the error but the internal loop will remain stable.

Conclusion: This qualitative analysis has shown that for the case where the delay of the secondary path exceeds by more than $0.5T_s$ the delay of the primary path, the risk of instability occurs for IIR, FIR and YKIIR feedforward compensators. For the YKFIR this risk does not exist and the poles of the internal loop are fixed and defined by the central controller.

Appendix B. A simplified YKFIR adaptive compensator

Choosing $R_0 = 0$ and $S_0 = 1$ for the central controller, the FUPLR, NFULMS, FUSBA and SFUSBA adaptation algorithms will use the same filter $L = \hat{G}$ (since in this case $P = A_M$) and the stability condition becomes : "$G/\hat{G} - \lambda/2$ should be strictly positive real" (where $\lambda = 0$ for scalar adaptation gain). The parameters will be adapted using Eq. (16) with $\mathbf{k}(t)$ given by Eq. (15) for a matrix adaptation gain and by Eq. (20) for a scalar adaptation gain. From Eq. (29) it results that in this case the control $\hat{u}(t+1)$ is given by :

$$\hat{u}(t+1) = \hat{u}(t+1|\hat{\mathbf{w}}(t+1)) = \hat{\mathbf{w}}^T(t+1)\mathbf{u}(t) \tag{B.1}$$

A YKFIR compensator with 60/0 parameters has been considered for simulations. A disturbance with a flat spectrum between 150 and 350 Hz has been used as disturbing noise. Figure B.14 gives the time evolution of the residual noise for the case of a matrix adaptation gain with constant trace (trace=60). Figure B.15 gives the time evolution of the residual noise for the case of a scalar adaptation gain with a constant trace of 60 (i.e. a scalar gain $\gamma = 1$. Figure B.16 shows the comparison between the PSD for the two adaptation schemes. the corresponding PSD (computed for the last 10s of the simulation). A global attenuation of 24.32 dB is obtained for the matrix algorithm and 22.86 dB for the scalar one.

References

[1] C. Jacobson, J. Johnson, C.R., D. McCormick, W. Sethares, Stability of active noise control algorithms, Signal Processing Letters, IEEE 8 (3) (2001) 74 –76.
[2] I. Landau, M. Alma, T. Airimitoaie, Adaptive feedforward compensation algorithms for active vibration control with mechanical coupling, Automatica 47 (10) (2011) 2185 – 2196.
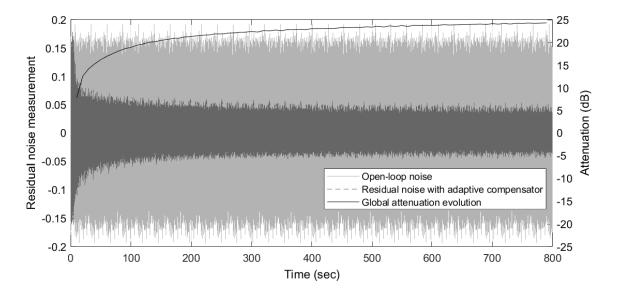
Figure B.14: Time domain evolution of the residual noise for the YKFIR 60/0 simplified adaptative compensator with matrix adaptation gain (constant trace of 60).
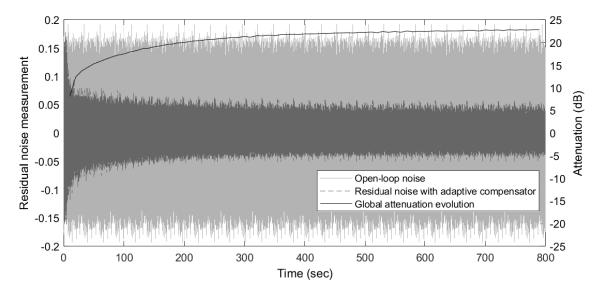
Figure B.15: Residual noise of the YKFIR 60/0 adaptation compensator with scalar gain (constant trace of 60, gain per parameter: 1).

[3] I. D. Landau, T.-B. Airimitoaie, M. Alma, A Youla–Kučera parametrized adaptive feedforward compensator for active vibration control with mechanical coupling, Automatica 48 (9) (2012) 2152 – 2158.
[4] S. Elliott, Signal processing for active control, Academic Press, San Diego, California, 2001.
[5] J. Zeng, R. de Callafon, Recursive filter estimation for feedforward noise cancellation with acoustic coupling, Journal of Sound and Vibration 291 (3-5) (2006) 1061 – 1079.

28
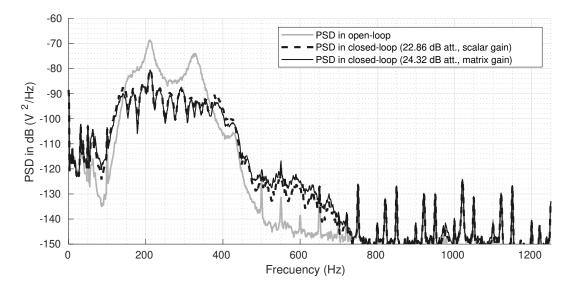
Figure B.16: PSD estimate of the YKFIR 60/0 adaptation compensator with scalar and matrix adaptation gains (constant trace of 60).

[6] R. Fraanje, Robust and fast schemes in broadband active noise and vibration control, Ph.D. thesis, University of Twente, Twente, The Netherlands (2004).

[7] J. Hu, J.-F. Lin, Feedforward active noise controller design in ducts without independent noise source measurements, IEEE Trans. on Control System Technology 8 (3) (2000) 443–455.

[8] I. D. Landau, T.-B. Airimitoaie, A. Castellanos Silva, A. Constantinescu, Adaptive and Robust Active Vibration Control—Methodology and Tests, Advances in Industrial Control, Springer, London, 2017.

[9] R. Melendez, I. Landau, L. Dugard, G. Buche, Data driven design of tonal noise feedback cancellers, in: Proceedings of the 20th IFAC World Congress, Toulouse, France, 2017, pp. 916–921.

[10] M. Kuo, D. Morgan, Active noise control systems-Algorithms and DSP implementation, Wiley, New York,, 1996.

[11] S. Kuo, D. Morgan, Active noise control: a tutorial review, Proceedings of the IEEE 87 (6) (1999) 943 – 973.

[12] I. D. Landau, R. Lozano, M. M'Saad, A. Karimi, Adaptive control, 2nd Edition, Springer, London, 2011.

[13] S. Haykin, Adaptive Filter Theory, Prentice Hall, Englewood Cliffs N.J., 1996.

[14] L. Eriksson, Development of the filtered-U LMS algorithm for active noise control, J. of Acoustical Society of America 89 (1) (1991) 257–261.

[15] B. Widrow, D. Shur, S. Shaffer, On adaptive inverse control, in: Proc. 15th Asilomar Conf. Circuits, Systems and Computers, Pacific Grove, CA, USA, 1981.

[16] I. D. Landau, T.-B. Airimitoaie, M. Alma, IIR Youla–Kučera parameterized adaptive feedforward compensators for active vibration control with mechanical coupling, IEEE Transactions on Control System Technology 21 (3) (2013) 765–779.

[17] P. Regalia, Adaptive IIR Filtering in Signal Processing and Control, Dekker, New York, 1995.

[18] J. Lu, C. Shen, X. Qiu, B. Xu, Lattice form adaptive infinite impulse response filtering algorithm for active noise control, The Journal of the Acoustical Society of America 113 (1) (2003) 327–335.

[19] I. Landau, G. Zito, Digital control systems – Design, identification and implementation, Springer, London, 2005.

ALGORITHMS FOR ADAPTIVE FEEDFORWARD NOISE ATTENUATION - A COMPARATIVE EXPERIMENTAL EVALUATION

Algorithms for adaptive feedforward noise attenuation – A comparative experimental evaluation

Tudor-Bogdan Airimitoaie, Ioan Doré Landau, Raul Melendez, and Luc Dugard

Abstract—Adaptive feedforward broad-band noise compensation is currently used when a correlated measurement with the disturbance (an image of the disturbance) is available. Most of the active feedforward noise control systems feature an internal "positive" acoustical feedback between the compensation system and the reference source (a correlated measurement with the disturbance) which has to be taken into account. Adaptive algorithms for active feedforward noise attenuation have been developed since 1985 from local optimization point of view and further improved and analysed. Later on, adaptive algorithms for feedforward active vibration control have been developed from a stability point of view and these algorithms can be used in adaptive feedforward noise control. The various algorithms existing in the literature of adaptive feedforward noise control can be viewed as particular cases of the algorithms developed from a stability point of view. In order to separate the problem of stabilizing the internal positive feedback loop from the minimization of the residual noise, the Youla–Kučera parametrization of the feedforward noise compensator has been proposed by Zeng and de Callafon (2006). This approach can be extended to the adaptive case and has been extensively studied in the field of active vibration control. Nevertheless, this approach can be used also in the adaptive active noise control. The paper tries to present, in an unified manner, the available algorithms and compensator structures for adaptive feedforward noise attenuation and to propose a comparative experimental evaluation on a relevant experimental test-bench (a duct silencer). A number of improvements of the current algorithms are also proposed and tested.

Index Terms—active noise control, adaptive feedforward compensation, Youla–Kučera parametrization, positive feedback coupling.

List of Acronyms

ANC	Active Noise Control
ANVC	Active Noise and Vibration Control
AVC	Active Vibration Control
FIR	Finite Impulse Response
FULMS	Filtered-u least mean squares
FUPLR	Filtered-u pseudo linear regression
FUSBA	Filtered-u stability based algorithm
FXLMS	Filtered-x least mean squares
IIR	Infinite Impulse Response
FIRYK	Youla–Kučera parametrized IIR adaptive feedforward compensator using a FIR Youla–Kučera filter
IIRYK	Youla–Kučera parametrized IIR adaptive feedforward compensator using an IIR Youla–Kučera filter
LMS	Least mean squares
NFULMS	Normalized FULMS
PAA	Parameter Adaptation Algorithm
PRBS	Pseudo random binary sequence
PSD	Power Spectral Density
SFUSBA	Scalar FUSBA
SPR	Strictly Positive Real (transfer function)
TET	Task execution time

Tudor-Bogdan Airimitoaie is with the Univ. Bordeaux, CNRS, Bordeaux INP, IMS, 33405 Talence, France (e-mail: tudor-bogdan.airimitoaie@u-bordeaux.fr).

Ioan Doré Landau, Raul Melendez, and Luc Dugard are with the Univ. Grenoble Alpes, CNRS, Grenoble INP, GIPSA-lab, 38000 Grenoble, France (e-mails: ioan-dore.landau@gipsa-lab.grenoble-inp.fr, raul.melendez@gipsa-lab.grenoble-inp.fr, and luc.dugard@gipsa-lab.grenoble-inp.fr).

I. Introduction

ADAPTIVE feedforward noise attenuation is widely used when a well correlated signal with the disturbance (image of the disturbance) is available ([1], [2], [3], [4]). The first references go back roughly to 1985 ([5]). In many systems, there is a positive acoustical coupling between the feedforward compensation system and the measurement of the image of the disturbance. This often leads to the instability of the system. In the context of this inherent "positive" feedback, the adaptive feedforward compensator should minimize the effect of the disturbance while simultaneously assuring the stability of the internal positive feedback loop. This problem has been clearly identified by the mid nineties [6], [7].

At the end of the nineties ([8]), adaptive feedback noise control emerged as an efficient solution for cancelling single or multiple tonal disturbances ([9], [10]) taking advantage of the internal model principle and the Youla–Kučera parametrization of the feedback controller. Nevertheless, the efficient use of the feedback approach for attenuation of broad-band noise is limited by the Bode integral. Therefore one can say that the adaptive feedforward noise compensation is particularly dedicated to the attenuation of broad-band noise with unknown and time-varying characteristics. For this reason, the present paper will focus on the experimental evaluation of the various feedforward compensator structures and adaptation algorithms in the presence of broad-band noise disturbances.

A major component of such a system is the PAA. In the field of ANC, the first algorithm used was the so called least mean squares (LMS) ([5]) derived from a local minimization of a quadratic criterion in terms of the residual noise. Many contributions have been done on the analysis of the properties of this algorithm and the improvement of the algorithm. Filtering of the regressor vector was one of the ways for improving the adaptation and the so called "Filtered-U LMS" (FULMS) ([11], [12], [13]) seems to be the most used algorithm in recent publications ([14], [15]).

For the analysis of these algorithms in the presence of an internal positive feedback an attempt is made in [12] where the asymptotic convergence in a stochastic environment of the FULMS algorithm is discussed. Further results on the same direction can be found in [13]. The authors use the Ljung's ODE method ([16]) for the case of a scalar vanishing adaptation gain. Unfortunately, this is not enough because nothing is said about the stability of the system with respect to initial conditions and when a non-vanishing adaptation gain is used (to keep adaptation capabilities). The authors have assumed that the positive feedback does not destabilize the system which is not a realistic assumption.

A different approach emerged in the area of ANVC, namely the design of the adaptation algorithms starting from a stability point of view and taking into account the internal positive feedback from the beginning. A first reference in ANC for a stability approach in the presence of the internal positive feedback is ([7]). Unfortunately, the applicability of the results is very limited since one assumes that the secondary (compensatory) path has a simple positive gain or it is characterized by a SPR transfer function (unrealistic hypothesis). In the field of AVC, the paper [17] provides a full synthesis procedure for asymptotically stable adaptation algorithms using IIR feedforard compensators in the presence of the internal feedback. These algorithms can be used also in ANC as it will be shown in this paper. It is important to note that most of the algorithms used for the adaptive feedforward compensation can be viewed as particular approximations of the algorithms derived from stability considerations.

An interesting idea is presented in the paper [4]: separate the stabilization of the internal positive feedback loop from the minimization of the residual noise. This can be done by using a Youla–Kučera parametrization of the feedforward compensator. A tuning procedure based on system identification has been proposed and tested on a silencer. This idea has been used in [18], [19] for developing direct adaptive feedforward compensation schemes using Youla–Kučera parametrization of FIR or IIR form for the feedforward compensator. These algorithms have been extensively tested and compared with other algorithms in the field of AVC [20]. Nevertheless, they can be used also in the field of ANC as it will be shown in this paper. These algorithms have a number of advantages with respect to IIR feedforward compensators including:

- Possibility to pre-assign the poles of the internal positive closed-loop (not possible with IIR(FIR) feedforward compensators);
- Easier satisfaction of the positive real condition for stability.

The objectives of this paper are:

- To comparatively evaluate experimentally in the context of ANC the various algorithms developed in AVC from the stability point of view and the algorithms currently used in ANC for attenuating broad-band noise disturbances;
- To compare experimentally the performance of Youla–Kučera parametrized feedforward compensators with those of the IIR (FIR) adaptive feedforward compensators for various types of PAA;
- To try to present in an unified manner the various PAA used in ANVC.
- To evaluate comparatively the complexity of the various configurations in terms of "performance" and "task execution time" (TET).

The experimental evaluation of the various algorithms and compensator configurations is done under identical protocols on an experimental test-bench which represents the core of a duct silencer.

The paper is organized as follows: in Section II, the experimental setting is presented. Section III describes the various paths of the system and gives their experimentally identified frequency characteristics (the identification procedure is presented in Appendix A). The IIR adaptive compensators together with the corresponding PAA are reviewed in Section IV. In Section V the Youla–Kučera based adaptive feedforward algorithms are presented. Section VI presents the results of the comparative experimental evaluation. Conclusions of these evaluations are given in Section VII.

II. EXPERIMENTAL SETUP

The view of the test-bench used for experiments is shown in Fig. 1 and its detailed scheme is given in Fig. 2. The actual dimensions of the test-bench are given in Fig. 3.

Fig. 1. Duct active noise control test-bench (Photo).

The speaker used as the source of disturbances is labeled as 1, while the control speaker is marked as 2. At pipe's open end, the microphone that measures the system's output (residual noise $e(t)$) is denoted as 3. Inside the pipe, close to the source of disturbances, the second microphone, labeled as 4, measures the perturbation's image, denoted as $y(t)$. Additionally, we denote $u(t)$ the control signal, and $s(t)$ the disturbance. The transfer function between the disturbance's speaker and the microphone ($1\rightarrow3$) is called *Global Primary Path*, while the transfer function between the control speaker and the microphone ($2\rightarrow3$) is denoted *Secondary Path*. The
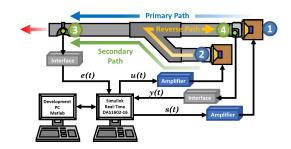
Fig. 2. Duct active noise control test-bench diagram.
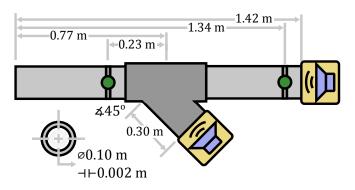
Fig. 3. Duct active noise control test-bench dimensions.

transfer function between microphones (4→3) is called *Primary Path*. The internal coupling found between (2→4) is denoted *Reverse Path*. These marked paths have a double differentiator behavior, since as input we have the voice coil displacement and as output the air acoustical pressure.

Both speakers are connected to an xPC Target computer with Simulink Real-time® environment through a pair of high definition power amplifiers and a data acquisition card. A second computer is used for development, design and operation with Matlab®. The sampling frequency has been chosen in accordance with the recommendations given in [20]. Taking into account that disturbances up to 400 Hz may need to be attenuated, a sampling frequency $f_s = 2500$ Hz has been chosen ($T_s = 0.0004$ sec), i.e., approximately six times the maximum frequency to attenuate.

In this configuration, speakers are isolated inside wood boxes filled with special foam in order to create anechoic chambers and reduce the radiation noise produced. These boxes have dimensions $0.15\,\mathrm{m} \times 0.15\,\mathrm{m} \times 0.12\,\mathrm{m}$, giving a chamber volume of $2.7\,\mathrm{L}$.

III. SYSTEM DESCRIPTION

The primary (T), secondary (G), and reverse (positive coupling) (M) paths are characterized by the asymptotically stable transfer operators:

$$X(q^{-1}) = q^{-d_x} \frac{B_X(q^{-1})}{A_X(q^{-1})}$$

$$= q^{-d_x} \frac{b_1^X q^{-1} + ... + b_{n_{B_X}}^X q^{-n_{B_X}}}{1 + a_1^X q^{-1} + ... + a_{n_{A_X}}^X q^{-n_{A_X}}}, \quad (1)$$

with $B_X = q^{-1} B_X^*$ for any $X \in \{G, M, T\}$. $\hat{G} = q^{-d_G} \frac{\hat{B}_G}{\hat{A}_G}$, $\hat{M} = q^{-d_M} \frac{\hat{B}_M}{\hat{A}_M}$, and $\hat{T} = q^{-d_T} \frac{\hat{B}_T}{\hat{A}_T}$ denote the identified (estimated) models of G, M, and T. Both B_G and B_M have a one step discretization delay.

The system's order is defined by (the indexes G, M, and T have been omitted):
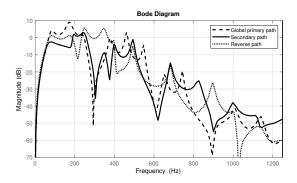
$$n = max(n_A, n_B + d). \quad (2)$$

Fig. 4. Frequency characteristics of the Primary, Secondary and Reverse paths identified models.

The frequency characteristics of the identified models for the primary[1], secondary and reverse paths are shown in Fig. 4. These characteristics present multiple resonances (low damped complex poles)[2] and anti-resonances (low damped complex zeros).

One can see that the secondary path has a high gain between 70 to 270 Hz, which means that disturbances can be efficiently attenuated in this zone. It is also clear that the reverse path has a significant gain on a large frequency range so its effect can not be neglected. The orders of the identified models are given in Table I.

Model	n_B	n_A	d
Primary (global)	20	24	7
Secondary	27	26	6
Reverse	22	25	5

TABLE I
ORDERS OF THE IDENTIFIED SYSTEM PATHS.

Details concerning the experimental model identification are given in Appendix A.

IV. IIR (FIR) ADAPTIVE FEEDFORWARD NOISE COMPENSATORS

The corresponding block diagrams in open-loop operation and with the compensator system are shown in Fig. 5. The signal $w(t)$ is the image of the disturbance measured when

---

[1] The primary path model has been exclusively used for simulation purposes only.

[2] The lowest damping is around 0.01.

the compensator system is not used (open-loop). The signal $\hat{y}(t)$ denotes the effective output provided by the measurement device when the compensator system is active and which will serve as input to the adaptive feedforward compensator $\hat{N}$. The output of this filter, denoted by $\hat{u}(t)$, is applied to the actuator through an amplifier. The transfer function G (the secondary path) characterizes the dynamics from the output of the compensator $\hat{N}$ to the residual noise measurement (amplifier + actuator + dynamics of the acoustical system). The unmeasurable value of the output of the primary path (when the compensation is active) is denoted $x(t)$.

(a)

(b)
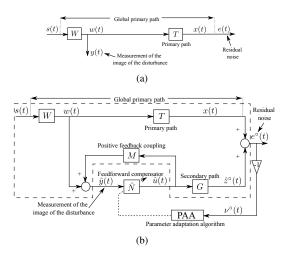
Fig. 5. Feedforward AVC: in open-loop (a) and with adaptive feedforward compensator (b).

The coupling between the output of the feedforward compensator and the measurement $\hat{y}(t)$ through the compensator actuator is denoted by M. As indicated in Fig. 5, this coupling is a "positive" feedback. The positive feedback may destabilize the system.[3] The system is no longer a pure feedforward compensator.

The objective is to estimate (and to adapt) the parameters of the feedforward compensator $N(q^{-1})$ such that the measured residual noise be minimized in the sense of a certain criterion. The optimal IIR feedforward compensator (unknown) is defined by:

$$N(q^{-1}) = \frac{R(q^{-1})}{S(q^{-1})}, \qquad (3)$$

where

$$R(q^{-1}) = r_0 + r_1 q^{-1} + \ldots + r_{n_R} q^{-n_R}, \qquad (4)$$
$$S(q^{-1}) = 1 + S_1 q^{-1} + \ldots + S_{n_S} q^{-n_S}$$
$$= 1 + q^{-1} S^*(q^{-1}). \qquad (5)$$

The estimated compensator is denoted by $\hat{N}(q^{-1})$ or $\hat{N}(\hat{\theta}, q^{-1})$ when it is a linear filter with constant coefficients or $\hat{N}(t, q^{-1})$ during estimation (adaptation) of its parameters. FIR compensators are obtained by taking $S = 1$ (i.e. $s_i = 0$, $\forall i = 1 : n_S$).

The input of the feedforward compensator is denoted by $\hat{y}(t)$ and it corresponds to the sum between the disturbance

image in the absence of compensation and of the output of the positive feedback path. In the absence of the compensation loop (open-loop operation): $\hat{y}(t) = w(t)$. The *a posteriori*[4] output of the feedforward compensator (which is the control signal applied to the secondary path) is denoted by $\hat{u}(t+1) = \hat{u}(t+1|\hat{\theta}(t+1))$. The input-output relationship for the estimated feedforward compensator is given by the equation of the *a priori* output:

$$\hat{u}^\circ(t+1) = \hat{u}(t+1|\hat{\theta}(t))$$
$$= -\hat{S}^*(t, q^{-1})\hat{u}(t) + \hat{R}(t, q^{-1})\hat{y}(t+1)$$
$$= \hat{\theta}^T(t)\phi(t) = \left[\hat{\theta}_S^T(t), \hat{\theta}_R^T(t)\right] \begin{bmatrix} \phi_{\hat{u}}(t) \\ \phi_{\hat{y}}(t) \end{bmatrix}, \quad (6)$$

where

$$\hat{\theta}^T(t) = [\hat{s}_1(t), \ldots \hat{s}_{n_S}(t), \hat{r}_0(t), \ldots \hat{r}_{n_R}(t)]$$
$$= [\hat{\theta}_S^T(t), \hat{\theta}_R^T(t)], \qquad (7)$$
$$\phi^T(t) = [-\hat{u}(t), -\hat{u}(t - n_S + 1), \hat{y}(t+1), \ldots \hat{y}(t - n_R + 1)]$$
$$= [\phi_{\hat{u}}^T(t), \phi_{\hat{y}}^T(t)], \qquad (8)$$

and $\hat{u}(t)$, $\hat{u}(t-1)$, ... are the *a posteriori* outputs of the feedforward compensator generated by

$$\hat{u}(t) = \hat{u}(t|\hat{\theta}(t)) = \hat{\theta}^T(t)\phi(t-1), \qquad (9)$$

where $\hat{y}(t+1)$, $\hat{y}(t)$, ... are the measurements provided by the primary transducer.[5]

The measured residual error satisfies the following equation:

$$e^\circ(t+1) = x(t+1) + \hat{z}^\circ(t+1). \qquad (10)$$

The *a priori* adaptation error is defined as

$$\nu^\circ(t+1) = -e^\circ(t+1) = -x(t+1) - \hat{z}^\circ(t+1). \quad (11)$$

The *a posteriori* adaptation (residual) error (which is computed) will be given by:

$$\nu(t+1) = \nu(t+1|\hat{\theta}(t+1)) = -x(t+1) - \hat{z}(t+1). \quad (12)$$

When using an estimated filter $\hat{N}$ with constant parameters: $\hat{u}^\circ(t) = \hat{u}(t)$, $\hat{z}^\circ(t) = \hat{z}(t)$ and $\nu^\circ(t) = \nu(t)$.

The development of the PAA for estimating in real-time the parameter vector $\hat{\theta}$ assumes that

- (Perfect matching condition) There exists a value of the feedforward compensator parameters such that[6]

$$\frac{N}{(1 - NM)}G = -T \qquad (13)$$

- and the characteristic polynomial of the "internal" feedback loop:

$$P(z^{-1}) = A_M(z^{-1})S(z^{-1}) - B_M(z^{-1})R(z^{-1}) \quad (14)$$

is a Hurwitz polynomial

---

[3]Different solutions for reducing the effect of this internal positive feedback are reviewed in [6], [3].

[4]In adaptive control and estimation the predicted output at t can be computed either on the basis of the previous parameter estimates (*a priori*) or on the basis of the current parameter estimates (*a posteriori*).

[5]$\hat{y}(t+1)$ is available before adaptation of parameters starts at $t+1$.

[6]The parenthesis (q^{-1}) or (z^{-1}) will be omitted in some of the following equations to make them more compact.

So the objective of the adaptation algorithm will be to allow the compensator $\hat{N}$ to approach the optimal compensator N at least in the frequency range of interest but assuring the asymptotic stability of the internal loop.

From the user point of view and taking into account the type of operation of adaptive disturbance compensation systems, one has to consider two modes of operation of the adaptive schemes:

- *Adaptive* operation. The adaptation is performed continuously with a non-vanishing adaptation gain and the feedforward compensator is updated at each sampling.
- *Self-tuning* operation. The adaptation procedure starts either on demand or when the performance is unsatisfactory. A vanishing adaptation gain is used.

Parameter Adaptation Algorithm (PAA)

A general formulation of the parameter adaptation algorithm is given below [21]:

$$\hat{\theta}(t+1) = \hat{\theta}(t) + F(t)\Phi(t)\nu(t+1) \tag{15}$$

$$\nu(t+1) = \frac{\nu^\circ(t+1)}{1 + \Phi^T(t)F(t)\Phi(t)} \tag{16}$$

$$F(t+1) = \frac{1}{\lambda_1(t)} \left[F(t) - \frac{F(t)\Phi(t)\Phi^T(t)F(t)}{\frac{\lambda_1(t)}{\lambda_2(t)} + \Phi^T(t)F(t)\Phi(t)} \right] \tag{17}$$

$$1 \geq \lambda_1(t) > 0 \quad ; \quad 0 \leq \lambda_2(t) < 2; F(0) > 0 \tag{18}$$

$$\Phi(t) = \phi_f(t) \tag{19}$$

where $\lambda_1(t)$ and $\lambda_2(t)$ allow to obtain various profiles for the adaptation gain matrix $F(t)$. Four cases are of interest:

- *Constant trace algorithm.* $\lambda_1(t)$ and $\lambda_2(t)$ are adjusted continuously to maintain constant the trace of the adaptation gain matrix. This allows to move in the optimal direction while maintaining the adaptation capabilities.
- *Decreasing adaptation gain* $(\lambda_1 = 1, \lambda_2 = 1)$. This is used in self-tuning regime and in some situations for initialization of the constant trace algorithm.
- *Variable forgetting factor.* The difference with respect to the decreasing adaptation gain is that in this option $\lambda_1(0) < 1$ but it will tend asymptotically to 1. This allows to get transiently a higher adaptation gain.
- *Constant scalar adaptation gain.* This is obtained by taking $F(t) = \gamma I$ where I is the identity matrix. One gets a scalar adaptation gain.

To initialize the algorithms often one can use the combination of the "decreasing gain" with the "constant trace" (i.e., allowing a larger gain at the beginning of the adaptation process) or the combination of the "variable forgetting factor" with the "constant trace". In both cases one switches to the constant trace when the trace of the adaptation gain matrix $F(t)$ reaches the specific desired trace.

The evolution of the adaptation gain matrix is given by:

$$F(t+1) = \frac{1}{\lambda_1(t)} \left[F(t) - \frac{F(t)\Phi(t)\Phi^T(t)F(t)}{\frac{\lambda_1(t)}{\lambda_2(t)} + \Phi^T(t)F(t)\Phi(t)} \right] . \tag{20}$$

For the decreasing gain one chooses

$$\lambda_1(t) = \lambda_1 = 1 ; \quad \lambda_2(t) = \lambda_2 = 1 \tag{21}$$

In the variable forgetting factor case, the evolution of $\lambda_1(t)$ is given by

$$\lambda_1(t) = \lambda_0\lambda_1(t-1) + 1 - \lambda_0 ; \quad 0 < \lambda_0 < 1 \tag{22}$$

with

$$\lambda_2(t) = \lambda_2 = 1 \tag{23}$$

the typical values being:

$$\lambda_1(0) = 0.95 \text{ to } 0.99 ; \quad \lambda_0 = 0.95 \text{ to } 0.99$$

The values of $\lambda_1(t)$ and $\lambda_2(t)$ in order to maintain constant the trace of the adaptation gain matrix are determined from the equation:

$$tr\left(F(t+1)\right) = \frac{1}{\lambda_1(t)} tr\left(F(t) - \frac{F(t)\Phi(t)\Phi^T(t)F(t)}{\alpha(t) + \Phi^T(t)F(t)\Phi(t)} \right)$$

fixing the ratio $\alpha(t) = \lambda_1(t)/\lambda_2(t) = const.$ (a typical value is $\alpha = 1$).

The updating of matrix F(t) is done using the U-D factorization for numerical robustness reasons. The details of this algorithm[7] are given in [20, Appendix B].

By taking $F(t) = \gamma I$, where I is the identity matrix, one gets a scalar adaptation gain (see columns 3 and 4 of Table II). The equation (15) for updating the parameter vector becomes:

$$\hat{\theta}(t+1) = \hat{\theta}(t) + \gamma\Phi(t)\frac{\nu^\circ(t+1)}{1 + \gamma\Phi^T(t)\Phi(t)}. \tag{24}$$

When using scalar adaptation gain, one can see that for very small values of γ one can approximate the above equation by

$$\hat{\theta}(t+1) = \hat{\theta}(t) + \gamma\Phi(t)\nu^\circ(t+1) \tag{25}$$

which corresponds almost to the adaptation algorithm used in FULMS except that since the adaptation gain is small and the residual error varies slowly, the quantity $\Phi(t)\nu^\circ(t+1)$ is replaced by $\Phi(t-1)\nu^\circ(t)$.

Filtering of the residual error

An interesting practical issue is the use of a filtered residual error (noise) in the adaptation algorithm. This idea comes from adaptive filtering and identification ([22], [7]). For a general presentation see [20]. A recent application of adaptation error filtering to AVC is presented in [23]. The use of this filtering on one hand may contribute to satisfy the SPR condition for stability and on the other hand (which is the most important) it will shape the resulting spectral density.[8]

In this case the adaptation error takes the form

$$\nu^\circ(t) = -\left[e^\circ(t) + V^*(q^{-1})e(t-1) \right], \tag{26}$$

where the filter $V(q^{-1})$ is given as

$$V(q^{-1}) = 1 + v_1 q^{-1} + \ldots + v_{n_V} q^{-n_V} = 1 + q^{-1}V^*(q^{-1}).$$

---

[7]Routines for the implementation of the algorithm can be downloaded from http://www.gipsa-lab.grenoble-inp.fr/~ioandore.landau/adaptivecontrol/

[8]In fact it will modify the quadratic criterion minimized by the adaptation algorithm by introducing a frequency dependent weight.

Summary of the algorithms for adaptive IIR (FIR) compensators

Table II summarizes the most important algorithms used with an IIR (FIR) configuration of the feedforward compensator. Column 1 gives the adaptation algorithms using a matrix adaptation gain derived from stability considerations (FUPLR and FUSBA). Column 2 gives the adaptation algorithms using scalar adaptation gain also derived from stability considerations (NFULMS and SFUSBA). Column 3 gives the now classical FULMS algorithm (which corresponds to the FXLMS algorithm when using an FIR compensator) which uses a scalar adaptation gain. The connections with the NFULMS have been enhanced above.

The last two rows of Table II summarize the stability conditions in a deterministic context (global asymptotic stability condition for any initial condition on the parameters of the compensator or local asymptotic stability condition) and the convergence condition in a stochastic environment (convergence of the parameters in the presence of a measurement noise affecting the residual noise measurement, assuming that the system is already asymptotically stable in deterministic context and that the parameters evolve inside the zone where the internal positive feedback loop is stable for each time t [21]).

A key role in the stability of the various adaptation algorithms is played by the filter L operating on the observation vector ϕ. It helps to satisfy the "strictly positive real condition" for asymptotic stability and parameter convergence.

For understanding the roles played by the filter L introduced on the observation vector, it is important to note that the equation of the residual error can be expressed as (see [17]):

$$\nu(t+1) = H(q^{-1})[\theta - \hat{\theta}(t+1)]^T \phi_f(t) \qquad (27)$$

where

$$H(q^{-1}) = \frac{A_M(q^{-1})G(q^{-1})}{P(q^{-1})L(q^{-1})} \qquad (28)$$

and

$$\phi_f(t) = L\phi(t). \qquad (29)$$

From these equations, one can understand that there is a phase difference between the residual error $\nu(t+1)$ and $\phi_f(t)$ and that $\phi_f(t)\nu(t+1)$ is an approximation of the inverse of the gradient vector. Therefore, for convergence, the angle between the direction of adaptation and the direction of the inverse of the true gradient (not computable) should be less than 90° which is effectively assured by the SPR stability condition on H. For time-varying adaptation gains, the stability condition is sharper:

$$H'(q^{-1}) = H(q^{-1}) - \frac{\lambda_2}{2}, \quad \max_t(\lambda_2(t)) \leq \lambda_2 < 2 \qquad (30)$$

should be SPR.

Several choices for the filter L will be considered, leading to different algorithms. For the case of matrix adaptation gain one has:

FUPLR: $L = \hat{G}$

FUSBA: $L = \frac{\hat{A}_M}{\hat{P}}\hat{G}$ with $\hat{P} = \hat{A}_M\hat{S} - \hat{B}_M\hat{R}$

The algorithm FUPLR, assuming that the SPR condition given in Table II is satisfied, assures a global stability of the algorithm for any initial conditions. The SPR stability condition can be relaxed for low adaptation gain provided that, in the average, the SPR condition is true (see [24], [16], [17]) but the performance will be impacted. To improve the performance one has to use the FUSBA algorithm which tries to make the $H(q^{-1})$ transfer function close to 1. This will depend on how good the estimation in real-time of $\hat{P}$ is. This can be achieved once an acceptable estimation of the parameters of $\hat{N}$ is available. Therefore, in order to use this algorithm, an initialization with the FUPLR algorithm should be done[9].

For the scalar adaptation gain one has the same choices for the filter L and the corresponding algorithms issued from stability consideration are (see column 3 of Table II): NFULMS and SFUSBA. The same considerations as for the matrix adaptation gain are valid in the case of constant scalar adaptation gain. The SFUSBA should be initialized using the NFULMS. Note also that FULMS and NFULMS use the same type of filter.

The following procedure is used at each sampling time for implementing the adaptive feedforward compensation:

1) Get the measured image of the disturbance $\hat{y}(t+1)$, the measured residual error $e°(t+1)$, and compute $\nu°(t+1) = -e°(t+1)$.
2) Compute $\phi(t)$ and $\phi_f(t)$ using (8) and (29).
3) Estimate the parameter vector $\hat{\theta}(t+1)$ using the PAA (15)-(19).
4) Compute (using (9)) and apply the control $\hat{u}(t+1)$.

V. Youla–Kučera Parametrized Adaptive Feedforward Compensators

The rationale behind the use of the Youla–Kučera parametrized feedforward compensator is to separate the problem of the stabilization of the positive internal loop from the problem of the minimization of the residual noise.

In order to achieve this, instead of a standard IIR feedforward compensator, one can use an Youla–Kučera parametrization of the adaptive feedforward compensator. The central compensator will assure the stability of the internal positive feedback loop and its performance are enhanced in real-time by the direct adaptation of the parameters of the Youla–Kučera Q filter.

A block diagram of such an adaptive feedforward compensator is shown in Fig. 6. FIR and IIR Q filters can be used. Details of the specific algorithms can be found in [18], [19]. The transfer operators of the various paths of the AVC system have been described in Section III.

---

[9]For the FUSBA algorithm the stability condition is a "local" result. Strictly speaking, it is valid only in the neighborhood of the equilibrium point. It assumes indeed that the estimated $\hat{P}$ is asymptotically stable. This requires inclusion of a stability test on $\hat{P}$.

	Paper (Matrix gain)	Paper (Scalar gain)	FULMS (Scalar gain)
$\hat{\theta}(t+1) =$	$\hat{\theta}(t) + F(t)\Phi(t)\frac{\nu^\circ(t+1)}{1+\Phi^T(t)F(t)\Phi(t)}$	$\hat{\theta}(t) + \gamma(t)\Phi(t)\frac{\nu^\circ(t+1)}{1+\gamma(t)\Phi^T(t)\Phi(t)}$	$\hat{\theta}(t) + \gamma(t)\Phi(t-1)\nu^\circ(t)$
Adapt. gain	$F(t+1)^{-1} = \lambda_1(t)F(t)+$ $+\lambda_2(t)\Phi(t)\Phi^T(t)$ $0 \le \lambda_1(t) < 1, 0 \le \lambda_2(t) < 2$ $F(0) > 0$	$\gamma(t) > 0$	$\gamma(t) > 0$
Adaptive	Decr. gain and const. trace	$\gamma(t) = \gamma = const$	$\gamma(t) = \gamma = const$
Self tuning	$\lambda_2 = const.$ $\lim_{t\to\infty} \lambda_1(t) = 1$	$\sum_{t=1}^{\infty} \gamma(t) = \infty, \quad \lim_{t\to\infty} \gamma(t) = 0$	$\sum_{t=1}^{\infty} \gamma(t) = \infty, \quad \lim_{t\to\infty} \gamma(t) = 0$
$\phi^T(t) =$	$[-\hat{y}(t),\dots,\hat{u}(t+1),\dots]$	$[-\hat{y}(t),\dots,\hat{u}(t+1),\dots]$	$[-\hat{y}(t),\dots,\hat{u}(t+1),\dots]$
$\Phi(t) =$	$L\phi(t)$ FUPLR: $L = \hat{G}$ FUSBA: $L = \frac{\hat{A}_M}{\hat{P}}\hat{G}$ $\hat{P} = \hat{A}_M\hat{S} - \hat{B}_M\hat{R}$	$L\phi(t)$ NFULMS: $L = \hat{G}$ SFUSBA: $L = \frac{\hat{A}_M}{\hat{P}}\hat{G}$ $\hat{P} = \hat{A}_M\hat{S} - \hat{B}_M\hat{R}$	$L\phi(t)$ $L = \hat{G}$
$M = \frac{B_M}{A_M}$	$B_M = b_{1_M}z^{-1} + b_{2_M}z^{-2} + \dots$ $A_M = 1 + a_{1_M}z^{-1} + a_{2_M}z^{-2} + \dots$	$B_M = b_{1_M}z^{-1} + b_{2_M}z^{-2} + \dots$ $A_M = 1 + a_{1_M}z^{-1} + \dots$	$B_M = b_{1_M}z^{-1} + b_{2_M}z^{-2} + \dots$ $A_M = 1$
Stability condition	$\frac{A_M G}{PL} - \frac{\lambda}{2} = SPR$ $\lambda = \max \lambda_2(t)$	$\frac{A_M G}{PL} = SPR$	Unknown
Conv. condition	$\frac{A_M G}{PL} - \frac{\lambda}{2} = SPR$ $\lambda = \lambda_2$	$\frac{A_M G}{PL} = SPR$	$\frac{G}{P\hat{G}} = SPR$

TABLE II

COMPARISON OF ALGORITHMS FOR DIRECT ADAPTIVE FEEDFORWARD COMPENSATION IN ANC WITH ACOUSTICAL COUPLING.
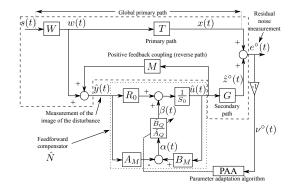
Fig. 6. Adaptive feedforward disturbance compensation using Youla–Kučera parametrization.

Infinite Impulse Response Youla–Kučera compensators (IIRYK)

The optimal IIR feedforward compensator which will minimize the residual noise can be written, using the Youla–Kučera parametrization, as

$$N = \frac{R}{S} = \frac{A_Q R_0 - B_Q A_M}{A_Q S_0 - B_Q B_M} \qquad (31)$$

where the optimal Youla–Kučera filter $Q(q^{-1})$ has an IIR structure

$$Q(q^{-1}) = \frac{B_Q(q^{-1})}{A_Q(q^{-1})} = \frac{b_0^Q + b_1^Q q^{-1} + \dots + b_{n_{B_Q}}^Q q^{-n_{B_Q}}}{1 + a_1^Q q^{-1} + \dots + a_{n_{A_Q}}^Q q^{-n_{A_Q}}}$$

and $R_0(q^{-1})$, $S_0(q^{-1}) = 1 + q^{-1}S_0^*(q^{-1})$ are the polynomials of the central (stabilizing) compensator [10] and $A_M(q^{-1})$,

---

[10]The characteristic polynomial of the internal loop with the central compensator: $P_0 = A_M S_0 - B_M R_0$ is a Hurwitz polynomial.

$B_M(q^{-1})$ are given in (1). The estimated IIRYK filter is expressed as:

$$\hat{Q}(q^{-1}) = \frac{\hat{B}_Q(q^{-1})}{\hat{A}_Q(q^{-1})} = \frac{\hat{b}_0^Q + \hat{b}_1^Q q^{-1} + \dots + \hat{b}_{n_{B_Q}}^Q q^{-n_{B_Q}}}{1 + \hat{a}_1^Q q^{-1} + \dots + \hat{a}_{n_{A_Q}}^Q q^{-n_{A_Q}}}$$

and its parameters are given by

$$\hat{\theta}^T = [\hat{b}_0^Q, \dots, \hat{b}_{n_{B_Q}}^Q, \hat{a}_1^Q, \dots, \hat{a}_{n_{A_Q}}^Q] = [\hat{\theta}_{B_Q}^T, \hat{\theta}_{A_Q}^T]. \qquad (32)$$

The estimated IIRYK filter is denoted by $\hat{Q}(q^{-1})$ or $\hat{Q}(\hat{\theta}, q^{-1})$ when it is a linear filter with constant coefficients or $\hat{Q}(t, q^{-1})$ during estimation (adaptation). The *a priori* output of the estimated feedforward compensator using an IIRYK parametrization for the case of time-varying parameter estimates is given by (using (31))

$$\begin{aligned} \hat{u}^\circ(t+1) &= \hat{u}(t+1|\hat{\theta}(t)) \\ &= -\hat{S}^*(t,q^{-1})\hat{u}(t) + \hat{R}(t,q^{-1})\hat{y}(t+1) \\ &= -S_0^*\hat{u}(t) + R_0\hat{y}(t+1) - \hat{A}_Q(t,q^{-1})^*\beta(t) \\ &\quad + \hat{B}_Q(t,q^{-1})\alpha(t+1), \end{aligned} \qquad (33)$$

and

$$\begin{aligned} \hat{u}(t+1) &= -S_0^*\hat{u}(t) + R_0\hat{y}(t+1) - \hat{A}_Q(t+1,q^{-1})^*\beta(t) \\ &\quad + \hat{B}_Q(t+1,q^{-1})\alpha(t+1), \end{aligned} \qquad (34)$$

where $\beta(t) = S_0\hat{u}(t) - R_0\hat{y}(t)$ (see also Fig. 6). The development of the PAA assumes that:

- (*perfect matching condition*) For the IIRYK parametrized feedforward compensator there exists a value of the parameters Q such that

$$\frac{G \cdot A_M(R_0 A_Q - A_M B_Q)}{A_Q(A_M S_0 - B_M R_0)} = -T. \qquad (35)$$

- the characteristic polynomial of the resulting internal loop:

$$P = A_Q(A_M S_0 - B_M R_0) = A_Q P_0, \qquad (36)$$

is a Hurwitz polynomial.

The equation of the residual error can be expressed as ([19]:

$$\nu(t+1|\hat{\theta}) = \frac{A_M(q^{-1})G(q^{-1})}{A_Q(q^{-1})P_0(q^{-1})L(q^{-1})}[\theta - \hat{\theta}]^T\phi_f(t) \quad (37)$$

with

$$\phi_f(t) = L(q^{-1})\phi(t)$$
$$= [\alpha_f(t+1), \dots \alpha_f(t - n_{B_Q} + 1),$$
$$\beta_f(t), \beta_f(t-1), \dots \beta_f(t - n_{A_Q})] \quad (38)$$

where $\alpha_f(t+1) = L(q^{-1})\alpha(t+1)$, $\beta_f(t) = L(q^{-1})\beta(t)$, and

$$\phi(t) = [\alpha(t+1), \dots \alpha(t - n_{B_Q} + 1),$$
$$\beta(t), \beta(t-1), \dots \beta(t - n_{A_Q})] \quad (39)$$

The PAA described in Section IV is used also for the Youla–Kučera feedforward compensators. Several choices for the filter L will be considered, leading to different algorithms:

FUPLR: $L = \hat{G}$
FUSBA: $L = \frac{\hat{A}_M}{\hat{P}}\hat{G}$ with

$$\hat{P} = \hat{A}_Q(\hat{A}_M S_0 - \hat{B}_M R_0) = \hat{A}_Q \hat{P}_0,$$

where $\hat{A}_Q$ is an estimation of the denominator of the ideal IIRYK filter computed on the basis of available estimates of the parameters of the filter $\hat{Q}$. In order to implement the FUSBA - IIRYK algorithm, it is necessary to make an initialization over a certain horizon for obtaining an estimation of $\hat{A}_Q$. This can be done by running the FUPLR -IIRYK for a certain time to get an estimate of $\hat{A}_Q$.

Finite Impulse Response Youla–Kučera Compensators (FIRYK)

FIR Youla–Kučera filters are obtained by taking $A_Q(q^{-1}) = 1$. The vector of parameters of the optimal FIRYK filter assuring perfect matching will be denoted by

$$\theta^T = [b_0^Q, \dots b_{n_{B_Q}}^Q] = \theta_{B_Q}^T. \quad (40)$$

The vector of parameters for the estimated $\hat{Q}$ filter

$$\hat{Q}(q^{-1}) = \frac{\hat{B}_Q(q^{-1})}{1} = \hat{b}_0^Q + \hat{b}_1^Q q^{-1} + \dots + \hat{b}_{n_{B_Q}}^Q q^{-n_{B_Q}} \quad (41)$$

is denoted by

$$\hat{\theta}^T = [\hat{b}_0^Q, \dots, \hat{b}_{n_{B_Q}}^Q] = \hat{\theta}_{B_Q}^T. \quad (42)$$

The major difference between the IIRYK configuration and the FIRYK configuration is reflected in the equation describing the evolution of the residual noise:

$$\nu(t+1|\hat{\theta}) = \frac{A_M(q^{-1})G(q^{-1})}{P_0(q^{-1})L(q^{-1})}[\theta - \hat{\theta}]^T\phi_f(t) \quad (43)$$

with

$$\phi_f(t) = [\alpha_f(t+1), \dots \alpha_f(t - n_{B_Q} + 1)] = L(q^{-1})\phi(t), \quad (44)$$

where $\alpha_f(t+1) = L(q^{-1})\alpha(t+1)$ and

$$\phi(t) = [\alpha(t+1), \dots \alpha(t - n_{B_Q} + 1)] \quad (45)$$

In eq. 43 the current poles of the internal closed-loop will no more depend upon the time-varying parameters of A_Q and are now fixed and defined by the central compensator.

The objective is to select a filter L such that the transfer function

$$H = \frac{A_M(q^{-1})G(q^{-1})}{P_0(q^{-1})L(q^{-1})} \quad (46)$$

is SPR when a constant adaptation gain is used or that the transfer function

$$H'(q^{-1}) = H(q^{-1}) - \frac{\lambda_2}{2}, \quad \max_t(\lambda_2(t)) \leq \lambda_2 < 2 \quad (47)$$

is SPR for time-varying adaptation gains.

Several choices for the filter L will be considered, leading to different algorithms (see Table III):

FUPLR: $L = \hat{G}$
FUSBA: $L = \frac{\hat{A}_M}{\hat{P}_0}\hat{G}$ with $\hat{P}_0 = \hat{A}_M S_0 - \hat{B}_M R_0$

The major difference with respect to the IIR and IIRYK compensators is that the FUSBA algorithm assures in this case global asymptotic stability and can be implemented from the beginning since the polynomial $\hat{P}_0$ is known from the beginning and remains unchanged during adaptation process. This is a significant advantage.

Table III gives the details of the adaptation gains used in the various cases as well as the structure of the filters. The implementation procedure is similar to that for the IIR compensators except that (8), (29), and (9) are replaced, respectively, by (39), (38), and (34) for IIRYK (or (45), (44), and (34) for FIRYK).

Design of the Central Compensator

The same central compensator $N_0(q^{-1}) = \frac{R_0(q^{-1})}{S_0(q^{-1})}$ can be used for FIRYK or IIRYK. The main objective is to guarantee the stability of the internal positive feedback loop. This can be achieved by using a pole placement design technique (see also [20, Chapter 7]) taking into account that the feedback is positive. All stable poles of the reverse path can be assigned as poles of the closed-loop (one can change their damping in order to impose a desired minimum value for the damping of the complex poles). Additional stable poles can be assigned. Sensitivity functions of the internal closed-loop have to be checked.

Youla–Kučera Parametrization—Some Remarks

Two major observations when using the Youla–Kučera parametrization have to be made:

- If an FIR Q filter is used, the poles of the internal closed-loop will be defined by the central compensator R_0, S_0 and they will remain unchanged independently of the values of the parameters of the Q filter. The stability condition for the FUSBA algorithm is global.
- If an IIR Q filter is used, the poles of the internal closed-loop will be defined by the central compensator but additional poles corresponding to the denominator of the Q filter will be added. The stability condition for the FUSBA algorithm is local and an initialization with the FUPLR algorithm is necessary.

	IIRYK	FIRYK	IIRYK	FIRYK
	Matrix adaptation gain		Scalar adaptation gain	
$\hat{\theta}(t+1) =$	$\hat{\theta}(t) + F(t)\Phi(t)\frac{\nu^\circ(t+1)}{1+\Phi^T(t)F(t)\Phi(t)}$		$\hat{\theta}(t) + \gamma(t)\Phi(t)\frac{\nu^\circ(t+1)}{1+\gamma(t)\Phi^T(t)\Phi(t)}$	
Adapt. gain	$F(t+1)^{-1} = \lambda_1(t)F(t) + \lambda_2(t)\Phi(t)\Phi^T(t)$ $0 \le \lambda_1(t) < 1,\ 0 \le \lambda_2(t) < 2,\ F(0) > 0$		$\gamma(t) > 0$	
Adaptive	Decr. gain and const. trace		$\gamma(t) = \gamma = const$	
Self tuning	$\lambda_2 = const.,\quad \lim_{t\to\infty}\lambda_1(t) = 1$		$\sum_{t=1}^{\infty}\gamma(t) = \infty,\quad \lim_{t\to\infty}\gamma(t) = 0$	
$\hat{\theta}(t) =$	$[\hat{b}_0^Q,\ldots,\hat{a}_1^Q,\ldots]$	$[\hat{b}_0^Q,\ldots]$	$[\hat{b}_0^Q,\ldots,\hat{a}_1^Q,\ldots]$	$[\hat{b}_0^Q,\ldots]$
$\phi^T(t) =$	$[\alpha(t+1),\ldots,\beta(t),\ldots]$ $\alpha(t) = B_M\hat{u}(t) - A_M\hat{y}(t)$ $\beta(t) = S_0\hat{u}(t) - R_0\hat{y}(t)$	$[\alpha(t+1),\ldots]$ $\alpha(t) = B_M\hat{u}(t)$ $-A_M\hat{y}(t)$	$[\alpha(t+1),\ldots,\beta(t),\ldots]$ $\alpha(t) = B_M\hat{u}(t) - A_M\hat{y}(t)$ $\beta(t) = S_0\hat{u}(t) - R_0\hat{y}(t)$	$[\alpha(t+1),\ldots]$ $\alpha(t) = B_M\hat{u}(t)$ $-A_M\hat{y}(t)$
$\hat{P} =$	$\hat{A}_Q(\hat{A}_M S_0 - \hat{B}_M R_0)$	$\hat{A}_M S_0 - \hat{B}_M R_0$	$\hat{A}_Q(\hat{A}_M S_0 - \hat{B}_M R_0)$	$\hat{A}_M S_0 - \hat{B}_M R_0$
$P =$	$A_Q(A_M S_0 - B_M R_0)$	$A_M S_0 - B_M R_0$	$A_Q(A_M S_0 - B_M R_0)$	$A_M S_0 - B_M R_0$
$\Phi(t) =$	$L\phi(t)$ FUPLR: $L = \hat{G}$ FUSBA: $L = \frac{\hat{A}_M}{\hat{P}}\hat{G}$		$L\phi(t)$ SFUPLR: $L = \hat{G}$ SFUSBA: $L = \frac{\hat{A}_M}{\hat{P}}\hat{G}$	
Stability condition	$\frac{A_M G}{PL} - \frac{\lambda}{2} = SPR \quad (\lambda = \max\lambda_2(t))$		$\frac{A_M G}{PL} = SPR$	
Conv. condition	$\frac{A_M G}{PL} - \frac{\lambda}{2} = SPR \quad (\lambda = \lambda_2)$		$\frac{A_M G}{PL} = SPR$	

TABLE III

COMPARISON OF ALGORITHMS FOR YOULA–KUČERA PARAMETRIZED ADAPTIVE FEEDFORWARD COMPENSATION IN ANC WITH ACOUSTICAL COUPLING.

When using an FIRYK structure, $\hat{A}_Q \equiv 1$ and the implementation of the FUSBA algorithm is much simpler since $\hat{P} = \hat{P}_0$ is constant and known once the central compensator is designed.

As for the direct feedforward algorithms described in Section IV, scalar adaptation gains can also be used. The same choices for the filter L apply and the corresponding algorithms issued from stability consideration are: NFULMS and SFUSBA (see also Table III).

VI. EXPERIMENTAL RESULTS

The objective of this section is to asses comparatively the performance of the various adaptive feedforward compensation schemes for attenuating broad-band noise disturbances with unknown and time-varying characteristics.

In defining the experimental protocols, a number of indicators have to be taken into account:

- Testing signals
- Type of structure for the feedforward compensator
- Number of parameters to be adapted
- Type of PAA used
- Computer load (complexity).

Testing Signals

Two broad band disturbances have been considered

- noise with a flat PSD between 70 and 270 Hz
- step change from a flat disturbance 70 - 170 Hz to a flat disturbance 170 - 270 Hz

These disturbances have been obtained using a PRBS with $N = 15$ and amplitude 0.1 passed through band-pass Butterworth filters of order 7 with the cut-off frequencies as indicated above.

A test horizon of 180 s has been chosen as a compromise between the time required to achieve all the experiments and the convergence horizon. For the best algorithms a few tests have been carried out on a larger horizon of 600 s showing the expected improvement in performance.

For testing the adaptation capabilities in the presence of step changes of the disturbance characteristics, a horizon of 360s with a step change occurring at 180 s has been selected.

Type of Structure

Standard IIR and FIR (particular case of IIR) compensators will be considered as well as the FIRYK and IIRYK compensators.

Number of Adjustable Parameters

The performances of the various compensators will depend on the number of parameters. A compromise between number of parameters and performance in terms of global attenuation and computer load is considered when choosing the number of parameters.

Type of Parameter Adaptation Algorithms

For this paper only the adaptive operation will be considered in the experimental evaluation. This means that only the "constant trace adaption gain" and the constant scalar adaptation gain will be considered. For a given complexity of the feedforward compensator the performances obtained with various PAA have been evaluated. The attenuation is measured on a sample of 15 s. One expresses the ratio between the variance of the residual noise in the absence of the compensator and the variance of the residual noise in the presence of the compensator in dB.

Computer Load

The indicator of the complexity of a scheme is given by the maximum TET (Task Execution Time) which measures the maximum duration of computation over a sampling period.

A. Results for IIR (FIR) Adaptive Feedforward Compensators

For each type of compensator the comparison has been done under the following protocols:

- Given PAA and variable number of parameters to be adapted
- Fixed number of parameters and various parameter adaptation algorithms

The PAA used for the experiments are implemented using an initial diagonal gain matrix with a gain of 0.002 per parameter.

Filter type	No. params. [num/den]	Attenuation [dB]	max. TET [s]
FIR	20/0	18.4	8.76e-5
FIR	30/0	21.0	9.79e-5
FIR	40/0	21.0	1.07e-4
FIR	50/0	20.8	1.16e-4

TABLE IV
INFLUENCE OF THE NUMBER OF PARAMETERS ON THE PERFORMANCE OF THE STANDARD FIR ADAPTIVE FEEDFORWARD COMPENSATOR USING THE FUSBA ALGORITHM (70-270 HZ BROAD-BAND DISTURBANCE, 180 S EXPERIMENTS).

Filter type	No. params. [num/den]	Attenuation [dB]
FIR	30/0	32.4
FIR	40/0	32.2

TABLE V
EXPERIMENTAL RESULTS USING FIR ADAPTIVE COMPENSATOR WITH THE FUSBA ALGORITHM (70-270 HZ BROAD-BAND DISTURBANCE, 600 S EXPERIMENTS).

We begin our discussion with the choice of the number of parameters (complexity) for both the FIR and the IIR compensators. The standard FIR adaptive feedforward compensator has been tested first. Experimental results for various number of parameters are shown in Table IV and Table V. From these tables, one can conclude that the FIR with 30/0 parameters is the best compromise in terms of performance over number of parameters.

Filter type	No. params. [num/den]	Attenuation [dB]
IIR	10/10	23.4
IIR	15/15	26.7
IIR	20/20	25.6

TABLE VI
INFLUENCE OF THE NUMBER OF PARAMETERS ON THE PERFORMANCE OF THE STANDARD IIR ADAPTIVE FEEDFORWARD COMPENSATOR USING THE FUSBA ALGORITHM (70-270 HZ BROAD-BAND DISTURBANCE, 180 S EXPERIMENTS).

A similar evaluation has been done for the standard IIR adaptive feedforward compensator. From the examination of the Table VI and Table VII one can conlude that 15/15

Filter type	No. params. [num/den]	Attenuation [dB]	max. TET [s]
IIR	15/15	39.5	8.92e-5
IIR	20/20	41.5	9.30e-5

TABLE VII
EXPERIMENTAL RESULTS USING IIR ADAPTIVE COMPENSATOR WITH THE FUSBA ALGORITHM (70-270 HZ BROAD-BAND DISTURBANCE, 600 S EXPERIMENTS).

parameters[11] gives the best compromise between performance and number of parameters. This IIR compensator has the same total number of parameters as the FIR compensator 30/0 evaluated previously.

Adaptation algorithm	Attenuation [dB]	max. TET [s]
Matrix (FUSBA)	39.5	8.92e-5
Matrix (FUPLR)	35.5	7.01e-5
Scalar (SFUSBA)	36.8	8.17e-5
Scalar (NFULMS)	35.1	6.63e-5
Scalar (FULMS)	34.6	6.14e-5

TABLE VIII
EXPERIMENTAL RESULTS FOR IIR 15/15 ADAPTIVE COMPENSATORS USING VARIOUS ADAPTATION ALGORITHMS (70-270 HZ BROAD-BAND DISTURBANCE, 600 S EXPERIMENTS).

It results that for a total number of 30 adapted parameters, the IIR 15/15 compensator gives the best results compared with the FIR with 30 parameters.

The IIR structure with 15/15 parameters has been chosen to be further evaluated. Results obtained using various adaptation algorithms are shown in Table VIII. These experiments have been run over 600 s. The maximum TET is also indicated. It can be observed that the matrix gain FUSBA algorithm gives the best results. The corresponding scalar version shows a loss of 6.8 % in performance and a reduction of the maximum TET by 8.4 %. The FULMS algorithm gives the lowest performance.

Figure 7 illustrates the evolution of the residual noise and of the attenuation over an horizon of 600 s for the IIR 15/15 feedforward compensator using the FUSBA algorithm with a matrix adaptation gain. Attenuation reaches almost the steady state value at 600 s.

Figure 8 shows the PSD for the FIR 30/0 and the IIR 15/15 using the FUSBA algorithm with matrix adaptation gain. Both compensators assure a significant attenuation of the disturbance. Nevertheless, both PSD show a strong unwanted amplification (around 325 Hz in the case of the IIR and around 350 Hz for the FIR) which is caused by the presence of very low damped poles in the internal closed-loop (the algorithm guarantees only that the final closed-loop poles will be inside the unit circle but these poles can be very close to the unit circle).

Figure 9 shows an estimation of the output sensitivity function of the internal loop (at 600 s) for the IIR 15/15 compensator. There is a peak of 25 db at 315 Hz (corresponding to a modulus margin[12] of 0.06) and there is a pair of low damped

---

[11]The first number indicates the number of adjustable parameters at the numerator and the second indicates the number of the adjustable parameters at the denominator.

[12]The modulus margin gives the minimum distance between the Nyquist plot and the critical point $[-1, 0]$.
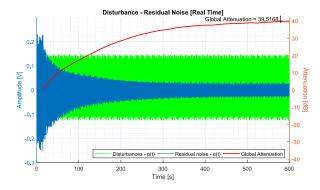
Fig. 7. Residual noise using the IIR 15/15 adaptive compensators using FUSBA matrix adaptation (70-270 Hz disturbance, 600 s experiments).
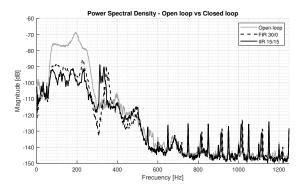

Fig. 8. PSD comparison of FIR 30/0 and IIR 15/15 standard adaptive compensators using FUSBA matrix adaptation (70-270 Hz disturbance, 600 s experiments).
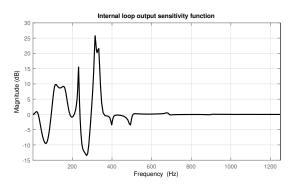

Fig. 9. Internal loop output sensitivity function for the IIR 15/15 adaptive compensator (70-270 Hz disturbance, 600 s experiments).

closed-loop poles at 315 Hz with a damping of 0.0090. This explains the peak in the PSD of the residual noise.

Figure 10 shows the phase of the estimated $\frac{A_M}{P}$ for the IIR 15/15 adaptive compensator using the FUSBA and the FUPLR algorithms. Since this transfer operator is not strictly positive real between 330 and 360 Hz, one can understand the beneficial effect of using the FUSBA algorithm (by filtering additionally the regressor by $\frac{A_M}{P}$). In the mean time, by averaging arguments, since the energy of the signal is concentrated between 70 to 270 Hz where $\frac{A_M}{P}$ is strictly positive real, the FUPLR (and the NFULMS) is stable.
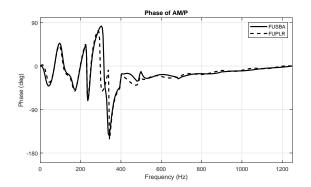
Fig. 10. Phase of $\frac{A_M}{P}$ for the IIR 15/15 adaptive compensator (70-270 Hz disturbance, 600 s experiments).
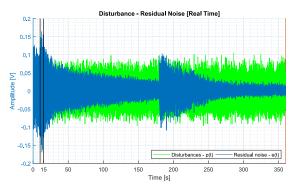
Fig. 11. Residual noise of the IIR 15/15 adaptive feedforward compensator for a change of disturbance from 170 - 270 Hz to 70 - 170 Hz at 180 s.

Figure 11 illustrates the adaptation capabilities of the IIR 15/15 FUSBA compensator. These experiments are run over 360 s. For the first 15 s, the system is in open-loop and the disturbance 70 - 170 Hz is applied until 10 s and then the disturbance 170 - 270 Hz is applied from 10 to 15 s. The adaptive compensation system is in operation from 15 to 360 s. During this period, the disturbance 170 - 270 Hz is applied from 15 to 180 s and the disturbance 70 - 170 Hz is applied from 180 to 360 s.

B. Results for IIRYK Adaptive Feedforward Compensators

The initial diagonal adaptation gain matrix used for IIRYK compensators has been set at 0.02 per parameter.

Filter type	No. params. [num/den]	Attenuation [dB]	max. TET [s]
IIRYK	25/25	29.0	7.85e-5
IIRYK	30/30	30.2	8.41e-5
IIRYK	40/40	33.2	1.01e-4

TABLE IX

INFLUENCE OF THE NUMBER OF PARAMETERS ON THE PERFORMANCE OF THE IIRYK ADAPTIVE FEEDFORWARD COMPENSATOR USING THE FUSBA ALGORITHM (70-270 HZ BROAD-BAND DISTURBANCE, 180 S EXPERIMENTS).

The number of parameters for the Youla-Kučera parametrized adaptive compensators has been chosen such that the maximum TET be equivalent to the one obtained for the standard IIR adaptive compensator with matrix gain.

Table IX shows that a total of 60 (30/30) parameters can be adapted for a maximum TET that is close to the one for the standard IIR 15/15 adaptive compensator given in Table VII. Table X shows the attenuation that can be obtained if the

Filter type	No. params. [num/den]	Attenuation [dB]	max. TET [s]
IIRYK	30/30	35.7	8.51e-5

TABLE X

EXPERIMENTAL RESULTS USING IIRYK ADAPTIVE COMPENSATOR WITH THE FUSBA ALGORITHM (70-270 HZ BROAD-BAND DISTURBANCE, 600 S EXPERIMENTS).

experiment is run over 600 s. The difference with respect to the 180 s long experiment is less significant than for the standard IIR compensator case. This is due to the fact that the IIRYK adaptive compensator converges more rapidly. Figure

Adaptation algorithm	Attenuation [dB]	max. TET [s]
Matrix (FUSBA)	30.2	8.41e-5
Matrix (FUPLR)	6.1	8.32e-5
Scalar (SFUSBA)	27.5	7.10e-5
Scalar (SFUPLR)	6.1	6.77e-5

TABLE XI

EXPERIMENTAL RESULTS FOR IIRYK 30/30 ADAPTIVE COMPENSATORS USING VARIOUS ADAPTATION ALGORITHMS (70-270 HZ BROAD-BAND DISTURBANCE, 180 S EXPERIMENTS).

12 illustrates the evolution of the residual noise and of the attenuation over an horizon of 600 s for the IIRYK 15/15 feedforward compensator using the FUSBA algorithm with a matrix adaptation gain. Attenuation reaches almost the steady state value at 600 s. Table XI gives a comparison of the various adaptation algorithms in terms of global attenuation and maximum TET. Clearly the FUSBA and the SFUSBA give the best results. The loss in performance when using a scalar adaptation gain is around 9% and the corresponding reduction of the maximum TET is about 15%. To understand why the FUPLR gives in this case far less good results than the FUSBA, one has to look at the phase of the estimated $\frac{A_M}{P}$ shown in Figure 13. One can see that $\frac{A_M}{P}$ is not positive real between 50 - 120 Hz, 160 - 310 Hz and 350 - 890 Hz. It is clear that in a large frequency spectrum the adaptation will not move in the right direction.

Figure 14 shows the PSD for the IIRYK 30/30 using the FUSBA algorithm. The peak at 306 Hz is due to a pole in the denominator of the Youla-Kučera filter at the same frequency with a damping of 0.00265.

Figures 15 shows the adaptation capabilities of the IIRYK adaptive compensator with 30/30 parameters. The same protocol is used as in the case of the standard IIR. The transients are shorter than for the IIR 15/15 while the steady states are comparable (even if one is better in high frequencies (IIRYK) and the other one is better in lower frequencies (IIR)).

C. Results for FIRYK Adaptive Feedforward Compensators

The initial gain of the adaptation algorithms used for FIRYK compensators has been set at 0.5 per parameter (this is possible since in this case one can take advantage of the global
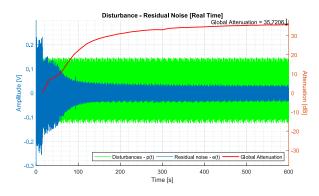
Fig. 12. Residual noise using the IIRYK 30/30 adaptive compensators with FUSBA matrix adaptation (70-270 Hz disturbance, 600 s experiments).


Fig. 13. Phase of $\frac{A_M}{P}$ for the IIRYK 30/30 adaptive compensator (70-270 Hz disturbance, 600 s experiments).
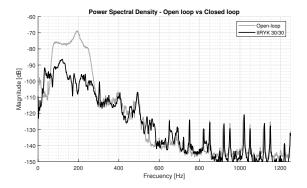
Fig. 14. PSD of the IIRYK 30/30 adaptive compensators using FUSBA matrix adaptation (70-270 Hz disturbance, 600 s experiments).

Filter type	No. params. [num/den]	Attenuation [dB]	max. TET [s]
FIRYK	20/0	17.2	6.43e-5
FIRYK	30/0	20.9	6.72e-5
FIRYK	40/0	22.7	7.06e-5
FIRYK	50/0	25.7	7.51e-5
FIRYK	60/0	27.0	7.87e-5
FIRYK	80/0	28.9	9.36e-5
FIRYK	100/0	31.2	1.11e-4

TABLE XII

INFLUENCE OF THE NUMBER OF PARAMETERS ON THE PERFORMANCE OF THE FIRYK ADAPTIVE FEEDFORWARD COMPENSATOR USING THE FUSBA ALGORITHM (70-270 HZ BROAD-BAND DISTURBANCE, 180 S EXPERIMENTS).
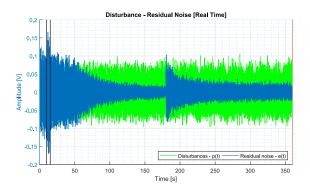
Fig. 15. Residual noise of the IIRYK 30/30 adaptive feedforward compensator for a change of disturbance from 170 - 270 Hz to 70 - 170 Hz at 180 s.

character of the stability condition for the FUSBA algorithm).

Table XII shows a comparison of the attenuation and maximum TET for various complexities of the FIRYK compensator. The FIRYK with 60 parameters (same number as

Filter type	No. params. [num/den]	Attenuation [dB]	max. TET [s]
FIRYK	60/0	28.3	8.03e-5

TABLE XIII

EXPERIMENTAL RESULTS USING FIRYK ADAPTIVE COMPENSATOR WITH THE FUSBA ALGORITHM (70-270 Hz BROAD-BAND DISTURBANCE, 600 S EXPERIMENTS).

for the IIRYK) has been chosen for further investigation. A 600 s experiment has been conducted for this FIRYK compensator and the results are given in Table XIII. Figure 16 shows both the time evolution of the residual error and of the attenuation. While the adaptation is much faster compared with the previous schemes, the steady state is less good (28.3 dB compared with the 35.7 dB for the IIRYK 30/30 and the 39.5 dB for the IIR 15/15 and the 32.4 for the FIR 30/0). Note however that the maximum TET is slightly smaller than for the other two schemes.

Adaptation algorithm	Attenuation [dB]	max. TET [s]
Matrix (FUSBA)	27.0	7.87e-5
Matrix (FUPLR)	unstable	-
Scalar (SFUSBA)	26.7	6.75e-5
Scalar (SFUPLR)	unstable	-

TABLE XIV

EXPERIMENTAL RESULTS FOR FIRYK 60/0 ADAPTIVE COMPENSATORS USING VARIOUS ADAPTATION ALGORITHMS (70-270 Hz BROAD-BAND DISTURBANCE, 180 S EXPERIMENTS).

Table XIV gives a comparison of the various adaptation algorithms in terms of global attenuation and maximum TET. It was observed that the FUPLR is unstable and this can be understood when looking to the phase plot of the estimated $\frac{A_M}{P}$ given in Figure 17. It can be observed that $\frac{A_M}{P}$ is not positive real in a large frequency range from 110 Hz to 760 Hz [13] and one absolutely needs to use the FUSBA algorithm. The

[13] Averaging can not be used since the region of non positive realness is much larger than the region where $\frac{A_M}{P}$ is SPR even within the range 70 - 270 Hz.

loss in performance when using a scalar adaptation gain is very small in this case (1%) while the computer load decreases by 14%.

Figure 18 shows the PSD of the FIRYK 60/0 using the FUSBA algorithm. The loss in performance with respect to the other schemes seems to be specifically in the region 210-270 Hz. Nevertheless, this curve indicates that the peak around 325 Hz is lower than in the previous cases (it will depend in fact on the design of the central compensator). The estimated pair of complex poles around this frequency have a damping of 0.04 (348 Hz) much higher than for the other schemes. Figure 19 shows the estimation of the output sensitivity function of the internal loop for the FIRYK 60/0 using the FUSBA algorithm. Note that the shape of this curve depends exclusively on the design of the central compensator and is not affected by the evolution of the Q filter parameters. As one can see, the maximum is about 10 dB which assures from the beginning of the adaptation process a modulus margin greater than 0.3.
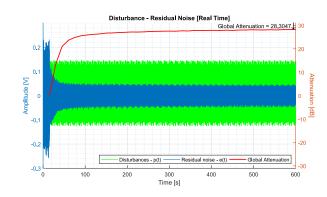

Fig. 16. Residual noise using the FIRYK 60/0 adaptive compensators with FUSBA matrix adaptation (70-270 Hz disturbance, 600 s experiments).
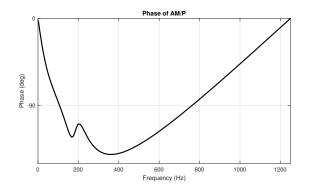
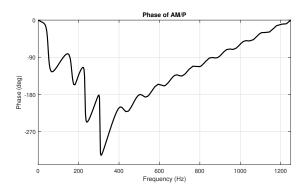Fig. 17. Phase of $\frac{A_M}{P}$ for the FIRYK 60/0 adaptive compensator (70-270 Hz disturbance, 600 s experiments).

Figure 20 shows the adaptation capabilities of the FIRYK adaptive compensator with 60/0 parameters. The same protocol is used as in the case of the standard IIR. As expected, the adaption transient is very fast and in addition the maximum value of the residual noise during the adaptation transient is much smaller compared with the IIR and the IIRYK.

Fig. 18. PSD of the FIRYK 60/0 adaptive compensators using FUSBA matrix adaptation (70-270 Hz disturbance, 600 s experiments).

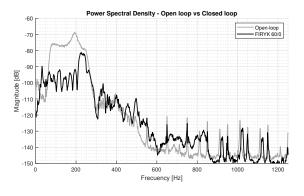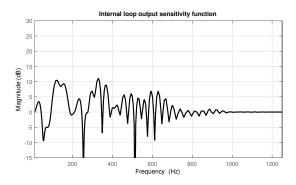Fig. 19. Internal loop output sensitivity function for the FIRYK 60/0 adaptive compensator (70-270 Hz disturbance, 600 s experiments).
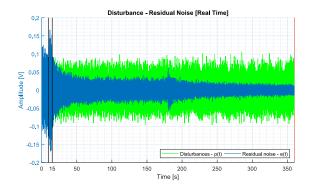
Fig. 20. Residual noise of the FIRYK 60/0 adaptive feedforward compensator for a change of disturbance from 170 - 270 Hz to 70 - 170 Hz at 180 s.

Filtering the Residual Noise for Parameter Adaptation

Figure 21 illustrates the effect of using a filtered residual noise in the adaptation algorithm upon the PSD of the residual noise. The comparison is done using the IIRYK 30/30 compensator with the FUSBA algorithm over 180 s (similar behavior is obtained also for the other compensator structures). The residual noise filter considered is a low pass FIR filter given by

$$V(q^{-1}) = 1 + 0.9q^{-1} \qquad (48)$$

The frequency response of this filter is shown in Fig. 22. As it can be observed, this filter enhances the attenuation
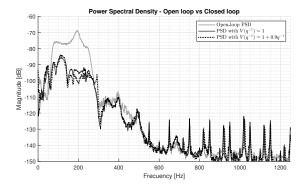
Fig. 21. PSD comparison of the residual noise in open-loop (solid grey line), using the adaptive compensator without filtering of the residual noise (solid black line), and using the adaptive compensator with filtering of the residual noise (dotted black line).

of disturbances at low frequencies. The global attenuation obtained with and without this filter is given in Table XV. One can see an improvement of about 9% when the filter is used.
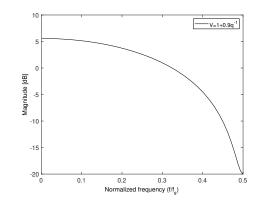
Fig. 22. Residual error filter.

Filter type	No. params.	Residual noise filter	Atn. [dB]
IIRYK	30/30	$V(q^{-1}) = 1$	30.2
IIRYK	30/30	$V(q^{-1}) = 1 + 0.9q^{-1}$	32.9

TABLE XV
EXPERIMENTAL RESULTS USING IIRYK ADAPTIVE COMPENSATOR WITH AND WITHOUT RESIDUAL NOISE FILTER (70-270 HZ BROAD-BAND DISTURBANCE, 180 S EXPERIMENTS).

Performance comparison - a summary

For a comparable complexity in terms of computer load, the IIR feeforward compensator with the matrix adaptation gain using the FUSBA algorithm provides the best steady state results in terms of attenuation followed by the IIRYK, FIR and FIRYK. In terms of adaptation transients, the FIRYK provides the best results. In terms of safety of operation (stability of the internal positive loop) without any doubt the FIRYK using the FUSBA algorithm (matrix adaptation gain) is the good choice since in this case the stability of the internal positive loop depends exclusively upon the stabilizing central compensator.

The steady state performance of the FIRYK can be enhanced by augmenting the number of adjustable parameters (which will increase however the computer load).

The use of the scalar adaptation gain leads to a slight degradation of the performances but does not lead to a substantial reduction of the computer load.

The use of a filtered residual noise measurement for adaptation may improve the overall performance.

VII. CONCLUSION

This study has provided the opportunity to assess comparatively the properties of various algorithms which can be used for adaptive feedforward noise compensation taking into account the inherent presence, in most of the applications, of an internal positive coupling. In many practical applications instabilities have been encountered using classical algorithms (FXLMS, FULMS, etc.) which do not take into account this internal positive coupling.

Based on extensive experimental tests one can state that FIRYK adaptive compensator structure using the FUSBA (or SFUSBA) algorithm is the good solution for a robust operation of the feedforward active noise attenuation. The main argument is that the stability of the internal positive loop is guaranteed by the design of the central compensator and is not influenced by the evolution of the adjustable filter parameters.

APPENDIX
IDENTIFICATION OF THE EXPERIMENTAL TEST-BENCH

The PRBS characteristics used in the identification process as excitation signal was: magnitude $= 0.14\,\text{V}$, register length $= 15$, frequency divider of 1, sequence length: $2^{15} - 1 = 32,767$ samples, guaranteeing an flat power spectrum up to $1250\,\text{Hz}$.

Since the transfer functions have a double differentiator behaviour (input: speaker's coil position, output: acoustical pressure), this is considered as the system's known part. The objective being to identify the unknown part only, the input sequence is filtered by a double discrete-time differentiator $D_F = (1 - q^{-1})^2$ such that $u'(t) = D_F \cdot u(t)$. The double differentiator is added to the identified model of the unknown part in order to obtain the complete model.

Once the input-output data have been acquired, the next step in the identification procedure is to estimate the order n of the model from experimental data (see (2)). The method of Duong ([20], [25]) has been used. Once an estimated order $\hat{n}$ is selected, one can apply a similar procedure to estimate $\hat{n}_A$, $\hat{n}-\hat{d}$, and $\hat{n}_{B'}+\hat{d}$, from which $\hat{n}_A$, $\hat{n}_{B'}$ and $\hat{d}$ are obtained ($n_{B'}$ is the order of the model's numerator without the double differentiator). In the method of Duong, the minimum of a quadratic criterion in terms of an unbiased plant-model error penalized by a complexity terms is searched. Fig. 23 shows in detail the system's order estimation results for the secondary path.

The value of $\hat{n} = 25$ minimizes the Duong criterion, but since the minimum is relatively flat, nearby values have also been considered. The final selection has been done by
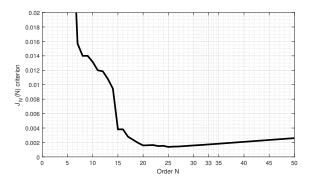

Fig. 23. Penalized criterion for order estimation (secondary path).

checking what order allows to capture all the oscillatory modes in the model and leads to the best statistical validation once the parameters are identified. For the secondary path, this order has been found to be $\hat{n} = 33$ (see Table I).

Comparative parameter estimations considering various plant + noise models and estimation algorithms led to the conclusion that an ARMAX model representation is the most appropriate for this system and the best results in terms of statistical validation (whiteness test on the residual error) have been obtained using the Output Error with Extended Prediction Model (termed *OEEPM* or *XOLOE*). See [20] and [26] for more details on the methodology.

REFERENCES

[1] S. Elliott and P. Nelson, "Active noise control," *Noise / News International*, pp. 75–98, June 1994.

[2] S. Elliott and T. Sutton, "Performance of feedforward and feedback systems for active control," *Speech and Audio Processing, IEEE Transactions on*, vol. 4, no. 3, pp. 214 –223, may 1996.

[3] S. Kuo and D. Morgan, "Active noise control: a tutorial review," *Proceedings of the IEEE*, vol. 87, no. 6, pp. 943 – 973, jun 1999.

[4] J. Zeng and R. de Callafon, "Recursive filter estimation for feedforward noise cancellation with acoustic coupling," *Journal of Sound and Vibration*, vol. 291, no. 3-5, pp. 1061 – 1079, 2006.

[5] B. Widrow and S. Stearns, *Adaptive Signal Processing*. Englewood Cliffs, New Jersey: Prentice-Hall, 1985.

[6] M. Kuo and D. Morgan, *Active noise control systems-Algorithms and DSP implementation*. New York,: Wiley, 1996.

[7] C. Jacobson, J. Johnson, C.R., D. McCormick, and W. Sethares, "Stability of active noise control algorithms," *Signal Processing Letters, IEEE*, vol. 8, no. 3, pp. 74 –76, mar 2001.

[8] F. Ben Amara, P. Kabamba, and A. Ulsoy, "Adaptive sinusoidal disturbance rejection in linear discrete-time systems - Part I: Theory," *Journal of Dynamic Systems Measurement and Control*, vol. 121, pp. 648–654, 1999.

[9] ——, "Adaptive sinusoidal disturbance rejection in linear discrete-time systems - Part II: Experiments," *Journal of Dynamic Systems Measurement and Control*, vol. 121, pp. 655–659, 1999.

[10] I. D. Landau, M. R., D. L., and B. G., "Robust and adaptive feedback noise attenuation in ducts," *IEEE Transactions on Control System Technology*, vol. 24, no. 12, pp. 1–8, December 2017.

[11] L. Eriksson, "Development of the filtered-U LMS algorithm for active noise control," *J. of Acoustical Society of America*, vol. 89, no. 1, pp. 257–261, 1991.

[12] A. Wang and W. Ren, "Convergence analysis of the Filtered-U algorithm for active noise control," *Signal Processing*, vol. 83, pp. 1239–1254, 1999.

[13] R. Fraanje, M. Verhaegen, and N. Doelman, "Convergence analysis of the Filtered-U LMS algorithm for active noise control in case perfect cancellation is not possible," *Signal Processing*, vol. 73, pp. 255–266, 2003.

[14] L. Xie, Z. cheng Qiu, and X. min Zhang, "Vibration control of a flexible clamped-clamped plate based on an improved FULMS algorithm and laser displacement measurement," *Mechanical Systems and Signal Processing*, vol. 75, pp. 209 – 227, 2016.

[15] X. Zhu, Z. Gao, Q. Huang, S. Gao, and E. Jiang, "Analysis and implementation of MIMO FULMS algorithm for active vibration control," *Transactions of the Institute of Measurement and Control*, vol. 34, no. 7, pp. 815–828, 2012.

[16] L. Ljung and T. Söderström, *Theory and practice of recursive identification*. Cambridge Massachusetts , London, England: The M.I.T Press, 1983.

[17] I. Landau, M. Alma, and T. Airimitoaie, "Adaptive feedforward compensation algorithms for active vibration control with mechanical coupling," *Automatica*, vol. 47, no. 10, pp. 2185 – 2196, 2011.

[18] I. D. Landau, T.-B. Airimitoaie, and M. Alma, "A Youla–Kučera parametrized adaptive feedforward compensator for active vibration control with mechanical coupling," *Automatica*, vol. 48, no. 9, pp. 2152 – 2158, 2012.

[19] ——, "IIR Youla–Kučera parameterized adaptive feedforward compensators for active vibration control with mechanical coupling," *IEEE Transactions on Control System Technology*, vol. 21, no. 3, pp. 765–779, May 2013.

[20] I. D. Landau, T.-B. Airimitoaie, A. Castellanos Silva, and A. Constantinescu, *Adaptive and Robust Active Vibration Control—Methodology and Tests*, ser. Advances in Industrial Control. Springer Verlag, 2017.

[21] I. D. Landau, R. Lozano, M. M'Saad, and A. Karimi, *Adaptive control*, 2nd ed. London: Springer, 2011.

[22] J. Treichler, M. Larimore, and J. Johnson, C., "Simple adaptive IIR filtering," in *Acoustics, Speech, and Signal Processing, IEEE International Conference on ICASSP '78.*, vol. 3, apr 1978, pp. 118 – 122.

[23] M. Beijen, M. Heertjes, J. V. Dijk, and W. Hakvoort, "Self-tuning mimo disturbance feedforward control for active hard-mounted vibration isolators," *Control Engineering Practice*, vol. 72, pp. 90 – 103, 2018.

[24] B. Anderson, R. Bitmead, C. Johnson, P. Kokotovic, R. Kosut, I. Mareels, L. Praly, and B. Riedle, *Stability of adaptive systems*. Cambridge Massachusetts , London, England: The M.I.T Press, 1986.

[25] H. N. Duong and I. D. Landau, "An IV based criterion for model order selection," *Automatica*, vol. 32, no. 6, pp. 909–914, 1996.

[26] R. Melendez, I. Landau, L. Dugard, and G. Buche, "Data driven design of tonal noise feedback cancellers," in *Proceedings of the 20th IFAC World Congress, Toulouse, France*, 2017, pp. 916–921.

D

DATA DRIVEN DESIGN OF TONAL FEEDBACK CANCELLERS

Data driven design of tonal noise feedback cancellers

Raúl A. Meléndez [*,★], **Ioan D. Landau** [*], **Luc Dugard** [*], **Gabriel Buche** [*]

[*] *Univ. Grenoble Alpes, CNRS, GIPSA-lab, F-38000 Grenoble, France,*
(e-mail: Raul.Melendez, Ioan-Dore.Landau, Luc.Dugard,
Gabriel.Buche@gipsa-lab.grenoble-inp.fr)

Abstract: This paper emphasizes the design methodology for active tonal noise feedback cancellers starting from data collected on the system. To design such control systems, an accurate dynamic model of the system is necessary. Physical modeling can provide qualitative results but fails to yield enough accurate models for control design. The main point in the methodology is identification of primary path (noise propagation) and secondary path (compensation) models from data. The procedure is investigated in details starting with transfer functions' order estimations, continuing with parameters estimation and model's validation. The second aspect is the design of a noise canceller using the Internal Model Principle and the sensitivity function shaping in order to reduce the "water-bed" effect. The estimated model's quality for control design is illustrated by the experimental performance of a tonal noise feedback canceller implemented on a test bench.

Keywords: Active noise control, System Identification, Internal model principle, Band stop filters, Sensitivity functions.

1. INTRODUCTION

Active noise control *(ANC)* has been under research for many years and applied in various kind of applications. In most cases feed-forward broadband noise compensation is currently used for ANC when a disturbance's image is available (correlated measurement with the disturbance). See Elliott and Nelson (1994), Elliott and Sutton (1996), Kuo and Morgan (1999), Zeng and de Callafon (2006).

However, these solutions, inspired by Widrows technique for adaptive noise cancellation, see Widrow and Stearns (1985), ignore the possibilities offered by feedback control systems and have a number of disadvantages: they require the use of an additional transducer, difficult choice for its location and presence, in most cases, of a "positive" coupling between the compensator system and the disturbance image's measurement, which can cause instabilities. To achieve the disturbance's rejection (asymptotically) without measuring it, a feedback solution can be considered.

Residual noise can be described as the result of acoustic waves which pass trough the system, and the noise cancellers' objective is to attenuate it. In many cases, these waves can be characterized in the frequency domain either as tonal disturbances or as narrow band perturbations. The common framework is the assumption that a narrow band disturbance is the result of a white noise or a Dirac impulse passed through the "disturbance's model." In the case of tonal (narrow band) noise disturbances, the basic idea is to use the "internal model principle" to get a strong attenuation, combined with output sensitivity function shaping, in order to avoid unwanted amplifications in the tonal disturbances' neighborhoods.

However, the real time performance of the noise cancellers strongly depends on the secondary path dynamic model's quality used for designing the feedback control law. Many studies have been carried out to develop dynamic models for control design, starting from the basic physical equations describing the system and trying to determine, from the systems' geometry, the values of some basic constants. See Nelson and Elliott (1993). Zimmer and Lipshitz (2003) give a very complete evaluation of the physical modeling in the context of active noise control in ducts. Unfortunately on one hand the resulting models are not very good, since it is hard for a given system to find the correct physical constants, and on the other hand it is a PDE model for which there are not simple control design methods available.

What is needed in practice is a finite dimension discrete-time model which reproduces the system's dynamical behavior. Once such a model is available, one can use digital control design techniques readily implementable on a real time computer. These models can be obtained directly from data using system identification techniques, see Ljung (1999); Landau et al. (2016); Carmona and Alvarado (2000). However these discrete-time models for active noise compensation present a number of peculiarities which require to develop a specific identification procedure. One of the major objectives of the paper is to clarify how system identification from data should be done in the context of active noise control. Previous identification results given in Ben Amara et al. (1999) and Zeng and de Callafon (2006) have been also considered.

The final quality test for an identified model is to verify how close are the real-time experimental results obtained and the designed controller's performances in simulation. As shown later, the results are very close, which indicates that the proposed procedure is reliable. Two control problems have been considered: the rejection of two tonal disturbances, and strong

attenuation of interferences, caused by tonal disturbances with very close frequencies. The Internal Model Principle *(IMP)* combined with the sensitivity functions' shaping will be used for control design.

2. EXPERIMENTAL SETUP

The test bench used for the experiments is shown in Fig. 1, and its detailed scheme is given in Fig. 2. The speaker used as the source of disturbances is labeled as 1, the control speaker is 2 and finally, at pipe's open end, the microphone that measures the system's output (residual noise) is denoted as 3. The transfer function between the disturbance's speaker and the microphone $(1 \rightarrow 3)$ is denominated *Primary Path*, while the transfer function between the control speaker and the microphone $(2 \rightarrow 3)$ is denominated *Secondary Path*. Both speakers are connected to a xPC Target computer with Simulink Real Time® environment through a pair of high definition power amplifiers and a data acquisition card. The current signals $u(t)$ and $p(t)$ are amplified and reach the speakers' voice coils and displace them, generating movement in the diaphragms and thus, sound waves. In Fig. 2, $y(t)$ is the system's output (residual noise measurement). Both primary and secondary paths have a double differentiator behavior, since as input we have the voice coil displacement, and as output the air acoustic pressure. A second computer is used for development, design and operation with Matlab®.
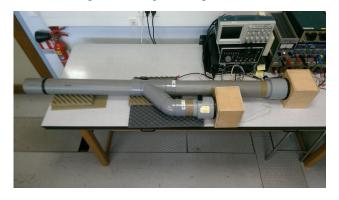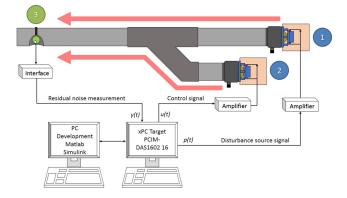

Fig. 1: Noise control test bench (Photo).

Fig. 2: Noise control test bench diagram.

PVC pipes of $0.10\,\text{m}$ diameter are used in this test bench, with couplings of $135°$ for the control speaker. Distances between disturbance speaker and microphone are $1.65\,\text{m}$, and to control input $0.80\,\text{m}$. Speakers are isolated inside wood boxes filled with special foam in order to create anechoic chambers and reduce the radiation noise produced.

3. SYSTEM DESCRIPTION

The linear time invariant *(LTI)* discrete-time model of the secondary path, or plant, used for controller design is

$$G(z^{-1}) = \frac{z^{-d}B(z^{-1})}{A(z^{-1})} = \frac{z^{-d}B'(z^{-1})}{A(z^{-1})}D_F(z^{-1}), \quad (1)$$

where $D_F(z^{-1})$ is a double differentiator filter and

$$A(z^{-1}) = 1 + a_1 z^{-1} + \cdots + a_{n_A} z^{-n_A}, \quad (2)$$
$$B'(z^{-1}) = b_1 z^{-1} + \cdots + b_{n_{B'}} z^{-n_{B'}}, \quad (3)$$

with d as the plant pure time delay in number of sampling periods [1]. The system's order is

$$n = max(n_A, n_{B'} + d) \quad (4)$$
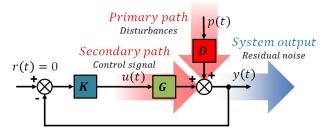
Fig. 3: Feedback regulation scheme.

Figure 3 shows the closed loop feedback regulation scheme, where the controller K is described by

$$K(z^{-1}) = \frac{R}{S} = \frac{r_0 + r_1 z^{-1} + \cdots + r_{n_R} z^{-n_R}}{1 + s_1 z^{-1} + \cdots + s_{n_S} z^{-n_S}}. \quad (5)$$

The plant's output $y(t)$ and the input $u(t)$ may be written as (see Fig. 3):

$$y(t) = \frac{q^{-d}B(q^{-1})}{A(q^{-1})} \cdot u(t) + p(t), \quad (6)$$
$$S(q^{-1}) \cdot u(t) = -R(q^{-1}) \cdot y(t). \quad (7)$$

In (6), $p(t)$ is the disturbances' effect on the measured output [2] and $R(z^{-1})$, $S(z^{-1})$ are polynomials in z^{-1} having the following expressions:

$$R = H_R \cdot R' = H_R \cdot (r'_0 + r'_1 z^{-1} + \ldots + r'_{n_{R'}} z^{-n_{R'}}), \quad (8)$$
$$S = H_S \cdot S' = H_S \cdot (1 + s'_1 z^{-1} + \ldots + s'_{n_{S'}} z^{-n_{S'}}), \quad (9)$$

where $H_S(z^{-1})$ and $H_R(z^{-1})$ represent prespecified parts of the controller (used for example to incorporate the internal model of a disturbance, or to open the loop at some frequencies) and $S'(z^{-1})$ and $R'(z^{-1})$ are solutions of the Bezout equation:

$$P = P_D \cdot P_F = (A \cdot H_S) \cdot S' + \left(z^{-d} B \cdot H_R \right) \cdot R'. \quad (10)$$

In (10) $P(z^{-1})$ represents the characteristic polynomial, which specifies the desired closed loop poles of the system. P_D represents the stable poles of the plant and P_F are auxiliary poles.

The transfer functions between the disturbance $p(t)$ and the system's output $y(t)$ and the control input $u(t)$, denoted respectively *output* and *input sensitivity functions*, are given by

$$S_{yp}(z^{-1}) = \frac{A(z^{-1})S(z^{-1})}{P(z^{-1})} \quad (11)$$

---

[1] The complex variable z^{-1} is used to characterize the system's behavior in the frequency domain and the delay operator q^{-1} for the time domain analysis.
[2] The disturbance passes through the *primary path*, and $p(t)$ is its output.

and

$$S_{up}(z^{-1}) = -\frac{A(z^{-1})R(z^{-1})}{P(z^{-1})}, \qquad (12)$$

4. DATA DRIVEN SYSTEM IDENTIFICATION

Model identification from experimental data is a well established methodology (see Landau et al. (2016); Ljung (1999)). Identification of systems is an experimental approach for determining a system's dynamic model. It includes four steps:

1. Input-output data acquisition under an experimental protocol and data pre-processing.
2. Estimation of the model complexity.
3. Estimation of the model parameters.
4. Validation of the identified model (complexity of the model and values of the parameters).

A complete identification operation must comprise the four stages indicated above. The typical input is a *PRBS*, which is a persistent excitation signal allowing unique parameter estimation even for high order system. Model validation is the final key point. It is important to emphasize that it does not exist one single algorithm that can provide in all the cases a good model (i.e. which passes the model validation tests). System identification should be viewed as an iterative process which has as objective to obtain a model which passes the model validation test and then can be used safely for control design. The procedure will be detailed for the secondary path's identification. The same methodology has been used for the primary path identification also (which is used only for simulation), and only the final results will be given.

4.1 Data Acquisition under the experimental protocol

For design and application reasons (the objective is to reject tonal disturbances up to 400 Hz), the sampling frequency was selected as $f_s = 2500\,\text{Hz}$ ($T_s = 0.0004\,\text{s}$) i.e. approximatively 6 times the maximum frequency to attenuate, in accordance with recommendation given in (see Landau et al. (2016)). The theoretical band pass of the system is 1975 Hz, using formula given in Zimmer and Lipshitz (2003).

The experimental protocol should assure persistent excitation for the number of parameters to be estimated, thus a PRBS has been used. This signal's magnitude is constant allowing an easy selection with respect to the magnitude constraint on the plant input. One of the key points is the design of a PRBS in order to satisfy a compromise between the frequencies range to be covered (particularly those in the low frequencies region), and the test duration. One should apply at least on complete PRBS sequence, and its characteristics, including duration, will depend on the number of cells in the registers length used for its generation.

For identification, the signals' characteristics used in both paths are: magnitude $= 0.15\,\text{V}$, register length $= 17$, frequency divider of 1, sequence length of $2^{17} - 1 = 131,071$ samples, guaranteeing a uniform power spectrum from about 70 Hz to 1250 Hz. Since the transfer functions have a double differentiator behavior, this is considered as a system's known part and the objective will be to identify the unknown part only. To do this, the input sequence will be filtered by a double discrete-time differentiator $D_F = (1 - q^{-1})^2$ such that $u'(t) = D_F \cdot u(t)$. The double differentiator will be concatenated with the identified model of the unknown part in the final models.

4.2 Complexity Estimation

The basic idea in complexity estimation is to have, on one hand an unbiased estimator of the system parameters, which allows to obtain an unbiased evolution of the prediction error quadratic criterion that tends toward zero when the correct order is reached, and on the other hand a penalty term for the model's complexity. In order to get an unbiased estimation of the error criterion, the *instrumental variable* approach is used, see Landau et al. (2016); Duong and Landau (1996). This assumes that the system is described by $Y(t) = Z(\hat{n})\hat{\theta}_{\hat{n}}$, where $\hat{\theta}_{\hat{n}}^T = [\hat{a}_1, \cdots, \hat{a}_{\hat{n}}, \hat{b}_1, \cdots, \hat{b}_{\hat{n}}]$, and $\hat{n}$ is the estimated order. So,

$$Z(\hat{n}) = [U(t-L-1), U(t-1), \cdots, U(t-L-\hat{n}), U(t-\hat{n})]$$

are the delayed inputs with $L > \hat{n}$, and $Y(t)$, $U(t)$ are defined by

$$Y^T(t) = [y(t), y(t-1)...]; \quad U^T(t) = [u'(t), u'(t-1)...].$$

The least squares criterion defined in Landau et al. (2016) is

$$V_{IV}(\hat{n}, N) = \min_{\hat{\theta}} \frac{1}{N} \left\| Y(t) - Z(\hat{n})\hat{\theta}_{\hat{n}} \right\|^2, \qquad (13)$$

where N is the number of samples. Adding a term which penalizes the model's complexity leads to

$$J_{IV}(\hat{n}, N) = V_{IV}(\hat{n}, N) + 2\hat{n}\frac{\log N}{N}. \qquad (14)$$

When identifying finite dimensional discrete-time models, J_{IV} will show a minimum value, function of $\hat{n}$, allowing to define the estimated order of the model. Once an estimated order $\hat{n}$ is selected, one can apply a similar procedure to estimate $\hat{n}_A$, $\hat{n} - \hat{d}$, and $\hat{n}_{B'} + \hat{d}$, from which $\hat{n}_A$, $\hat{n}_{B'}$ and $\hat{d}$ are obtained.
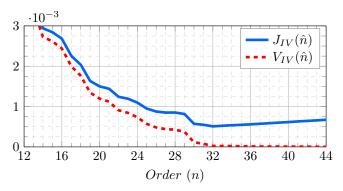
Results for the secondary path order estimation (without the double differentiator) are shown in Fig. 4, where both non-penalized and penalized criteria V_{IV}, J_{IV} are represented. As it can be seen, the minimum is very flat (which is understandable since we are trying to approximate an infinite-dimensional system). It is therefore necessary to explore the model's properties for n between 32 and 42, in order to decide what order to take. Two additional criteria will be used to decide upon the best order estimation: I) comparison between the Power Spectral Densities *(PSD)* of the identified model's output, and the output's real data (in order to see if the identified model captures all the vibrations modes in the frequency range of operation); and II) comparison of the validation tests for the various models.

To do this it is necessary to estimate the values of n_A, $n_{B'}$ and d for each order n selected, and to proceed with parameter estimation. To illustrate the details of orders estimations, the model with $n = 40$ is considered (the procedure for other values of n is similar). For the secondary path, Fig.4b shows that the minimum for $n - d$ is 32. From Fig.4c one can see that the minimum for n_A is given by $n_A = 38$. From Fig.4d one concludes that $n_{B'} + d = 38$. Taking in account the definition of order n, one concludes that $n_A = 38$, $n_{B'} = 30$ and $d = 8$, therefore the effective estimated order of this model is $n_e = 38$. Similarly for a model with $n = 38$, one gets $n_A = 37$, $n_{B'} = 30$, $d = 8$ (which means an effective order $n_e = 38$)[3].
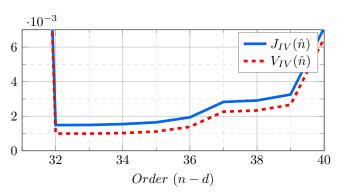
4.3 Parameters Estimation

The algorithms used for parameter estimation will depend on the assumptions made on the measurements' noise characteristics, which have to be confirmed by the model validation.
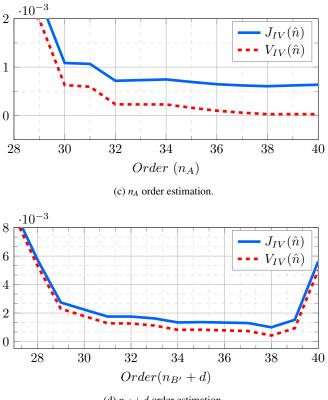
---

[3] Complete model's $n_B = n_{B'} + 2$, due to the double differentiator addition.

(a) Instrumental Variable (n) order estimation.

(b) Instrumental Variable ($n-d$) order estimation.

(c) n_A order estimation.

(d) $n_{B'}+d$ order estimation.

Fig. 4: Secondary path, Instrumental Variable order estimation.

It is important to emphasize that none single *plant + noise* structure exists that can describe all the situations encountered in practice. It is the validation stage which will allow to decide what method (and implicitly what noise model) has to be used.

(a) Model with $n = 40$.

(b) Model with $n = 38$.
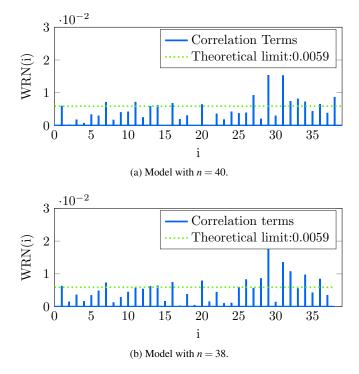
Fig. 5: Whiteness validation tests for the secondary path.

Among various models, it was found that the *ARMAX* model gives the best representation in this case, and between the available methods for that model, Output Error with Extended Prediction method *(XOLOE)* brought the best results in terms of validation for a given order model. The details of the algorithm are given in Landau et al. (2016), section 5.4.2.

4.4 Model Validation

The validation procedure associated with the identification of ARMAX models is based on a whiteness test.

Whiteness test: Let $\{\varepsilon(t)\}$ be the centered (measured value minus average) sequence of the residual prediction errors. One computes estimations of the normalized autocorrelations as:

$$R(i) = \frac{1}{N} \sum_{t=1}^{N} \varepsilon(t)\varepsilon(t-i) \tag{15}$$

$$R(0) = \frac{1}{N} \sum_{t=1}^{N} \varepsilon^2(t) \; ; \; RN(i) = \frac{R(i)}{R(0)} \tag{16}$$

$$i = 1, 2, 3, \ldots, n_A, \ldots, n$$

One considers as a validation criterion (extensively tested on applications):

$$RN(0) = 1 \; ; \; |RN(i)| \leq \frac{2.17}{\sqrt{N}} \; ; \; i \geq 1. \tag{17}$$

Fig. 5 shows the validation results (whiteness test) for the unknown part model with $n = 40$ (effective $n_e = 38$) and $n = 38$ ($n_e = 38$). The results are summarized in Table 1. Model $n = 40$ leads to better results, which is confirmed in Fig. 6 where the PSD of real data's measures is compared with the two complete models outputs' PSD (including the double differentiator). Therefore the *XOLOE* model $n = 40$ is chosen. It has 18 oscillatory modes with damping comprised between 0.0097 and 0.3129; also 13 pairs of oscillatory zeros

Fig. 6: System output PSD.

Fig. 7: Frequency characteristics of the identified primary and secondary paths models

with damping comprised between -0.0159 and 0.5438. The presence of these low damped zeros make the control system's design difficult. Fig. 7 gives the frequency characteristics of the identified complete models for the primary and secondary paths.
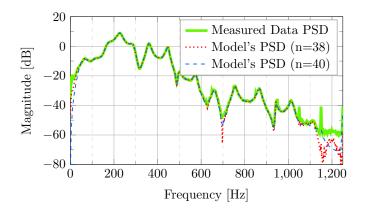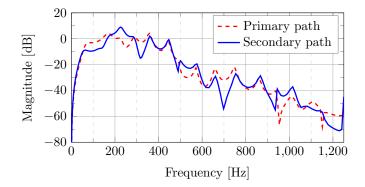
Table 1: Summary of Whiteness tests validations

Method	Model	Error energy	Maximum $RN(i)$	$RN(i)$ over limit
$XOLOE$	$n = 40$	1.3307e-06	0.0154	15
$XOLOE$	$n = 38$	1.3337e-06	0.0177	14

5. CONTROLLER DESIGN

The basic specifications are that the attenuation of two tonal disturbances located at $170\,\text{Hz}$ and $285\,\text{Hz}$ must be at least $-40\,\text{dB}$, and the maximum amplification at other frequencies be less than $7\,\text{dB}$. Furthermore, in order to improve robustness, the input sensitivity function should be below $-20\,\text{dB}$ at frequencies over $600\,\text{Hz}$ (beyond the system's bandpass).

In order to strongly attenuate the two tonal disturbances the IMP has been used, so the RS controller to be designed requires a fixed part H_S to incorporate the disturbance's model, as described in section 3. See (Landau et al., 2016). The tonal disturbances can be modeled by:

$$p(t) = \frac{N_p(q^{-1})}{D_p(q^{-1})} \cdot \delta(t), \quad (18)$$

with $\delta(t)$ as a Dirac impulse. D_p has roots on the unit circle. In practice, the contribution of N_p is negligible for steady state
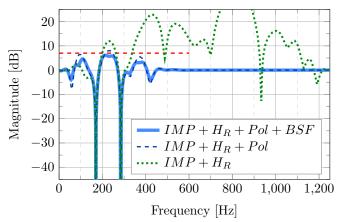

Fig. 8: Frequency characteristics for Output sensitivity, S_{yp}.
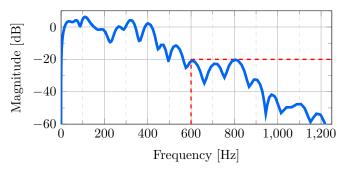
Fig. 9: Frequency characteristics for Input sensitivity, S_{up}.

analysis in comparison with D_p. Then $H_S(q^{-1}) = D_p(q^{-1})$, and for this specific case, $H_S = H_{S_1} H_{S_2}$ where:

$$H_{S_i}(q^{-1}) = D_{p_i}(q^{-1}) = 1 - 2\cos\left(2\pi \frac{f_i}{f_s}\right) q^{-1} + q^{-2}, \quad (19)$$

with $f_1 = 170\,\text{Hz}$ and $f_2 = 285\,\text{Hz}$. Also, since the system has a zero gain at $0\,\text{Hz}$ and a very low gain at $1250\,\text{Hz}$, the loop has been opened at these frequencies by choosing $H_R = (1 + q^{-1})(1 - q^{-1})$. The dominant closed loop poles P_D have been chosen equal to those of the secondary path. Eq. (10) has unique solution for S' and R' of minimal degree for

$$n_P = \deg P(z^{-1}) \le n_A + n_{H_S} + n_B + n_{H_R} + d - 1, \quad (20)$$

$$n_{S'} = \deg S'(z^{-1}) = n_B + n_{H_R} + d - 1, \quad (21)$$

$$n_{R'} = \deg R'(z^{-1}) = n_A + n_{H_S} - 1. \quad (22)$$

Fig. 8 shows the resulting output sensitivity function S_{yp} (curve $IMP + H_R$). The specifications for maximum gain are violated. To overcome this, 30 auxiliary real poles with value $p_i = 0.25$ have been added in the form $P_F(z^{-1}) = (1 - p_i z^{-1})^{n_F}$, without augmenting the controller's order (curve $IMP + H_R + Pol$). The resulting sensitivity function is improved but the limit is still violated. To further shape the sensitivity function, *Band-Stop Filters* (BSF) have been used (Landau et al. (2016)); 3 on S_{yp}, and 3 on S_{up} to obtain a correct behavior (see table 2). The resulting output sensitivity function is shown in Fig. 8. Also the resulting input sensitivity function is shown in Fig. 9.

Table 2: Band-Stop Filters for sensitivity functions.

	Freq.[Hz]	Ampli.[dB]		Freq.[Hz]	Ampli.[dB]
	90	-6.00		600	-6.00
S_{yp}	231	-8.00	S_{up}	800	-1.00
	370	-5.00		945	+5.00

Fig. 10 displays the system's output for a simulation using the models estimated for the primary and secondary paths. A pair of sinusoidal signals at 170 Hz and 285 Hz were used as disturbances $p(t)$ from 1 s to 11 s. Control starts at 6 s and ends at 11 s. A global attenuation of 86.4 dB was achieved, with attenuations of -88.6 dB at 170 Hz, and -94 dB at 285 Hz.
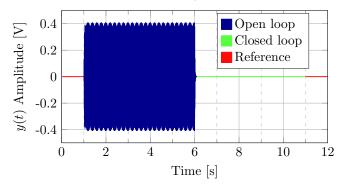

Fig. 10: Simulation results.

6. EXPERIMENTAL RESULTS

The experimental results have been obtained by implementing the designed controller on the test-bench described in Section 2.

Fig. 11 shows the result for a real time test. Two tonal sinusoidal signals at 170 Hz and 285 Hz were used as disturbances $p(t)$ from 1 s to 11 s. Control starts by closing the loop at 6 s and ends at 11 s. Performances during the first second and the last one are used as a reference for the ambient noise (no control, no disturbance). A global attenuation of 76.88 dB was achieved, with disturbance attenuations of -94.5 dB at 170 Hz, and -94 dB at 285 Hz. These results are very close to those obtained in simulation. Fig. 12 displays the effective residual PSD estimation, calculated as a difference between the open-loop PSD and the closed-loop PSD of the residual noise.
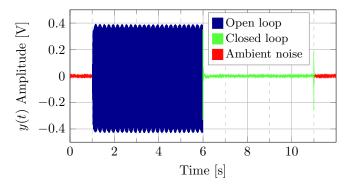

Fig. 11: Real-time experiment results: tonal disturbances.

Fig. 13 displays the results for a second real-time test. Two pairs of sinusoidal interference signals (170 Hz+170.5 Hz and 285 Hz+285.5 Hz) with amplitude of 0.14 V were used as disturbances $p(t)$ from 1 s to 20 s. Control starts by closing the loop at 10 s and ends at 20 s. Performances during first and last second are used as a reference for ambient noise again. A global attenuation of 59.55 dB was achieved.

REFERENCES

Ben Amara, F., Kabamba, P., and Ulsoy, A. (1999). Adaptive sinusoidal disturbance rejection in linear discrete-time sys-
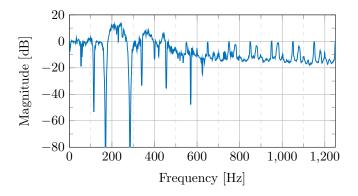
Fig. 12: Effective residual attenuation PSD estimation.
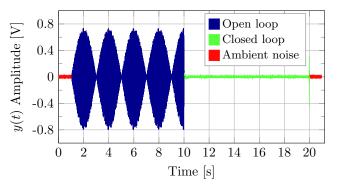
Fig. 13: Interference attenuation: residual noise in open loop and closed loop.

tems - Part II: Experiments. *Journal of Dynamic Systems Measurement and Control*, 121, 655–659.

Carmona, J.C. and Alvarado, V.M. (2000). Active noise control of a duct using robust control theory. *IEEE-CST*, 8(6), 930–938.

Duong, H.N. and Landau, I.D. (1996). An IV Based Criterion for Model Order Selection. *Automatica*, 32(6), 909–914.

Elliott, S. and Nelson, P. (1994). Active noise control. *Noise / News International*, 75–98.

Elliott, S. and Sutton, T. (1996). Performance of feedforward and feedback systems for active control. *IEEE Speech Audio Proces.*, 4(3), 214–223.

Kuo, S. and Morgan, D. (1999). Active noise control: a tutorial review. *Proceedings of the IEEE*, 87(6), 943 – 973.

Landau, I.D., Airimioaie, T.B., and Castellanos-Silva, A. (2016). *Adaptive and Robust Active Vibration Control*. Springer, London.

Ljung, L. (1999). *System Identification - Theory for the User*. Prentice Hall, Englewood Cliffs, second edition.

Nelson, P. and Elliott, S. (1993). *Active Control of Sound*. Academic Press.

Widrow, B. and Stearns, S. (1985). *Adaptive Signal Processing*. Prentice-Hall, Englewood Cliffs, New Jersey.

Zeng, J. and de Callafon, R. (2006). Recursive filter estimation for feedforward noise cancellation with acoustic coupling. *Journal of Sound and Vibration*, 291(3-5), 1061 – 1079.

Zimmer, B.J. and Lipshitz, S.P. (2003). An improved acoustic model for active noise control in a duct. *Journal of Dynamic Systems, Measurement, and Control*, 125, 382–395.

E

ACTIVE NOISE CONTROL: ADAPTIVE VS ROBUST APPROACH

Active Noise Control : Adaptive vs. Robust Approach

Ioan Doré Landau, Raúl Meléndez

Abstract—Active noise control is often concerned with the strong attenuation of single or multiple tonal noise disturbances which may have unknown and time varying frequencies. Currently in applications, adaptive feed-forward compensation is used which requires the use of an additional transducer and introduces an instability risk due to a positive internal coupling. However for these types of noise a feedback approach can be efficiently used and this will be illustrated in this paper. One considers the case of two tonal disturbances located in two distinct frequency regions subject to frequency variations within a given range as well the case of interferences between tonal disturbances of very close frequencies. The objective is to minimize the measured residual noise in a predefined location. These problems occurs often in ventilation systems (active silencers). To solve these problems robust and adaptive solutions are considered. A robust controller design using sensitivity function shaping is considered. The maximum achievable attenuation is inverse proportional to the range of frequency variations of the tonal disturbances. To further improve the performance an add-on direct adaptive feedback approach using the Internal Model Principle and the Youla Kucera parametrization is considered. The adaptive approach allows both to improve the performance within the given frequency ranges as well as to extend the admissible domain of frequencies variations. Experimental results obtained on a relevant test bench will illustrate the performance of the two designs.

Index Terms—Active noise control, System Identification, Internal model principle, Youla-Kučera parametrization, Adaptive control, Robust control.

I. INTRODUCTION

Active disturbance rejection is a key issue in active vibration control and active noise control. The popular approach for active noise control is to use adaptive feed-forward compensation. This approach, inspired by Widrows technique for adaptive noise cancellation, see [1], ignores the possibilities offered by feedback control systems and have a number of disadvantages: 1) it requires the use of an additional transducer for obtaining an image of the disturbance, 2) difficult choice for positioning this additional transducer and, 3) in most cases, there exists a "positive" coupling between the compensator system and the disturbance image's measurement, which can cause instabilities. See for example [2]. To achieve the disturbance's rejection (asymptotically) without measuring it, a feedback solution can be considered. This approach is particularly pertinent for single or multiple time varying tonal or narrowband disturbance noise.

The common framework is the assumption that a narrow band or a tonal disturbance noise is the result of a white noise or a Dirac impulse passed through the "disturbance's model." More specifically the model for a single narrow-band or tonal disturbance is a notch filter with poles on the unit circle and zeros inside the unit circle (for details see [3]).

In managing the vibration attenuation by feedback, the shape of the modulus of the "output sensitivity function" (the transfer function between the disturbance and the residual acceleration/force) is fundamental both from performance and robustness considerations. Three basic concepts are to be considered: the Bode Integral, the Modulus margin and the Internal Model Principle (IMP). The problem of robust control design in the context of active noise control has been considered in [4] and the shaping of the output sensitivity function has been achieved using the convex optimization procedure introduced in [5]. See also [6], [7] for Hinf and LMI approaches.

In this paper, one considers multiple unknown and time varying tonal disturbances located within two distinct relatively small frequency ranges. To be specific, two cases will be considered: (i) the case of two time varying tonal disturbances located in two distinct frequency regions and (ii) the case of four simultaneous tonal disturbances, two located in one limited frequency range and the other two in another frequency range. In this context, a very important problem is to be able to counteract the very low frequency oscillations which are generated when the two frequencies are very close (interference). Since these disturbances are located within two relatively small frequency ranges, it is possible to consider a robust linear control design which will shape the output sensitivity function in such a way that a sufficient attenuation is introduced in these two frequency regions but avoiding significant amplification at other frequencies (both for performance and robustness reason). It will be shown in this paper that an elementary procedure for shaping appropriately the modulus of the sensitivity functions can be implemented using stop band filters as shaping tools. For a basic reference on this approach see [3].

To further improve the performance an add-on direct adaptive feedback approach using the Internal Model Principle and the Youla Kucera parametrization is considered [3]. The adaptive approach allows both to improve the performance within the given frequency ranges as well as to extend the admissible domain of frequencies variations. See also [8].

The performance of these approaches depend to a large extent on the quality of the dynamic model of the compensator system used for controller design. To obtain such reliable model, identification from data of a finite dimensional discrete time model has to be used since the physical modeling does not in general provide enough good models for design.

Experimental results on a noise silencer for noise attenuation in ducts will illustrate comparatively the performance of the robust and adaptive approach.

II. THE TEST BENCH

The detailed scheme of the noise silencer test bench used for the experiments is given in Fig. 1. Its actual photo is shown in Fig. 2. The speaker used as the source of disturbances is labeled as 1, the control speaker is 2 and finally, at pipe's open end, the microphone that measures the system's output (residual noise) is denoted as 3. The transfer function between the disturbance's speaker and the microphone (1→3) is denominated *Primary Path*, while the transfer function between the control speaker and the microphone (2→3) is denominated *Secondary Path*. Both speakers are connected to a PC Target computer with Simulink Real Time® environment through a pair of high definition power amplifiers and a data acquisition card. In Fig. 1, $y(t)$ is the system's output (residual noise measurement) and $u(t)$ is the control signal. Both primary and secondary paths have a double differentiator behaviour, since as input we have the voice coil displacement, and as output the air acoustic pressure. A second computer is used for development, design and operation with Matlab®.
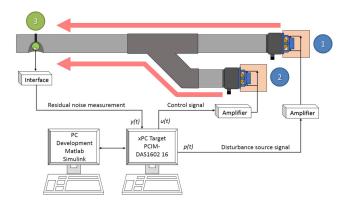

Fig. 1. Active noise control test bench diagram.
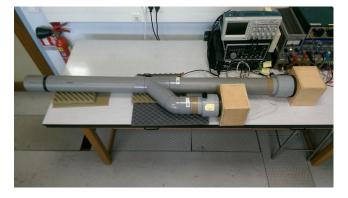
Fig. 2. Active noise control test bench (Photo).

PVC pipes of 0.10 m diameter are used in this test bench, with couplings of 135° for the control speaker. Distances between disturbance loudspeaker and microphone are 1.65 m, and to control input 0.80 m. Speakers are isolated inside wood boxes filled with special foam in order to create anechoic chambers and reduce the radiation noise produced.

III. SYSTEM DESCRIPTION

The linear time invariant *(LTI)* discrete-time model of the secondary path, (the plant), used for controller design is

$$G(z^{-1}) = \frac{z^{-d}B(z^{-1})}{A(z^{-1})} = \frac{z^{-d}B'(z^{-1})D_F(z^{-1})}{A(z^{-1})}, \quad (1)$$

where $D_F(z^{-1}) = (1 - z^{-1})^2$ is a double differentiator filter and

$$A(z^{-1}) = 1 + a_1 z^{-1} + \cdots + a_{n_A} z^{-n_A}, \quad (2)$$
$$B'(z^{-1}) = b_1 z^{-1} + \cdots + b_{n_{B'}} z^{-n_{B'}}, \quad (3)$$

with d as the plant pure time delay in number of sampling periods[1]. The system's order (without the double differentiator) is:

$$n = max(n_A, n_{B'} + d) \quad (4)$$
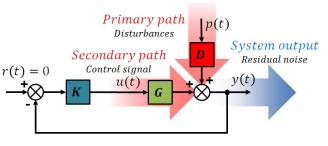
Fig. 3. Feedback regulation scheme.

Figure 3 shows the closed loop feedback regulation scheme[2], where the controller K is described by:

$$K(z^{-1}) = \frac{R}{S} = \frac{r_0 + r_1 z^{-1} + \cdots + r_{n_R} z^{-n_R}}{1 + s_1 z^{-1} + \cdots + s_{n_S} z^{-n_S}}. \quad (5)$$

The plant's output $y(t)$ and the input $u(t)$ may be written as (see Fig. 3):

$$y(t) = \frac{q^{-d}B(q^{-1})}{A(q^{-1})} \cdot u(t) + p(t), \quad (6)$$

$$S(q^{-1}) \cdot u(t) = -R(q^{-1}) \cdot y(t). \quad (7)$$

In (6), $p(t)$ is the disturbances' effect on the measured output[3] and $R(z^{-1})$, $S(z^{-1})$ are polynomials in z^{-1} having the following expressions:

$$R = H_R \cdot R' = H_R \cdot (r'_0 + r'_1 z^{-1} + \ldots + r'_{n_{R'}} z^{-n_{R'}}), \quad (8)$$

$$S = H_S \cdot S' = H_S \cdot (1 + s'_1 z^{-1} + \ldots + s'_{n_{S'}} z^{-n_{S'}}), \quad (9)$$

---

[1]The complex variable z^{-1} is used to characterize the system's behavior in the frequency domain and the delay operator q^{-1} for the time domain analysis.

[2]The measurement noise is not represented

[3]The disturbance passes through the *primary path*, and $p(t)$ is its output.

where $H_S(z^{-1})$ and $H_R(z^{-1})$ represent prespecified parts of the controller (used for example to incorporate the internal model of a disturbance, or to open the loop at some frequencies) and $S'(z^{-1})$ and $R'(z^{-1})$ are solutions of the Bezout equation:

$$P = (A \cdot H_S) \cdot S' + \left(z^{-d}B \cdot H_R\right) \cdot R'. \qquad (10)$$

In (10) $P(z^{-1})$ represents the characteristic polynomial, which specifies the desired closed loop poles of the system.

The transfer functions between the disturbance $p(t)$ and the system's output $y(t)$ and the control input $u(t)$, denoted respectively *output sensitivity* and *input sensitivity functions*, are given by

$$S_{yp}(z^{-1}) = \frac{A(z^{-1})S(z^{-1})}{P(z^{-1})} \qquad (11)$$

and

$$S_{up}(z^{-1}) = -\frac{A(z^{-1})R(z^{-1})}{P(z^{-1})}, \qquad (12)$$

IV. SYSTEM IDENTIFICATION

System identification from experimental data (see [3], [9]) will be used for obtaining the dynamic model of the compensator system used for controller design .

For design and application reasons (the objective is to reject tonal disturbances up to 400 Hz), the sampling frequency was selected as $f_s = 2500\,\text{Hz}$ ($T_s = 0.0004\,\text{s}$) i.e. approximatively 6 times the maximum frequency to attenuated (see [3]).

A Pseudo Random Binary Sequence (PRBS) has been used as excitation signal. Its characteristics are: magnitude = $0.15\,\text{V}$, register length = 17, frequency divider of 1, sequence length of $2^{17} - 1 = 131,071$ samples, guaranteeing a uniform power spectrum from about $70\,\text{Hz}$ to $1250\,\text{Hz}$. Since the transfer functions has a double differentiator behaviour (input: speaker's coil position, output: acoustic pressure), this is considered as a system's known part and the objective will be to identify the unknown part only. To do this, the input sequence will be filtered by a double discrete-time differentiator $D_F = (1 - q^{-1})^2$ such that $u'(t) = D_F \cdot u(t)$. The double differentiator will be concatenated with the identified model of the unknown part in the final model used for controller design.

The criterion used for order estimation has the form:

$$J_{IV}(\hat{n}, N) = V_{IV}(\hat{n}, N) + 2\hat{n}\frac{\log N}{N}, \qquad (13)$$

where $\hat{n}$ is the estimated order of the system and N is the number of data and the optimal estimated order is the one which minimize the criterion J_{IV}. The first term of the criterion $V_{IV}(\hat{n}, N)$ is a prediction error criterion to which a term penalizing the model's complexity is added. The effective order estimation was done using the algorithms given in [3], [10] which uses *instrumental variables* for obtaining an unbiased value for the error criterion V_{IV} since one can not ignore the measurement noise. Once an estimated order $\hat{n}$ is selected, one can apply a similar procedure to estimate $\hat{n}_A$, $\hat{n} - \hat{d}$, and $\hat{n}_{B'} + \hat{d}$, from which $\hat{n}_A$, $\hat{n}_{B'}$ and $\hat{d}$ are obtained.
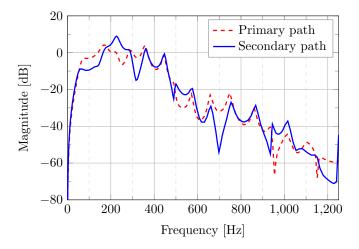
Fig. 4. Frequency characteristics of the identified primary and secondary paths models.

A model with the orders n=40, nA=38, nB'=30 and d=8 has been chosen.

Comparison of several models obtained with various parameter estimation algorithms in terms of statistical validation led to the conclusion that an ARMAX model representation is the most appropriate for this system. Among the various methods which can be used for this structure[4], *XOLOE* algorithm gives the best results for a given order model, in terms of whiteness test validation (see [3]).

Therefore the *XOLOE* model with $n = 40$ has been chosen. It has 18 oscillatory modes with damping comprised between 0.0097 and 0.3129; also 13 pairs of oscillatory zeros with damping comprised between -0.0159 and 0.5438. Fig. 4 gives the frequency characteristics of the identified complete models for the primary and secondary paths[5].

V. ROBUST CONTROL DESIGN

Control specifications

The controller will be designed to attenuate in regions of $\pm 5\,\text{Hz}$ around the two nominal frequencies $170\,\text{Hz}$ and $285\,\text{Hz}$. The attenuation must be al least of $-17\,\text{dB}$ and any undesired amplification should be less that $7\,\text{dB}$. Also since our model may be not fully representative of the system's behaviour at high frequencies, magnitudes at the input sensitivity function should be below $-20\,\text{dB}$ at frequencies over $600\,\text{Hz}$ (improving robustness versus additive plant model uncertainties in high frequencies).

In addition the gain of the controller should be zero at 0 Hz since the plant does not have gain at zero frequency and the gain of the controller should be zero also at the Nyquist frequency $(0.5f_s)$ for robustness reasons. These control specifications will be achieved through the sensitivity functions' shaping.

---

[4]Recursive Extended Least Squares *(RELS)*, Output Error with Extended Prediction Model *(OEEPM)* or *(XOLOE)*, Recursive Maximum Likelihood *(RML)*

[5]Primary path model has been identified using the same procedure. This model is used for simulations only

Design procedure

To achieve the constraints at 0Hz and at $0.5f_s$, a fixed part (H_R) [6] will be introduced in the controller:

$$H_R(q^{-1}) = (1 - q^{-1})(1 + q^{-1}) = 1 - q^{-2}, \qquad (14)$$

Three major tools will be used for design

- Choice of the dominant poles
- Use of the band stop filters for shaping the sensitivity functions
- Choice of the auxiliary poles for further improving performance and robustness

The use of auxiliary poles will be done such that the characteristic polynomial take the form

$$P(z^{-1}) = P_D(z^{-1}) \cdot P_F(z^{-1}), \qquad (15)$$

where P_D are the dominant poles obtained from the identified dynamic model, and P_F will be the auxiliary poles determined by the controller's requirements.

It is shown in [3] that very accurate shaping of the output or the input sensitivity functions can be obtained by the use of band-stop filters (BSF). These are IIR filters obtained from the discretization of continuous-time filters of the form

$$F(s) = \frac{s^2 + 2\zeta_{num}\omega_0 s + \omega_0^2}{s^2 + 2\zeta_{den}\omega_0 s + \omega_0^2} \qquad (16)$$

using the bilinear transform $s = \frac{2}{T_s}\frac{1-z^{-1}}{1+z^{-1}}$. The use of BSFs introduces an attenuation $M = 20\log\left(\frac{\zeta_{num}}{\zeta_{den}}\right)$ at the normalized discretized frequency $\omega_d = 2 \cdot \arctan\left(\frac{\omega_0 T_s}{2}\right)$. Depending on whether the filter is designed for shaping the output or the input sensitivity function, the numerator of the discretized filter is included in the fixed part of the controller denominator H_{S_0} or numerator H_{R_0}, respectively. The filter denominator is always included in the desired closed loop characteristic polynomial. As such, the filter denominator influences the design of the controller indirectly since S_0' and R_0' are solutions of the Bezout equation (10). These filters will be used for a fine shaping of both the output and input sensitivity functions.

The steps for the design of the linear controller are:

1) include all (stable) secondary path poles in the closed loop characteristic polynomial.
2) open the loop at 0 Hz and at 1250 Hz by setting the fixed part of the controller numerator as in Eq. (14).
3) 7 BSFs on S_{yp} have been used around each of the frequencies where attenuation is desired in order to assure the desired attenuation within ± 5 Hz .
4) 11 BSF has been used on S_{up} to reduce its magnitude above 600 Hz.
5) to improve robustness 17 auxiliary real poles located at 0.17 have been added to the characteristic polynomial.

Figure 5 shows the characteristics of the output sensitivity function through the various steps of the design. The performance and robustness specifications are achieved (as well as on the input sensitivity function, not shown here).
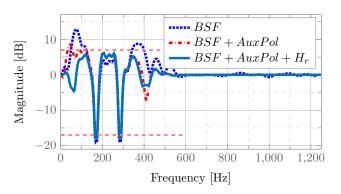
---

[6]$H_i, H_{R_i}, H_{R_i}, P_{F_i}$ will denote any given controller's fixed part.

Fig. 5. Robust controller design: Output sensitivity function.

VI. ADAPTIVE CONTROL DESIGN

The adaptive approach uses the Youla-Kucera parametrization of the controller combined with the Internal Model Principle. The basic reference for this approach used in active vibration control is [3] A key aspect of this methodology is the use of the Internal Model Principle (IMP). It is supposed that $p(t)$ is a deterministic disturbance given by

$$p(t) = \frac{N_p(q^{-1})}{D_p(q^{-1})} \cdot \delta(t), \qquad (17)$$

where $\delta(t)$ is a Dirac impulse and N_p, D_p are coprime polynomials of degrees n_{N_p} and n_{D_p}, respectively[7]. In the case of stationary narrow-band disturbances, the roots of $D_p(z^{-1})$ are on the unit circle.

Internal Model Principle[11]: The effect of the disturbance (17) upon the output

$$y(t) = \frac{A(q^{-1})S(q^{-1})}{P(q^{-1})} \cdot \frac{N_p(q^{-1})}{D_p(q^{-1})} \cdot \delta(t), \qquad (18)$$

where $D_p(z^{-1})$ is a polynomial with roots on the unit circle and $P(z^{-1})$ is an asymptotically stable polynomial, converges asymptotically towards zero *iff* the polynomial $S(z^{-1})$ in the RS controller has the form (based on eq. (9))

$$S(z^{-1}) = D_p(z^{-1})H_{S_0}(z^{-1})S'(z^{-1}). \qquad (19)$$

Thus, the pre-specified part of $S(z^{-1})$ should be chosen as $H_S(z^{-1}) = D_p(z^{-1})H_{S_0}(z^{-1})$ and the controller is computed solving

$$P = AD_pH_{S_0}S' + z^{-d}BH_{R_0}R', \qquad (20)$$

where P, D_p, A, B, H_{R_0}, H_{S_0} and d are given[8].
In the context of this paper for the Youla-Kučera parametrization, one considers a finite impulse response (FIR) filter of the form:

$$Q(z^{-1}) = q_0 + q_1 z^{-1} + \cdots + q_{n_Q} z^{-n_Q}, \qquad (21)$$

to which one associate the vector of parameters:

$$\theta = [q_0 \; q_1 \ldots q_{n_Q}]^T. \qquad (22)$$

---

[7]Throughout the paper, n_X denotes the degree of the polynomial X.
[8]Of course, it is assumed that D_p and B do not have common factors.

Under Youla-Kučera parametrization or *Q-parametrization*, the equivalent polynomials $R(z^{-1})$ and $S(z^{-1}$ of the controller $K(q^{-1})$ take the form

$$R(q^{-1}) = R_0 + A \cdot Q \cdot H_{S_0} \cdot H_{R_0} \tag{23}$$

$$S(q^{-1}) = S_0 - q^{-d} B \cdot Q \cdot H_{S_0} \cdot H_{R_0}, \tag{24}$$

with

$$R_0(z^{-1}) = r_0^0 + r_1^0 z^{-1} + \ldots + r_{n_R}^0 z^{-n_{R_0}} = R_0' \cdot H_{R_0} \tag{25}$$

$$S_0(z^{-1}) = 1 + s_1^0 z^{-1} + \ldots + s_{n_S}^0 z^{-n_{S_0}} = S_0' \cdot H_{S_0}, \tag{26}$$

where A, B and d correspond to the identified model of the secondary path, $R_0(z^{-1})$, $S_0(z^{-1})$ are the central controller's polynomials, and H_{S_0}, H_{R_0} are the controller fixed parts.

Using the output sensitivity function, the expression of the output can be written as:

$$y(t) = \frac{S_0}{P} \cdot w(t) - Q \cdot \frac{q^{-d} B H_{S_0} H_{R_0}}{P} \cdot w(t), \tag{27}$$

with

$$w(t) = A \cdot y(t) - q^{-d} B \cdot u(t) = A \cdot p(t) \tag{28}$$

as a disturbance's observer. The objective is to find a value of Q such that $y(t)$ is driven to zero.

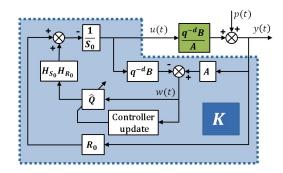A block diagram of the adaptive scheme is given in Figure 6.

Fig. 6. Adaptive Youla-Kučera parametrization scheme.

The estimation of the polynomial Q at time t is denoted:

$$\hat{Q}(t, q^{-1}) = \hat{q}_0(t) + \hat{q}_1(t) q^{-1} + \cdots + \hat{q}_{n_Q}(t) q^{-n_Q} \tag{29}$$

and is caracterized by the parameter vector:

$$\hat{\theta}(t) = [\hat{q}_0(t) \ \hat{q}_1(t) \ldots \hat{q}_{n_Q}(t)]^T, \tag{30}$$

Since this is a regulation problem $y(t)$ is expected to go to zero and as such it is an a priori adaptation error denoted $\varepsilon^0(t+1)$ for a given estimated polynomial $\hat{Q}(t, q^{-1})$:

$$\varepsilon^0(t+1) = \frac{S_0}{P} \cdot w(t+1) - \hat{Q}(t) \frac{q^{-d} B^* H_{S_0} H_{R_0}}{P} \cdot w(t), \tag{31}$$

with $B(q^{-1}) = q^{-1} \cdot B^*(q^{-1})$. In a similar way, we can define an *a posteriori* error like

$$\varepsilon(t+1) = \frac{S_0}{P} \cdot w(t+1) - \hat{Q}(t+1) \frac{q^{-d} B^* H_{S_0} H_{R_0}}{P} \cdot w(t), \tag{32}$$

which can be further expressed as

$$\varepsilon(t+1) = [Q - \hat{Q}(t+1)] \cdot \frac{q^{-d} B^* H_{S_0} H_{R_0}}{P} \cdot w(t) + \eta(t+1) \tag{33}$$

where $\eta(t)$ tends asymptotically towards zero (see [3]for details).

Denoting filtered versions of observer output $w(t)$ as

$$w_1(t) = \frac{S_0(q^{-1})}{P(q^{-1})} \cdot w(t) \tag{34}$$

$$w_2(t) = \frac{q^{-d} B^* H_{R_0} H_{S_0}}{P} \cdot w(t) \tag{35}$$

and

$$\varphi^T(t) = [w_2(t) \ w_2(t-1) \ldots w_2(t - n_Q)], \tag{36}$$

Eq. (33) can be rewritten as:

$$\varepsilon(t+1) = [\theta^T - \hat{\theta}^T(t+1)] \cdot \varphi(t) + \eta^*(t+1). \tag{37}$$

This type of equation allows immediately to develop an adaptation algorithm (see [12]):

$$\hat{\theta}(t+1) = \hat{\theta}(t) + F(t)\varphi(t)\varepsilon(t+1) \tag{38}$$

$$\varepsilon(t+1) = \frac{\varepsilon^0(t+1)}{1 + \varphi^T(t) F(T) \varphi(t)} \tag{39}$$

$$\varepsilon^0(t+1) = w_1(t+1) - \hat{\theta}^T(t) \varphi(t). \tag{40}$$

$$F(t+1) = \frac{1}{\lambda_1(t)} \left[F(t) - \frac{F(t)\varphi(t)\varphi^T(t)F(t)}{\frac{\lambda_1(t)}{\lambda_2(t)} + \varphi^T(t)F(t)\varphi(t)} \right] \tag{41}$$

where λ_1, λ_2 allows to obtain different profiles for the evolution of the adaptation gain $F(t)$. Finally the control to be applied is given by

$$S_0 \cdot u(t+1) = -R_0 \cdot y(t+1) - H_{R_0} H_{S_0} \hat{Q}(t+1) \cdot w(t+1). \tag{42}$$

For the stability analysis of this algorithm see[12].

VII. EXPERIMENTAL RESULTS

The robust and adaptive design have been comparatively evaluated on the duct silencer described in Section II. For all the adaptive experiments $n_Q = 3$ (4 parameters)

A. Interference test

Figure 7 shows the performance of the robust controller in the presence of two pairs of sinusoidal noise signals acting simultaneously, and located first at170 Hz and 170.5 Hz, 285 Hz from 10s to 20s and then with modified central frequencies located at 285.5 Hz, 180 Hz and 180.5 Hz, and respectively at 295 Hz and 295.5 Hz. One can see that the controller gives good performance from 10s to 20s (global attenuation of 36.56 dB) but the performance is degraded after 20s and this is understandable since one operates outside the the region considered for the design. Figure 8 shows the performance of the adaptive controller for the same configuration. The performance are very good (global attenuation of 71.45 dB).
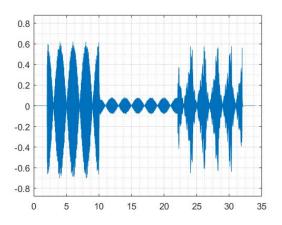
Fig. 7. Acoustic interference attenuation using a robust controller. Noise frequencies:170,170.5,285,285.5 Hz then 180,180.5,295, 295.5 Hz.
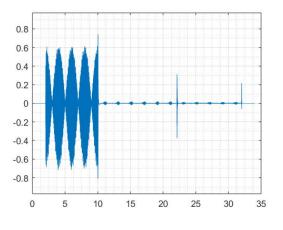

Fig. 8. Acoustic interference attenuation using an adaptive controller. Noise frequencies:170,170.5,285,285.5 Hz then 180,180.5,295, 295.5 Hz.

B. Step Changes in Frequency

In this test, two simultaneous signals of constant frequency act as disturbances. After a given amount of time a step change in the frequencies of both signals is done. Both frequencies are decreased or increased with a constant value and remain at those new constant frequencies for 4s . Figures 9 and 10 show the performance of the robust and adaptive controller. The red curves gives the magnitude of the residual noise in open loop and the blue curves give the magnitude of the residual noise in closed loop. The frequencies of the disturbances are indicated in the plots. One can clearly see that the adaptive controller has better performance than the robust controller even within the frequency domain of variations used for robust controller design.

VIII. Conclusion

The paper has shown that robust and adaptive approaches can be considered for active attenuation of multiple narrow band noise disturbances by feedback. However the adaptive approach offer better performance.
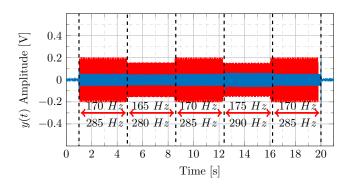

Fig. 9. Step changes in frequencies using the robust controller.
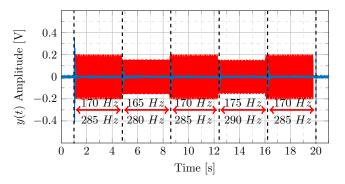
Fig. 10. Step changes in frequencies using the adaptive controller.

References

[1] B. Widrow and S. Stearns, *Adaptive Signal Processing*. Englewood Cliffs, New Jersey: Prentice-Hall, 1985.

[2] J. Zeng and R. de Callafon, "Recursive filter estimation for feedforward noise cancellation with acoustic coupling," *Journal of Sound and Vibration*, vol. 291, no. 3-5, pp. 1061 − 1079, 2006.

[3] I. D. Landau, T.-B. Airimitoaie, A. Castellanos-Silva, and A. Constantinescu, *Adaptive and Robust Active Vibration Control*. London: Springer, 2016.

[4] J. C. Carmona and V. M. Alvarado, "Active noise control of a duct using robust control theory," *IEEE-CST*, vol. 8, no. 6, pp. 930–938, November 2000.

[5] J. Langer and I. D. Landau, "Combined pole placement/sensitivity function shaping method using convex optimization criteria," *Automatica*, vol. 35, no. 6, pp. 1111–1120, 1999.

[6] C. A. S. L. Stefan Liebich, Daniel Rüschen, "Active noise cancellation in headphones by digital robust feedback control," in *24th European Signal Processing Conference (EUSIPCO)*, 2016, pp. 1843–1847.

[7] A. S. S. Tansel Yucelen and F. Pourboghrat, "Active noise control in a duct using output feedback robust control techniques," in *American Control Conference*, 2010, pp. 3506–3511.

[8] R. Marino, G. Santosuosso, and P. Tomei, "Robust adaptive compensation of biased sinusoidal disturbances with unknown frequency," *Automatica*, vol. 39, pp. 1755–1761, 2003.

[9] L. Ljung, *System Identification - Theory for the User*, 2nd ed. Englewood Cliffs: Prentice Hall, 1999.

[10] H. N. Duong and I. D. Landau, "An IV Based Criterion for Model Order Selection," *Automatica*, vol. 32, no. 6, pp. 909–914, 1996.

[11] B. Francis and W. Wonham, "The internal model principle of control theory," *Automatica*, vol. 12, no. 5, pp. 457 − 465, 1976.

[12] I. D. Landau, R. Lozano, M. M'Saad, and A. Karimi, *Adaptive control*, 2nd ed. London: Springer, 2011.

WHY ONE SHOULD USE YOULA-KUČERA PARAMETRIZATION IN ADAPTIVE FEEDFORWARD NOISE ATTENUATION?

Why one should use Youla-Kucera parametrization in adaptive feeforward noise attenuation?

Ioan Doré Landau, Tudor-Bogdan Airimitoaie, Raul Melendez, and Luc Dugard

Abstract— A crucial problem in adaptive feedforward noise attenuation is the presence of an "internal" positive acoustical feedback between the compensation system and the reference source which is a cause of instabilities. Adaptive algorithms for feedforward active compensation having an infinite impulse response (IIR) or a finite impulse response (FIR) structure have been developed from a stability point of view. Nevertheless, in order to separate the problem of stabilizing the internal positive feedback loop from the minimization of the residual noise, the Youla–Kučera (YK) parametrization of the feedforward compensator has been proposed and algorithms have been developed from a stability point of view. Since the stability of the internal loop is a key issue in practice, the present paper using a unified presentation of the algorithms available discusses the stability conditions associated with the various algorithms and their properties. It is shown that the FIRYK configuration offers, from the stability point of view, the best option. Experimental results obtained on a relevant test-bench will illustrate the theoretical analysis.

I. INTRODUCTION

Adaptive feedforward broad-band noise compensation is currently used when a correlated measurement with the disturbance (an image of the disturbance) is available. Most of the active feedforward noise control systems feature an internal "positive" acoustical feedback between the compensation system and the reference source (a correlated measurement with the disturbance). This internal positive feedback loop often leads to the instability of the system if it is not taken into account in the design stage ([1]).
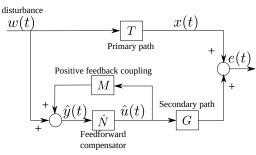

Fig. 1. Adaptive active noise feedforward compensation.

Figure 1 gives the basic block diagram of the adaptive feedforward compensation in the presence of the internal

positive coupling between the output of the compensator and the measurement of the image of the incoming noise. The incoming noise propagates through the so called *primary path* and its effect is compensated through a secondary noise source (*secondary path*) driven by a feedforward compensator. The input to the feedforward compensator is the sum of the image of the incoming noise and of the internal acoustical positive feedback.

Single and multiple narrow-band disturbances can be efficiently attenuated by adaptive feedback configurations ([2], [3]). Nevertheless, the efficient use of the feedback approach for attenuation of broad-band noise is limited by the Bode integral. Therefore adaptive feedforward noise compensation is particularly dedicated to the attenuation of broad-band noise with unknown and time-varying characteristics.

Stability analysis of the adaptive feedforward compensation schemes taking into account the internal positive loop is an important aspect (see [4], [5], [6], [7], [8]). The stability analysis makes the assumption that there exists a compensator N such that the internal positive loop (formed by M and N in feedback) is stable and such that the perfect matching of the primary path is achieved.[1]

Starting with [6], a new approach emerged in the area of active noise and vibration control (ANVC), namely the design of the adaptation algorithms starting from a stability point of view and taking into account the internal positive feedback from the beginning. In the field of active vibration control (AVC), the paper [7] provides a full synthesis procedure for asymptotically stable adaptation algorithms using infinite impulse response (IIR) feedforard compensators in the presence of the internal feedback. These algorithms can be used also in active noise control (ANC) as it will be shown in this paper.

Since assuring the stability of the internal positive feedback loop is essential in applications, in [9] it is proposed to separate the stabilization of the internal positive feedback loop from the minimization of the residual noise by using a Youla–Kučera (YK) parametrization of the feedforward compensator. A tuning procedure based on system identification has been proposed and tested on a silencer. This idea has been used in [10] for developing direct adaptive feedforward compensation schemes using the YK parametrization of finite impulse response (FIR) form or IIR form [11] for the feedforward compensator. While these algorithms have been developed and tested in the context of AVC [8], they can be

used also in the field of ANC. Even if the various algorithms proposed for IIR or FIR compensators assure the stability of the full system under some strictly positive real (SPR) conditions, they do not guarantee that the poles of the internal positive loop are not too close to the unit circle. One may ask if such a situation may occur. Considering the block diagram shown in Fig. 1, one can view this system as a Model Reference Adaptive System. In order to achieve perfect matching, the internal closed loop which is the effective feedforward compensator will try to cancel all the zeros of the secondary path which are not zeros of the primary path. This will imply that the poles of the internal closed loop will tend towards the zeros of the secondary path. Unfortunately, as it will be shown in the experimental section, the model of the secondary path in the context of noise attenuation in ducts (typical application field) have very low damped complex zeros. Therefore, as it will be shown, despite very good attenuation properties, the FIR (IIR) compensators will lead to the presence of closed-loop poles extremely close to the unit circle. So the problem of securing a disk of radius less than 1 is very important from a practical point of view, even if one has to accept slightly less good performances. YK parametrized adaptive feedforward compensators can offer such a solution. An FIRYK configuration will allow to define from the beginning the desired closed-loop poles (design of the central controller) and these poles will remain unchanged independently of the values of the parameters of the FIRYK filter.

The FIRYK configuration offers also another advantage: by an appropriate design of the central controller one can remove the SPR condition for stability (or more exactly, it will only depend on the precision of the estimation of the reverse path M, and current techniques of system identification extract excellent models from data).

There is also another advantage of using an FIRYK configuration. A necessary condition for perfect matching is that the transportation delay[2] of the secondary path should be smaller or equal than the transportation delay of the primary path. For most applications till recently, the design of the physical system has been done such that this constraint be satisfied. Nevertheless, there are potential application fields where, because of thermal constraints, this condition can not be fulfilled. It will be shown that despite the violation of the delay constraints, the FIRYK can still operate with good performance while all the other configurations except the FIR are unstable (but the FIR gives poor performance).

The paper is organized as follows: in Section II, the various structures and algorithms will be presented under a unified form called "Generalized Youla-Kučera". Section III will examine comparatively various particular configurations and algorithms proposed in terms of stability conditions. Results obtained on an experimental test-bench (a core of a duct silencer) will illustrate some important properties of the algorithms in Section IV.

II. BASIC EQUATIONS AND NOTATIONS

The block diagram associated with an adaptive feeforward compensator using a generalized Youla-Kučera structure for adaptive feedforward compensators is shown in Fig. 2.
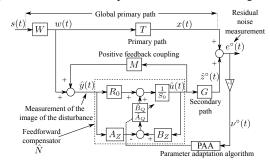
Fig. 2. Adaptive feedforward disturbance compensation using the generalized Youla–Kučera parametrization.

The primary (T), secondary (G), and reverse (positive coupling) (M) paths represented in Fig. 2 are characterized by the asymptotically stable transfer operators:

$$X(q^{-1}) = \frac{B_X(q^{-1})}{A_X(q^{-1})} = \frac{b_1^X q^{-1} + ... + b_{n_{B_X}}^X q^{-n_{B_X}}}{1 + a_1^X q^{-1} + ... + a_{n_{A_X}}^X q^{-n_{A_X}}}, \tag{1}$$

with $B_X = q^{-1}B_X^*$ for any $X \in \{D, G, M\}$. $\hat{G} = \frac{\hat{B}_G}{\hat{A}_G}$, $\hat{M} = \frac{\hat{B}_M}{\hat{A}_M}$, and $\hat{D} = \frac{\hat{B}_D}{\hat{A}_D}$ denote the identified (estimated) models of G, M, and D.

Polynomials A_Z and B_Z are defined as:

$$A_Z = a_0^Z + a_1^Z q^{-1} + ... \tag{2}$$

$$B_Z = b_1^Z q^{-1} + ... \tag{3}$$

The optimal feedforward compensator which will minimize the residual noise can be written as:

$$N = \frac{R}{S} = \frac{A_Q R_0 - B_Q A_Z}{A_Q S_0 - B_Q B_Z} \tag{4}$$

where the optimal filter $Q(q^{-1})$ has an IIR structure

$$Q = \frac{B_Q}{A_Q} = \frac{b_0^Q + b_1^Q q^{-1} + \ldots + b_{n_{B_Q}}^Q q^{-n_{B_Q}}}{1 + a_1^Q q^{-1} + \ldots + a_{n_{A_Q}}^Q q^{-n_{A_Q}}} \tag{5}$$

and $R_0(q^{-1})$, $S_0(q^{-1}) = 1 + q^{-1}S_0^*(q^{-1})$ are the polynomials of the central (stabilizing) filter and $A_Z(q^{-1})$, $B_Z(q^{-1})$ are given in (2) and (3)[3].

The estimated QIIR filter is denoted by $\hat{Q}(q^{-1})$ or $\hat{Q}(\hat{\theta}, q^{-1})$ when it is a linear filter with constant coefficients or $\hat{Q}(t, q^{-1})$ during estimation (adaptation). The vector of parameters of the optimal QIIR filter assuring perfect matching will be denoted by

$$\theta^T = [b_0^Q, \ldots, b_{n_{B_Q}}^Q, a_1^Q, \ldots, a_{n_{A_Q}}^Q] = [\theta_{B_Q}^T, \theta_{A_Q}^T]. \tag{6}$$

The vector of parameters for the estimated $\hat{Q}$IIR filter

$$\hat{Q}(q^{-1}) = \frac{\hat{B}_Q(q^{-1})}{\hat{A}_Q(q^{-1})} = \frac{\hat{b}_0^Q + \hat{b}_1^Q q^{-1} + \ldots + \hat{b}_{n_{B_Q}}^Q q^{-n_{B_Q}}}{1 + \hat{a}_1^Q q^{-1} + \ldots + \hat{a}_{n_{A_Q}}^Q q^{-n_{A_Q}}} \tag{7}$$

is denoted by

$$\hat{\theta}^T = [\hat{b}_0^Q, \ldots, \hat{b}_{n_{B_Q}}^Q, \hat{a}_1^Q, \ldots, \hat{a}_{n_{A_Q}}^Q] = [\hat{\theta}_{B_Q}^T, \hat{\theta}_{A_Q}^T]. \tag{8}$$

The input of the feedforward filter (called also reference) is denoted by $\hat{y}(t)$ and it corresponds to the measurement provided by the primary microphone. In the absence of the compensation loop (open-loop operation) $\hat{y}(t) = w(t)$. The output of the feedforward compensator (which is the control signal applied to the secondary path) is denoted by $\hat{u}(t+1) = \hat{u}(t + 1/\hat{\theta}(t + 1))$ (*a posteriori* output).

The *a priori* output of the estimated feedforward compensator using an IIRYK parametrization for the case of time-varying parameter estimates is given by (using (4))

$$\begin{aligned}
\hat{u}^\circ(t + 1) &= \hat{u}(t + 1|\hat{\theta}(t)) \\
&= -\hat{S}^*(t, q^{-1})\hat{u}(t) + \hat{R}(t, q^{-1})\hat{y}(t + 1) \\
&= -S_0^* \hat{u}(t) + R_0 \hat{y}(t + 1) - \hat{A}_Q(t, q^{-1})^* \beta(t) \\
&\quad + \hat{B}_Q(t, q^{-1})\alpha(t + 1),
\end{aligned} \tag{9}$$

and

$$\begin{aligned}
\hat{u}(t + 1) &= -S_0^* \hat{u}(t) + R_0 \hat{y}(t + 1) - \hat{A}_Q(t + 1, q^{-1})^* \beta(t) \\
&\quad + \hat{B}_Q(t + 1, q^{-1})\alpha(t + 1),
\end{aligned} \tag{10}$$

where $\beta(t) = S_0 \hat{u}(t) - R_0 \hat{y}(t)$ (see also Fig. 2).

The objective is to develop stable recursive algorithms for adaptation of the parameters of the Q filter such that the measured residual error (noise in ANC) be minimized in the sense of a certain criterion. This has to be done for broadband disturbances $w(t)$ (or $s(t)$) with unknown and variable spectral characteristics and an unknown primary path model.

The algorithms for adaptive feedforward compensation have been developed under the following basic hypotheses

1) (Perfect matching condition) There exists a value of the Q parameters such that

$$\frac{G \cdot A_M(R_0 A_Q - A_Z B_Q)}{A_Q(A_M S_0 - B_M R_0) - B_Q(B_Z A_M - B_M A_Z)} = -T.$$

2) The characteristic polynomial of the internal closed-loop for $A_Q = 1$ and $B_Q = 0$

$$P_0(z^{-1}) = A_M(z^{-1})S_0(z^{-1}) - B_M(z^{-1})R_0(z^{-1})$$

is a Hurwitz polynomial.

3) (Stability of the internal loop) The characteristic polynomial of the internal closed-loop for the values of A_Q and B_Q assuring perfect matching is a Hurwitz polynomial:

$$P = A_Q(A_M S_0 - B_M R_0) - B_Q(B_Z A_M - B_M A_Z)$$

A first step in the development of the algorithms is to establish for a fixed estimated compensator a relation between the error on the Q-parameters (with respect to the optimal

values) and the adaptation error ν. This is summarized in the following lemma.

Lemma 1: Under the hypotheses 1–3 for the system described by eqs. (1)–(10) using an estimated generalized Youla-Kučera parameterized feedforward compensator with constant parameters, one has:

$$\nu(t + 1/\hat{\theta}) = \frac{A_M G}{A_Q P_0 - B_Q(B_Z A_M - B_M A_Z)}[\theta - \hat{\theta}]^T \phi(t), \tag{11}$$

with $\phi(t)$ given by:

$$\begin{aligned}
\phi^T(t) = [&\alpha(t + 1), \alpha(t), \ldots, \alpha(t - n_{B_Q} + 1), \\
&- \beta(t), -\beta(t - 1), \ldots, -\beta(t - n_{A_Q})].
\end{aligned} \tag{12}$$

where:

$$\begin{aligned}
\alpha(t + 1) &= B_M \hat{u}(t + 1) - A_M \hat{y}(t + 1) = \\
&= B_M^* \hat{u}(t) - A_M \hat{y}(t + 1) \tag{13a} \\
\beta(t) &= S_0 \hat{u}(t) - R_0 \hat{y}(t). \tag{13b}
\end{aligned}$$

The proof of this lemma follows the proof given in Appendix A of [11] with the appropriate change of notations and is omitted.

For assuring the stability of the system, one needs to filter the observation vector $\phi(t)$. Filtering the vector $\phi(t)$ through an asymptotically stable filter $L(q^{-1}) = \frac{B_L}{A_L}$, (11) for $\hat{\theta} = constant$ becomes

$$\begin{aligned}
\nu(t + 1/\hat{\theta}) &= \frac{A_M G}{(A_Q P_0 - B_Q(B_Z A_M - B_M A_Z))L} \cdot \\
&\quad \cdot [\theta - \hat{\theta}]^T \phi_f(t) \tag{14}
\end{aligned}$$

with

$$\begin{aligned}
\phi_f(t) = L(q^{-1})\phi(t) = [&\alpha_f(t + 1), \ldots, \alpha_f(t - n_{B_Q} + 1), \\
&\beta_f(t), \beta_f(t - 1), \ldots, \beta_f(t - n_{A_Q})] \tag{15}
\end{aligned}$$

where

$$\alpha_f(t + 1) = L(q^{-1})\alpha(t + 1), \; \beta_f(t) = L(q^{-1})\beta(t). \tag{16}$$

When the parameters of $\hat{Q}$ evolve over time and neglecting the non-commutativity of the time-varying operators, eq. (14) transforms into[4]

$$\begin{aligned}
\nu(t + 1/\hat{\theta}(t + 1)) &= \frac{A_M G}{[A_Q P_0 - B_Q(B_Z A_M - B_M A_Z)]L} \cdot \\
&\quad \cdot [\theta - \hat{\theta}(t + 1)]^T \phi_f(t). \tag{17}
\end{aligned}$$

Equation (17) has the standard form for an *a posteriori* adaptation error ([12]), which immediately suggests to use

[4]Nevertheless, exact algorithms can be developed taking into account the non-commutativity of the time varying operators - see [12].

the following parameter adaptation algorithm (PAA):

$$\hat{\theta}(t+1) = \hat{\theta}(t) + F(t)\psi(t)\nu(t+1) \; ; \tag{18a}$$

$$\nu(t+1) = \frac{\nu^0(t+1)}{1 + \psi^T(t)F(t)\psi(t)} \; ; \tag{18b}$$

$$F(t+1) = \frac{1}{\lambda_1(t)}\left[F(t) - \frac{F(t)\psi(t)\psi^T(t)F(t)}{\frac{\lambda_1(t)}{\lambda_2(t)} + \psi^T(t)F(t)\psi(t)}\right] \tag{18c}$$

$$1 \geq \lambda_1(t) > 0; 0 \leq \lambda_2(t) < 2; F(0) > 0 \tag{18d}$$

$$\psi(t) = \phi_f(t), \tag{18e}$$

where $\lambda_1(t)$ and $\lambda_2(t)$ allow to obtain various profiles for the matrix adaptation gain $F(t)$ (see [12]). By taking $\lambda_2(t) \equiv 0$ and $\lambda_1(t) \equiv 1$, one gets a constant adaptation gain matrix. Choosing $F = \gamma I$, $\gamma > 0$ one gets a scalar adaptation gain. The equation (18a) for updating the parameter vector becomes:

$$\hat{\theta}(t+1) = \hat{\theta}(t) + \gamma\Phi(t)\frac{\nu^\circ(t+1)}{1 + \gamma\Phi^T(t)\Phi(t)}. \tag{19}$$

III. SPECIFIC CASES

1) For $A_Z = -1$, $B_Z = 0$, $R_0 = 0$, $S_0 = 1$: we are in the context of IIR (FIR) adaptive feedforward compensators discusssed in [7]. In this context there are two basic algorithms:
FUPLR (Filtered-U pseudo linear regression): $L = \hat{G}$ and
FUSBA (Filtered-U stability based algorithm): $L = \frac{\hat{A}_M}{\hat{P}}\hat{G}$, with $\hat{P} = \hat{A}_M\hat{S} - \hat{B}_M\hat{R}$.

The stability condition for FUPLR is: $\frac{A_M G}{P\hat{G}} - \frac{\lambda}{2} = SPR$ with $\lambda = \max\lambda_2(t)$ and for the FUSBA the stability condition is: $\frac{A_M\hat{P}G}{\hat{A}_M P\hat{G}} - \frac{\lambda}{2} = SPR$ $(\lambda = \max\lambda_2(t))$. For the FUSBA algorithm, the SPR condition is milder. Note that the FUSBA algorithm requires initialization over a certain horizon using FUPLR. This implies that the SPR condition for FUPLR is fulfilled at least in the average [13], [7]. Note that the stability conditions for FUPLR is "global" while for the FUSBA is "local" (one implicitly assumes that the FUPLR algorithm brings the parameters in the vicinity of the equilibrium point).

2) For $A_Z = A_M$, $B_Z = B_M$: we are in the context of the IIRYK feedforward compensator which has been discussed in [11]. In this context one has two basic algorithms:
FUPLR: $L = \hat{G}$ and
FUSBA: $L = \frac{\hat{A}_M}{\hat{P}}\hat{G}$, where $\hat{P} = \hat{A}_Q(A_M S_0 - B_M R_0)$.
The stability condition associated to the FUPLR is that $\frac{A_M G}{P\hat{G}} - \frac{\lambda}{2} = SPR$ $(\lambda = \max\lambda_2(t))$ and the stability condition associated with th FUSBA is that: $\frac{A_M\hat{P}G}{\hat{A}_M P\hat{G}} - \frac{\lambda}{2} = SPR$ $(\lambda = \max\lambda_2(t))$.

In this case also the FUSBA algorithm requires initialization using the FUPLR algorithm.[5] This implies that the SPR condition for the FUPLR is satisfied at least on the average. The FUPLR stability condition is "global" while the FUSBA condition is "local".

----

[5]Or with an approximated FUSBA algorithm (using the filter $L = \frac{\hat{A}_M}{\hat{P}_0}\hat{G}$).

3) For $A_Z = A_M$, $B_Z = B_M$, $A_Q = 1$: we are in the context of the FIRYK feedforward compensator (see [11]). One can consider two adaptation algorithms:
FUPLR: $L = \hat{G}$ and
FUSBA: $L = \frac{\hat{A}_M}{\hat{P}_0}\hat{G}$, where $\hat{P}_0 = (\hat{A}_M S_0 - \hat{B}_M R_0)$.
The stability condition associated with the FUPLR is that: $\frac{A_M G}{P_0\hat{G}} - \frac{\lambda}{2} = SPR$ $(\lambda = \max\lambda_2(t))$. The stability condition associated with the FUSBA is that: $\frac{A_M\hat{P}_0\hat{G}}{\hat{A}_M P_0\hat{G}} - \frac{\lambda}{2} = SPR$ $(\lambda = \max\lambda_2(t))$. In this case, for both FUPLR and FUSBA the stability conditions are "global". The main difference with respect to the previous cases is twofold:

- The FUSBA algorithm can be implemented from the beginning since P_0 is known and constant and the stability condition is global.
- The design of the central controller can be used for fulfilling the SPR conditions.[6]

If the central controller is designed such that $\hat{P}_0 = \hat{A}_M$, then FUPLR and FUSBA are almost the same and the fulfillment of the SPR condition will depend only on the quality of the estimation of the transfer M. This is a key point because not only the stability of the internal loop will be assured for any finite value of the parameters of the FIR Youla-Kučera filter but in addition the system will be operated under a global stability condition easy to fulfill and allowing to use high values of the adaptation gain leading to fast adaptation.

A consequence of this property is that the YKFIR configuration can be safely used even if the perfect matching condition is not fulfilled. Such a situation occurs in practice when the pure delay (propagation delay) on the secondary path is larger than the pure delay of the primary path. This will be illustrated in the experimental results section.

For all the configurations, scalar adaptation gains can also be used. The same filter L is used and the algorithms corresponding to FUPLR and FUSBA are termed: NFULMS[7] and SFUSBA respectively. The stability conditions are the same as for the matrix case except that in this case $\lambda = 0$.

Youla–Kučera Parametrization—Some Remarks

Two major observations when using the Youla–Kučera parametrization have to be made:

- If an FIR Q filter is used, the poles of the internal closed-loop will be defined by the central compensator R_0, S_0 and they will remain unchanged independently of the values of the parameters of the Q filter. The stability condition for the FUSBA algorithm is global.
- If an IIR Q filter is used, the poles of the internal closed-loop will be defined by the central compensator but additional poles corresponding to the denominator of the Q filter will be added. The stability condition for the FUSBA algorithm is local and an initialization with the FUPLR algorithm is necessary.

----

[6]The main objective of the central controller is to stabilize the internal loop.

[7]For the case of FIR and IIR structures the FXLMS and respectively the FULMS can be interpreted as approximations of the NFULMS algorithm.

IV. Experimental Results

The core of a noise silencer is used as a test bench. Two configurations have been considered: Configuration A shown in Fig. 3 (the pure delay of the secondary path is smaller than the pure delay of the primary path) and configuration B shown in Fig. 4 (the pure delay of the secondary path is larger than the pure delay of the primary path).
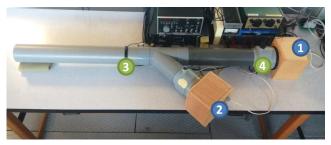

Fig. 3.   Duct active noise control test-bench. Configuration A (Photo).

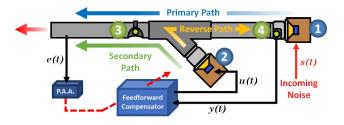Fig. 4.   Duct active noise control test-bench. Configuration B (Photo).

Fig. 5.   Duct active noise control test-bench diagram.

Figure 5 gives the block diagram of the system. The speaker used as the source of disturbances is labeled as 1, while the control speaker is marked as 2. At the pipe's open end, the microphone that measures the system's output (residual noise $e(t)$) is denoted as 3. Inside the pipe, close to the source of disturbances, the second microphone, labeled as 4, measures the image of the incoming noise, denoted as $\hat{y}(t)$. The various paths are indicated on the figure. The system is connected to an xPC Target computer with Simulink Real-time® environment. The sampling frequency is $f_s = 2500$ Hz. The various paths have been identified by standard experimental identification techniques which are described in [14]. The various paths' models are characterized by the presence of multiple very low damped complex poles

and complex zeros. The orders for the various models are summarized in Table I for configurations A and B.

Config.	A	A	A	B	B	B
Model	n_B	n_A	d	n_B	n_A	d
Primary (global)	20	24	7	20	27	8
Secondary	27	26	6	20	27	9
Reverse	22	25	5	33	33	4

TABLE I
ORDERS OF THE IDENTIFIED SYSTEM PATHS. CONFIGURATION A AND B.

1) Configuration A: The objective is to illustrate first the properties of the FIRYK configuration and the importance of the design of the central controller for the fulfillment of the SPR condition for stability. In the first design, the central controller introduces some attenuation in the region of operation (70 to 270 Hz). In the second design, the central controller was computed such that $P_0 = \hat{A}_M$ without introducing attenuation. Table II gives the results obtained using the two different central controllers with 60 adapted parameters. In the case $P_0 \neq \hat{A}_M$, the FUPLR algorithm

Cl. Poles	$P_0 \neq \hat{A}_M$	$P_0 = \hat{A}_M$
Adaptation algorithm	Atten. [dB]	Atten. [dB]
Matrix (FUSBA)	27.0	27.3
Matrix (FUPLR)	unstable	27.2
Scalar (SFUSBA)	26.7	27.1
Scalar (SFUPLR)	unstable	27.2

TABLE II
EXPERIMENTAL RESULTS FOR FIRYK 60/0 ADAPTIVE COMPENSATORS USING VARIOUS ADAPTATION ALGORITHMS (70-270 HZ BROAD-BAND DISTURBANCE, 180 S EXPERIMENTS).

is unstable. This can be easily understood by looking to the phase of the estimated transfer function $\frac{\hat{A}_M}{P_0}$ shown in Fig. 6 (obtained when using the FUSBA algorithm). Since the noise to be attenuated has an almost flat power spectral density (PSD) between 70 and 270 Hz, it is clear that the SPR condition is violated in a too large frequency spectrum (even using averaging arguments). By using the second design, for both FUPLR and FUSBA, the SPR condition will be the same and both algorithms will be stable and will provide identical performances as illustrated in Table II.

Figure 7 shows the PSD in open loop and in the presence of the FIRYK compensator[8]. As it can be seen, there is no significant amplification at the frequencies outside the attenuation zone. The estimation of the output sensitivity function of the internal loop for the FIRYK 60/0 using the FUSBA algorithm shows a maximum below 10 dB (modulus margin greater than 0.3). Figure 8 shows the PSD of an FIR and of an IIR adaptive compensator. Despite the fact that they assure a better attenuation in the region 70-270 Hz there is a very strong amplification outside the attenuation zone indicating the presence of a pair of very low damped complex poles (in the region around 320 Hz).

[8]The number of the parameters of the compensator is denoted by nb/na (nb for the numerator, nb for the denominator)
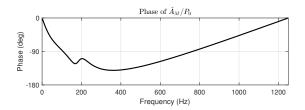
Fig. 6. Phase of $\frac{\hat{A}_M}{P}$ for the FIRYK 60/0 adaptive compensator (70-270 Hz disturbance, 600 s experiments).
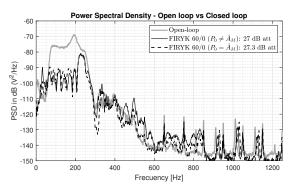

Fig. 7. PSD of the FIRYK 60/0 adaptive compensators using FUSBA matrix adaptation (70-270 Hz disturbance, 600 s experiments).
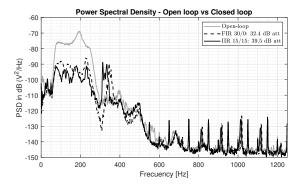

Fig. 8. PSD comparison of FIR 30/0 and IIR 15/15 standard adaptive compensators using FUSBA matrix adaptation (70-270 Hz disturbance, 600 s experiments).

Further analysis shows for the IIR configuration that the estimated output sensitivity function has a maximum of 26 dB in this region corresponding to a modulus margin of less than 0.06 (extremely close to instability).

2) Configuration B: In this configuration, all compensators are unstable except the FIR and the FIRYK. Figure 9 shows the PSD of the residual noise obtained over a test horizon of 800 s for the FIR and the FIRYK compensators. Clearly the FIRYK compensator offers much better results in terms of attenuation (20.6 dB versus 10.4 dB for a broad band noise covering the range 150-350 Hz).

V. CONCLUDING REMARK

In summary one can say that the FIRYK adaptive feedforward compensator offers a robust solution (with respect to the risk of instability of the internal loop) for adaptive feedforward noise attenuation.
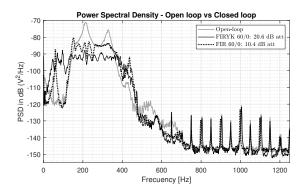

Fig. 9. PSD of the FIR and the FIRYK adaptive compensators using FUSBA (60 parameters, 150-350 Hz disturbance, 800 s experiments).

REFERENCES

[1] M. Bai and H. Lin, "Comparison of active noise control structures in the presence of acoustical feedback by using the H∞ synthesis technique," *J. of Sound and Vibration*, vol. 206, pp. 453–471, 1997.

[2] F. Ben Amara, P. Kabamba, and A. Ulsoy, "Adaptive sinusoidal disturbance rejection in linear discrete-time systems - Part II: Experiments," *Journal of Dynamic Systems Measurement and Control*, vol. 121, pp. 655–659, 1999.

[3] I. D. Landau, R. Melendez, L. Dugard, and G. Buche, "Robust and adaptive feedback noise attenuation in ducts," *IEEE Transactions on Control System Technology*, vol. 24, no. 12, pp. 1–8, December 2017.

[4] A. Wang and W. Ren, "Convergence analysis of the Filtered-U algorithm for active noise control," *Signal Processing*, vol. 83, pp. 1239–1254, 1999.

[5] R. Fraanje, M. Verhaegen, and N. Doelman, "Convergence analysis of the Filtered-U LMS algorithm for active noise control in case perfect cancellation is not possible," *Signal Processing*, vol. 73, pp. 255–266, 2003.

[6] C. Jacobson, J. Johnson, C.R., D. McCormick, and W. Sethares, "Stability of active noise control algorithms," *Signal Processing Letters, IEEE*, vol. 8, no. 3, pp. 74 –76, mar 2001.

[7] I. Landau, M. Alma, and T. Airimitoaie, "Adaptive feedforward compensation algorithms for active vibration control with mechanical coupling," *Automatica*, vol. 47, no. 10, pp. 2185 – 2196, 2011.

[8] I. D. Landau, T.-B. Airimitoaie, A. Castellanos Silva, and A. Constantinescu, *Adaptive and Robust Active Vibration Control—Methodology and Tests*, ser. Advances in Industrial Control. Springer Verlag, 2017.

[9] J. Zeng and R. de Callafon, "Recursive filter estimation for feedforward noise cancellation with acoustic coupling," *Journal of Sound and Vibration*, vol. 291, no. 3-5, pp. 1061 – 1079, 2006.

[10] I. D. Landau, T.-B. Airimitoaie, and M. Alma, "A Youla–Kučera parametrized adaptive feedforward compensator for active vibration control with mechanical coupling," *Automatica*, vol. 48, no. 9, pp. 2152 – 2158, 2012.

[11] ——, "IIR Youla–Kučera parameterized adaptive feedforward compensators for active vibration control with mechanical coupling," *IEEE Transactions on Control System Technology*, vol. 21, no. 3, pp. 765–779, May 2013.

[12] I. D. Landau, R. Lozano, M. M'Saad, and A. Karimi, *Adaptive control*, 2nd ed. London: Springer, 2011.

[13] B. Anderson, R. Bitmead, C. Johnson, P. Kokotovic, R. Kosut, I. Mareels, L. Praly, and B. Riedle, *Stability of adaptive systems*. Cambridge Massachusetts , London, England: The M.I.T Press, 1986.

[14] R. Melendez, I. Landau, L. Dugard, and G. Buche, "Data driven design of tonal noise feedback cancellers," in *Proceedings of the 20th IFAC World Congress, Toulouse, France*, 2017, pp. 916–921.

EVALUATION EXPÉRIMENTALE DES TECHNIQUES D'ATTÉNUATION ACTIVE DE BRUIT PAR CONTRE-RÉACTION ADAPTATIVE

Evaluation expérimentale des techniques d'atténuation active de bruit par contre-réaction adaptative

I. Landau, R. Melendez, L. Dugard. GIPSA-LAB – France.

Les techniques d'atténuation active de bruit par contre-réaction offre de performances très intéressantes et sont d'une complexité moindre que les techniques de compensation active de bruit par pré-compensation adaptative. Par rapport aux techniques utilisant la pré-compensation adaptative, elles ont l'avantage de ne pas nécessiter un microphone supplémentaire pour obtenir une image du bruit perturbateur, de nécessiter un nombre plus réduit de paramètres à adapter, et de ne pas introduire une réaction interne positive source de possible instabilités. Ces techniques font appel au principe du modèle interne (le régulateur doit contenir le modèle de la perturbation) et utilisent la paramétrisation Youla-Kucera pour le régulateur qui permet de réduire significativement le nombre de paramètres à adapter. Les algorithmes d'adaptation paramétriques utilisés sont de type à gain d'adaptation matriciel ou scalaire. On évaluera les performances de ces approches en présence de plusieurs configurations: a) Perturbation tonales (bande étroite) multiples de fréquences inconnues et variables; b) Atténuation des phénomènes d'interférence pour des perturbations tonales ayant des fréquences rapprochées, inconnues et variable; c) Atténuation dynamique de bruit tonal de fréquence variable; d) Atténuation de bruit bande large (plus exactement d'une largeur de bande limitée). Les mesures concernent: l'atténuation globale, l'atténuation des raies, l'amplification maximale à d'autre fréquences que celles qui sont atténues, durée des transitoires. Des fichiers audio illustreront les performances en complément des différentes courbes. Les expérimentations seront faites sur un banc de test existant au GIPSA-Lab consistant en un tube principal excité par un haut-parleur (voie primaire de propagation) sur le quel est branché en amont du microphone de mesure du bruit résiduel un autre tube par lequel le bruit de compensation produit par un haut-parleur commandé est envoyé (la voie secondaire).

[Airimiţoaie, 2012] Airimiţoaie, T.-B. (2012). *Commande robuste et calibrage des systèmes de contrôle actif de vibrations*. PhD thesis, Université de Grenoble.

[Airimiţoaie et al., 2018] Airimiţoaie, T.-B., Landau, I.-D., Meléndez, R., and Dugard, L. (2018). *Algorithms for adaptive feedforward noise attenuation - A comparative experimental evaluation*.

[Airimiţoaie et al., 2011] Airimiţoaie, T., Landau, I. D., Dugard, L., and Popescu, D. (2011). Identification of mechanical structures in the presence of narrow band disturbances - application to an active suspension. In *19th Mediterranean Conference on Control Automation (MED)*, pages 904–909.

[Airimitoaie and Landau, 2016] Airimitoaie, T. and Landau, I. D. (2016). Robust and adaptive active vibration control using an inertial actuator. *IEEE Transactions on Industrial Electronics*, 63(10):6482–6489.

[Alma, 2011] Alma, M. (2011). *Rejet adaptatif de perturbations en contrôle actif de vibrations*. PhD thesis, Université de Grenoble.

[Alma et al., 2012] Alma, M., Martinez, J. J., Landau, I. D., and Buche, G. (2012). Design and tuning of reduced order h-infinity feedforward compensators for active vibration control. *IEEE Transactions on Control Systems Technology*, 20(2):554–561.

[Amara et al., 1999a] Amara, F. B., Kabamba, P., and Ulsoy, A. (1999a). Adaptive sinusoidal disturbance rejection in linear discrete-time systems - part II:experiments. *Journal of Dynamic Systems Measurement and Control*, 121:655–659.

[Amara et al., 1999b] Amara, F. B., Kabamba, P., and Ulsoy, A. (1999b). Adaptive sinusoidal disturbance rejection in linear discrete-time systems - part I:theory. *Journal of Dynamic Systems Measurement and Control*, 121:648–654.

[Anderson et al., 1986] Anderson, B., Bitmead, R., Johnson, C., Kokotovic, P., Kosut, R., Mareels, I., and Praly, L. (1986). *Stability of adaptive systems*. The M.I.T Press, Cambridge Massachusetts , London, England.

[Åström and Murray, 2008] Åström, K. and Murray, R. (2008). *Feedback Systems: An Introduction for Scientists and Engineers*. Princeton University Press.

[Babaee et al., 2016] Babaee, S., Overvelde, J., Chen, E., and Tournat, V. (2016). Reconfigurable origami-inspired acoustic waveguides. *Science Advances*, 2:e1601019.

[Bai and H.H.Lin, 1997] Bai, M. and H.H.Lin (1997). Comparison of active noise control structures in the presence of acoustical feedback by using the hinf synthesis technique. *Journal. of Sound and Vibration*, 206:453–471.

[Baz, 2018] Baz, A. M. (2018). *Active and Passive Vibration Damping*. Wiley.

[Ben-Amara et al., 1999] Ben-Amara, F., Kabamba, P. T., and Ulsoy, A. G. (1999). Adaptive sinusoidal disturbance rejection in linear discrete-time systems—part ii: Experiments. *Journal of Dynamic Systems, Measurement, and Control*, 121:655–659.

[Bengtsson, 1977] Bengtsson, G. (1977). Output regulation and internal models- a frequency domain approach. *Automatica*, 13(4):333345.

[Bierman, 1977] Bierman, G. (1977). *Factorization methods for discrete sequential estimation*. Academic Press, New York.

[Billoud, 2001] Billoud, D. G. (2001). Ll-6508 active control at lord corporation - a reality.

[Bodson, 2005] Bodson, M. (2005). Rejection of periodic disturbances of unknown and time-varying frequency. *International Journal of Adaptive Control and Signal Processing*, 19:67–88.

[Bodson and Douglas, 1997] Bodson, M. and Douglas, S. (1997). Adaptive algorithms for the rejection of sinusoidal disturbances with unknown frequency. *Automatica*, 33:2213–2221.

[Bordeneuve-Guibé and Nistor, 2002] Bordeneuve-Guibé, J. and Nistor, I. (2002). Practical application of active noise control in a duct using predictive control. In *4th International Armament Conference on Scientific Aspects Of Armament Technology*, Waplewo, Pologne.

[Burges, 1981] Burges, J. (1981). Active adaptive sound control in a duct: A computer simulation. *Journal of the Acoustical Society of America*, 70(3):715–726.

[Carme et al., 2016] Carme, C., Schevin, O., Romerowski, C., and Clavard, J. (2016). Active noise control applied to open windows. In *INTER-NOISE 2016*, Hamburg, Germany.

[Carmona and Alvarado, 2000] Carmona, J. C. and Alvarado, V. M. (2000). Active noise control of a duct using robust control theory. *IEEE Transactions on Control System Technology*, 8(6):930–938.

[Coanda, 1930] Coanda, H. (1930). Procédé de protection control le bruit. French Patent FR 722.274.

[Cocchi et al., 2000] Cocchi, A., Garai, M., and Guidorzi, P. (2000). Active noise control in heating, ventilation and air conditioning systems. In *7th International Congress on Sound and Vibration*, Garmisch-Partenkirchen, Germany.

[Constantinescu, 2001] Constantinescu, A. (2001). *Command robuste et adaptative d'une suspension active*. PhD thesis, Institute National Polytechnique de Grenoble.

[Constantinescu and Landau, 2003] Constantinescu, A. and Landau, I. (2003). Direct controller order reduction by identification in closed loop applied to a benchmark problem. *European Journal of Control*, 9(1).

[Crawford and Stewart, 1997] Crawford, D. and Stewart, R. (1997). Adaptive iir filtered-v algorithms for active noise control. *Journal of the Acoustical Society of America*, 101(4).

[de Bedout et al., 1997] de Bedout, J., Franchek, M., Bernhard, R., and Mongeau, L. (1997). Adaptive-passive noise control with self-tuning helmholtz resonators. *Journal of Sound and Vibration*, 202(1):109–123.

[Ding, 2003] Ding, Z. (2003). Global stabilization and disturbance suppression of a class of nonlinear systems with uncertain internal model. *Automatica*, 39(3):471–479.

[Duong and Landau, 1994] Duong, H. N. and Landau, I. D. (1994). On statistical properties of a test for model structure selection using the extended instrumental variable approach. *IEEE Transactions on Automatic Control*, 39(1):211–215.

[Duong and Landau, 1996] Duong, H. N. and Landau, I. D. (1996). An iv based criterion for model order selection. *Automatica*, 32(6):909–914.

[Elliott, 2001] Elliott, S. (2001). *Signal processing for active control*. Academic Press.

[Elliott and Nelson, 1993] Elliott, S. and Nelson, P. (1993). Active noise control. *IEEE Signal Processing Magazine*, 10(4):12–35.

[Elliott and Nelson, 1994] Elliott, S. and Nelson, P. (1994). Active noise control. *Noise / News International*, pages 75–98.

[Elliott and Sutton, 1996] Elliott, S. and Sutton, T. (1996). Performance of feedforward and feedback systems for active control. *Speech and Audio Processing, IEEE Transactions on*, 4(3):214 –223.

[Eriksson, 1991a] Eriksson, L. (1991a). Development of the filtered-u algorithm for active noise control. *Acoustic Society of America*, 89(1):257–265.

[Eriksson, 1991b] Eriksson, L. (1991b). Development of the filtered-u lms algorithm for active noise control. *Journal of Acoustical Society of America*, 89(1):257–261.

[Eriksson et al., 1987] Eriksson, L., Allie, M., and Greiner, R. (1987). The selection and application of an iir adaptive filter for use in active sound attenuation. *IEEE Transactions on Acoustics, Speech and Signal Processing*, 35(4):433–437.

[Feintuch, 1976] Feintuch, P. (1976). An adaptive recursive lms filter. *Proceedings of the IEEE*, 64(11):1622–1624.

[Fleming et al., 2007] Fleming, A., Niederberger, D., Moheimani, S., and Morari, M. (2007). Control of resonant acoustic sound fields by electrical shunting of a loudspeaker. *IEEE Transactions on Control Systems Technology*, 15(4):689–703.

[Fraanje et al., 1999] Fraanje, R., Verhaegen, M., and Doelman, N. (1999). Convergence analysis of the filtered-u lms algorithm for active noise control in case perfect cancellation is not possible. *Signal Processing*, 73:255–266.

[Francis and Wonham, 1976] Francis, B. and Wonham, W. (1976). The internal model principle of control theory. *Automatica*, 12(5):457–465.

[Fuller and von Flotow, 1995] Fuller, C. and von Flotow, A. (1995). Active control of sound and vibration. *IEEE Control Systems*, 15(6):9–19.

[Gouraud et al., 1997] Gouraud, T., Gugliemi, M., and Auger, F. (1997). Design of robust and frequency adaptive controllers for harmonic disturbance rejection in a single-phase power network. *Proceedings of the European Control Conference, Bruxelles*.

[Guicking, 2007] Guicking, D. (2007). *Active Control of Sound and Vibration History - Fundamentals - State of the Art*. Festschrift DPI, 1-32, Herausgeber (ed.), Universitätsverlag Göttingen.

[Guidorzi, 1981] Guidorzi, R. P. (1981). Invariants and canonical forms for systems structural and parametric identification. *Automatica*, 17(1):117–133.

[Guo et al., 2018a] Guo, X., Gusev, V., Bertoldi, K., and Tournat, V. (2018a). Manipulating acoustic wave reflection by a nonlinear elastic metasurface. *Journal of Applied Physics*, 123:124901.

[Guo et al., 2018b] Guo, X., Gusev, V., Bertoldi, K., and Tournat, V. (2018b). Nonlinear elastic metasurface design achieving acoustic wave scattering control. In *12th International Congress on Artificial Materials for Novel Wave Phenomena (Metamaterials)*, pages 498–500.

[Hall, 1991] Hall, A. (1991). Order identification of arma models based on instrumental variable estimators. *IEEE Transactions on Automatic Control*, 36(9):1116–1117.

[Hansen et al., 2007] Hansen, C. H., Xiaojun Qiu, G. B., and Howard, C. Q. (2007). Optimization of active and semi-active noise and vibration control systems. In *14th International Congress on Sound & Vibration*, Cairns, Australia.

[Heuberger et al., 1995] Heuberger, P., Van den Hof, P., and Bosgra, O. (1995). A generalized orthonormal basis for linear dynamical systems. *Automatic Control, IEEE Transactions on*, 40(3):451–465.

[Hillerstrom and Sternby, 1994] Hillerstrom, G. and Sternby, J. (1994). Rejection of periodic disturbances with unknown period - a frequency domain approach. *Proceedings of American Control Conference, Baltimore*, pages 1626–1631.

[Hong and Bernstein, 1998] Hong, J. and Bernstein, D. (1998). Bode integral constraints, collocation, and spillover in active noise and vibration control. *IEEE Transactions on Control Systems Technology*, 6(1):111–120.

[Hu and Lin, 2000] Hu, J. and Lin, J.-F. (2000). Feedforward active noise controller design in ducts without independent noise source measurements. *IEEE Transactions on Control System Technology*, 8(3):443–455.

[Jacobson et al., 2001] Jacobson, C., Johnson, C.R., J., McCormick, D., and Sethares, W. (2001). Stability of active noise control algorithms. *Signal Processing Letters, IEEE*, 8(3):74–76.

[Johnson, 1976] Johnson, C. (1976). Theory of disturbance - accomodating controllers. In Control and Dynamical Systems.

[Johnson, 1979] Johnson, C., J. (1979). A convergence proof for a hyperstable adaptive recursive filter (corresp.). *IEEE Transactions on Information Theory*, 25(6):745–749.

[Krylov, 2014] Krylov, V. V. (2014). Acoustic black holes: recent developments in the theory and applications. *IEEE Transactions on Ultrasonics, Ferroelectrics, and Frequency Control*, 61(8):1296–1306.

[Krysinski and Malburet, 2008] Krysinski, T. and Malburet, F. (2008). *Mechanical Vibrations: Active and Passive Control*. ISTE Ltd.

[Kuo and Morgan, 1996] Kuo, M. and Morgan, D. (1996). *Active noise control systems - Algorithms and DSP implementation*. Academic Press, New York.

[Kuo and Morgan, 1999] Kuo, S. and Morgan, D. (1999). Active noise control: a tutorial review. *Proceedings of the IEEE*, 87(6):943–973.

[Landau, 1979] Landau, I. (1979). *Adaptive control - the model reference approach*. Marcel Dekker, New York,USA.

[Landau, 1976] Landau, I.-D. (1976). Unbiased recursive identification using model reference adaptive techniques. *IEEE Transactions on Automatic Control*, 21(2):194–202.

[Landau, 1980] Landau, I. D. (1980). An extension of a stability theorem applicable to adaptive control. *IEEE Transactions on Automatic Control*, 25(4):814–817.

[Landau et al., 2012] Landau, I.-D., Airimiţoaie, T.-B., and Alma, M. (2012). A youla-kučera parametrized adaptive feedforward compensator for active vibration control with mechanical coupling. *Automatica*, 48(9):2152–2158.

[Landau et al., 2013] Landau, I.-D., Airimiţoaie, T.-B., and Alma, M. (2013). Iir youla-kučera parameterized adaptive feedforward compensators for active vibration control with mechanical coupling. *IEEE Transactions on Control System Technology*, 21(3):765–779.

[Landau et al., 2016] Landau, I. D., Airimiţoaie, T.-B., and Castellanos-Silva, A. (2016). *Adaptive and Robust Active Vibration Control: Methodology and Tests*. Springer, London.

[Landau et al., 2019a] Landau, I.-D., Airimiţoaie, T.-B., Meléndez, R., and Dugard, L. (2019a). Beyond the delay barrier in adaptive feedforward active noise attenuation. *Journal of Sound and Vibration*.

[Landau et al., 2019b] Landau, I.-D., Airimiţoaie, T.-B., Meléndez, R., and Dugard, L. (2019b). Why one should use youla-kučera parametrization in adaptive feedforward noise attenuation? In *58th IEEE Conference on Decision and Control (IEEE-CDC)*, Nice, France.

[Landau et al., 2011a] Landau, I. D., Alma, M., and Airimiţoaie, T.-B. (2011a). Adaptive feedforward compensation algorithms for active vibration control with mechanical coupling. *Automatica*, 47(10):2185–2196.

[Landau et al., 2011b] Landau, I. D., Alma, M., Constantinescu, A., Martinez, J., and Noë, M. (2011b). Adaptive regulation - rejection of unknown multiple narrow band disturbances (a review on algorithms and applications). *Control Engineering Practice*, 19(10):1168–1181.

[Landau et al., 2005] Landau, I.-D., Constantinescu, A., and Rey, D. (2005). Adaptive narrow band disturbance rejection applied to an active suspension - an internal model principle approach. *Automatica*, 41(4):563–574.

[Landau et al., 2011c] Landau, I. D., Lozano, R., M'Saad, M., and Karimi, A. (2011c). *Adaptive control*. Springer, London, 2nd edition.

[Landau and Meléndez, 2017] Landau, I.-D. and Meléndez, R. (2017). Active noise control: Adaptive vs robust approach. In *25th Mediterranean Conference on Control and Automation (MED)*, pages 799–804, Valletta, Malta.

[Landau et al., 2019c] Landau, I.-D., Meléndez, R., Dugard, L., and Buche, G. (2019c). Robust and adaptive feedback noise attenuation in ducts. *IEEE Transactions on Control Systems Technology*, 27(2):872–879.

[Landau and Silveira, 1979] Landau, I. D. and Silveira, H. (1979). A stability theorem with applications to adaptive control. *IEEE Transactions on Automatic Control*, 24(2):305 – 312.

[Landau and Zito, 2006] Landau, I. D. and Zito, G. (2006). *Digital Control Systems: Design, Identification and Implementation (Communications and Control Engineering)*. Springer-Verlag, Berlin, Heidelberg.

[Larimore et al., 1980] Larimore, M., Treichler, J., and Johnson, C., J. (1980). Sharf: An algorithm for adapting iir digital filters. *IEEE Transactions on Acoustics, Speech and Signal Processing*, 28(4):428–440.

[Ljung, 1977a] Ljung, L. (1977a). Analysis of recursive stochastic algorithms. *IEEE Transactions on Automatic Control*, 22(4):551–575.

[Ljung, 1977b] Ljung, L. (1977b). On positive real transfer functions and the convergence of some recursive schemes. *IEEE Trans. on Automatic Control*, AC-22:539–551.

[Ljung, 1999] Ljung, L. (1999). *System Identification - Theory for the User*. Prentice Hall, Englewood Cliffs, second edition.

[Ljung and Söderström, 1983] Ljung, L. and Söderström, T. (1983). *Theory and practice of recursive identification*. The MIT Press, Cambridge Massachusetts, London, England.

[Lu et al., 2014] Lu, B., Chen, X., Liu, Y., and Tian, Q. (2014). Application simulation of active noise control in dental treatment. *Open Journal of Acoustics and Vibration*, 2:19–27.

[Lueg, 1934] Lueg, P. (1934). Process of silencing sound oscillations. US Patent 2,043,416.

[Marchal, 2014] Marchal, R. (2014). *Métamatériaux Acoustiques Actifs*. PhD thesis, Université Pierre et Marie Curie - Paris 6.

[Marino et al., 2003] Marino, R., Santosuosso, G., and Tomei, P. (2003). Robust adaptive compensation of biased sinusoidal disturbances with unknown frequency. *Automatica*, 39:1755–1761.

[Marino and Tomei, 2007] Marino, R. and Tomei, P. (2007). Output regulation for linear minimum phase systems with unknown order exosystem. *IEEE Transactions on Automatic Control*, 52(10):2000–2005.

[Matsuhisa et al., 1992] Matsuhisa, H., Ren, B., and Sato, S. (1992). Semiactive control of a duct noise by a volume-variable resonator. *Japan Society of Mechanical Engineers International Journal Series 3, Vibration, Control Engineering, Engineering for Industry*, 35(2):223–228.

[Meléndez et al., 2017] Meléndez, R., Landau, I.-D., Dugard, L., and Buche, G. (2017). Data driven design of tonal feedback cancellers. *IFAC-PapersOnLine*, 50(1):916–921. 20th World Congress of the International Federation of Automatic Control (WC-IFAC).

[Miljković, 2016] Miljković, D. (2016). Active noise control: From analog to digital — last 80 years. In *39th International Convention on Information and Communication Technology, Electronics and Microelectronics (MIPRO)*, pages 1151–1156.

[Montazeri and Poshtan, 2010] Montazeri, A. and Poshtan, J. (2010). A computationally efficient adaptive iir solution to active noise and vibration control systems. *IEEE Transactions on Automatic Control*, AC-55:2671–2676.

[Montazeri and Poshtan, 2011] Montazeri, A. and Poshtan, J. (2011). A new adaptive recursive rls-based fast-array iir filter for active noise and vibration control systems. *Signal Processing*, 91(1):98–113.

[Mosquera et al., 1999] Mosquera, C., Gomez, J., Perez, F., and Sobreira, M. (1999). Adaptive iir filters for active noise control. In *Sound and Vibration, 6th International Congress on ICSV 1999.*, pages 1571–1582.

[Nelson and Elliott, 1993] Nelson, P. and Elliott, S. (1993). *Active Control of Sound*. Academic Press.

[Olson and May, 1953] Olson, H. F. and May, E. G. (1953). Electronic sound absorber. *The Journal of the Acoustical Society of America*, 25(6):1130–1136.

[Popov, 1960] Popov, V. M. (1960). Criterii de stabilitate pentru sistemele automate conţinând elemente neunivoce, probleme de automatizare. *Publishing House of the Romanian Academy*, pages 143–151.

[Popov, 1963] Popov, V. M. (1963). Solution of a new stability problem for controlled systems. *Automatic Remote Control*, 24(1):1–23.

[Popov, 1966] Popov, V. M. (1966). *Hiperstabilitatea Sistemelor Automate*. Editura Academiei Republicii Socialiste România.

[Popov, 1973] Popov, V. M. (1973). *Hyperstability of Control Systems*. Springer-Verlag.

[Rotunno and de Callafon, 2003] Rotunno, M. and de Callafon, R. (2003). Design of model-based feedforward compensators for vibration compensation in a flexible structure. Department of Mechanical and Aerospace Engineering. University of California, San Diego. Internal report.

[Söderström, 1977] Söderström, T. (1977). On model structure testing in system identification. *International Journal of Control*, 26(1):1–18.

[Söderström and Stoica, 1988] Söderström, T. and Stoica, P., editors (1988). *System Identification*. Prentice-Hall, Inc., New Jersey, USA.

[Serrani, 2006] Serrani, A. (2006). Rejection of harmonic disturbances at the controller input via hybrid adaptive external models. *Automatica*, 42(11):1977–1985.

[Sharma and Renu, 2016] Sharma, M. K. and Renu, V. (2016). Ambulance siren noise reduction using lms and fxlms algorithms. *Indian Journal of Science and Technology*, 9(47).

[Silva, 2014] Silva, A. C. (2014). *Compensation adaptative par feedback pour le contrôle actif de vibrations en présence d'incertitudes sur les paramètres du procédé*. PhD thesis, Université de Grenoble.

[Snyder, 1994] Snyder, S. (1994). Active control using iir filters - a second look. In *IEEE International Conference on Acoustics, Speech, and Signal Processing (ICASSP).*, volume ii, pages II/241 –II/244 vol.2.

[Snyder, 2000] Snyder, S. D. (2000). *Active Noise Control Primer*. Springer Verlag.

[Stanfield and Skaves, 2012] Stanfield, C. and Skaves, D. (2012). *Fundamentals of HVACR*. Always learning. Prentice Hall.

[Stoica, 1981] Stoica, P. (1981). On a procedure for structural identification. *International Journal of Control*, 33(6):1177–1181.

[Sun and Chen, 2002] Sun, X. and Chen, D.-S. (2002). A new infinte impulse response filter-based adaptive algorithm for active noise control. *Journal of Sound and Vibration*, 258(2):385–397.

[Sun and Meng, 2004] Sun, X. and Meng, G. (2004). Steiglitz-mcbride type adaptive iir algorithm for active noise control. *Journal of Sound and Vibration*, 273(1-2):441–450.

[Tay et al., 1997] Tay, T. T., Mareels, I. M. Y., and Moore, J. B. (1997). *High Performance Control*. Birkh auser Boston.

[Treichler et al., 1978] Treichler, J., Larimore, M., and Johnson, C., J. (1978). Simple adaptive iir filtering. In *IEEE International Conference on Acoustics, Speech, and Signal Processing (ICASSP)*, volume 3, pages 118–122.

[Tsypkin, 1997] Tsypkin, Y. (1997). Stochastic discrete systems with internal models. *Journal of Automation and Information Sciences*, 29(4-5):156–161.

[Valentinotti, 2001] Valentinotti, S. (2001). *Adaptive Rejection of Unstable Disturbances: Application to a Fed-Batch Fermentation*. Thèse de doctorat, École Polytechnique Fédérale de Lausanne.

[Valentinotti et al., 2003] Valentinotti, S., Srinivasan, B., Holmberg, U., Bonvin, D., Cannizzaro, C., and Rhiel, M. (2003). Optimal operation of fed-batch fermentations via adaptive control of overflow metabolite. *Control Engineering Practice*, 11(6):665 – 674.

[Venugopal and Bernstein, 2000] Venugopal, R. and Bernstein, D. S. (2000). Adaptive disturbance rejection using armarkov/toeplitz models. *IEEE Transactions on Control System Technology*, 8(2):257–269.

[Wang and Ren, 2003] Wang, A. and Ren, W. (2003). Convergence analysis of the filtered-u algorithm for active noise control. *Signal Processing*, 83:1239–1254.

[Wellstead, 1978] Wellstead, P. (1978). An instrumental product moment test for model order estimation. *Automatica*, 14(1):89–91.

[Widrow, 1971] Widrow, B. (1971). *Adaptive filters*. Holt, Rinehart and Winston. Kalman, R.E. and DeClaris, H.

[Widrow et al., 1975] Widrow, B., Glover, J.R., J., McCool, J., Kaunitz, J., Williams, C., Hearn, R., and Zeidler, J. (1975). Adaptive noise cancelling: Principles and applications. *Proceedings of the IEEE*, 63(12):1692–1716.

[Widrow et al., 1981] Widrow, B., Shur, D., and Shaffer, S. (1981). On adaptive inverse control. In *Proceedings 15th Asilomar Conferenece Circuits, Systems and Computers*, Pacific Grove, CA, USA.

[Widrow and Stearns, 1985] Widrow, B. and Stearns, S. (1985). *Adaptive Signal Processing*. Prentice-Hall, Englewood Cliffs, New Jersey.

[Xie et al., 2016] Xie, L., cheng Qiu, Z., and min Zhang, X. (2016). Vibration control of a flexible clamped-clamped plate based on an improved fulms algorithm and laser displacement measurement. *Mechanical Systems and Signal Processing*, 75:209–227.

[Young et al., 1980] Young, P., Jakeman, A., and McMurtrie, R. (1980). An instrumental variable method for model order identification. *Automatica*, 16(3):281–294.

[Zeng and de Callafon, 2006] Zeng, J. and de Callafon, R. (2006). Recursive filter estimation for feedforward noise cancellation with acoustic coupling. *Journal of Sound and Vibration*, 291(3-5):1061–1079.

[Zhou et al., 1996] Zhou, K., Doyle, J. C., and Glover, K. (1996). *Robust and optimal control*. Prentice Hall, Upper Saddle River, New Jersey.

[Zhu et al., 2012] Zhu, X., Gao, Z., Huang, Q., Gao, S., and Jiang, E. (2012). Analysis and implementation of mimo fulms algorithm for active vibration control. *Transactions of the Institute of Measurement and Control*, 34(7):815–828.

[Zimmer et al., 2003] Zimmer, B. J., Lipshitz, S. P., Morris, K. A., Vanderkooy, J., and Obasi, E. E. (2003). An improved acoustic model for active noise control in a duct. *Journal of Dynamic Systems, Measurement, and Control*, 125:382–395.

Abstract

The aim of this thesis is the development and application of different control methods for Active Noise Control in the presence of uncertain and time-varying disturbances. A model-based controller design is applied and a full methodology for model identification is introduced. In this context, a reconfigurable test bench based on a noise silencer for ducts has been designed and built. It is fully equipped with sensors and actuators in order to test the developed algorithms in diverse configurations.

A feedback scheme is established for the case where narrow-band disturbances are present. Based on the Internal Model Principle, fixed linear and robust controllers are designed and compared with the proposed adaptive feedback controller using a Youla-Kučera parametrization. For the case where disturbances have broadband characteristics, a feedforward scheme is proposed. This approach requires the introduction of an additional sensor which creates an internal positive coupling, requiring a specific design in order to avoid possible instabilities. In this framework, Infinite (IIR) and Finite (FIR) Impulse Responses adaptive feedforward compensators, as well as Youla-Kučera parametrized adaptive feedforward compensators are compared.

The estimated models' quality for control design as well as the control capabilities themselves are illustrated by the experimental performance of the controllers implemented on the test bench for various tests setup conditions.

Résumé

Le but de cette thèse est le développement et l'application de différentes méthodes de contrôle pour le contrôle actif du bruit en présence de perturbations incertaines et variables dans le temps. Une conception de contrôleur basée sur un modèle est appliquée et une méthodologie complète pour l'identification du modèle est introduite. Dans ce contexte, un banc d'essai reconfigurable basé sur un silencieux de bruit pour gaines a été conçu et construit. Il est entièrement équipé de capteurs et d'actionneurs afin de tester les algorithmes développés dans diverses configurations.

Un schéma contre-réaction feedback est établi pour les cas où des perturbations en bande étroite sont présentes. Sur la base du Principe du Modèle Interne, des contrôleurs linéaires fixes et robustes sont conçus et comparés avec le contrôleur par contre-réaction adaptatif proposé en utilisant un paramétrage Youla-Kučera. Dans le cas où les perturbations présentent des caractéristiques à large bande, un système de rétroaction feedforward est proposé. Cette approche nécessite l'introduction d'un capteur supplémentaire qui crée un couplage positif interne, nécessitant une conception spécifique afin d'éviter d'éventuelles instabilités. Dans ce cadre, les compensateurs adaptatifs IIR et FIR, ainsi que les compensateurs adaptatifs avec paramétrage Youla-Kučera sont comparés.

La qualité des modèles estimés pour la conception des contrôles ainsi que les capacités de contrôle elles-mêmes sont illustrées par les performances expérimentales des contrôleurs mis en œuvre sur le banc d'essai pour diverses conditions de configuration des tests.